UNIVERSITÀ DEGLI STUDI DI TRIESTE
e
UNIVERSITÀ CA' FOSCARI DI VENEZIA

XXXII CICLO DEL DOTTORATO DI RICERCA IN

_____CHIMICA_____

PALLADIUM CATALYZED COPOLYMERIZATIONS: FROM LIGAND ARCHITECTURE TO MACROMOLECULE MICROSTRUCTURE

Settore scientifico-disciplinare: **CHIM/03**

DOTTORANDO / A
ANNA DALL'ANESE

COORDINATORE
PROF. BARBARA MILANI

SUPERVISORE DI TESI
PROF. BARBARA MILANI

CO-SUPERVISORE DI TESI
PROF. FULVIA FELLUGA

ANNO ACCADEMICO 2018/2019

TABLE OF CONTENTS

LIST OF ABBREVIATIONS

Ar-BIAN: Acenaphthene/bis(aryl-imino)acenaphthene based α-diimines

Ar-BIP: Phenanthrene based α-diimines

Ar-DAB: 1,4-diaza-1,3-butadiene or 1,4-diaza-2,3-methyl-buta-1,3-diene based α-diimines

BAr^F: $B(3,5–(CF_3)_2C_6H_3)_4^-$

Bd: branching degree

BF_4: tetrafluoroborate

BQ: 1,4-benzoquinone

Bpy: 2,2'–bipyridyl

BINAPHOS: bisnaphthyl-diphenylphosphino-phosphito

CP: copolymer

$CDCl_3$: deuterated chloroform

CD_2Cl_2: deuterated dichloromethane

CO: carbon monoxide

Cod: *cis,cis*–1,5–cyclooctadiene

COSY: correlation spectroscopy

DAPP: 1,3-bis-(di-anisol)phosphino propane

DCM: dichloromethane

DQCOSY: double quantum correlation spectroscopy

E or Et: ethylene

GOC: growing oligomeric chain

GPC: gel permeation chromatography or growing polymeric chain

HFIP: 1,1,1,3,3,3–hexafluoro–2–propanol

HMBC: heteronuclear multiple bond correlation

HSQC: heteronuclear single quantum coherence/correlation spectroscopy

L: labile ligand

MA: methyl acrylate

Mw: mass average molar mass

Mn: number average molar mass

MS: 4-methyl styrene

NMR: Nuclear magnetic resonance

NOESY: Nuclear Overhauser effect spectroscopy

nBA: n-butyl acrylate

ORTEP: Oak Ridge Thermal Ellipsoid Plot

OTf: triflate, $CF_3SO_3^-$

OTs: tosilate

Phen: phenanthroline

Py: pyridine

Pyr-DAB: pyrene-tagged DAB ligands

PF_6: hexafluorophosphate

PPh_3: triphenylphosphine

RU: repeating unit

SbF_6: hexafluoroantimonate

S: styrene

TBA: tert-butyl acrylate

TBS: 4-tert-butyl styrene

TFE: 2,2,2-trifluoroethanol

THF: tetrahydrofuran

TOCSY: total correlation spectroscopy

TON: turnover number

TOF: turnover frequency

TsOH: *p*–toluensulphonic acid

ABSTRACT

Polyolefins represent one of the major products of the plastic industry, that satisfy 55 % of the worldwide plastic demand. However, due to their chemical composition, they suffer of scarce surface properties, such as dyeability, compatibility with other materials, printability and adhesion. In this regard, the introduction of polar functional groups into the polyolefin skeleton would overcome this problem. Up to now this target is industrially achieved by radical polymerization reactions, that require harsh conditions of temperature and pressure and do not allow the control on the microstructure of the produced functionalized polyolefin. The direct, homogeneously catalyzed copolymerization reaction of ethylene with polar vinyl monomers would overcome all of these limits, allowing to use milder reaction conditions but, most importantly, to have a precise control on the copolymer microstructure. Much efforts have been done in this direction, and in the last two decades a wide number of systems based on palladium catalysts with a great variety of ligands has been reported. However, the catalytic performances of these systems, in terms of activity/productivity values, incorporation of the polar monomers, molecular weight and molecular weight distribution and copolymer microstructure, do not satisfy the requirements for a potential industrial application, thus better performing catalysts are needed.

This PhD thesis aims to develop new homogeneous catalysts for the target reaction based on palladium(II) complexes with bidentate nitrogen-donor ligands (N-N). The strategy of this research project is based on expanding the library of N-N donor ligands reported in literature, and to study the influence of the ligand design on the catalytic outcome. In each Chapter the synthesis and characterization of different N-N ligands will be reported, along with the synthesis and characterization of the relevant Pd(II) complexes, and the study of their catalytic behaviour including the characterization of the catalytic products.

Chapter 1 consists in an overview on the principal catalytic systems reported in literature for the synthesis of functionalized polyolefins, with a focus on systems based on N-N ligands reported in recent years.

Chapter 2 deals with the exploitation of the concept of ligand desymmetrisation, and in particular with the application of pyridylimine-based palladium complexes to the cooligomerization of ethylene and acrylic esters. This kind of systems have been widely studied and applied to several catalytic reactions, but this represent the first example of a detailed catalytic study in such cooligomerization reaction. The monocationic palladium complexes of general formula [Pd(N-N')(CH_3)(CH_3CN)][X] (where X = OTf, PF_6^-, SbF_6^-) yield cooligomers with a maximum productivity of almost 1.1 kg P/g Pd and with an incorporation of polar monomer (methyl acrylate)

that is in the range of 10-25 %, making such products interesting for potential industrial applications. An effect of both the ligand skeleton and the different counter anions on catalysis is observed. In particular, the productivity increases with increasing the coordinating capability of X^-, which is counterintuitive and differs from what is usually observed. Moreover a first attempt to recycle the homogeneous catalyst is reported.

Chapter 3 focuses on the variation of the ligand backbone with respect to the usual α-diimine ligands, that feature either the acenaphthene (BIAN) or the 1,4-diaza-2,3-methyl-buta-1,3-diene (DAB) backbone. A family of phenanthrene derived α-diimines is reported, and the relevant neutral, [Pd(Ar-BIP)(CH_3)Cl], and cationic, [Pd(Ar-BIP)(CH_3)(CH_3CN)][PF_6], complexes are synthesized and characterized, and the latter applied to the copolymerization of ethylene and methyl acrylate, leading to copolymers with M_n values up to 37000 and a content of polar monomer of 5.3 mol %. NMR characterization of the copolymers produced in 2,2,2-trifluoroethanol points out that the polar monomer is inserted both at the end of the branches and into the main chain, with a more selective enchainment than that achieved when the copolymerization is carried out in dichloromethane. *In situ* NMR investigations allowed us to detect relevant intermediates of the catalytic cycle and shed light on the nature of possible deactivation species. Ligand desymmetrisation is also applied to the phenanthrene-based α-diimines, and the relevant non-symmetrical Ar,Ar'-BIP ligands are here reported and their coordination chemistry to Pd(II) investigated.

In *Chapter 4* another aspect of ligand design is evaluated, namely the introduction of a bulky substituent, like butoxy pyrene, on the *para* position of the N-aryl rings of α-diimines with the DAB backbone (pyr-DAB). The relevant monocationic palladium complexes, [Pd(pyr-DAB)(CH_3)(CH_3CN)][SbF_6], give excellent results in the copolymerization of ethylene with acrylic esters, leading to macromolecules with peculiar features. When they are obtained in trifluoroethanol, the polar vinyl monomer is prevailingly inserted into the main polymeric chain, which represents a remarkable difference with respect to most of the other α-diimine based systems reported up to now; when dichloromethane is the reaction medium, instead, an opposite selectivity of the enchainment of methyl acrylate is found, that is the usual insertion into the termination of the branches. To shed a light on this behavior, the study of the reactivity by NMR spectroscopy of the most productive precatalyst with methyl acrylate and ethylene in both deuterated dichloromethane and deuterated trifluoroethanol is assessed.

Another reaction of interest is the copolymerization of carbon monoxide with vinyl arenes, to obtained perfectly alternating polyketones. In *Chapter 5* a brief introduction on the subject is reported, with a focus on pyridylimine-based Pd(II) catalytic systems. The introduction of polycyclic aromatic moieties on the N_{imino} fragment of pyridylimine ligands and their effect on the

copolymerization of CO with either styrene or its derivatives (4-methyl styrene and 4-*tert*-butyl styrene) is investigated. The highlight of this work is represented by the effect of the vinyl arene on the produced macromolecules, in particular on their stereochemistry, that is studied in terms of microtacticity by ^{13}C NMR spectroscopy. This analysis shows that, when catalysts with aldimine ligands are used, the stereochemistry of the obtained polyketones is affected not by the ligand itself but by the different comonomer used.

As a general conclusion, the results of this PhD project show the importance of ligand design in the catalytic synthesis of functionalized macromolecules and represent a significant improvement of the state of the art, in particular in the field of homogeneously-catalyzed functionalized polyolefin synthesis. Focusing on the ethylene/methyl acrylate copolymerization, the data discussed in *Chapters 3* and *4* allow us to state that, in order to have better copolymerization catalysts, a possible strategy to follow is not to design systems that give good ethylene homopolymerization catalysts, but instead to move towards complexes that, at the same time, have a good affinity for the polar vinyl monomers.

RIASSUNTO

Le poliolefine rappresentano uno dei principali prodotti dell'industria della plastica, e soddisfano il 55% della richiesta di plastica di tutto il mondo. Ciò nonostante, a causa della loro composizione chimica, le poliolefine presentano scarse proprietà di superficie, come tingibilità, compatibilità con altri materiali, stampabilità e proprietà di adesione. A questo proposito, l'introduzione di gruppi funzionali polari nello scheletro delle poliolefine, ottenendo poliolefine funzionalizzate, rappresenta un possibile metodo per superare questo problema. Le tecnologie attualmente applicate industrialmente per la sintesi di poliolefine funzionalizzate si basano su reazioni di polimerizzazione radicaliche, che richiedono condizioni drastiche di pressione e temperatura, e non permettono il controllo della microstruttura delle macromolecole prodotte.

La copolimerizzazione diretta e controllata, via catalisi omogenea, dell'etilene con monomeri vinilici polari rappresenta il metodo più efficace ed ecocompatibile per superare queste limitazioni, permettendo di utilizzare condizioni di reazione più blande e, ancor più importante, di avere un controllo preciso sulla microstruttura del copolimero ottenuto.

Molti sforzi sono stati compiuti in tal senso, e nelle ultime due decadi un vasto numero di sistemi catalitici basati su complessi di palladio con una gran varietà di leganti è stato riportato in letteratura. Tuttavia, le prestazioni dei catalizzatori riportati fino ad ora, in termini di attività/produttività, di grado di incorporazione del monomero polare, di peso molecolare e sua distribuzione, e di microstruttura dei copolimeri ottenuti, non soddisfano i requisiti richiesti per una potenziale applicazione industriale, e pertanto vi è una forte interesse nello sviluppo di catalizzatori migliori.

Lo scopo principale di questa tesi di dottorato riguarda proprio lo sviluppo di nuovi catalizzatori omogenei, basati su complessi di palladio(II) con leganti bidentati azotati (N-N), per la reazione di copolimerizzazione dell'etilene con monomeri vinilici polari per ottenere poliolefine funzionalizzate. La strategia su cui si è basato il progetto di ricerca ha riguardato l'ampliamento della libreria dei leganti N-N riportati in letteratura, e lo studio dell'influenza della progettazione del legante sui risultati catalitici. Ogni Capitolo si articola nella sintesi e caratterizzazione di diversi leganti N-N, nella sintesi e caratterizzazione dei relativi complessi di Pd(II) e nello studio del loro comportamento catalitico nella reazione target, comprendente anche la caratterizzazione parziale delle macromolecole prodotte.

Il *Capitolo 1* consiste in una panoramica sui principali sistemi catalitici riportati in letteratura per la sintesi delle poliolefine funzionalizzate, con un focus sui sistemi basati su leganti N-N riportati di recente.

Il *Capitolo 2* riguarda l'applicazione del concetto di desimmetrizzazione del legante, con particolare riferimento allo studio di molecole appartenenti alla classe delle piridilimmine quali leganti ancillari per complessi di palladio utilizzati come catalizzatori nella cooligomerizzazione dell'etilene con esteri acrilici. Questo tipo di sistemi sono stati ampiamente utilizzati in diverse reazioni catalitiche, ma questo studio rappresenta il primo esempio di uno studio catalitico dettagliato in questa reazione di cooligomerizzazione. I complessi di palladio monocationici di formula generale [Pd(N-N')(CH_3)(CH_3CN)][X] (dove X = OTf, PF_6^-, SbF_6^-) danno cooligomeri con una produttività massima di 1.1 kg P/g Pd e con un contenuto di monomero polare (metil acrilato) che va dal 10 al 25 %, rendendo così tali prodotti interessanti per potenziali applicazioni industriali. Si è osservato un effetto molto pronunciato sia dello scheletro del legante che dei diversi controanioni sui risultati catalitici. In particolare, la produttività aumenta all'aumentare del potere coordinante di X^-, un andamento controintuitivo che differisce da quello che viene solitamente osservato. Inoltre, è stato effettuato con successo un primo tentativo di riciclo del catalizzatore omogeneo.

Il *Capitolo 3* si concentra sulla variazione dello scheletro del legante rispetto a quello solitamente studiato per le α-diimine, che sono caratterizzate da uno scheletro derivante o dall'acenaftene (BIAN) o dall'1,4-diaza-2,3-metil-buta-1,3-diene (DAB). Questo capitolo riguarda la classe delle α-diimine derivanti dal fenantrene (Ar-BIP). I relativi complessi neutri, [Pd(Ar-BIP)(CH_3)Cl], e cationici, [Pd(Ar-BIP)(CH_3)(CH_3CN)][PF_6], sono sintetizzati, caratterizzati e testati nella copolimerizzazione dell'etilene con il metil acrilato, ottenendo dei copolimeri con valori di M_n fino a 37 000, e con un contenuto di monomero polare del 5.3 mol %. La caratterizzazione NMR dei copolimeri prodotti in 2,2,2-trifluoroetanolo indica che il monomero vinilico polare è inserito sia in terminazione di catena che in catena principale, con un'incorporazione più selettiva rispetto a quella che si ha quando la copolimerizzazione viene condotta in diclorometano. L'analisi NMR *in situ* ha permesso di individuare gli intermedi di reazione più rilevanti del ciclo catalitico e di portare alla luce la natura delle possibili specie coinvolte nella disattivazione del catalizzatore. Il concetto di desimmetrizzazione è stato successivamente applicato anche alle α-diimine a scheletro fenantrenico, studiando i relativi leganti Ar,Ar'-BIP non simmetrici assieme alla loro chimica di coordinazione al Pd(II).

Nel *Capitolo 4* è stato investigato un ulteriore aspetto della progettazione del legante, che ha riguardato l'introduzione di un sostituente ingombrante, come il butossi pirene, sulla posizione *para* degli anelli arilici di α-diimine a scheletro DAB (pyr-DAB). I relativi complessi di palladio monocationici, [Pd(pyr-DAB)(CH_3)(CH_3CN)][SbF_6], hanno dato risultati eccellenti quali catalizzatori per la copolimerizzazione dell'etilene con esteri acrilici, dando delle macromolecole con caratteristiche peculiari. Quando la reazione di copolimerizzazione viene condotta in

trifluoroetanolo, il monomero vinilico polare viene inserito prevalentemente nella catena polimerica principale, il che rappresenta una significativa differenza rispetto ai sistemi catalitici basati sulle α-diimine riportati fino ad oggi. Quando invece, il mezzo di reazione è il diclorometano, il metil acrilato viene inserito in terminazione di catena, con una selettività nell'incorporazione del monomero polare opposta alla precedente. Per far luce su questo comportamento, si è studiata la reattività con metil acrilato ed etilene del precatalizzatore più produttivo, mediante spettroscopia NMR *in situ*, sia in diclorometano che in trifluoroetanolo deuterato.

Un'altra reazione di interesse è la copolimerizzazione del monossido di carbonio con vinil areni, per ottenere polichetoni perfettamente alternati. Il *Capitolo 5* si articola in una breve introduzione sull'argomento, con un focus sui sistemi catalitici di Pd(II) basati su piridilimmine. In questa parte del lavoro di ricerca si è studiata l'introduzione di frammenti policiclici aromatici sulla porzione $N_{imminico}$ del legante piridilimminico e il loro effetto sulla copolimerizzazione del CO sia con lo stirene che con i suoi derivati (4-metil stirene e 4-*tert*-butil stirene). Il punto di maggiore interesse di questo lavoro è rappresentato dall'effetto del vinil arene sulle macromolecole prodotte, in particolare sulla loro stereochimica, che viene studiata in termini di microtatticità con spettroscopia NMR del carbonio ^{13}C. Quest'analisi mostra che, quando i catalizzatori contengono i derivati aldimminici come leganti ancillari, la stereochimica del polichetone risultante è influenzata non solo dal legante ma anche dal diverso comonomero usato.

In conclusione, i risultati ottenuti durante questo progetto di dottorato mostrano l'importanza della progettazione del legante nella sintesi catalitica di macromolecole funzionalizzate, e rappresentano un significativo miglioramento rispetto allo stato dell'arte, in particolare nel campo della sintesi delle poliolefine funzionalizzate mediante catalisi omogenea. Concentrandosi sulla copolimerizzazione etilene/metil acrilato, i dati discussi nei *Capitoli 3* e *4* ci permettono di affermare che, per avere migliori catalizzatori di copolimerizzazione, la strategia da seguire non è quella di progettare sistemi che diano esclusivamente buoni catalizzatori di omopolimerizzazione dell'etilene, bensì di spostarsi verso complessi che mostrino, allo stesso tempo, una buona affinità per i monomeri vinilici polari.

CHAPTER 1
Introduction

1.1. From polyolefins to functionalized polyolefins

Polyolefins, in particular polypropylene (PP), linear low density polyethylene (LLDPE), low density polyethylene (LDPE) and high density polyethylene (HDPE), account for more than 55% of the plastic market demand worldwide,[1] and Europe alone in 2017 had a plastic converter demand of almost 25 million tonnes.[2] Despite their large use in different sectors of industry, however, polyolefins suffer of scarce surface properties such as dyeability, compatibility with other materials, printability and adhesion.[3] To overcome this problem, a feasible solution would be the introduction of functional polar groups into the polyolefin skeleton: these should give to the final products the desired surface properties and possibly expand their range of applications. Up to now, the functionalized polyolefins that are present on the market are produced with processes based on post-polymerization functionalization or radical polymerization. These technologies are not the most efficient from an industrial perspective, since they require high energies, have a low cost-efficiency and moreover do not allow precise control on the macromolecule microstructure, a very important feature. This makes the available range of functionalized polyolefins quite narrow, but on the other hand pushes industry and academia to find new approaches to the matter. In particular, the direct, homogeneously catalysed copolymerization of terminal alkenes with polar vinyl monomers would be an environmentally friendly approach to the matter, solving also the problem of the control on the macromolecule microstructure and the incorporation of the polar vinyl monomer.[4] Until now, this remains one of the "holy grails" in the field of polymer synthesis, despite the enormous efforts and the large number of publications on the topic appeared in the last few years, since none of these provided solutions efficient enough to be applied to industry.

The Ziegler-Natta and the metallocene catalysts, industrially applied for the production of polyolefins, are based on early transition metals, like Ti(IV) and Zr(IV). These metals are too oxophilic, and, therefore, the corresponding catalysts are easily poisoned by monomers that contain polar functional moieties.[5] Late transition metals, introduced in the 90's as catalysts for ethylene and α-olefin polymerization,[6] are more tolerant to functional groups, making them suitable candidates for application as catalysts in functionalized polyolefin synthesis. From the industrial point of view acrylic esters are the comonomers of interest, and linear macromolecules having a content of polar monomer around 20 % or lower, inserted into the main polymer chain, are the desired products (Scheme 1.1).

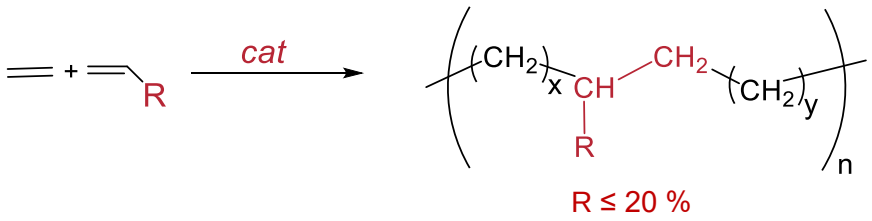

Scheme 1.1. Synthesis of functionalized polyolefins from ethylene/generic acrylic ester.

The breakthrough in the field was, indeed, Brookhart's discovery, in 1995, that organometallic monocationic Pd(II) complexes, $[Pd(CH_3)(Et_2O)(N\text{-}N)][BAr^F]$, are excellent catalysts for polyolefin synthesis.[6a] One year later he demonstrated that the same complexes are able to catalyse the copolymerization of ethylene with methyl acrylate (MA), taken as the model reaction for the synthesis of functionalized polyolefins.[7a] The coordination sphere of the metal centre features a methyl fragment, diethyl ether as labile ligand, and a neutral α-diimine as ancillary ligand (N-N); BAr^F is the non-coordinating counteranion (BAr^F = 3,5-$(CF_3)_2C_6H_3$). The α-diimine is characterized by either the 1,4-diaza-1,3-butadiene (DAB) or the acenaphthene (BIAN) skeleton, and two N-aryl rings bearing bulky substituents, such as isopropyl groups, on the *ortho* positions (Figure 1.1). The latter represents the key feature of these complexes: the aryl rings, orthogonally oriented with respect to the coordination plane, create a proper steric hindrance around the metal centre, that disfavours the termination step of the growing of the polymeric chain leading to macromolecules, in place of higher olefins and/or ethylene oligomers. The ligand backbone has also a remarkable effect on the catalytic performances of these complexes:[7] moving from the acenaphthene or the 1,4-diaza-1,3-butadiene (**L1** and **L2**) to the 1,4-diaza-2,3-methyl-buta-1,3-diene backbone (**L3**), an increase of one order of magnitude in catalyst activity was achieved, together with an increase also in the molecular weight of the produced ethylene/MA copolymers (Figure 1.1). The content of polar monomer inserted is not affected by these variations, being always around 4.0 %. The produced copolymers are branched macromolecules with the polar monomer incorporated at the end of the branches (Scheme 1.2a). In addition, these catalysts are active under mild reaction conditions of temperature and pressure (T = 303 K, $P_{ethylene}$ = 1.0-6.0 atm), and using dichloromethane as a solvent.

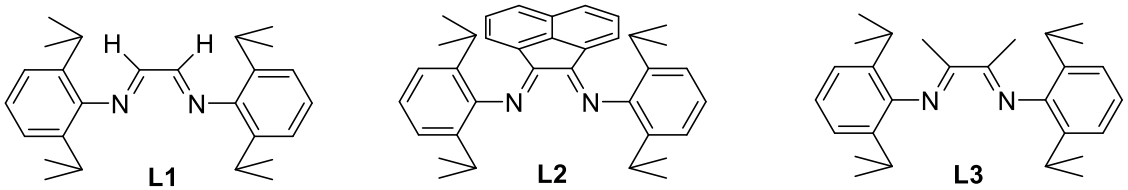

6.1 g CP/g Pd · h
5.0 % MA
Mn = 300

6.1 g CP/g Pd · h
4.7 % MA
Mn = 10 000

57 g CP/g Pd · h
4.0 % MA
Mn = 42 000

Figure 1.1. Classic Brookhart-type α-diimine and activities of the relevant Pd(II) catalysts. Reaction conditions: CH_2Cl_2, 308 K, P_E = 6 atm, [MA] = 5.8 M.

This represented the starting point for the development of novel homogeneous catalysts for this copolymerization reaction to yield functionalized polyolefins.

A few years later, Pugh *et al.* reported neutral Pd(II) complexes based on anionic phosphino sulfonate derivatives (P-O) (Figure 1.2).[8] In particular, the catalyst having the P-O ligand, a methyl group and dimethylsulfoxide as labile ligand, [Pd(CH_3)(dmso)(P-O)] (**L4**), has an activity of 169 g CP/g Pd · h in the synthesis of ethylene/MA copolymers with molecular weight values around 2000, and an incorporation of the polar monomer of 52 %. The produced copolymers are linear macromolecules with the polar monomer incorporated into the main polymer chain (Scheme 1.2b). In addition, these catalysts are active under a bit harsher reaction conditions of temperature and pressure (T = 368 K, $P_{ethylene}$ = 5 atm), and using toluene as a solvent.

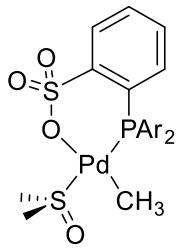

L4

169.2 g CP/g Pd h
52 % MA
Mn = 1800

Figure 1.2. Example of a phosphino sulfonate derivative and its activity in the ethylene/methyl acrylate copolymerization; reaction conditions: toluene, 368 K, P_E = 5 atm.

The palladium catalysts based on P-O ligands have proven to be quite versatile, since they are able to catalyse the copolymerization of ethylene with a wide number of acrylates and other polar vinyl monomers, like acrylonitrile, nitrogen-containing polar monomers, vinyl acetate, alkyl vinyl ethers, vinyl fluoride, acrylic acid, vinyl sulfonate.[9]

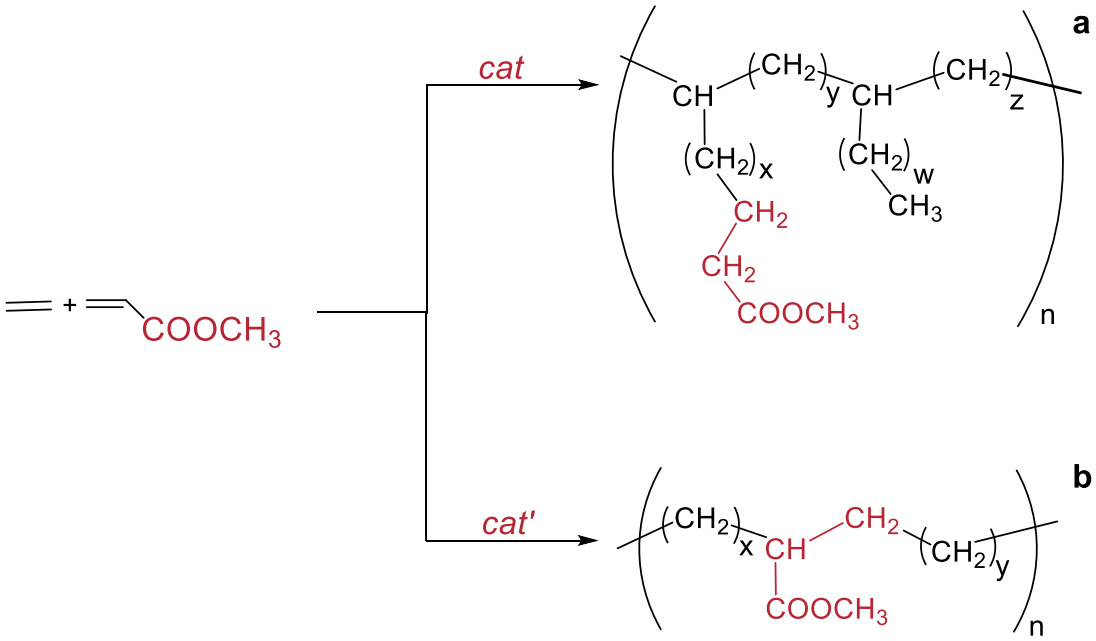

Scheme 1.2. Synthesis of functionalized polyolefins from ethylene/methyl acrylate copolymerization: a) branched and b) linear macromolecule.

The generally recognized mechanism for this catalytic copolymerization reaction is based on two migratory-insertion reactions: that of the polar vinyl monomer into the Pd-C bond of the growing polymer chain, and that of ethylene in the same bond. These two reactions, in competition with each other, take place in a random way, meaning that there is no rule to describe the order followed by the two events to happen.

The main difference between the N-N and the P-O based catalysts lies in the reaction that takes place after the migratory-insertion of the polar vinyl monomer. NMR spectroscopy, in particular variable temperature experiments, is the technique of choice to disclose the different pathways followed. The data obtained have been also validated by DFT calculations.

For catalysts based on α-diimines, the migratory-insertion of methyl acrylate into the Pd-C bond can occur with either a primary or a secondary regiochemistry, the latter usually being favoured. The 4-membered metallacycle that is formed, due to its high strain, undergoes a rapid β-hydrogen elimination and reinsertion, that produces the 5-membered metallacycle in the first place, that is further converted into the 6-membered metallacycle, that represents the catalyst resting state. The chelate intermediates have to be opened by the incoming monomers to continue the growth of the polymeric chain. This phenomenon of subsequent eliminations/reinsertions is known as chain walking mechanism and leads to branched macromolecules with the ester group located at the end of the branches.[7b]

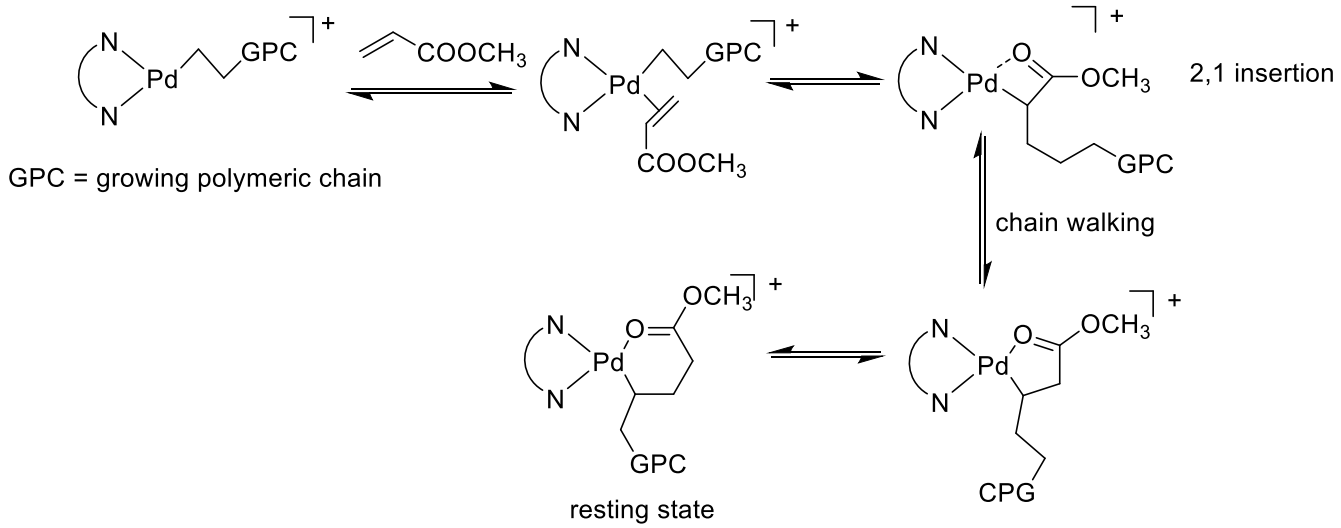

Scheme 1.3. Proposed mechanism for the ethylene/polar vinyl monomer copolymerization with α-diimine Pd(II) complexes.

For catalysts with P-O ligands, due to their asymmetric character, the polar vinyl monomer can coordinate either *cis* or *trans* relative to the oxygen atom in the ligand; after coordination, the migratory-insertion of methyl acrylate into the Pd-alkyl bond takes place in a 1,2 or 2,1 fashion, with the latter being generally preferred for electron poor vinyl monomers (Scheme 1.4).[10] In both cases, a metallacycle is formed (5-membered for the 1,2 insertion, 4-membered for the 2,1 insertion), with the functional group preferentially coordinated *trans* to the O atom of the ligand. This metallacycle does not undergo the sequence of β-hydrogen elimination-reinsertion reactions observed for catalysts with α-diimines and does not represent the catalyst resting state. Instead, it is easily cleaved by an incoming ethylene molecule, that coordinates and inserts, thus continuing the copolymerization and resulting in the main chain polar vinyl monomer incorporation. For this system the resting state is the insertion of the monomer, both ethylene and acrylate, into Pd-alkyl bond formed after the insertion of the polar monomer.

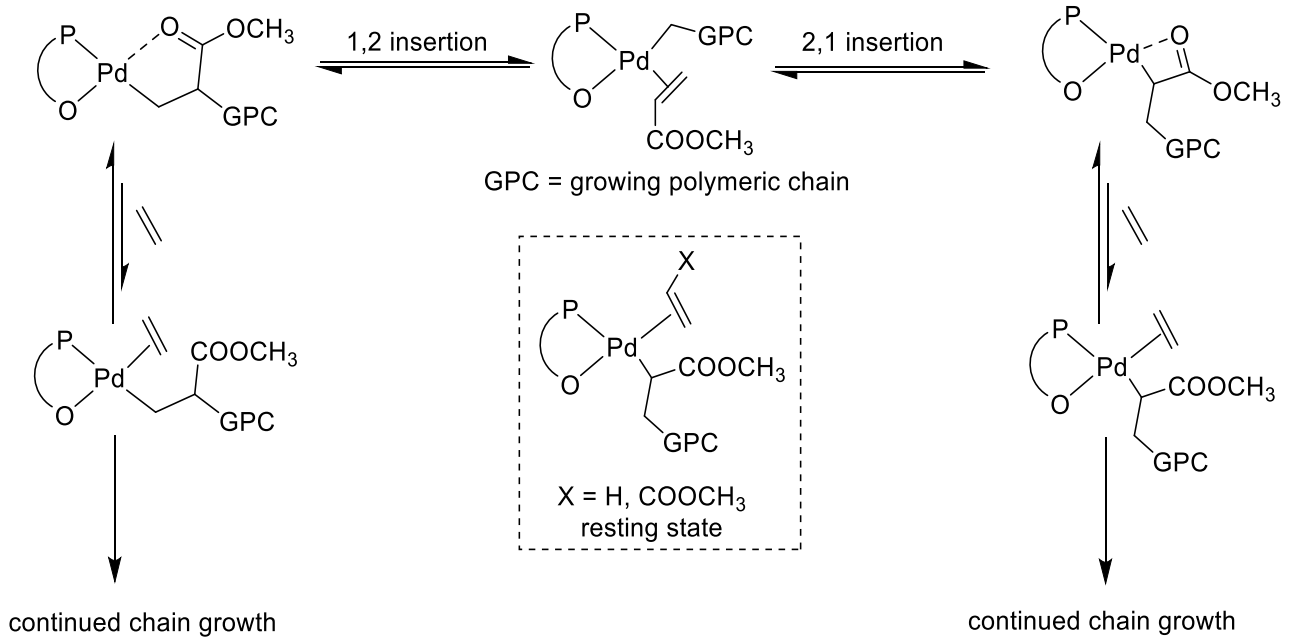

Scheme 1.4. Proposed mechanism for the ethylene/polar vinyl monomer copolymerization with phosphino sulfonate Pd(II) complexes.

From these seminal works it appears quite clearly that the choice of the ancillary ligand is fundamental in the control of the microstructure of the products. In the two decades that followed these fundamental discoveries, much work has been done on the tuning of the ligands: in this Chapter a brief overview about catalysts with non-nitrogen donor ligands will be presented, and a more detailed discussion about those with N-N donor ligands will be considered.

1.2. An overview about non-nitrogen donor ligands

Bisphosphinemonoxide (BPMO) palladium complexes were among the first other kind of ligands introduced for the ethylene/acrylic ester copolymerization reaction (Figure 1.3).[11] Taking inspiration from the phosphino sulfonate ligands, also BPMOs possess one strong and one weak σ-donor, and this unbalance should be beneficial in obtaining highly linear and random copolymers. The first BPMO Pd(II) catalysts reported, of formula [Pd(**L5**)(CH_3)(2,6-lut)][SbF_6] (2,6-lut = 2,6-lutidine) or [Pd(**L5**)(*o*-acetoanilido)][X] (X = SbF_6^-, BAr^F), were found to be not active in the copolymerization with methyl acrylate, whereas they resulted to be active with polar monomers that are usually challenging, such as vinyl and allyl acetate, halogenated monomers, acrylonitrile,[11] with moderate activities (up to 7.6 kg mol^{-1} h^{-1}) and low levels of incorporated monomer (0.7-4.1 %), by carrying out the reaction in toluene, at 353 K, with an ethylene pressure of 30 bar. Second

generation o-acetoanilido Pd(II) BPMO complexes resulted to be active in the copolymerization of ethylene with methyl acrylate, reaching activities of 540 kg mol^{-1} h^{-1} in just one hour of reaction, and also with other polar monomers.[12] In all cases, the produced macromolecules are indeed linear, random copolymers with the polar vinyl monomer inserted prevailingly inside the main chain, but also in the terminations, with M_n ranging from 1600 to 33000.

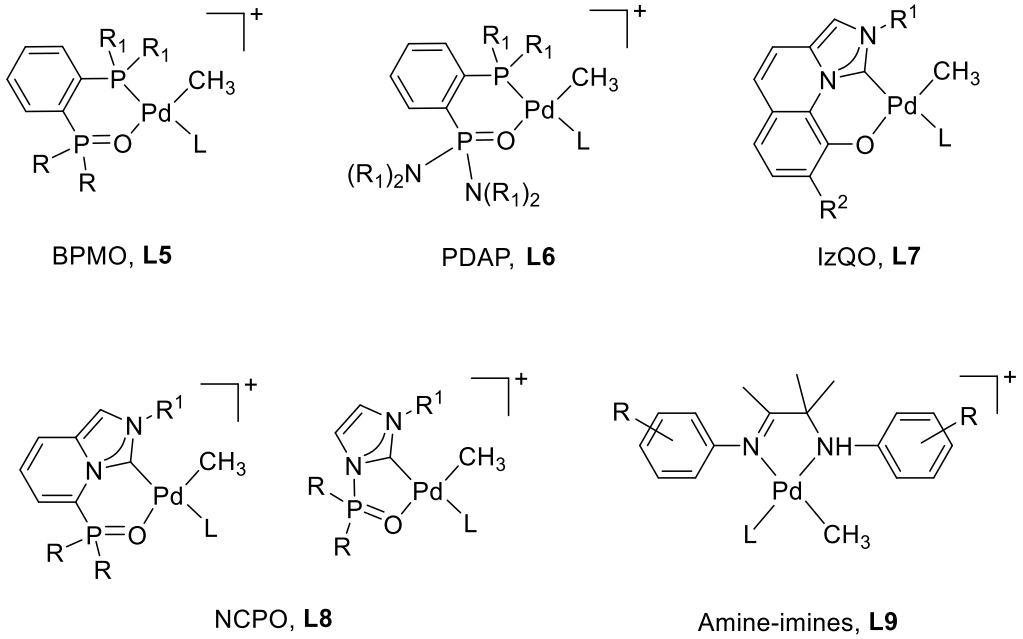

Figure 1.3. Different classes of Pd(II) complexes with non-nitrogen donor ligands.

Closely related to BPMO ligands are phosphonic diamide-phosphines (PDAP), that again exploit the difference between a P(III) and a P(V) atom. The relevant palladium complexes [Pd(**L6**)(CH_3)(2,6-lut)][BAr^F] generated active catalysts in the ethylene-polar vinyl monomers copolymerization. In particular, taking methyl acrylate into consideration, the productivities are in the range of 26 to 740 kg product per mol of palladium, and up to 5.4% of MA inserted, under reaction conditions similar to those applied for BPMO derivatives. The microstructure of the produced macromolecules shows that the polar vinyl monomer is inserted almost exclusively inside the main polymeric chain (94 *vs* 6 % in the termination ends), which mimics the microstructure of commercially available linear low density polyethylene, however with not so high M_w (21 or 85 kDa according to the catalyst used).[13]

Ligands with a N-heterocyclic carbene (NHC) moiety have also been considered.[14] Palladium complexes with NHC ligands with a quinoline backbone (IzQO) were tested in the

copolymerization of both ethylene and propylene with different monomers. Focusing on the E/MA reaction, the [Pd(**L7**)(CH_3)(2,6-lut)] complex bearing a 2,6-di(isopropyl)-substituted aryl ring on the N-donor atom *cis* to the CH_3 ligand showed an activity of 10.6 kg mol^{-1} h^{-1} and an incorporation of the acrylate of 0.8% in toluene, at 373 K and with 40 bar of ethylene pressure.[14a] Similar complexes were also successfully applied in the copolymerization of ethylene with 1,1-disubstituted ethylenes bearing a polar functional group, such as methyl methacrylate.[14b] N-heterocyclic carbene-phosphine oxide ligands (NCPO) were also considered for the model reaction.[14c] The modification of the weak σ-donor with respect to the previously reported IzQO derivatives did not have beneficial effects in the copolymerization reaction, both in terms of activity (4.8 kg mol^{-1} h^{-1}) and in terms of inserted methyl acrylate (0.27 %). With all these catalysts the obtained copolymers have the polar monomer inserted both in main chain and in the terminations of the branches, and molecular weight values in the range 4.0-7.8 kg/mol.

Finally, also imine-amine derivatives were synthesized, and the relevant complexes used in the copolymerization of ethylene with methyl acrylate.[15] The relevant [Pd(**L9**)(CH_3)(CH_3CN)][BAr^F] complex gave lower yields compared to the classical Brookhart DAB system (0.096-0.191 g of isolated product *vs* 0.861 g) and also lower molecular weights values (4.5-15.3 *vs* 53.4 kg/mol), under mild reaction conditions of temperature (298-318 K) and pressure (0.5 atm of ethylene pressure). The imine-amine complexes had however the interesting property of inserting the acrylate both in the main chain and in the termination of the branches, which represents a significant difference from Brookhart-type catalysts.

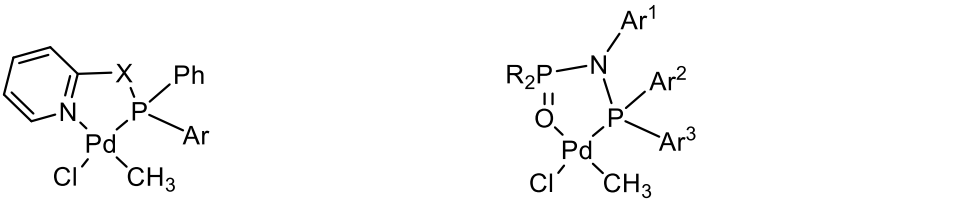

L10

X = CH_2, NH, O, CHC_6F_5

L11

R = Ph, iPr;
Ar^1 = Ph, 4-OMe-C_6H_4, 4-CF_3-C_6H_4
Ar^2 = Ph, 2-OMe-C_6H_4;
Ar^3 = 2-OMe-C_6H_4, 2-[2',6'-$(OMe)_2$-C_6H_3]-C_6H_4

Figure 1.4. Examples of PPy and PNPO derivatives.

Other P-X ligands have also appeared recently; in particular, Chen and coworkers reported both phosphine-pyridine ligands (PPy) and diphosphazane monoxide (PNPO) ligands (Figure 1.4).[16] In the first case, the relevant [Pd(**L10**)(CH_3)Cl] was tested upon activation with $NaBAr^F$ in the

reaction of ethylene with several polar vinyl monomers, yielding however cooligomers and not copolymers, with an activity in the case of the reaction with methyl acrylate of 0.2 kg mol^{-1} h^{-1} and 0.8 % of methyl acrylate inserted, both in the main chain and in the terminations,[16a] under relatively mild conditions of temperature and pressure (293 K, 8 atm). The PNPO palladium complexes of the general formula [Pd(**L11**)(CH_3)Cl], tested under similar conditions of pressure but at higher temperatures, gave instead copolymers with moderate activities (up to 16.7 kg mol^{-1} h^{-1}) and good levels of inserted monomer (up to 6.8%), both in main chain and in the chain ends, with low M_n (up to 6100).

1.3. Nitrogen donor ligands

In the last two decades, much of the development relevant to α-diimine ligands has been focused on the variation of the substituents on the N-aryl rings rather than on the ligand backbone. However, some reports on the diversification of the ligand skeleton can be found: one of the first, reported by Guo, Wu and coworkers, deals with N-N donor ligands with either a camphyl or a 1,4-diaza-2,3-aryl-buta-1,3-diene skeleton (Figure 1.5, **L12** and **L13**). The palladium complex [Pd(**L12**)(CH_3)Cl] upon activation with $NaBAr^F$ and methyl acrylate gave a macromolecule very similar in the Mn and the branching degree to that produced with the classical Brookhart-type DAB catalyst under the same reaction conditions (dichloromethane, 308 K, 1 bar, 36 h), but with a turnover frequency (TOF) that is 6 times lower.[17] Complexes with ligands having aryl groups on the backbone either are inactive in the copolymerization of ethylene with methyl acrylate or show TOF similar to those of the camphyl-substituted ligand but produce low molecular weight copolymers with low incorporation of MA (Mn from 1500 to 12000, % MA from 0.30 to 1.2 %).

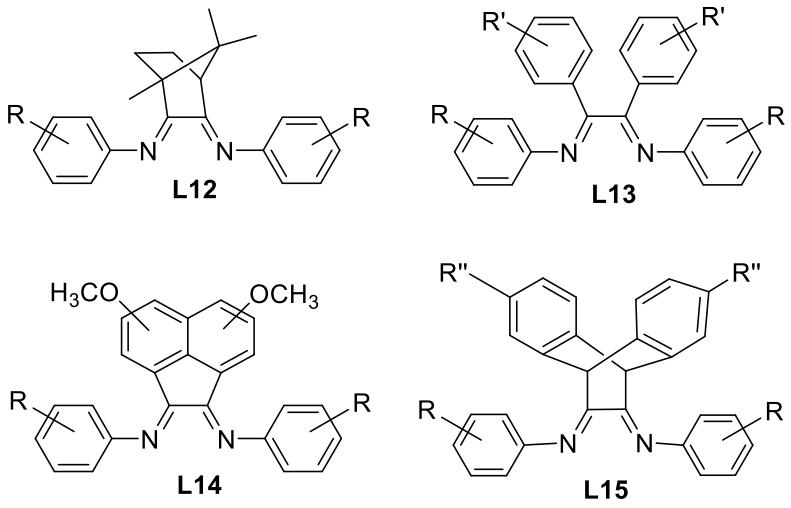

Figure 1.5. Variation of the α-diimine ligand skeleton.

Modification on the acenaphthene backbone has been reported by Chen and coworkers, by introducing either methyl or methoxy groups in the skeleton (Figure 1.5, **L14**).[19] Comparing the activities of the [Pd(**L14**)(CH_3)Cl] with those of the classic Ar-BIAN Brookhart precatalyst under the same reaction conditions (dichloromethane, 303 K, 1 atm ethylene pressure), an improvement in the activity of almost one order of magnitude is achieved when a methoxy group is placed in the third position of the acenaphthene skeleton (3.33 *vs* 0.67 kg mol^{-1} h^{-1}), but with the contemporary decrease in content of methyl acrylate from 4.3% to 1.9%. The molecular weight values of the macromolecules obtained with Ar-BIAN-modified catalysts are in the range 5.4-19.0 kg/mol.

Dibenzobarrelene-based α-diimines (Figure 1.5, **L15**) have been applied as ancillary ligands both for nickel[18] and palladium.[20] The palladium(II) precatalysts [Pd(**L15**)(CH_3)(CH_3CN)][BAr^F] resulted to be active in the ethylene/methyl acrylate copolymerization under different reaction conditions of temperature and pressure (temperatures in the range 288-323 K, pressures in the range of 0.2-21 bar). The activities are moderate (3.63-13.28 kg mol^{-1} h^{-1}), with different degrees of monomer incorporation according to the different reaction conditions tested and goes up to 4.64%. These catalysts have proven to be thermally resistant, being active up to 323 K and yielding copolymers with relatively high Mn (up to 39.2 kg/mol) and a high branching degree (up to 111);[20] moreover, by using different ethylene pressure in the copolymerization experiments resulted in changes in the branching topology of the resulting macromolecule, allowing a fine tuning on its properties.

Much more work has been done on the variation of the substituents on the aryl rings of the iminic nitrogen atoms, in particular on their *ortho* positions. The attention has been focused on changing the isopropyl groups of the classic Brookhart α-diimine ligands for more sterically hindered groups, or exploiting the so-called second sphere strategy, that should influence the outcome of the catalysis by promoting intermolecular interactions. One example of this strategy is represented by α-diimines that have on one of the two N-aryl rings nitrogen-containing groups (Figure 1.6, **L16**).[21] The relevant palladium complexes, however, have not been applied in the copolymerization with methyl acrylate as comonomer, but with other polar vinyl monomers such as allyl ether, allyl acetate and allyl benzene, thus expanding the scope of polar monomer substrates for α-diimine Pd(II) catalysts. The activities of such systems towards the mentioned polar vinyl monomers are in the range of 0.1-5.8 $kg \cdot mol^{-1} \cdot h^{-1}$, and the content of polar vinyl monomer inserted goes from 0.2 (for allyl acetate) to 7.9 % (for allyl benzene), with molecular weight values ranging from 1.9 to 59.6 kDa. The introduction of nitrogen-containing group has the effect of inducing metal-nitrogen interactions, that greatly reduce the branching densities in the polymeric products.

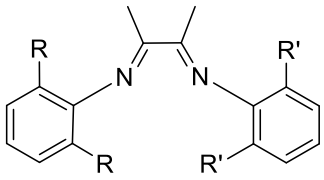

L16

L16a, R = R' = morpholine
L16b, R = R' = piperidine
L16c, R = pyrrolidine, R' = $CH(CH_3)_2$
L16d, R = morpholine, R' = $CH(CH_3)_2$
L16e, R = piperidine, R' = $CH(CH_3)_2$

Figure 1.6. α-diimines with nitrogen-containing second-sphere substituents.

Benzhydryl substituted α-diimines (Figure 1.7, **L17-L19**) were applied first in Ni(II) catalyzed ethylene homopolymerization[22] and subsequently also in the model copolymerization reaction.[23] The relevant palladium(II) neutral complex [Pd(**L17a**)(CH_3)Cl], upon activation with $NaBAr^F$, has an activity one order of magnitude higher than the corresponding complex with **L3** (3.7 *vs* 0.33 kg mol_{Pd}^{-1} h^{-1}), under the same reaction conditions (toluene, P_E = 1 atm, 15 h, 293 K). The product has a higher Mn and a lower content of methyl acrylate, inserted in the termination of the branches (0.4 *vs* 3.2 %) due to the increased steric bulk of the ligand. The branching degree also decreases in the new benzhydryl-substituted system.

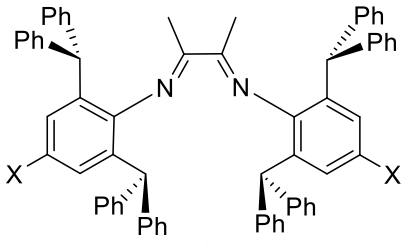

L17

L17a, X = Me
L17b, X = OMe
L17c, X = Cl
L17d, X = CF_3

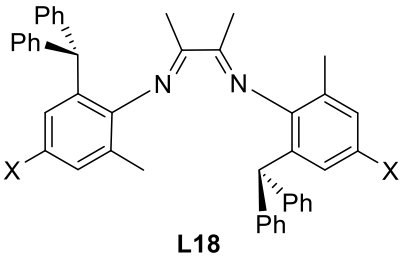

L18

L18a, X = OMe, R = Me
L18b, X = Me, R = Me
L18c, X = Cl, R = Me
L18d, X = NO_2, R = Me
L18e, X = Me, R = An

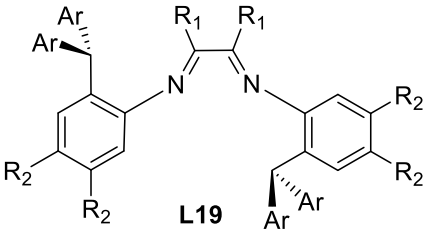

L19

L19a, R_1 = Me, R_2 = H, Ar = Ph
L19b, R_1 = An, R_2 = H, Ar = Ph
L19c, R_1 = Me, R_2 = OMe, Ar = 3,4-OMe-C_6H_3
L19d, R_1 = An, R_2 = OMe, Ar = 3,4-OMe-C_6H_3
L19e, R_1 = Me, R_2 = OMe, Ar = 3,4-OMe-C_6H_3

Figure 1.7. α-diimines with benzhydryl- or benzhydryl-derived substituents.

When a subtle steric unbalance is introduced in the system,[24] the activity of the relevant Pd(II) complexes and the molecular weight of the produced macromolecules drops significantly from ethylene homo- to copolymerization with methyl acrylate; for example, for complexes with **L19a-c**,

the activity drop is of two orders of magnitude (from 125-147 kg mol^{-1} h^{-1} of the homo- to 0.37-0.92 kg mol^{-1} h^{-1} of the copolymerization).[24a] The substitution of the phenyl rings of the benzhydryl moiety does not bring any positive effect on the activity of the corresponding precatalysts, that remain in the range of moderate (7.5 kg mol^{-1} h^{-1}) to low (0.70 kg mol^{-1} h^{-1}), along with low contents of inserted monomer (0.87-1.67 %).[24b]

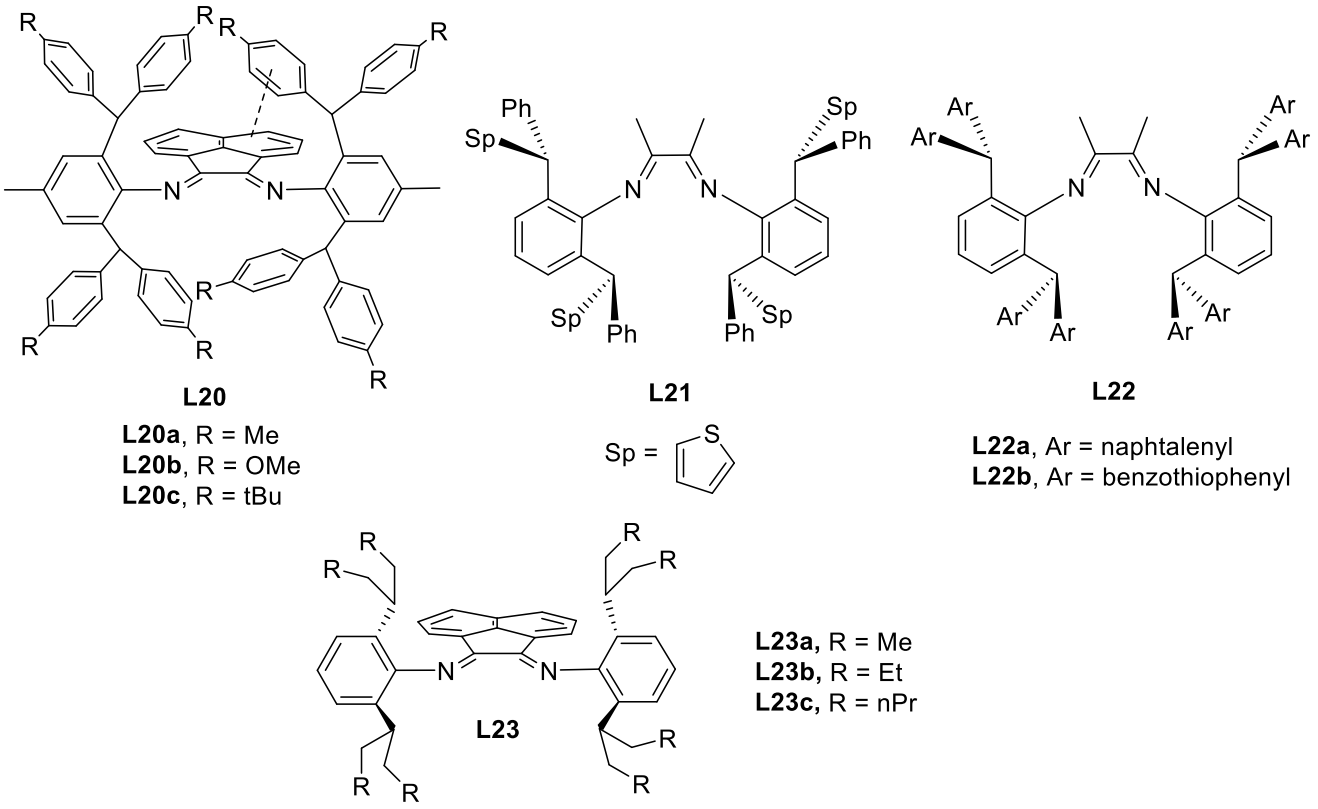

Figure 1.8. Other benzhydryl-derived α-diimines.

Similar acenaphthene or 1,4-diazabutadiene-based α-diimines with para-substituted phenyl rings were reported during the last year by Dai and coworkers (Figure 1.8, **L20**-**L22**).[25] In the case of the BIAN derivatives, in particular, π-π stacking interactions between the backbone and the substituents on the N-aryl rings are evident from the X-ray diffraction of the palladium complexes, and create an additional axial steric bulk around the metal centre, resulting in a low branching density of the obtained copolymers, that are produced with moderate activities in dichloromethane, at 303 K and with an ethylene pressure of 2 atm (2.3-5.3 kg mol^{-1} h^{-1}) and low levels of incorporation of methyl acrylate (1.04 % maximum). When one of the phenyl groups is replaced by a thiophene,[26] under an ethylene pressure of 8 atm and at 303 K, high activities are reached (70-105 kg mol^{-1} h^{-1}), and the produced macromolecules have high Mn (up to 1.24 10^6) with low monomer incorporation (up to

1.7 %), and a microstructure similar to that of low density polyethylene (LDPE), with the methyl acrylate inserted in the branch end. The activities, the Mn and the branching density decrease upon increasing the ethylene pressure, with a higher incorporation of polar monomer (1.8-6.8 %). At higher temperature (333 K) higher comonomer incorporation and branching density are obtained, with lower activity and Mn. If the phenyl is replaced by naphthalene or benzothiophene moieties, quite high activities are reached in the ethylene/methyl acrylate copolymerization at 8 atm of ethylene pressure, in toluene/dichloromethane or chloroform solvent mixture (30.3 kg mol^{-1} h^{-1} for the benzothiophene-derived catalyst, and 12.4 kg mol^{-1} h^{-1} for the naphthalene one), with low incorporation of the monomer (<0.1-0.88 %) and low branching degrees (9-18 branches /1000 C). These catalysts are, however, active towards acrylates that do not work with the Brookhart catalyst with **L3**, i.e. allyl ethers, allyl benzene, alkenes bearing halide groups.[27] When bulky but flexible substituents are placed in the *ortho* positions of the N-aryl rings (Figure 1.8, **L23**),[28] lower activities (1.3-3.2 kg mol^{-1} h^{-1}), insertion of methyl acrylate (0.28-1.60 %) and branching density in the products are obtained with respect to the system with ligand **L3**, whereas the Mn values are higher when the steric bulk of the substituent is increased.

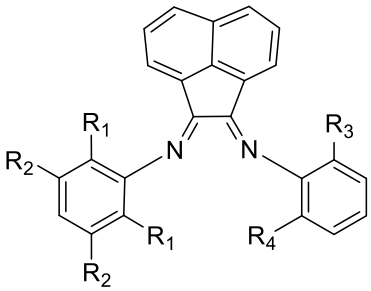

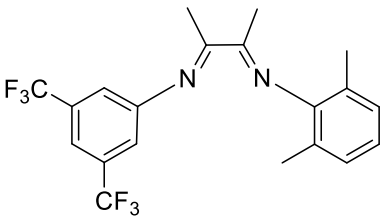

L28

L24, R_1 = H, R_2 = CF_3, R_3 = R_4 = Me
L25, R_1 = Me, R_2 = H, R_3 = R_4 = Me
L26, R_1 = H, R_2 = CF_3, R_3 = Me, R_4 = OMe
L27, R_1 = CF_3, R_2 = H, R_3 = Me, R_4 = OMe

Figure 1.9. Non-symmetrical BIAN and DAB-based α-diimines.

Taking inspiration from the non-symmetric P-O ligands, that possess one hard and one soft coordination site, and with the aim to evaluate if just a subtle unbalance of the electronic and steric properties of the two donor atoms would have been sufficient to affect the catalytic performances of the catalysts, the concept of ligand desymmetrisation was also applied to DAB and BIAN ligands. Milani *et al.* reported several α-diimines having a non-symmetrical distribution of substituents on the N-aryl rings (Figure 1.9, **L24**-**L28**).[29] When ligand **L24** is taken into consideration, and the catalytic activity of the relevant [Pd(**L24**)(CH_3)(L)][PF_6] (L = CH_3CN, dmso) compared to that of

the corresponding complex with 2,6-dimethyl groups on both the N-aryl rings (**L25**), an increase of two times in the productivity is reached with the catalyst having the non-symmetrical ligand (Table 1.1, run 1, 2 *vs* 3, 4), together with better results for the compounds that have the dimethylsulfoxide as labile ligand, with also an increase in the content of methyl acrylate inserted. It has to be pointed out that catalytic products are ethylene/MA cooligomers and not copolymers, thus indicating that the decrease in steric hindrance on just one of the two aryl rings is enough to change the selectivity of the reaction from polymerization to oligomerization. The introduction of methoxy substituents (**L26**, **L27**) results, in contrast with what was previously reported in literature,[20,23,30] in an unexpected detrimental effect on the catalytic outcome (Table 1.1, run 5-8 *vs* 2) and overcomes the possible beneficial effect of the non-symmetrical ligand.[29c] The 1,4-diaza-2,3-butadiene backbone was also considered as a platform for non-symmetrical substitution.[29b] As expected, moving from the BIAN to the DAB skeleton (**L28**) an increase in the productivity was achieved (Table 1.1, run 1 *vs* 9), that, however, is not as pronounced as for the relevant symmetrical species.[7a] Unlike to what observed for the BIAN derivatives,[29] moving from the symmetrical to the non-symmetrical DAB no increase in productivity was observed, likely this is due to the remarkable production of volatile alkenes that, with the used setup of the catalytic reactor, was not possible to quantify.

Table 1.1. Ethylene/methyl acrylate cooligomerization: effect of the ligand.[a]
Precatalyst: [Pd(**N-N**)(CH_3)(L)][PF_6].

Run	N-N	L	Yield (mg)	g P / g Pd[b]	mol % MA[c]	Alkenes/esters[d]
1	**L24**	CH_3CN	297.0	133.2	14.7	C4-C16
2	**L24**	dmso	520.8	233.5	12.5	C4-C16
3	**L25**	CH_3CN	171.4	79.4	10.4	-
4	**L25**	dmso	221.8	99.5	6.6	-
5	**L26**	CH_3CN	133.7	60.0	36	C4-C6
6	**L26**	dmso	52.8	23.7	38	C4-C6
7	**L27**	CH_3CN	157.1	70.4	25	C4-C12
8	**L27**	dmso	208.3	93.4	23	C4-C16
9	**L28**	CH_3CN	1280	544.6	4.5	C4-C6

[a] Reaction conditions: $n_{Pd}=2.1\cdot10^{-5}$ mol, 2,2,2-trifluoroethanol: V=21 mL, T=308 K, P_E=2.5 bar; methyl acrylate (MA) V=1.13 mL, [MA]/[Pd]=600, t=24 h; [b] Isolated yield; g P/g Pd=grams of product per gram of palladium; [c] Calculated by using ^{1}H NMR spectroscopy; [d] Determined by GC/MS.

The possibility of having non-symmetrical-substituted benzhydryl derived N-aryl rings was also assessed (Figure 1.10, **L29-L31**).[31] The results obtained when mixed ligands are used[31a] are worse than those obtained with the reference benzhydryl-derived ligand **L17a** under the same reaction conditions (toluene/dichloromethane, 303 K, PE = 1 atm), in terms of activity, molecular weight, branching degree; the latter parameter is not influenced by the variation in the ethylene pressure, but by the steric bulk of the ligand, and it decreases with the increasing steric bulk in the *ortho* positions substituents. The best results are obtained with the palladium catalyst having **L30b** as ancillary ligand (2.83 kg mol^{-1} h^{-1}, 1.2 % MA). The introduction of a secondary or tertiary amide on the sixth position of one of the N-aryl rings does not produce any improvement in these kind of benzhydryl-derived systems, leading to catalysts with moderate activities (7.7 kg mol^{-1} h^{-1}) and low incorporation of the polar monomer in the branch ends (up to 2.4 % maximum).

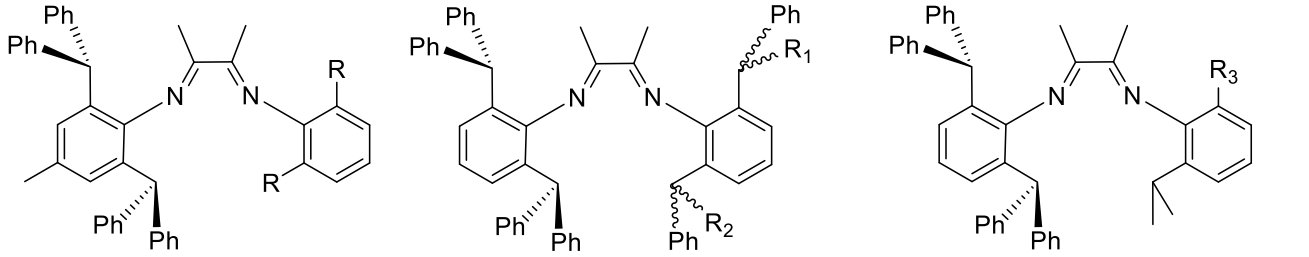

L29a, R = H
L29b, R = Me
L29c, R = iPr

L30a, R_1= R_2 = Me
L30b, R_1 = Me, R_2= Ph

L31a, R_3 = N-methyl formamide
L31b, R_3 = N,N-dimethyl formamide

Figure 1.10. Non-symmetrical benzhydryl-derived α-diimines.

The effect of electron-donating or withdrawing substituents on the *para* position of the N-aryl rings was studied by Chen and co-workers, that reported the beneficial effect in the copolymerization of ethylene/methyl acrylate of having electron-donating groups such as methyl or methoxy on the fourth position;[23] recently ethoxy,[32] ferrocenyl,[33] fluorinated tails[34] or bulky tails[35] substituents were also considered: their effects in the model reaction will be described in detail in Chapter 4.

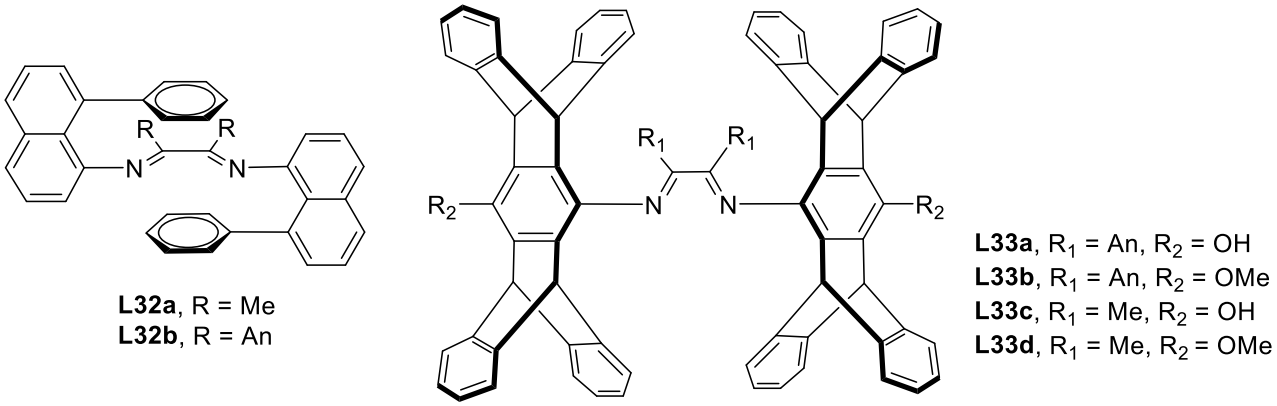

Figure 1.11. α-diimines with fused aromatic rings.

Other than substituents on the N-aryl rings, also the aryl rings themselves have been modified. One of the first examples, consisting in the introduction of bulky 8-*p*-tolylnaphtyl substituents (Figure 1.11, **L32**), was reported by Brookhart.[36] The corresponding palladium catalysts yielded both the desired copolymer and the methyl acrylate homopolymer, that is not commonly obtained with α-diimine Pd(II) catalysts. The activity is lower than that of the classic Brookhart-type catalyst, while the content of methyl acrylate inserted is similar (around 2%). The behaviour at higher concentrations of polar monomer and pressures is comparable to previously reported catalysts.

More recently, large fused aromatic rings such as pentiptycenyl[37] or bispentiptycenyl[38] have been reported, but just in the first case applied to the reaction of interest. The pentiptycenyl-derived systems afforded the desired copolymers with good levels of monomer incorporation (1.0-1.8 %), high molecular weight products (90.1 kg/mol for the Pd(II) complex with ligand **L33c**) and high activities (19.1 kg mol^{-1} h^{-1} for the Pd(II) complex with ligand **L33d**).[37]

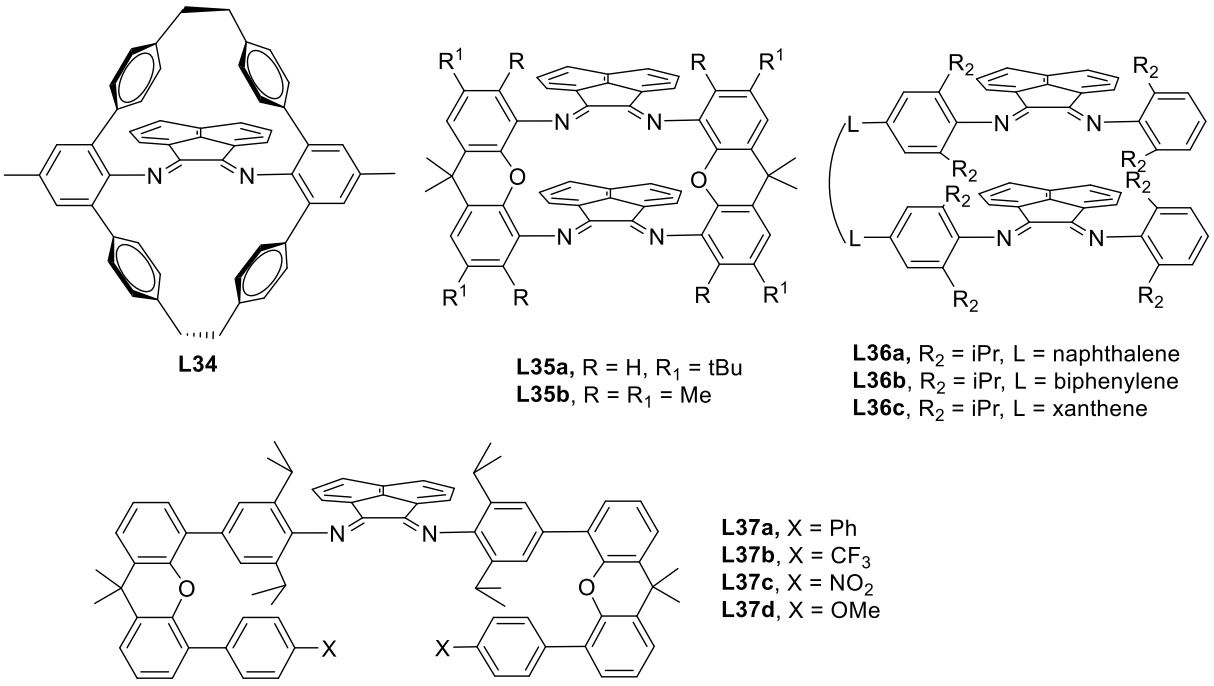

Figure 1.12. Bulky substitueted and bis(bidentate) α-diimines.

Another take on the bulky-substituent strategy was reported by Guan and Popeney, where the use of a cyclophane-based BIAN ligand (**L34**) was reported. With respect to the classic BIAN system, under the same reaction conditions (P_E = 6 bar, 308 K, toluene), the cyclophane-BIAN has proven to be more efficient in incorporating the polar monomer (20 % of MA inserted in the branch ends at [MA] = 4.0 M vs 4.0 % MA inserted at [MA] = 5.8 M).

Osakada *et al.* reported the first dinuclear palladium catalysts applied to the copolymerization reaction (**L35a,b**).[39] The ligand features two bidentate compartments connected together by a BIAN skeleton (Figure 1.12, **L35**). The relevant catalyst has higher TON both in ethylene and methyl acrylate with respect to the reported Pd(II) mesityl-substituted BIAN complex (TON_E 586 *vs* 376, TON_{MA} 32 *vs* 4.2, respectively), but the most important feature of this double-decker type system is that the polar monomer is inserted both into the main chain and in the chain ends, with a preference for the first, that represents a huge difference with all the other α-diimine catalysts. Copolymers with high molecular weights (up to 63.7 kDa) are obtained, and a decrease in the content of incorporated MA and of the in chain/termination ratio was observed by increasing the ethylene pressure. Starting from this system, also double-decker α-diimines with just one bridge have been reported (Figure 1.12, **L36a-c**),[40] but the relevant Pd(II) complexes do not incorporate the polar vinyl monomer under the applied reaction conditions (toluene, P_E = 9 atm, 293 K). Mononuclear systems of similar nature (Figure 1.12, **L37**), instead,[41] resulted to be active in the ethylene/methyl

acrylate copolymerization, and even more active than the classic BIAN complex (0.88 vs 2.13 kg mol^{-1} h^{-1}), with a lower degree of incorporation of acrylate (0.64-1.59 vs 2.53 %) and a higher Mn in the case of the complex with **L37a** (98.3 kDa).

As a general conclusion of this overview about the catalysts reported in the open literature for the target reaction it is possible to state that the huge number of examples reported and their variety highlight the influence on the catalytic outcome of even simple ligand modification, that is the main method to gain advances in homogeneous catalysis in general, and in functionalized polyolefin synthesis, in particular. In addition, for all the catalytic systems based on α-diimine ligands, but one, the polar vinyl monomer is always inserted at the end of the branches, thus pointing out how difficult it is to overcome the chain walking process.

With the aim of a potential industrial application in mind, the ideal catalyst has to show high productivity and be able, at the same time, to control the architecture of the produced macromolecules in terms of molecular weight and molecular weight distribution, content of the incorporated polar monomer and its distribution into the polymer chain. Since none of the catalytic systems reported up to now satisfies these requirements, the challenge to design new ligands and the relevant complexes for the synthesis of ethylene/polar vinyl monomer copolymer is still ongoing and appealing.

1.4. Bibliography

1. PlasticsEurope Market Research Group (PEMRG) / Consultic Marketing & Industrieberatung GmbH

2. Source: PlasticsEurope Market Research Group (PEMRG) and Conversio Market & Strategy GmbH

3. a) Boffa, L. S., Novak, B. M. *Chem Rev*. **2000**, *100*, 1479; ; b) Nakamura, A., Ito, S., Nozaki, K. *Chem. Rev.* **2009**, *109*, 5215; c) Franssen, N. M. G., Reek, J. N. H., de Bruin, B. *Chem. Soc. Rev.* **2013**, *42*, 5809.

4. a) Carrow, B. P., Nozaki, K. *Macromolecules* **2014**, *47*, 2541; b) Chen, Z., Brookhart, M. *Acc. Chem. Res.* **2018**, *51*, 1831; c) Chen, C. *Nat. Rev. Chem*. **2018**, *2*, 6.

5. Ittel, S. D., Johnson, L. K., Brookhart, M. *Chem. Rev*. **2000**, *100*, 1169.

6. a) Johnson, L. K, Killian, C. M., Brookhart, M. *J. Am. Chem. Soc.* **1995**, *117*, 6414; b) Britovsek, G. J. P., Gibson, V. C., Kimberlye, B. S., Maddox, P. J., McTavish, S. J., Solan, G. A., White, A. J. P., Williams, D. J. *Chem. Commun*. **1998**, 849; c) Gibson, V. C., Spitzmesser, S. K. *Chem. Rev*. **2003**, *103*, 283.

7. a) Johnson, L. K., Mecking, S., Brookhart, M. *J. Am. Chem. Soc* **1996,** *118*, 267 b) Mecking, S., Johnson, L. K., Brookhart, M. *J. Am. Chem. Soc.* **1998**, *120*, 888.

8. Drent, E., van Dijk, R., van Ginkel, R., van Oort, B., Pugh, R. I. *Chem. Comm*. **2002**, 964.

9. a) Kochi, T.; Noda, S.; Yoshimura, K.; Nozaki, K. *J. Am. Chem. Soc.* **2007**, *129*, 8948; b) Skupov, K. M.; Piche, L.; Claverie, J. P. *Macromolecules* **2008**, *41*, 2309; c) Ito, S.; Munakata, K.; Nakamura, A.; Nozaki, K. *J. Am. Chem. Soc.* **2009**, *131*, 14606; d) Luo, S.; Vela, J.; Lief, G. R.; Jordan, R. F. *J. Am. Chem. Soc.* **2007**, *129*, 8946; d) Shen, Z.; Jordan, R.J. *Macromolecules* **2010**, *43*, 8706; e) Rünzi, T.; Fröhlich, D.; Mecking, S. *J. Am. Chem. Soc.* **2010**, *132*, 17690; f) Bouilhac, C.; Rünzi, T.; Mecking, S. *Macromolecules* **2010**, *43*, 3589; g) Skupov, K. M.; Hobbs, J.; Marella, P.; Conner, D.; Golisz, S.; Goodall, B. L.; Claverie, J. P. *Macromolecules* **2009**, *42*, 6953.

10. Nakamura, A., Anselment, T. M. J., Claverie, J., Goodall, B., Jordan, R. F., Mecking, S., Rieger, Bernhard, Sen, A., van Leeuwen, P. W. N. M., Nozaki, K. *Acc. Chem. Res*. **2013**, *47*, 1438.

11. Carrow, B. P., Nozaki, K. *J. Am. Chem. Soc*. **2012**, *134*, 8802.

12. Mitsushige, Y., Carrow, B. P., Ito, S., Nozaki, K. *Chem. Sci.* **2016,** *7*, 737.

13. Zhang, W., Waddell, P. M., Tiedemann, M. A., Padilla, C. E., Mei, J., Chen, L., Carrow, B. P. *J. Am. Chem. Soc.* **2018**, *140*, 8841.

14. a) Nakano, R., Nozaki, K. *J. Am. Chem. Soc*. **2015**, *137*, 10934; b) Yasuda, H., Nakano, R., Ito, S., Nozaki, K. *J. Am. Chem. Soc*. **2018**, *147*, 1876; c) Tao, W., Akita, S., Nakano, R., Ito, S., Hoshimoto, Y., Ogoshi, S., Nozaki, K. *Chem. Commun*. **2017**, *53*, 2630.

15. Hu, H., Chen, D., Gao, H., Zhong, L., Wu, Q. *Polymer Chem.* **2016**, *7*, 529.

16. a) Si, G., Na, Y., Chen, C. *Chem. Cat. Chem*. **2018**, *10*, 5355; b) Chen, M., Chen, C. *Angew. Chem. Int. Ed*. **2018**, *57*, 3094.

17. Guo, L., Gao, H., Guan, Q., Hu, H., Deng, J., Liu, J., Liu, F., Wu, Q. *Organometallics* **2012**, *31*, 6054.

18. Zhong, L., Li, G., Liang, G., Gao, H., Wu, Q. *Macromolecules* **2017**, *50*, 2675.

19. Zou, W., Chen, C. *Organometallics* **2016**, *35*, 1794.

20. Zhong, S., Tan, Y., Zhong, L., Gao, J., Liao, H., Jiang, L., Gao, H., Wu, Q. *Macromolecules* **2017**, *50*, 5661.

21. Li, M., Wang, X., Luo, Y., Chen, C. *Angew. Chem. Int. Ed*. **2017**, *56*, 11604.

22. a) Rhinehart, J. L., Brown, L. A., Long, B. K. *J. Am. Chem. Soc*. **2013**, *135*, 16314; b) Rhinehart, J. L., Mitchell, N. E., Long, B. K. *ACS Catal*. **2014,** *4*, 2501.

23. Dai, S., Sui, X., Chen, C. *Angew. Chem. Int. Ed*. **2015**, *54*, 9948.

24. a) Sui, X., Hong, C., Pang, W., Chen, C. *Mat. Chem. Front*. **2017**, *1*, 967; b) Ma, X., Hu, X., Zhang, Y., Mu, H., Cui, L., Jian, Z. *Polym. Chem*. **2019**, *10*, 2596.

25. Gong, Y., Li, S., Tan, C., Kong, W., Xu, G., Zhang, S., Liu, B., Dai, S. *Journal of Catalysis* **2019**, *378*, 184.

26. Na, Y., Dai, S., Chen, C. *Macromolecules* **2018**, *51*, 4040.

27. Dai, S., Chen, C. *Angew. Chem. Int. Ed.* **2016**, *55*, 13281.

28. Guo, L., Sun, W., Li, S., Xu, G., Dai, S. *Polym. Chem*. **2019**, *10*, 4866.

29. a) Meduri, A, Montini, T., Ragaini, F., Fornasiero, P., Zangrando, E., Milani, B. *Chem. Cat. Chem*. **2013**, *5*, 1170; b) Rosar, V., Montini, T., Balducci, G., Zangrando, E., Fornasiero, P., Milani, B. *Chem. Cat. Chem*. **2017**, *9*, 3402; c) Rosar, V., Meduri, A., Montini, T., Fornasiero, P., Zangrando, E., Milani, B. *Dalton Trans*. **2018**, *47*, 2778.

30. Guironnet, D., Roesle, P., Rünzi, T., Gottker-Schnetmann, I., Mecking, S. *J. Am. Chem. Soc.* **2009**, *131*, 422.

31. a) Dai, S., Zhou, S., Zhang, W., Chen, C. *Macromolecules* **2016**, *49*, 8855; b) Zhai, F., Solomon, J. B., Jordan, R. F. *Organometallics* **2017**, *36*, 1873.

32. a) Kimiaghalam, M., Isfahani, H. N., Zohuri, G. H., Keivanloo, A. *Appl. Organometal. Chem.* **2017**, 4153; b) Kimiaghalam, M., Isfahani, H. N., Zohuri, G. H., Keivanloo, A. *Inorg. Chim. Acta* **2017**, *464*, 99.

33. Zhao, M., Chen, C. *ACS Catal.* **2017**, *7*, 7490.

34. Mundil, R., Sokolohorskyj, A., Hošek, J., Cvačka, J., Císařová, I., Kvičala, J., Merna, J. *Polym. Chem*. **2018**, *9*, 1234.

35. Guo, L., Liu, Y., Sun, W., Du, Q., Yang, Y., Kong, W., Liu, Z., Chen, D. *Journal of Organometallic Chemistry* **2018**, *877*, 12.

36. Allen, K. E., Campos, J., Daugulis, O., Brookhart, M. *ACS Catal*. **2015**, *5*, 456.

37. Liao, Y., Zhang, Y., Cui, L., Mu, H., Jian, Z. *Organometallics* **2019**, *38*, 2075.

38. Kanai, Y., Foro, S., Plenio, H. *Organometallics* **2019**, *38*, 544.

39. Takano, S., Takeuchi, D., Osakada, K., Akamatsu, N., Shishido, A. *Angew. Chem. Int. Ed*. **2014**, *53*, 9246.

40. Na, Y., Wang, X., Lian, K., Zhu, Y., Li, W., Luo, Y., Chen, C. *Chem. Cat. Chem*. **2017**, *9*, 1062.

41. Wang, R., Zhao, M., Chen, C. *Polym. Chem*. **2019**, *7*, 3933.

CHAPTER 2

Pd(II) complexes with pyridylimines: a detailed catalytic study on ethylene/acrylic esters cooligomerization

Overview

In this Chapter, pyridylimine ligands (N–N') and the relevant palladium complexes of the general formula [Pd(N–N')(CH_3)Cl] and [Pd(N–N')(CH_3)(CH_3CN)][X] (where X = PF_6^-, SbF_6^-, OTf) have been studied. The ligands feature a 2,6-diisopropyl substituted aryl ring on the iminic nitrogen atom, a pyridine ring, that in one case has a methyl group on its sixth position, and different substituents on the iminic carbon (hydrogen, methyl, phenyl). Pyridylimine complexes with transition metals have been extensively reported in literature and applied for several catalytic reaction, but this study represents the first detailed catalytic investigation on their behaviour in the ethylene/acrylic esters cooligomerization. The monocationic complexes of the general formula [Pd(N–N')(CH_3)(CH_3CN)][X] have been tested in the model cooligomerization of ethylene with methyl acrylate, and proven to be active also in the reaction with other acrylic esters. Moreover, the effect of the counter anion and of the presence of acetonitrile has been also investigated. A first recycling test of the homogeneous catalyst was also implemented with promising results.

Part of this Chapter will result in a future publication:

Dall'Anese, A., Degrassi, M., Balducci, G., Montini, T., Fornasiero, P., Milani, B., manuscript in preparation

2.1. Introduction.

Pyridylimines (N-N'), also named as (imino)pyridines, can be seen as molecules strictly related to pyridyl(bis)imines, introduced at the end of the '90s by the independent discoveries by Brookhart and Gibson.[1] The related iron(II) and cobalt(II) complexes of general formula [M(pyridyl(bis)imine)X_2] (X= Cl^-, Br^-) (Figure 2.1), when activated with MAO (MAO = methylaluminoxide) generated active catalysts for ethylene homopolymerization under very mild reaction conditions of T (308 or 323 K) and $P_{ethylene}$ (10 bar), and leading to highly linear polyethylene with values of activity 3750-20600 g/mmol·h·bar for Fe-derivatives and of 450-1740 g/mmol·h·bar for Co ketimine systems.[1b]

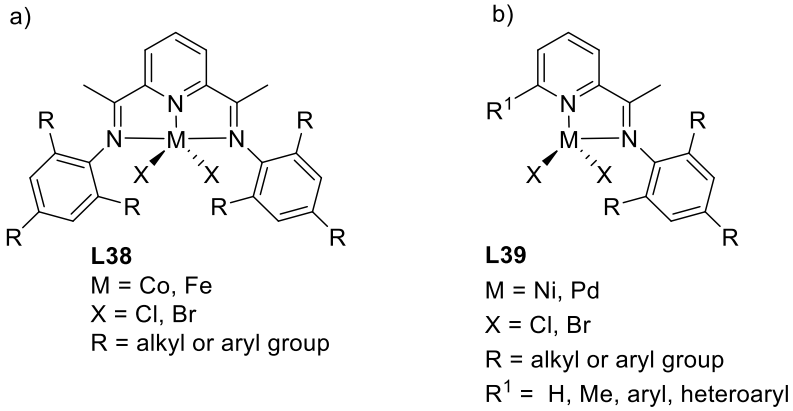

Figure 2.1. General structure of a) Fe(II) and Co(II) complexes with pyridyl(bis)imines; b) Ni(II) and Pd(II) complexes with pyridylimines.

Bidentate (imino)pyridines were then taken into consideration: these ligands and the relevant transition metal complexes are very easy to synthesize and handle, and both the pyridine and the iminic moieties can be modulated with different substituents. Transition metal complexes (Fe, Co, Ni, Pd, Cu) with pyridylimines have been widely studied,[2] and the lower coordination number with respect to pyridyl(bis)imines and both the lower steric hindrance around the coordination plane of the catalysts give to these systems unique properties, leading to catalysts that are active for the synthesis of low molecular weight polyolefins or oligomers starting from ethylene. Low molecular weight polymers can be obtained by increasing the steric hindrance on the iminic fragment, thus slowing down the chain transfer reaction with respect to propagation. As an example, reported by Brookhart and coworkers in 2016, Ni(II) dibromide complexes with half-sandwich N-N' ligands upon activation with MAO, give branched polyethylene with M_n up to $2.6 \cdot 10^4$ g/mol and with an activity up to $5.0 \cdot 10^{-4}$ h^{-1},[3] thanks to the peculiar conformation of the precatalyst (Figure 2.2a).

Similar results have been achieved with the introduction of an aryl ring substituted with benzhydryl group on the iminic moiety (Figure 2.2b).[4]

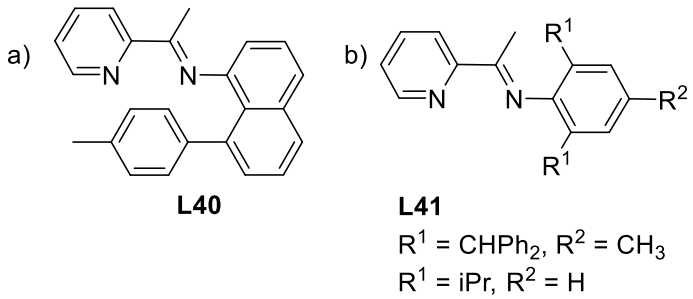

Figure 2.2. Sterically hindered pyridylimine ligands.

Other uses of complexes with pyridylimines that have been reported recently are as catalysts for Suzuki couplings,[5] for the selective synthesis of (Z)-allylboronates,[6] Heck coupling reactions between aryl halides and methyl acrylate.[7] Antitumoral activity has also been assessed, both for Pd(II) and Ir(III) complexes.[8] Examples of transition metal pyridylimine complexes can also be found in the field of metallosupramolecular chemistry.[9] In our group, Pd(II) complexes with pyridylimines have been widely employed as precatalysts for the copolymerization of CO with vinyl arenes, to obtain perfectly alternating polyketones.[10] This topic will be presented in Chapter 5.

As presented in *Chapter 1*, our research is focused mainly on the development of catalytic systems based on Pd(II) complexes with N-N donor ligands for the synthesis of functionalized polyolefins. Other than the classical Brookhart type systems with α-diimines, phosphinosulfonate (P-O) and P-N ligands have been extensively used for this reaction (Figure 1.4, **L10**).[11]

The P-O ligands are intrinsically non symmetrical, both from an electronic and a steric point of view, and this desymmetrisation is beneficial for the outcome of the catalysis. Recently, Chen and coworkers,[11b] inspired by the P-O ligands, introduced a P-N derivative (Figure 2.3), where the sulfonate moiety of P-O molecules is replaced by a pyridine ring. The relevant complexes produce cooligomers/copolymers with a slightly higher TOF (200 g CP/g Pd · h *vs* 169 g CP/g Pd·h) with respect to the classical P-O complex, and a lower incorporation of polar monomer and of molecular weight.

These results and the similarities with pyridylimines prompted us to look in the literature for applications of Pd(II) complexes with N-N' ligands to the copolymerization of ethylene with polar vinyl monomers. To the best of our knowledge, just one example was present, reported by Meneghetti *et al.*,[12] where the complex with the specific N-N' ketimine having the aryl ring substituted in 2,6 positions with an isopropyl group $[Pd(CH_3)(CH_3CN)(N\text{-}N')][BAr^F]$ (BAr^F = Tetrakis(3,5-bis(trifluoromethyl)phenyl)borate, Figure 2.4) is the catalyst of choice. The complex

was proven to be a good catalyst for ethylene oligomerization, with a long lifetime (up to 72 h) under different reaction conditions (10-60 °C, 2-6 bar of ethylene pressure), reaching a value of activity of 105 kg of oligomer mol^{-1} h^{-1} (6 h, 60 °C, 6 bar ethylene pressure). The catalyst was also active in the ethylene cooligomerization with methyl or benzyl acrylate, giving 3 and 5 mL of cooligomers respectively, with a degree of incorporation of acrylic ester of 9.3 and 8.2% in the two cases. However, no values of productivity or activity were reported, and no further catalytic investigation was performed.

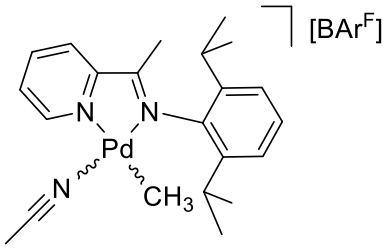

Figure 2.4. The Pd(II)-pyridylimine complex reported by Meneghetti *et al.*[12]

This publication represented the starting point to extend the research on catalysts for the copolymerization of ethylene with acrylic esters to pyridylimine complexes. We studied a small series of pyridylimines, that feature the 2,6-diisopropyl substituted aryl ring on the iminic moiety and have different substituents on the iminic carbon (H, CH_3, Ph). In one case, also the effect of the steric hindrance on the sixth position of the pyridine ring was assessed (Figure 2.5).

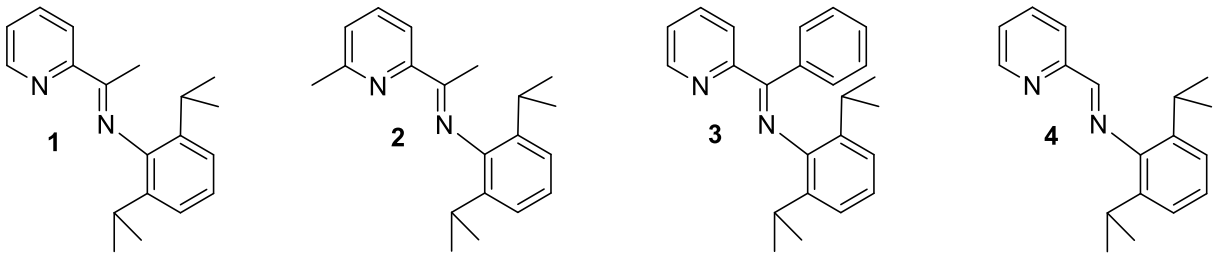

Figure 2.5. The family of pyridylimines under study.

The relevant neutral [Pd(CH_3)Cl(N-N')] and monocationic [Pd(CH_3)(CH_3CN)(N-N')][X] (X = OTf, PF_6^-, SbF_6^-) complexes have been synthesized, characterized and applied as precatalysts in the reaction of interest. The detailed catalytic study and the reactivity of such complexes with methyl acrylate will be hereby presented.

2.2. Results and discussion

*2.2.1. Synthesis and characterization of ligands **1-4**.*

Ligands **1**, **2**, and **4**, already known in literature,[6,12,13] have been obtained through a condensation reaction between either 2-acetylpyridine, or 2-acetyl-6-methylpyridine or 2-pyridinecarboxaldehyde and 2,6-di(isopropyl)aniline in methanol, at room temperature, with formic acid as catalyst (Scheme 2.1).

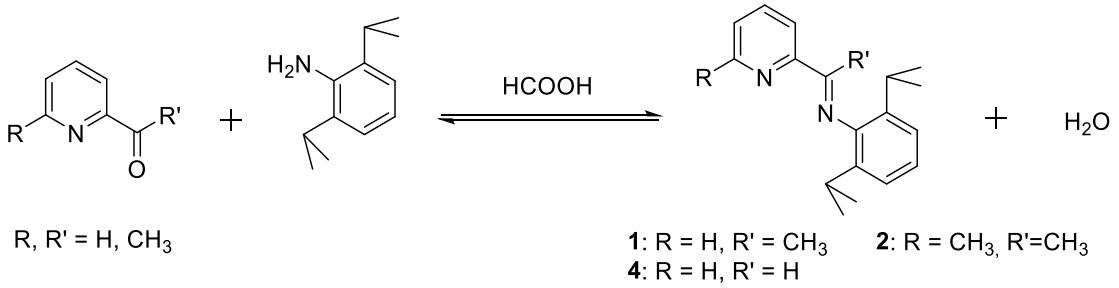

Scheme 2.1. General synthesis of pyridylimine ligands **1**, **2**, **4**.

1, **2** and **4** have been isolated as yellow solids in good yields (between 60 and 80 %). This synthetic procedure resulted to be ineffective for the synthesis of ligand **3**, synthesized in this work for the first time. Other procedures were tested, in order to find a suitable one (Scheme 2.2).

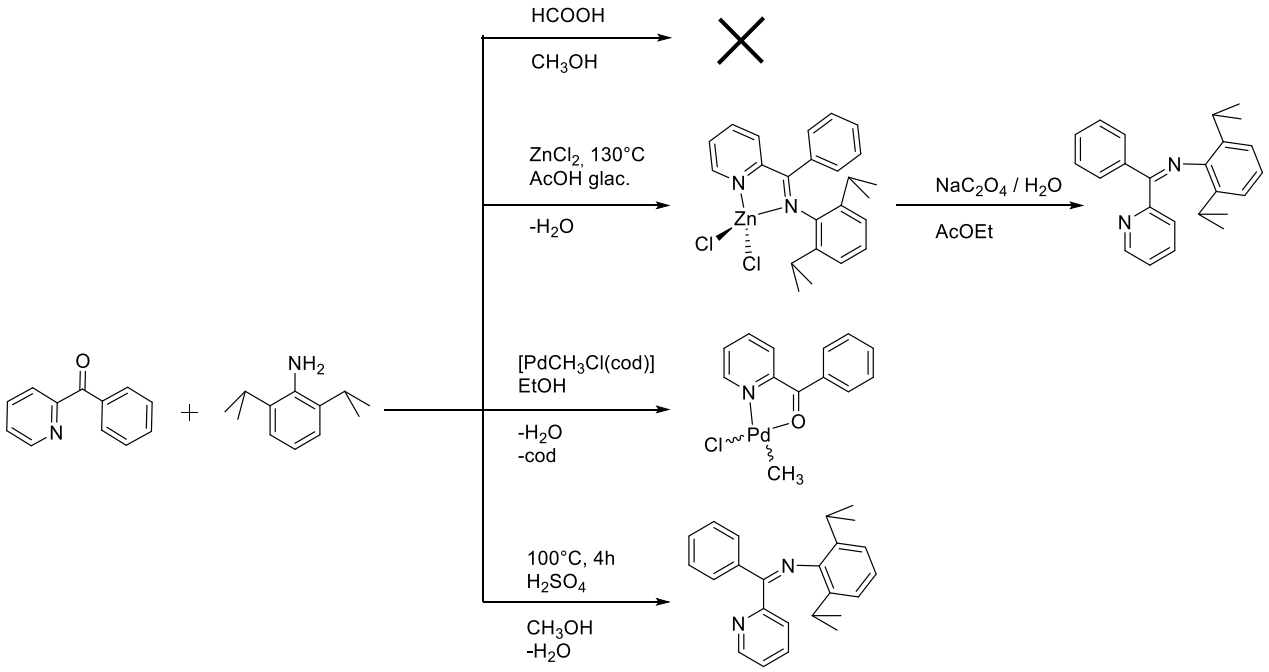

Scheme 2.2. Tentative synthetic pathways for ligand **3**.

First, a template synthesis with $ZnCl_2$ as templating agent was tested, by using a previously reported methodology for the synthesis of benzoylpyridine-derived pyridylimines.[3] [$ZnCl_2$(**3**)] was obtained,

as confirmed by the ^{1}H-NMR spectrum (Figure S2.6) and XRD analysis on single crystals (Figure S2.7). However, the next step of the synthesis, that consists in the removal of the zinc by using an aqueous solution of sodium oxalate, resulted in the complete hydrolysis of the ligand. The template synthesis with [Pd(cod)Cl(CH_3)][10b] as templating agent resulted to be ineffective as well, as the product of the reaction was [PdCl(CH_3)(benzoil-py)], as confirmed by the NMR analysis (Figure S2.8). The chosen synthetic pathway for **3** was based on in the microwave-assisted condensation reaction between benzoyl pyridine and the 2,6-di(isopropyl)aniline, with sulphuric acid as catalyst, even though **3** was isolated with a poor yield (16%).

All the ligands have been characterized in solution with mono- ad bi-dimensional NMR spectroscopy. The ^{1}H NMR spectra for ligands **1**, **2** and **4** and the relevant proton-signal assignments are in agreement with the ones reported in literature (Figure S2.1, S2.2, S2.11).[6,12,13] In the ^{1}H-NMR spectrum of ligand **3** (Figure 2.6) two sets of signals of comparable intensity, broadened and partially overlapped, are observed, indicating the presence of two species in solution, the geometrical isomers *E* and *Z*, in a 1 : 1.26 ratio (Scheme 2.3).

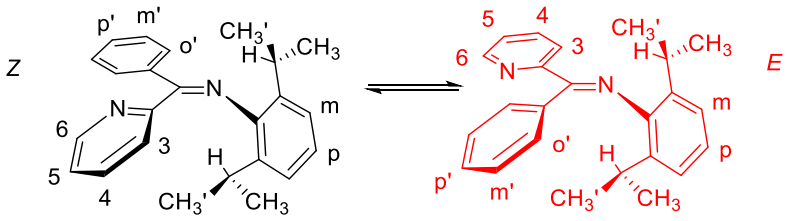

Scheme 2.3. Geometrical isomers of ligand **3**.

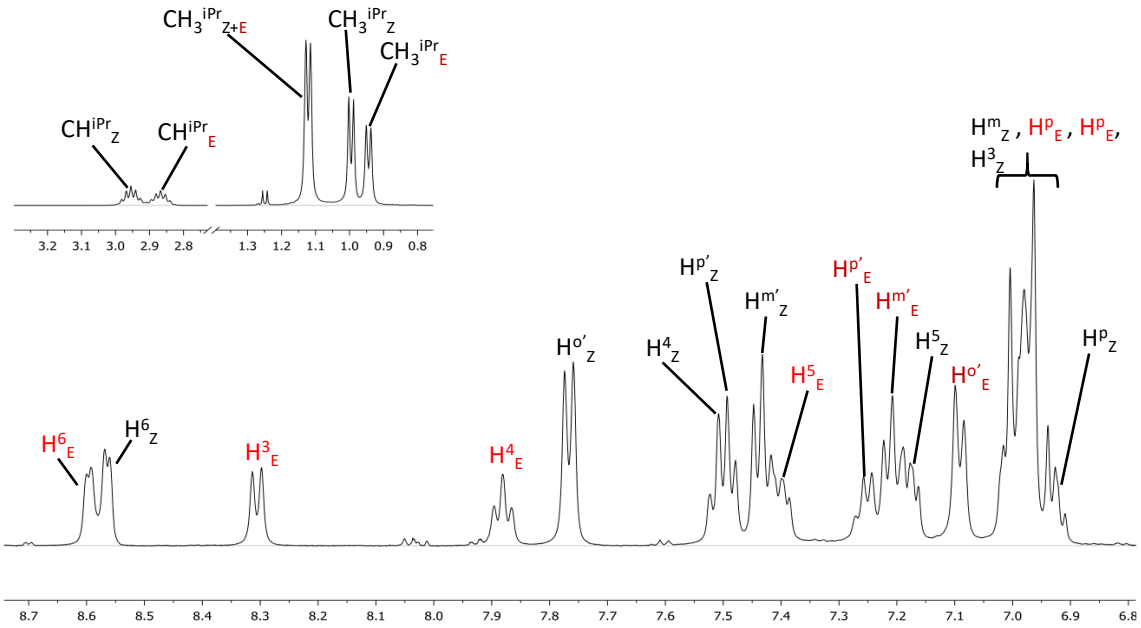

Figure 2.6. ^{1}H-NMR spectrum (CD_2Cl_2, 298 K) of ligand **3**, aromatic region and inset of aliphatic region.

In the NOESY spectrum (Figure 2.7) exchange peaks between the signals of the pyridine protons H^3, H^4 e H^5 in the two isomers and between those of protons of the phenylenic ring on the iminic carbon atom are evident, indicating that the two isomers are in slow equilibrium on the NMR time scale, at room temperature.

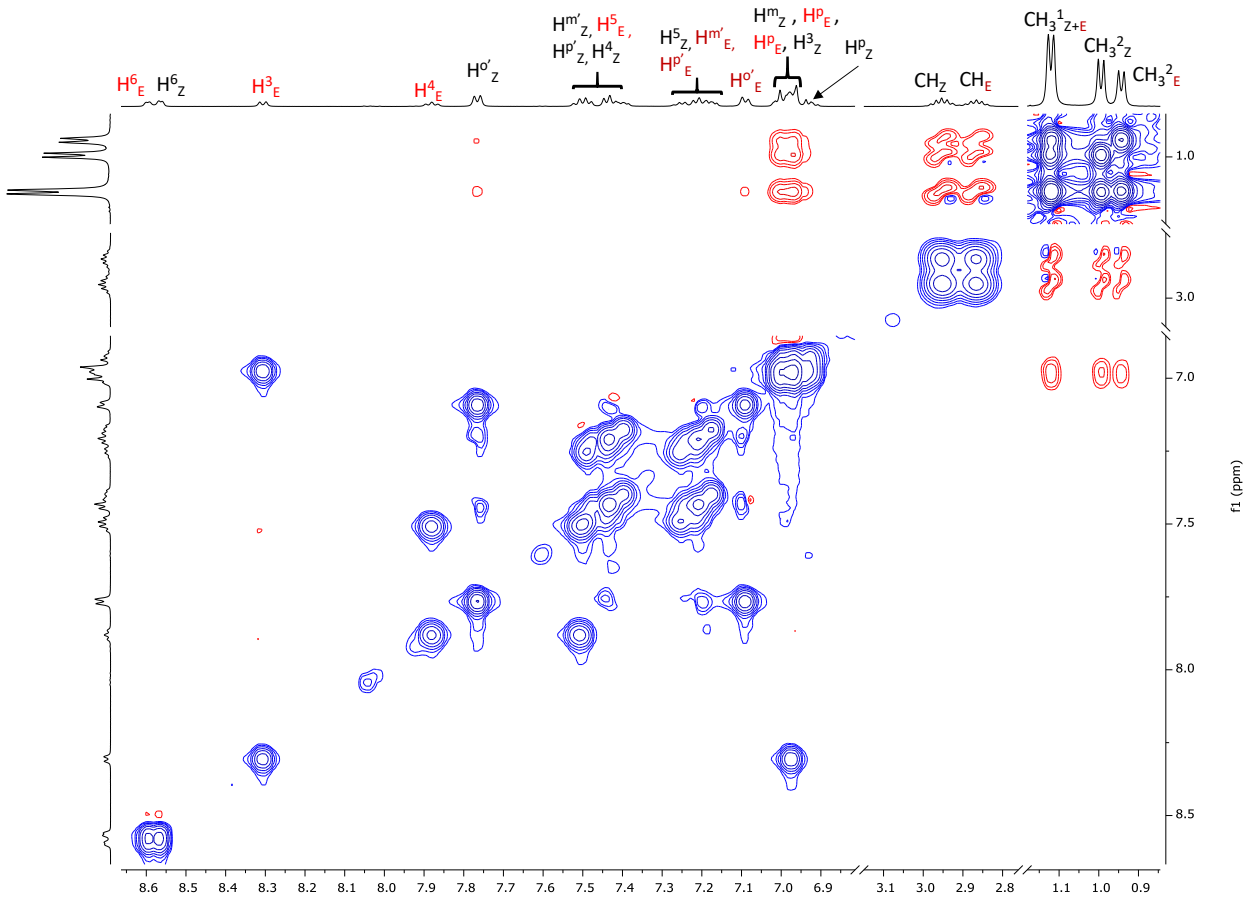

Figure 2.7. ^{1}H,^{1}H-NOESY spectrum (CD_2Cl_2, 298 K) of ligand **3**; in blue: exchange peaks.

For ligand **3,** single crystals suitable for X-ray diffraction were obtained directly from the reaction mixture. In the unit cell only the *Z* isomer is present (Figure 2.8). The crystallographic structure shows that the pyridine plane has a 20° angle with respect to the plane that contains the C=N iminic bond, whereas the phenyl and the aryl substituent on the iminic fragment form between each other a dihedral angle of 88°. The proton H^3 falls into the shielding cone of the phenyl substituent, in agreement with its low frequency resonance in the ^{1}H NMR spectrum. The bond distances of the iminic fragment and between the iminic carbon and the pyridine ring or the phenyl ring on the backbone have the expected values for C=N double bonds and C-C single bonds, thus indicating that no conjugation between the phenyl ring and the pyridine moiety and/or the isopropyl-substituted aryl ring.

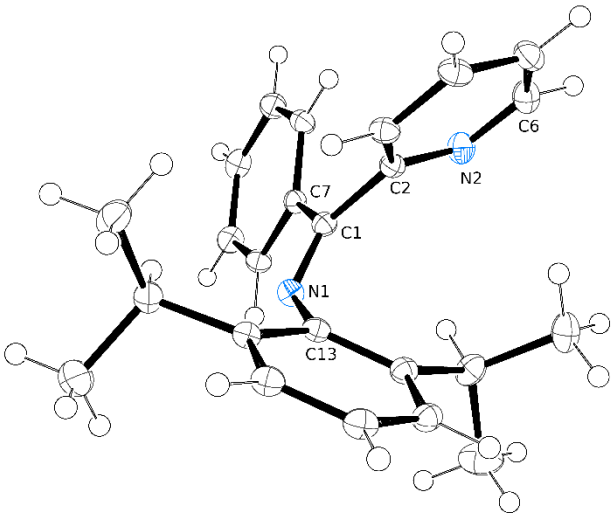

Figure 2.8. ORTEP representation (50% probability ellipsoids) of the molecule of ligand **3** in the crystal structure; for the sake of clarity, only the major population (76%) of a disordered iPr group has been included; most significant bond distances and dihedral angles (Å, °): C13-N1 1.419(1), N1-C1 1.278(1), C1-C2(py) 1.500(1), C1-C7(Ph) 1.490(1); [Ph(i-Pr)2]-[Py] 63.03(5), [Ph]-[Ph(i-Pr)2] 88.29(5), [Ph]-[Py] 64.16(5) .

*2.2.2. Synthesis and characterization of neutral Pd-complexes **1a-4a**.*

Ligands **1-4** were reacted with [Pd(cod)(CH_3)Cl] (cod = *cis,cis*-1,5-ciclooctadiene) to yield the neutral derivatives [Pd(CH_3)Cl(N–N')], **1a – 4a**. The desired complexes were isolated as yellow or orange solids in high yields (77-98%) (Scheme 2.4).

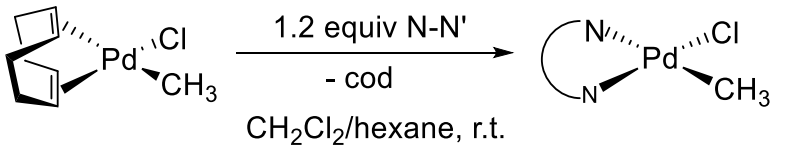

	N-N'	yield (%)
1a	**1**	98
2a	**2**	88
3a	**3**	86
4a	**4**	77

Scheme 2.4. Synthesis of the neutral Pd(II) complexes.

Complexes **2a-4a** were characterized in solution by mono- and bi-dimensional NMR experiments.

For all the Pd(II) complexes with pyridylimine ligands, both neutral and cationic, two isomers are possible, since the non-symmetrical ligand is coordinated in a non-symmetrical chemical environment. For the sake of clarity, we identify as *cis* the species with the Pd-CH_3 bond on the same side of the Pd-N_{imino} bond (N_{imino} = iminic nitrogen), and as the *trans* the one having the Pd-CH_3 bond on the opposite side of the Pd-N_{imino} bond (Figure 2.9).

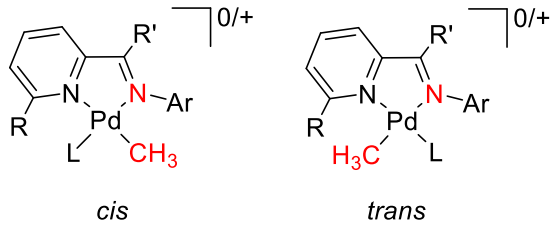

Figure 2.9. *cis* and *trans* isomers for neutral and cationic Pd(II) complexes (L= Cl^-, CH_3CN).

In agreement with data previously reported,[12] complex **1a** is present in solution as the *cis* isomer only (Figure 2.10), and this is further confirmed by NOESY experiment (Figure S2.15). An analogous situation is observed for complex **2a** (Figure 2.11).

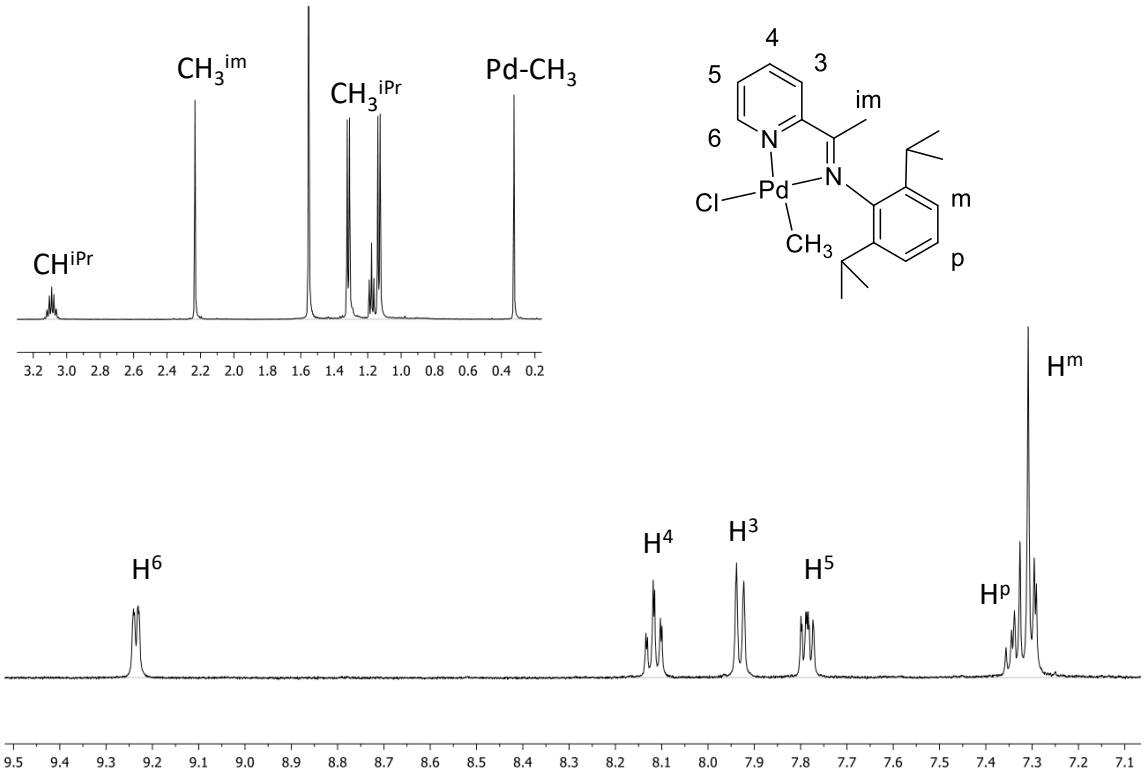

Figure 2.10. ^{1}H-NMR spectrum (CD_2Cl_2, 298 K) of complex **1a,** aromatic region, inset aliphatic region.

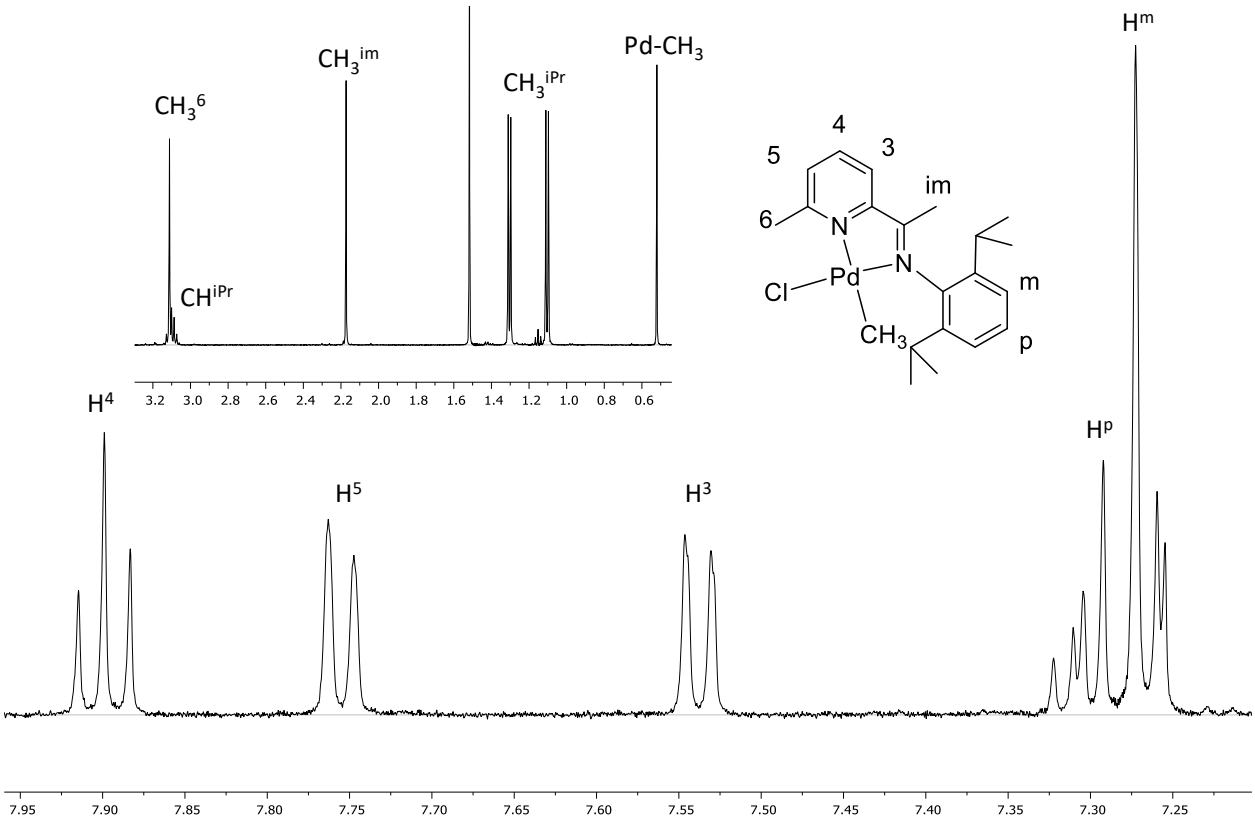

Figure 2.11. ^{1}H-NMR spectrum (CD_2Cl_2, 298 K) of complex **2a**.

For complex **3a**, two sets of signals are observed in the ^{1}H-NMR spectrum (Figure 2.12), with a relative intensity of 14:1, which means that in solution both the *cis* and the *trans* isomers are present. The Overhauser effect between the protons of the palladium-methyl fragment (s, 0.37 ppm) and those of the isopropyl group that resonates at 1.31 ppm allows us to identify the major species as the *cis* isomer (Figure S2.22). This attribution is in agreement with the fact that H^6 of the same species resonates at high frequency (9.28 ppm) due to its proximity to the Pd-Cl moiety.[14]

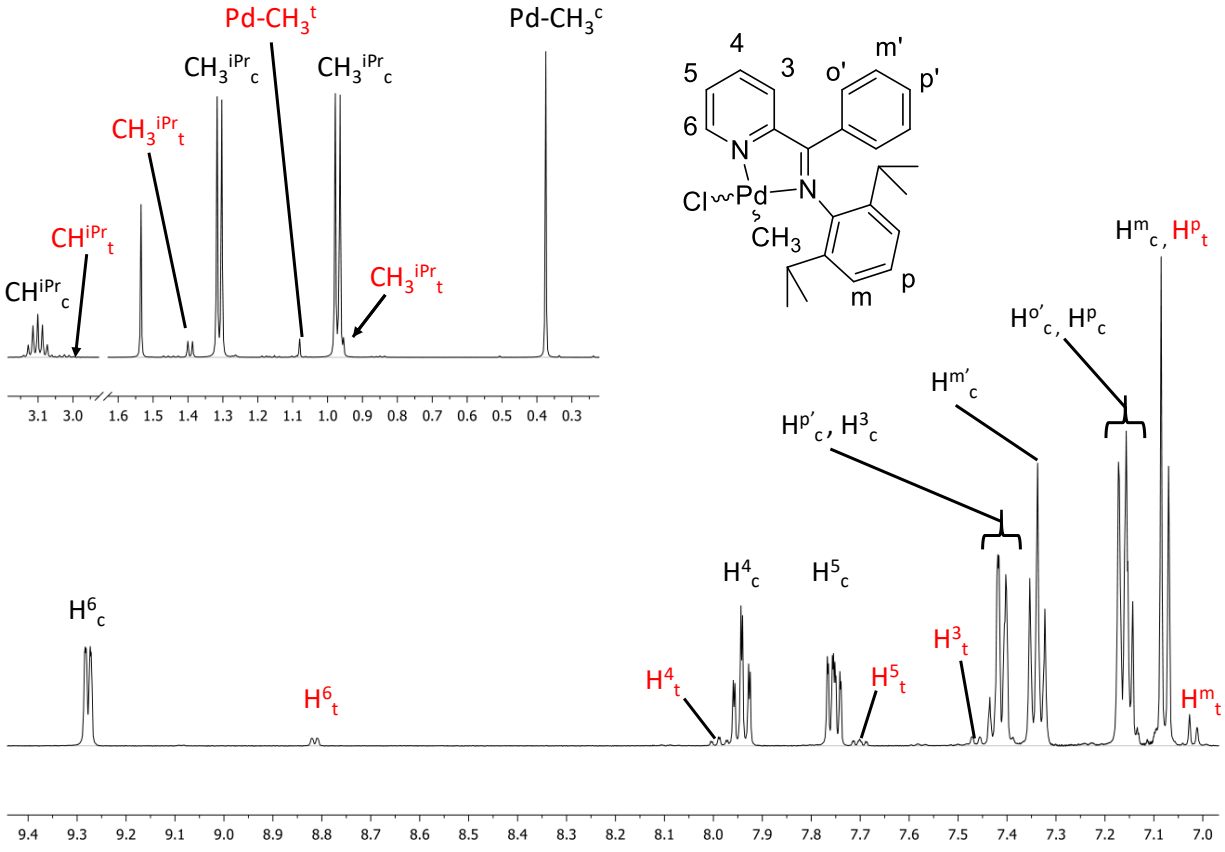

Figure 2.12. ^{1}H-NMR spectrum (CD_2Cl_2, 298 K) of complex **3a**.

In the ^{1}H-NMR spectrum of complex **4a** (Figure 2.13), again only one set of signals is present. This species is recognized as the *cis* isomer, thanks to the correlation peaks between the Pd-CH_3 singlet and the signals of the isopropyl moiety (Figure 2.14). The singlet of the iminic proton shows three cross-peaks: one with the doublet at 1.11 ppm and the multiplet at 3.26 ppm, due to the isopropyl substituents, and the last one with the doublet at 7.84 ppm, which is subsequently assigned to H^3.

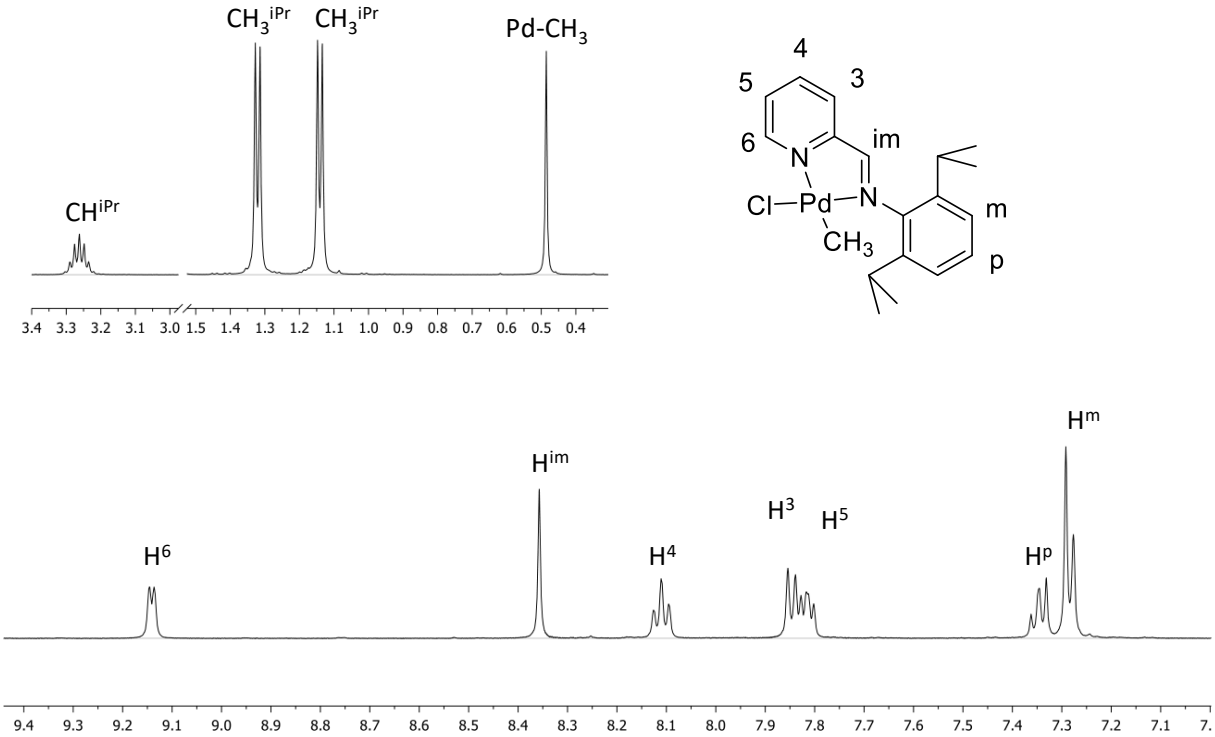

Figure 2.13. ^{1}H-NMR spectrum (CD_2Cl_2, 298 K) of complex **4a**.

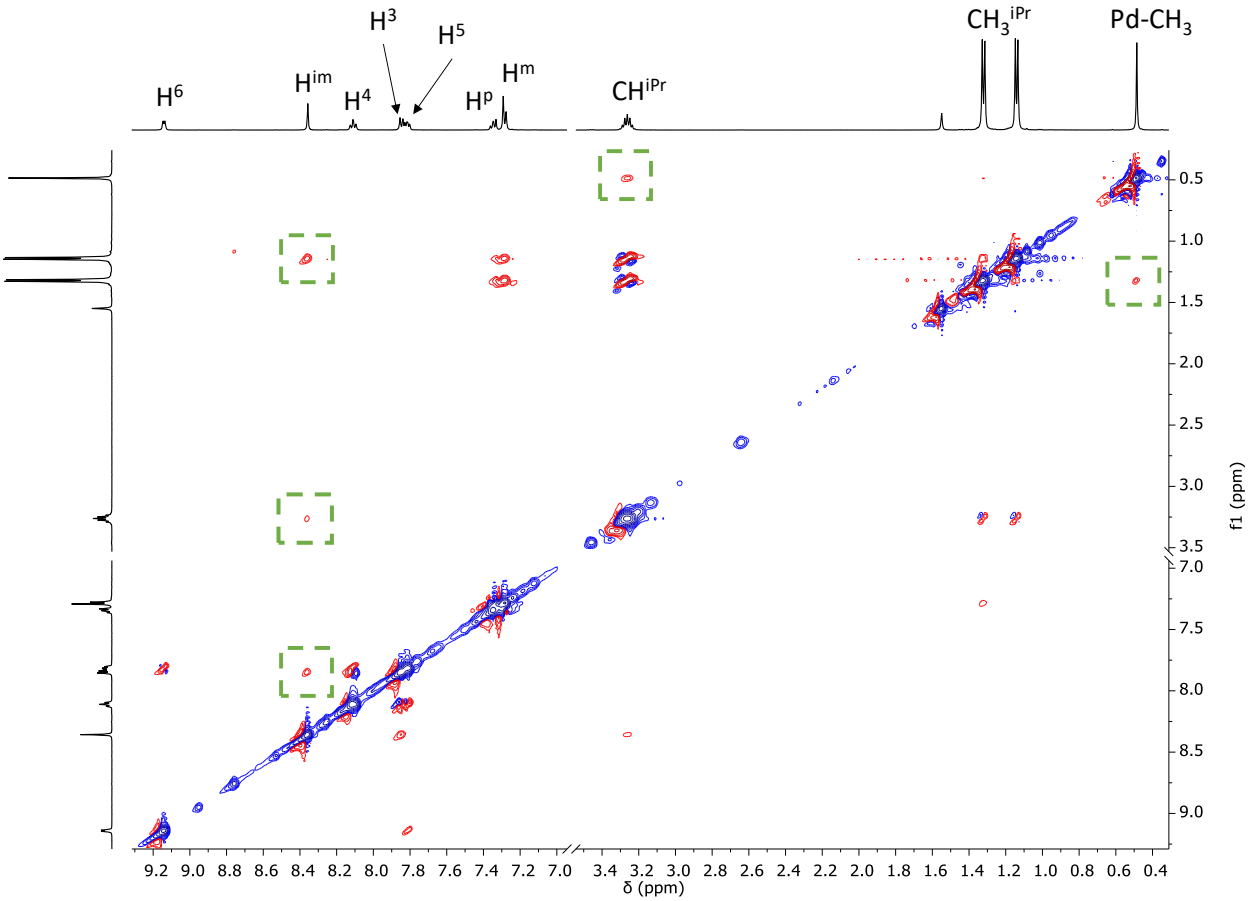

Figure 2.14. ^{1}H,^{1}H-NOESY (CD_2Cl_2, 298 K) of complex **4a**, selected correlation peaks evidenced by dashed green squares.

Upon layering diethyl ether over a dichloromethane solution of complex **3a**, and leaving it at 277 K for two weeks, it was possible to obtain crystals suitable for X ray analysis. In the unit cell only the *cis* isomer was found, which is also the prevailing species in solution (Figure 2.15).

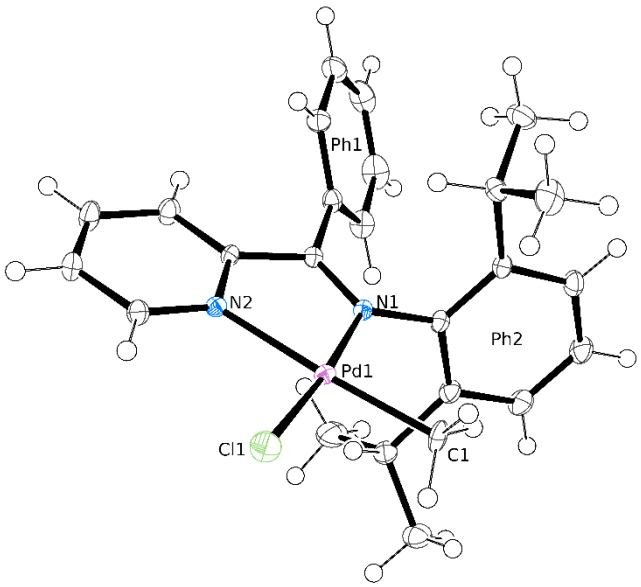

Figure 2.15. ORTEP representation (50% probability ellipsoids) of the single crystallographically independent molecule of compound **3a** in the crystal structure; two CH_2Cl_2 solvent molecules have been omitted for clarity. Most significant bond distances (Å), bond and torsion angles (°): Pd-C1 2.051(2), Pd-Cl1 2.3038(4), Pd-N1 2.056(1), Pd-N2 2.114(1), N1-Pd-N2 78.67(5), C1-Pd-Cl1 88.70(5), Ph1 57.36(6), Ph2 77.77(5).

The expected square planar geometry around palladium is confirmed by the X ray analysis. In agreement with the stronger *trans*-influence of the methyl group bonded to palladium with respect to that of the chlorido, the Pd-$N_{pyridine}$ bond is significantly longer than Pd-N_{imino}. Comparing these data with the ones reported in literature for similar pyridylimine complexes (Figure 2.16),[10b] the Pd-C bond in this case is longer than for all of the reported complexes (2.051(2) *vs* 2.0284(15), 2.030(2), 2.0414(17) Å), and is in agreement with the increasing basicity of the ligand, that implies a decrease in the σ-donation of the methyl group to palladium.

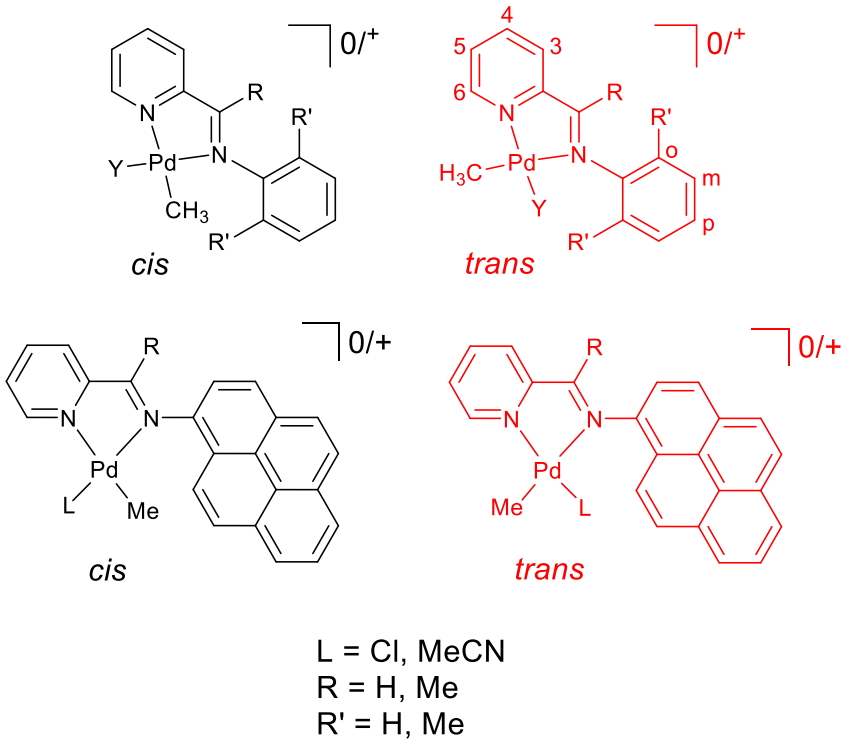

Figure 2.16. Previously reported Pd(II) complexes with N-N' ligands.

The Pd-$N_{pyridine}$ distances are shorter, as expected (2.114(1) *vs* 2.121(2), 2.1319(5), 2.1495(13) Å), and the Pd-N_{imino} lengths are slightly longer in our case (2.056(1) *vs* 2.0343(14), 2.0352(14), 2.051(2) Å). The dihedral angle values show that the planes of aryl substituents on both the iminic carbon (Ph1) and iminic nitrogen (Ph2) are almost orthogonal to the coordination plane.

2.2.3. Synthesis and characterization of cationic Pd-complexes ***1b-4b, 1c, 1d****.*

The monocationic complexes [Pd(CH_3)($NCCH_3$)(N–N')][X] (X = PF_6^-, SbF_6^-, OTf) **1b-4b**, **1c**, **1d**, were synthesized according to literature procedures,[10b,15] through the dehalogenation reaction of the corresponding neutral complexes **1a-4a**, by using an appropriate silver salt. The reaction is run under inert atmosphere, in dichloromethane, with a small excess of both dry acetonitrile and AgX with respect to palladium (X = PF_6^-, SbF_6^-, OTf) (Scheme 2.5). The cationic complexes were obtained upon concentration of the dichloromethane solution and addition of cold diethyl ether, isolating them in excellent yields (around 90%).

	X	yield (%)
1b	PF_6	99
2b	PF_6	87
3b	PF_6	99
4b	PF_6	87
1c	SbF_6	96
1d	OTf	71

Scheme 2.4. Synthesis of the monocationic complexes **1b-4b, 1c, 1d**.

The complexes **1b-4b, 1c, 1d** have all been characterized by NMR spectroscopy, in CD_2Cl_2, at room temperature. In the ^{1}H NMR spectrum of **1b** recorded 5 minutes after dissolving the complex, one set of intense signals is present, alongside with signals of very low intensity that are clearly visible in the isopropyl region, thus suggesting the prevalence in solution of one species (Figure 2.16a). After another 5 minutes, the intensity of the second set of signals increases (Figure 2.16b), and after 3 hours and 40 min the relative intensities between signals of the two sets do not change anymore (Figure 2.16c). After 18 h, formation of methane is evident together with peaks of a new species that, according to literature,[12] has been identified as the dicationic bischelated complex $[Pd(\mathbf{1})_2]^{2+}$ (Figure 2.16d).

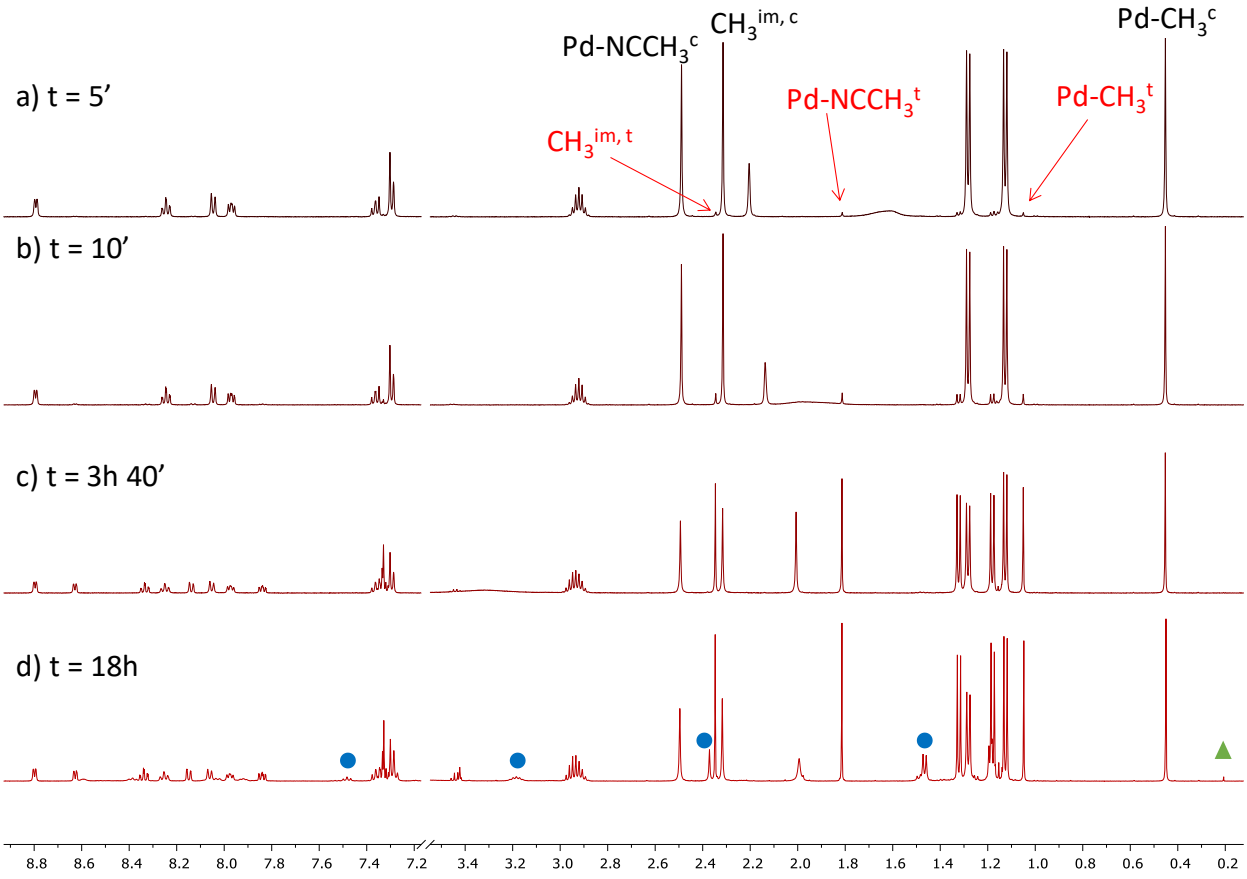

Figure 2.17. ^{1}H NMR spectra of **1b**: evolution with time (CD_2Cl_2, 298 K); ● = $[Pd(\mathbf{1})_2]^{2+}$; ▲ = CH_4.

The signal to proton assignments were made on the equilibrium mixture. Bi-dimensional NMR experiments, in particular NOESY, allowed to identify the *cis* isomer as both the main species at the equilibrium (ratio *cis* : *trans* = 1.3 : 1, Figure 2.17), and the isomer observed immediately after dissolution of **1b**.

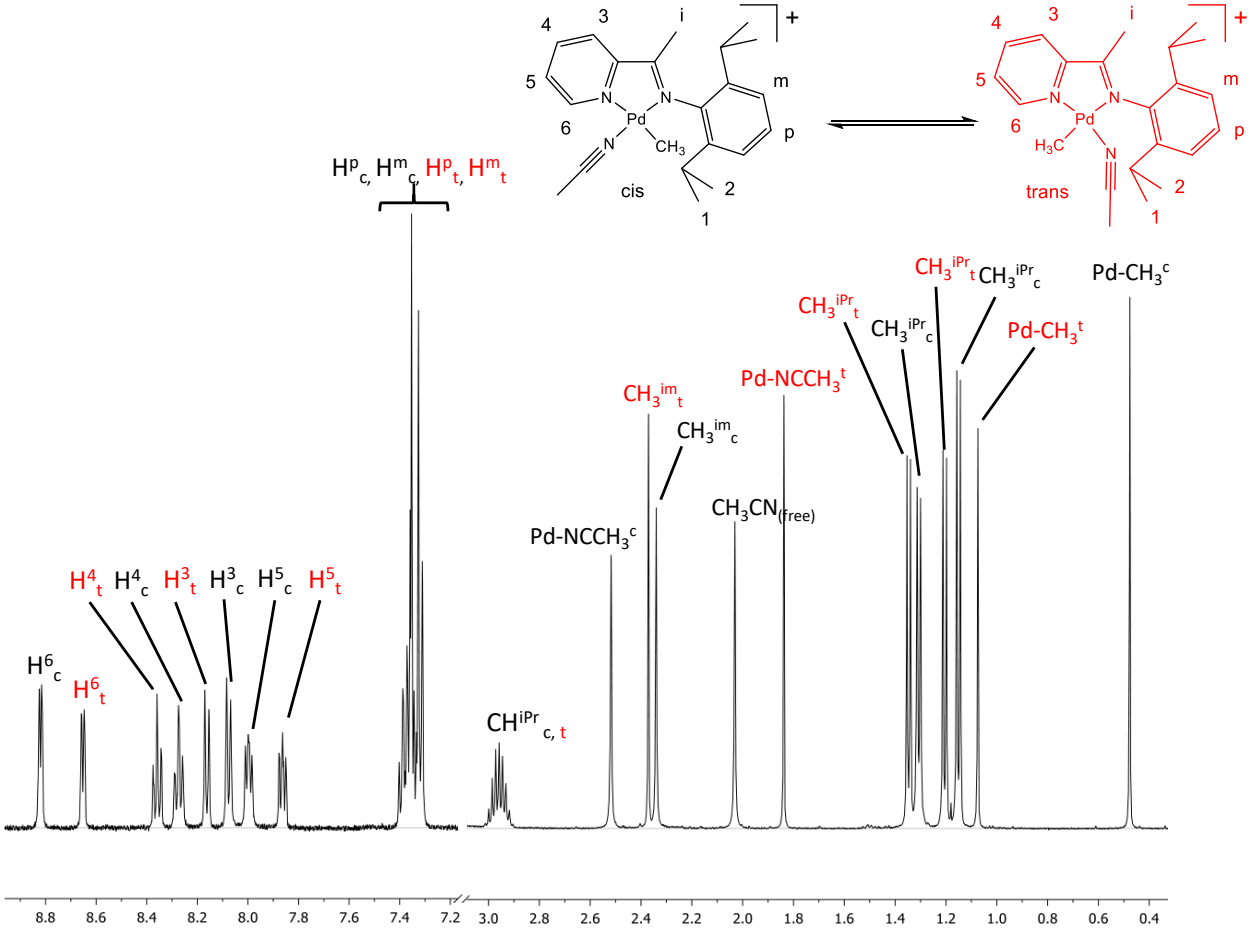

Figure 2.18. ^{1}H-NMR spectrum (CD_2Cl_2, 298 K, t = 3h40') of 1**b**, aliphatic and aromatic region not in scale.

A similar process is observed for the other cationic complexes having ligand **1**: in the ^{1}H-NMR spectrum of complexes **1c** (Figure S2.30) and **1d** (Figure S2.31) in CD_2Cl_2 recorded right after dissolving them, the signals of both isomers are observed, in a *cis* : *trans* ratio of 3 : 1 for **1c** and 4.5 : 1 for **1d**. After 10 minutes, the ratio changes for the two complexes (Figures S2.30, S2.31). These variations indicate that the initial mixture of isomers is the kinetic one, and that the thermodynamic composition is reached after a few hours. According to literature, this phenomenon was not observed for analogous palladium complexes with other pyridylimines like those reported by Milani *et al*,[10] whereas it was reported for the complex [Pd(CH_3)(CH_3CN)(**1**)][BAr^F].[12] In the latter case, the *cis* : *trans* ratio at the equilibrium was 1 : 2, reached after 15 minutes from the dissolution.

To have a better understanding of the isomerization process of the cationic complexes, a kinetic study was performed. ^{1}H NMR spectra of a 10 mM solution of the desired complex in CD_2Cl_2 (99% purity, from vial) where recorded every 20 minutes, for a total of 12 hours. The three cationic complexes **1b**-**1d** reached the equilibrium at different times, precisely after 1 h 20' for **1d**, 3 h 40' for **1b** and 9 h for **1c**. The observed constant k_{obs} values were calculated, by assuming the isomerization follows a reversible and unimolecular reaction (Scheme 2.5, Figure 2.19, Table 2.1), as it is for analogous complexes of Pd(II) with α-diimines.[16]

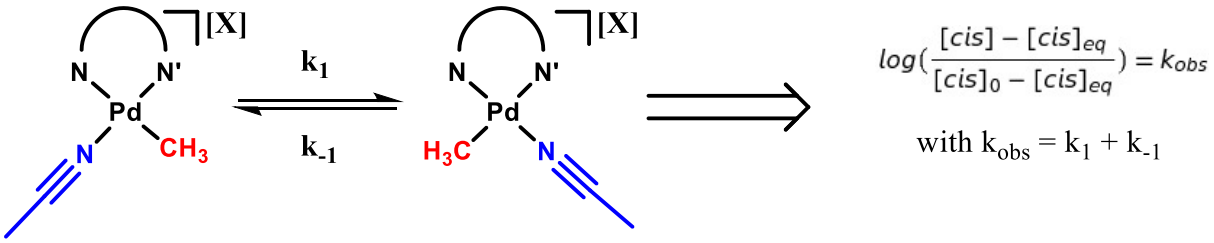

Scheme 2.5. *cis-trans* isomerization of cationic complexes and relevant kinetic law.

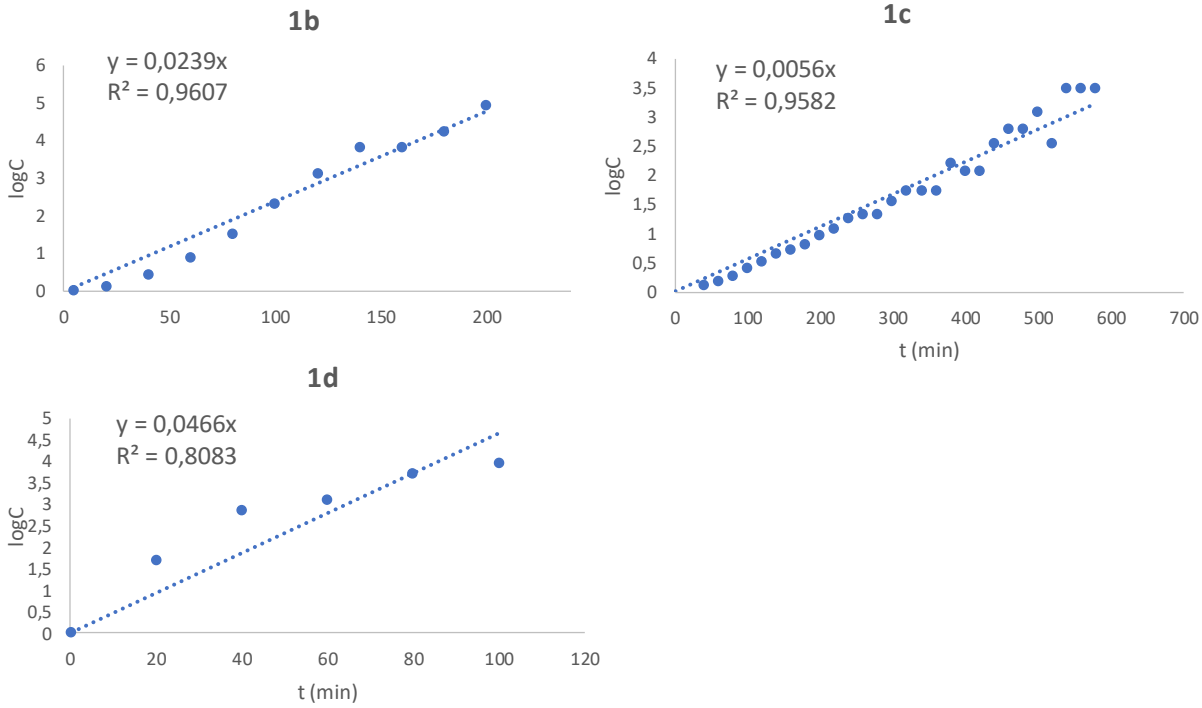

Figure 2.19. Isomerization kinetic curves of **1b**, **1c**, **1d** at 298 K.

Table 2.1. Observed kinetic constants of the isomerization process and equilibrium composition in CD_2Cl_2 for complexes **1b, 1c** e **1d**.

Anion	k_{obs} (s^{-1})	*cis*/*trans* ratio
OTf (1d)	$4.6 \cdot 10^{-2}$	1.26
PF_6^- (1b)	$2.4 \cdot 10^{-2}$	1.28
SbF_6^- (1c)	$5.6 \cdot 10^{-3}$	1.30

The data reported in Table 2.1 show that the rate of isomerization follows the order $SbF_6^- < PF_6^- <$ OTf, whereas the *cis*/*trans* ratio at the equilibrium is the same. From the isomerization kinetic curves it is clear that the used model suits well for **1b**, **1c**, even though with not so high R^2, whereas this is not true for **1d**, where the R^2 is very low (Figure 2.19). This might be attributed to the low number of points taken during the isomerization process, that it is faster than that of **1b** and **1c**. The only difference among complexes **1b-1d** lies in the counteranion and as expected, the ^1H NMR spectra of the three complexes at the equilibrium are very similar, except for the resonances of H^6 and Pd-$NCCH_3$ of the *cis* isomer, and that of H^4 and H^3 of the *trans* species, that are shifted at low frequencies going from OTf to PF_6^- to SbF_6^- (Table 2.2, Figure 2.20). These variations are in agreement with the coordinating capability of the counteranion, that decreases in the same order and suggest that, in solution, the counteranion might be preferentially located close to the H^6 and the Pd-$NCCH_3$ moiety of the *cis* isomer, and close to H^4 and the H^3 position of the pyridine moiety in the case of the *trans* isomer, thus affecting their resonances. This effect, in combination with the results of the kinetic study, suggests that the counteranion might be involved in the *cis*/*trans* isomerization process. In particular, the more coordinating anion, triflate, might favour a mechanism of isomerization consisting of different steps: i. the cleavage of the Pd-$N_{pyridine}$ bond, leading to an intermediate with a readily available coordination site, and the pyridilimine ligand coordinated as a monodentate ligand through the iminic nitrogen atom; ii. the exchange of two nitrogen atoms ($N_{pyridine}$-N_{imino}) at the same coordination site (flipping); iii. The coordination of the second nitrogen atom to Pd leading to the *trans* isomer (Scheme 2.6). This hypothesis is also in agreement with the fact that at the beginning, when the *cis* isomer is the prevailing species, the higher *trans*-influence of the methyl coordinated to Pd in *trans* position with respect to the Pd-$N_{pyridine}$ makes this bond more labile than the Pd-N_{imino} bond. This hypothesis might also explain the observation that for the triflate derivative the isomerization process does not follow a first order kinetic. Triflate, the most coordinating anion of the series, might coordinate to palladium in the rate determining step leading to a kinetic law of a higher order.

Table 2.2. Selected chemical shifts (ppm) for complexes **1b, 1c** and **1d.**[a]

Anion	H^6_c	H^5_c	Pd-$NCCH_3^c$	Pd-CH_3^c	H^4_t	H^3_t	$CH_3{}^i_t$	Pd-CH_3^t
OTf	8.91	8.02	2.53	0.44	8.37	8.22	2.36	1.05
PF_6^-	8.80	7.97	2.49	0.45	8.34	8.15	2.35	1.05
SbF_6^-	8.73	7.96	2.48	0.46	8.32	8.11	2.34	1.05

[a] ^{1}H NMR spectra in CD_2Cl_2 at 298 K, 10 mM solution of the complex.

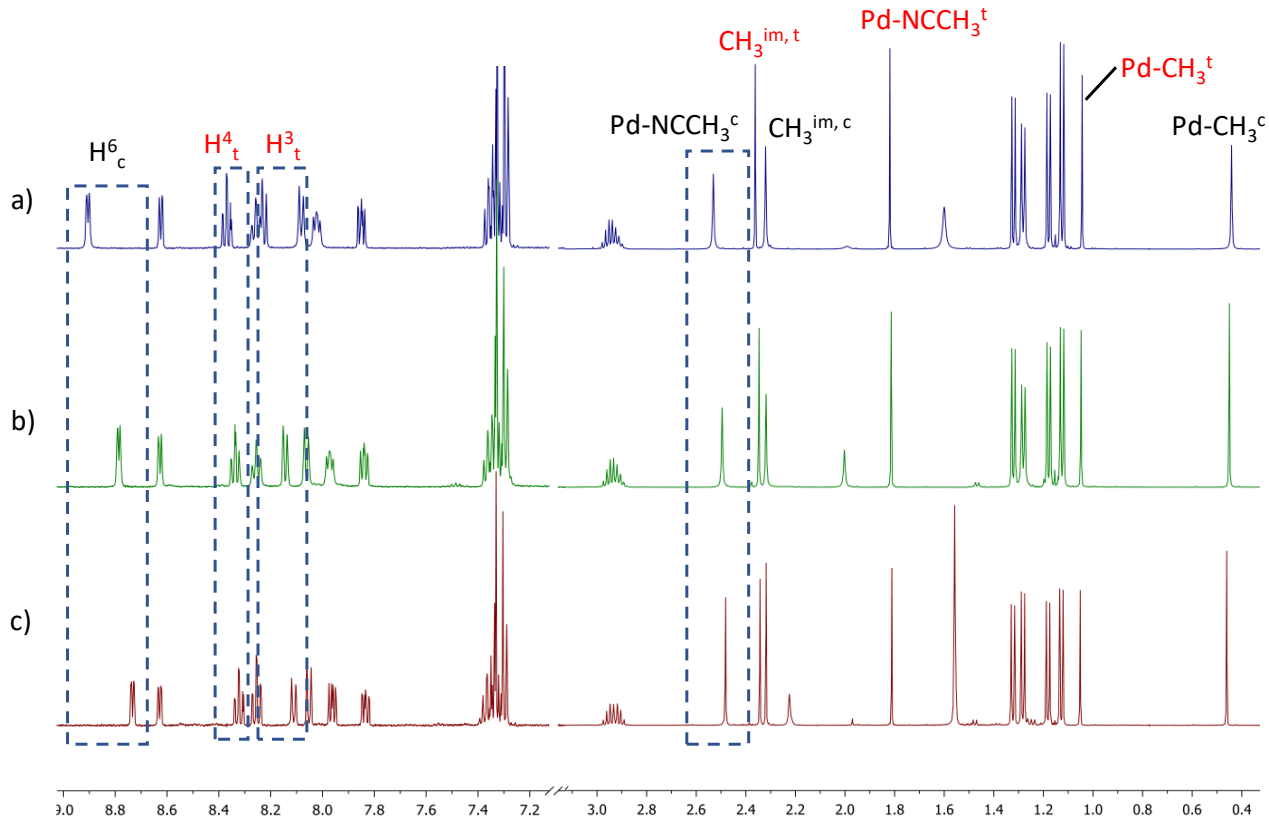

Figure 2.20. ^{1}H-NMR spectra (CD_2Cl_2, 298 K) of complexes **1d** (a), **1b** (b), **1c** (c) at the equilibrium. Selected resonances in dashed blue squares, aliphatic and aromatic region not in scale.

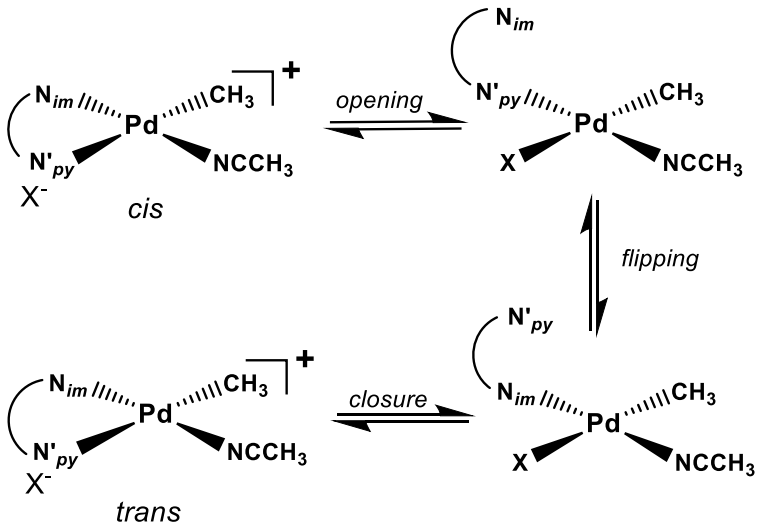

Scheme 2.6. Possible *cis*/*trans* isomerization mechanism (N = N_{imino}, N' = $N_{pyridine}$, X^- = counteranion).

To confirm this hypothesis, some preliminary $^1H,^{19}F$-HOESY experiments were performed for complexes **1b-d**. However, this kind of analysis did not give any evidence of an Overhauser effect between the fluorine atoms of the counteranion and the H^6 or the Pd-$NCCH_3$ protons of the cation. Further studies are required to prove or discard our hypothesis.

The ^{19}F NMR spectra of complexes **1b-1d** confirm the presence of the three different counteranions (Figure S2.29). In addition, for complex **1b**, in the ^{19}F NMR spectra recorded at different times, it was possible to observe that the intensity of the PF_6^- doublet decreased with time, with the simultaneous growth of another signal that, in agreement with literature,[17] was assigned to $PO_2F_2^-$, that is one of the possible products of the metal-catalyzed hydrolysis of PF_6^- (Figure 2.21).

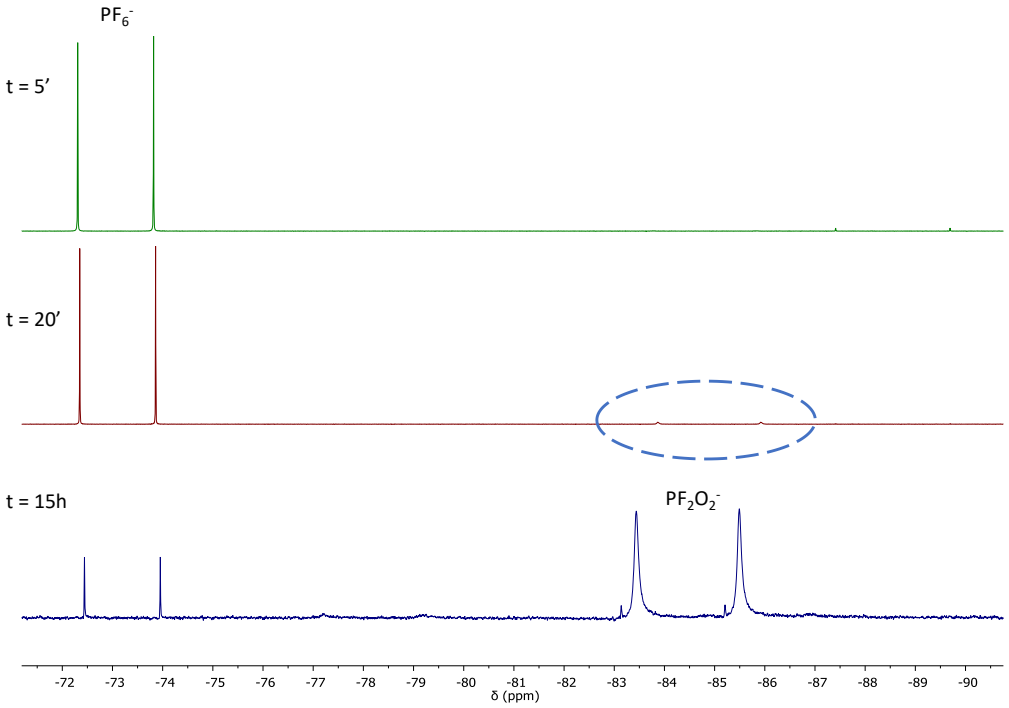

Figure 2.21. ^{19}F-NMR spectra (CD_2Cl_2, 298 K) of complex **1b**: evolution with time.

Differently from all the other cationic complexes, **2b** shows in the ^{1}H-NMR spectrum (Figure 2.22) the presence in solution of just one species, that is recognized as the *cis* isomer thanks to bi-dimensional NMR experiments (Figure 2.23). No spectral variation with time is observed.

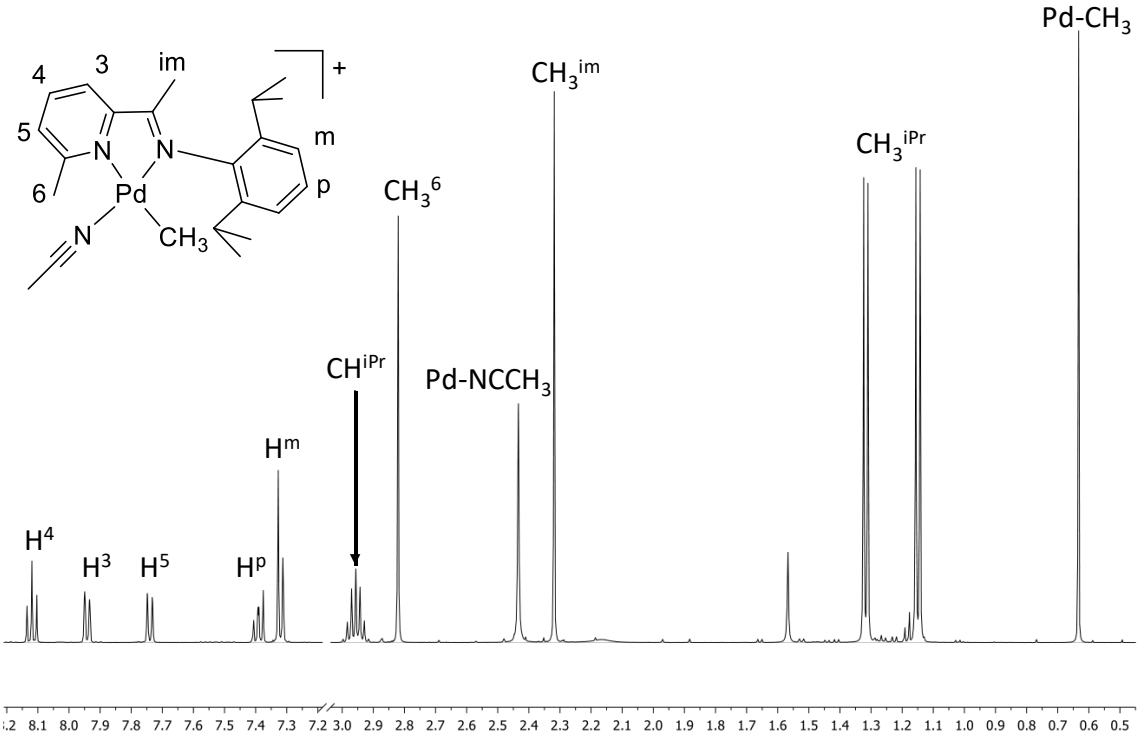

Figure 2.22. ^{1}H-NMR spectrum (CD_2Cl_2, 298 K) of complex **2b.**

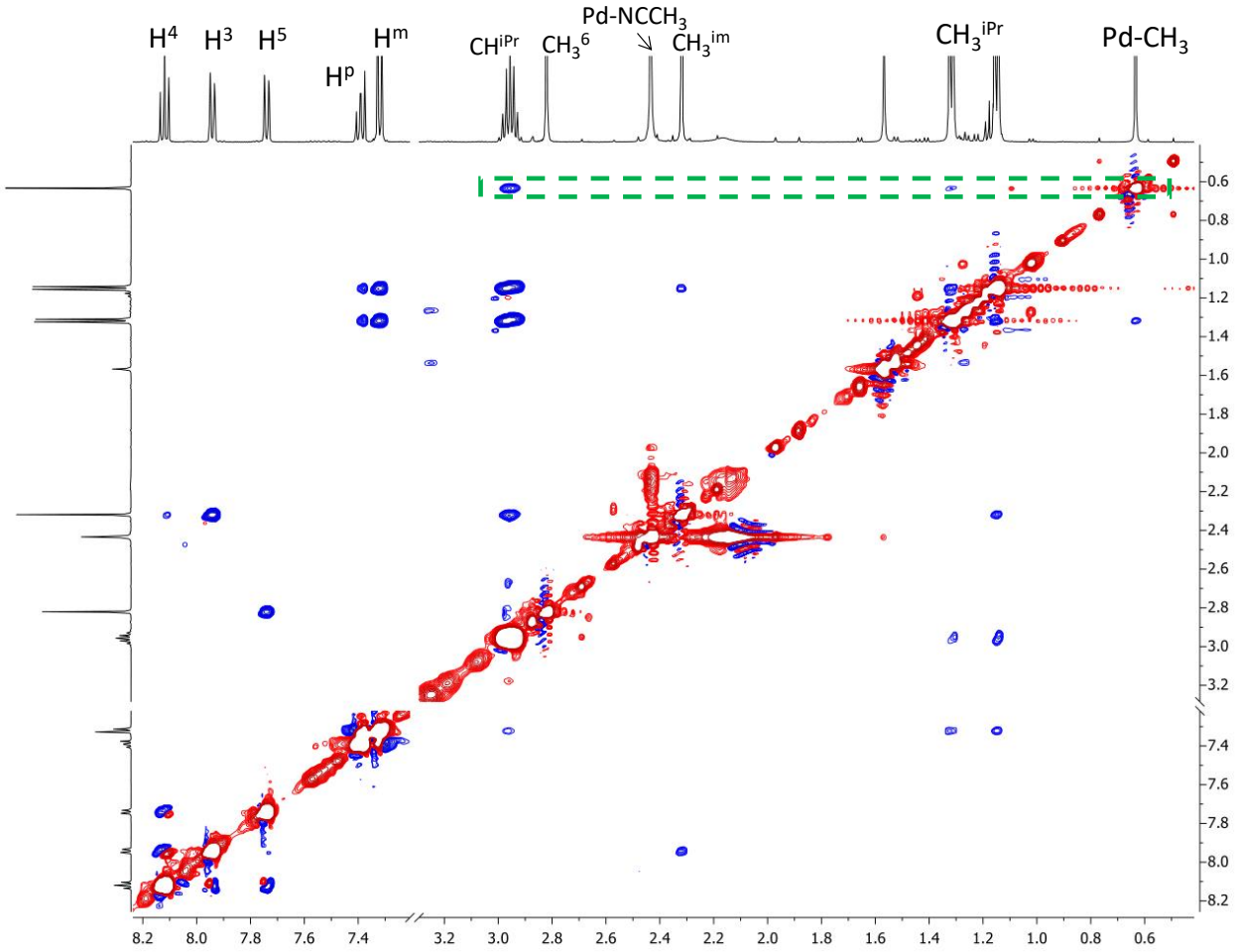

Figure 2.23. $^{1}H,^{1}H$-NOESY (CD_2Cl_2, 298 K) of complex **2b.**

Single crystals suitable for X-ray diffraction were obtained for **2b** by slow diffusion of n-hexane into the solution of the complex in dichloromethane. In the unit cell only the *cis* isomer is present, as it is also observed in solution (Figure 2.24).

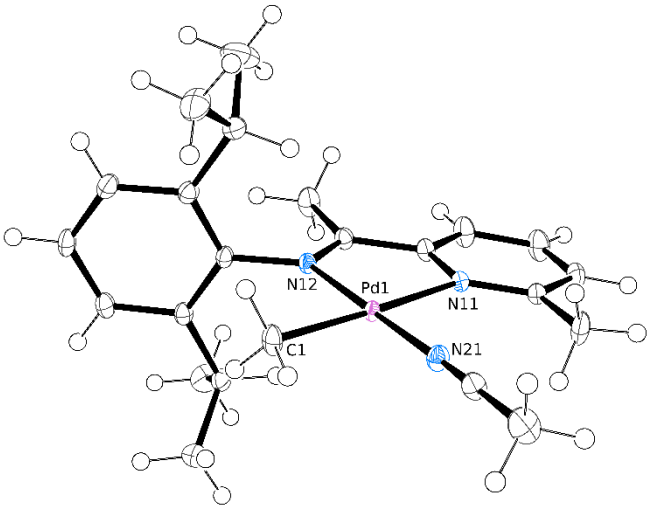

Figure 2.24. ORTEP representation (50% probability ellipsoids) of the cation of **2b** in the crystal structure, counteranion and solvent omitted for clarity. Selected bond distances (Å) and angles (°), and torsion angles with respect of the coordination plane: Pd1-C1 2.024(2), Pd1-N21 2.001(2), Pd1-N11 2.182(2), Pd1-N12 2.029(2), C1-Pd-N21 84.90(8), N11-Pd-N12 78.91(7), N11-Pd-N21 103.47(7), Ph 83.33(6).

As expected, the palladium has the square planar coordination geometry; the distance of the Pd-$N_{pyridine}$ bond is longer than the Pd-N_{imino} one, in agreement with the different *trans*-influence of methyl and acetonitrile ligands. The plane of the aryl ring is orthogonal to the coordination plane.

In the ^{1}H NMR spectra of **3b** and **4b** the number of signals and their integration indicates the presence in solution of *cis* and *trans* isomers, already immediately after the dissolution of the complexes. For both complexes the composition of the solution varies with time.

Indeed, after dissolving complex **3b** in CD_2Cl_2, an orange solution is obtained, and the main isomer is the *cis*, whereas at the equilibrium the *trans* prevails, with a *cis* : *trans* ratio of 1 : 3. The equilibrium is reached overnight. The isomerization process can be seen to the naked eye, both in solution and at the solid state, thanks to a change in the colour from orange to yellow. The proton-signal assignations have been made comparing previously reported data and mono- and bidimensional NMR spectroscopy. Complex **4b** similarly reaches the equilibrium overnight, with a final *cis* : *trans* ratio of 3.2 : 1.

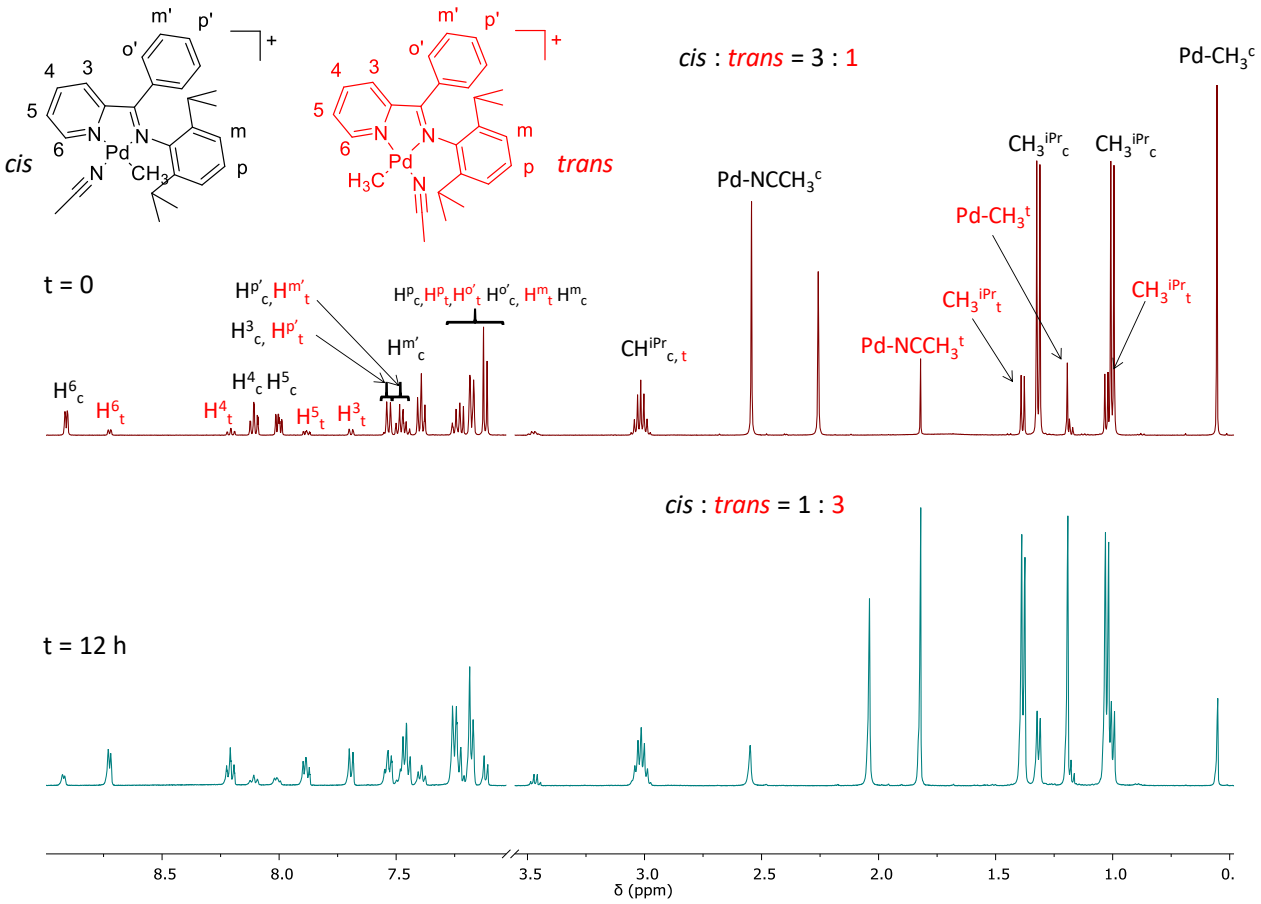

Figura 2.25. ^{1}H-NMR spectrum (CD_2Cl_2, 298 K) of complex **3b**: right after dissolving it (top), after 12 h (bottom).

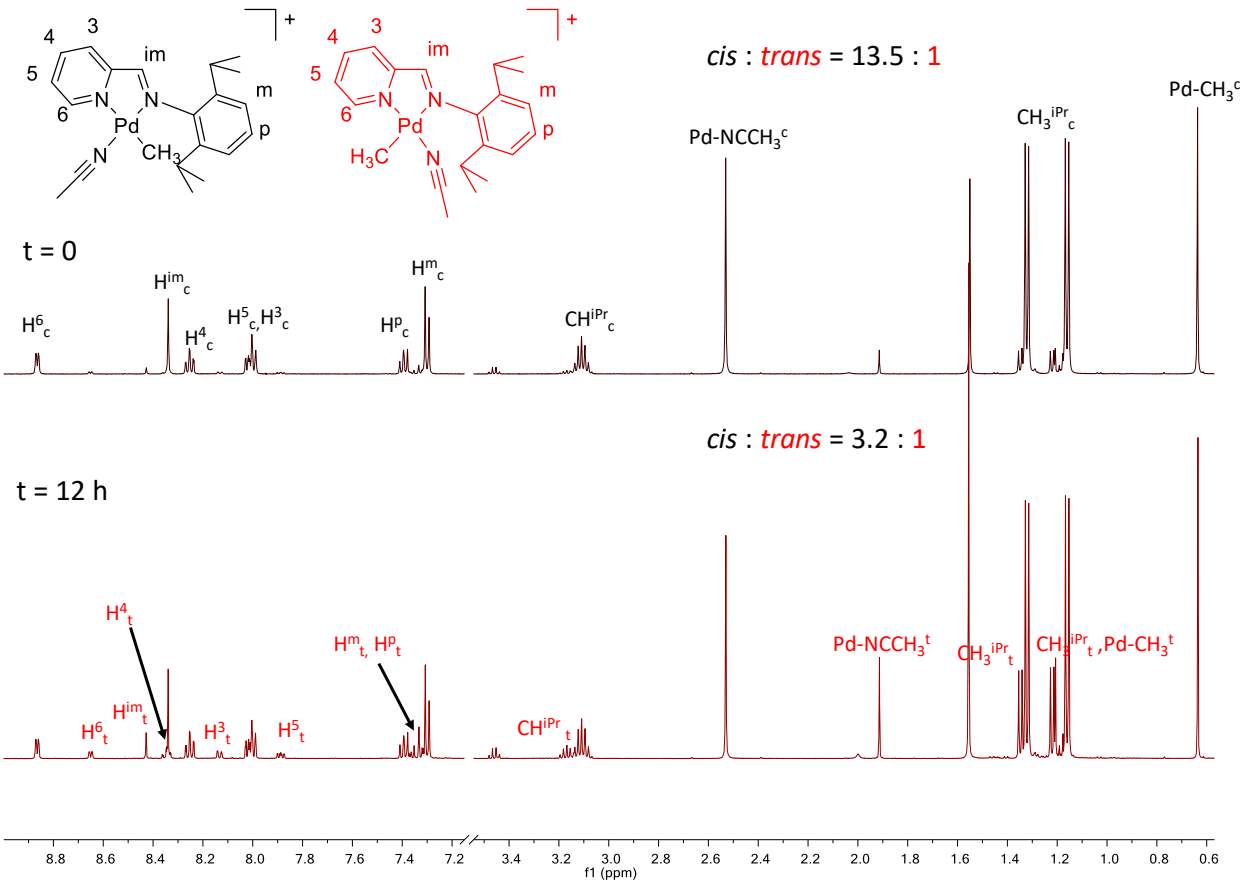

Figure 2.26. ^{1}H-NMR spectrum (CD_2Cl_2, 298 K) of complex **4b.**

From the analysis of NMR data, it is possible to draw some general conclusions regarding the isomeric distribution in pyridylimine complexes. As far as it concerns the neutral derivatives, the only species, or the prevailing one, in solution is in all cases the *cis* isomer. The *trans* is present in small percentage just for complex **3a** (Table 2.3), having the phenyl substituent on the iminic carbon atom. As already reported in literature,[10,12] going from neutral to monocationic derivatives, there is a lack in the stereoselectivity of the coordination of the ligand to the palladium center. Taking into consideration the series of cationic complexes under investigation at the equilibrium, the *cis* isomer is the only species present or the prevailing one for complexes **2b** and **4b**; for complexes **1b-1d** almost a 1 : 1 ratio between the two isomers is observed, whereas for complex **3b** the major species is the *trans* isomer. The distribution of the two isomers in the neutral and monocationic complexes can be driven by steric and/or electronic reasons. In agreement with our previous hypothesis, for the neutral complexes, the prevalence of the *cis* isomer can be attributed to electronic reasons: assuming that the methyl and the chlorido ligands have a similar steric hindrance, the most stable isomer is the one that has the methyl, which is the ligand with the higher *trans*-influence, in *trans* position to the nitrogen atom having the lower Lewis basicity, that is the pyridine nitrogen, giving the *cis* isomer. In the cationic complexes there is a marked difference in

the steric hindrance of the coordinated ligands, methyl and acetonitrile, that can be also involved in affecting the coordination of the ligands to the palladium centre.

For complex **2b**, the only isomer present is the *cis* one, likely due to the steric hindrance induced by the methyl group on the sixth position of the pyridine ring. The amount of the *trans* isomer increases going from the aldimine (**4b**) to the ketimine with the methyl (**1b**) to the ketimine with the phenyl ring on the iminic carbon (**3b**). This trend should not be due to the steric hindrance around palladium, that does not change, but likely it might suggest that going from the aldimine to the ketimine with the phenyl the relative strength of the Lewis basicity of the two nitrogen atoms varies, being for ligand **4** the N_{py} the least basic between two, whereas for ligand **3** it is the strongest, and for **1** the two N atoms should have a similar Lewis basicity.

Table 2.3. Isomeric distribution at the equilibrium of the investigated neutral and cationic complexes.

	[Pd(CH_3)(Cl)(**N-N'**)]		[Pd(CH_3)($NCCH_3$)(**N-N'**)][PF_6]	
N-N'	*cis* (%)	*trans* (%)	*cis* (%)	*trans* (%)
1	99.9	0	56.5	43.5
2	99.9	0	99.9	0
3	93.3	6.7	24.8	75.2
4	99.9	0	91.0	9.0

*2.2.4. Ethylene/acrylic esters cooligomerization with Pd-complexes **1b-4b**, **1c-d**.*

The cationic complexes **1b-4b**, **1c**, **1d** were tested as precatalysts in the cooligomerization of ethylene with methyl acrylate (MA). The precatalyst **1b** was used also in the cooligomerization of ethylene with different acrylic esters such as *tert*-butyl acrylate (*t*BA) and methyl methacrylate (MMA). The cooligomerization reactions were performed in 2,2,2-trifluoroethanol (TFE) as solvent, over 18 h, with a pressure of ethylene of 2.5 bar, at 308 K and with [acrylic ester]/[Pd] ratio of 600. Complexes **1b** and **1d** were also tested in dichloromethane under the same conditions.

Before workup, a sample for GC-MS was taken in order to analyze the presence of alkene oligomers. The catalytic products were isolated as clear oils and characterized by NMR spectroscopy after removal of the volatile fraction at reduced pressure. The molecular weight of the produced cooligomers was estimated by integration of the ^{1}H NMR spectra.

The analogous complex [Pd(CH_3)(CH_3CN)(**1**)][B(Ar^F)] has already been reported in literature[12] as catalyst for the cooligomerization of ethylene with methyl acrylate or benzyl acrylate. However, no data regarding the productivity or its detailed catalytic behaviour are presented. Therefore, this work represents the first detailed study of the catalytic activity of pyridylimine-based palladium(II) complexes in the cooligomerization of ethylene with polar vinyl monomers.

Table 2.4. Ethylene/MA Cooligomerization: effect of N-N'.[a]
Precatalyst: [Pd(CH_3)($NCCH_3$)(**N–N'**)][PF_6].[a]

Run	**N-N'**	Yield (g)	g P/g Pd[b]	MA (% mol)[c]	TON MA[d]	TON E[d]	Higher alkenes[e]	M_n[c]
1	**1**	1.9235	863.8	13.1	337	2232	C4-C12, C5-C11 esters	293
2	**2**	0.0278	12.4	-	-	-	C4, traces of C6	-
3	**3**	0.3456	154.5	15.5	70	374	C4-C12, C5-C11 esters	312
4	**4**	0.3608	157.8	25.5	100	292	C4-C12, C5-C11 esters	303

[a] Reaction conditions: n_{Pd} = 21 x 10^{-6} mol; V_{TFE} = 21 mL; V_{MA} = 1.13 mL; [MA]/[Pd] = 600; T = 308 K; P_{et} = 2.5 bar; t = 18 h; [b] Productivity, grams product per gram of Pd, calculated on the isolated products; [c] Based on ^{1}H NMR spectroscopy on isolated product; [d] Turnover number = mol of substrate converted per mol of catalyst; [e] Evaluated with GC-MS analysis.

From the data reported in Table 2.4 it is clear how even slight variations in the N-N' ligand affect significantly the catalytic behaviour of the relevant complexes. Complex **1b** gives the most productive catalyst of the series (777.8 g P/g Pd, g P/g Pd = grams of product per gram of palladium). Instead, complex **2b**, which differs from **1b** just for the presence of a methyl substituent on the sixth position of the pyridine ring, is inactive, leading just to the formation of butenes. No formation of Pd black was evident.

Catalysts with ligands **4** and **3**, respectively the aldimine and the ketimine with a phenyl substituent on the iminic carbon, show similar productivities, that are one fifth of that obtained with catalyst with ligand **1** (Table 2.4, run 3 and 4 *vs* 1). In the case of the reaction catalyzed by **3b**, the low productivity can be traced back to the formation of inactive palladium metal, the sign of decomposition of the active species, that is common for Pd(II) complexes with nitrogen donor ligands.[10b,15,18] The data obtained for **4b** agree with data previously reported in literature, where catalysts with aldimine ligands were found less productive than those having the corresponding ketimines.[10,19] Again, no formation of metallic palladium was evident. The turnover number values

for both comonomers decrease going from **1b**, to **3b** to **4b**, and this effect is more pronounced in the case of ethylene rather than methyl acrylate (Table 2.4, run 1 *vs* 3 *vs* 4), suggesting a higher affinity of the complexes under investigation for the polar vinyl monomer, especially in the case of complex with ligand **4**. This is also reflected by the values of inserted MA, which increase following the same order and with precatalysts **4b** the content of inserted MA reaches the value of 25.5%, which is the highest of the series. The trend of the MA content might be attributed to the steric hindrance of the ancillary ligand, which decreases in the same order and is the lowest for **4**. It should be noted that for precatalysts **1b** the TON with respect to ethylene is almost 7 times as high as that with respect to methyl acrylate, whereas for **3b** and **4b** the difference is lower, thus suggesting that **1b** might be a potential good catalyst for ethylene oligomerization. For all the catalytic experiments, the GC-MS analysis of the product shows traces of higher alkenes and esters.

The characterization of the catalytic products was performed by NMR spectroscopy. In particular, in the ^{1}H NMR spectrum of the product of the catalysis with **2b** (Figure 2.32), the observed signals do not belong either to the precursor or to the free ligand. After a thorough NMR characterization, the main species formed is recognized to be the 5-membered metallacycle that is formed after the insertion of methyl acrylate into the Pd-H bond (see Scheme 2.8, intermediate D'). In paragraph 2.2.4 the reactivity of **2b** will be presented to try to elucidate this outcome.

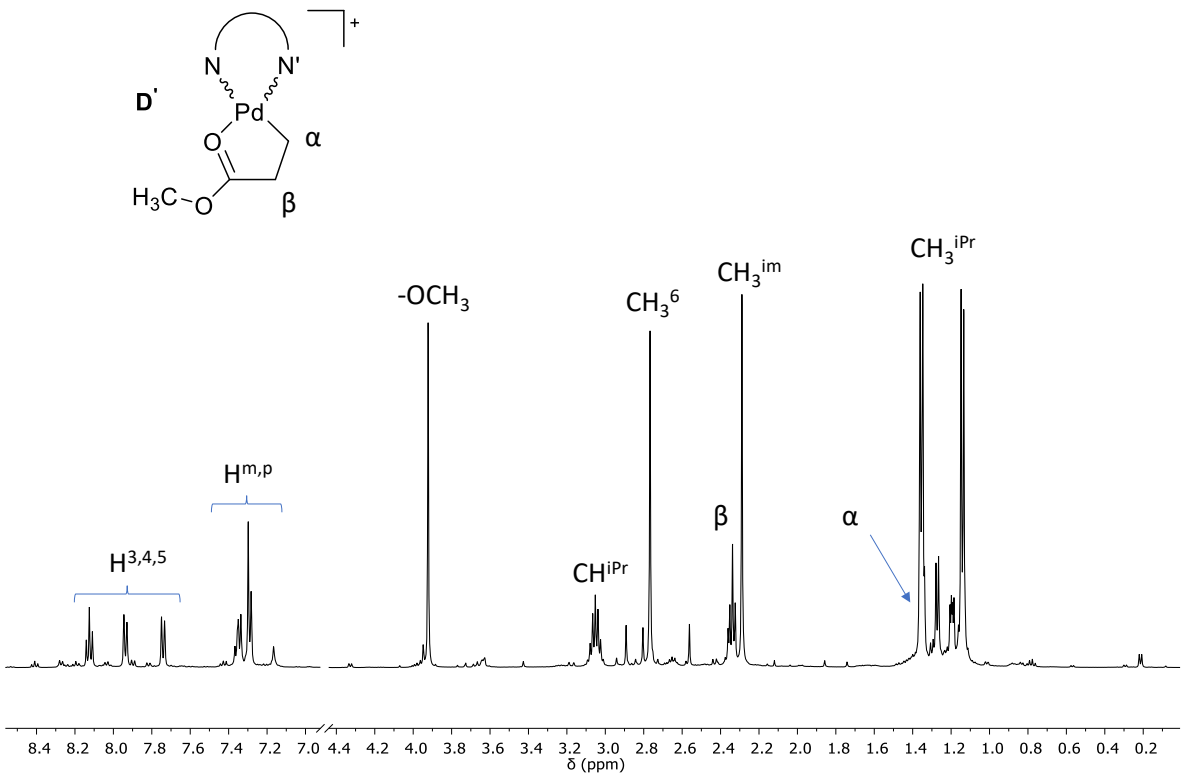

Figure 2.30. ^{1}H-NMR spectrum (CD_2Cl_2, 298 K) of the catalytic product of the cooligomerization of ethylene/methyl acrylate with **2b**.

The ^{1}H NMR spectra of the catalytic products obtained with the other precatalysts (Figure 2.31) confirm the cooligomeric nature of the products, that have the polar vinyl monomer inserted at the end of the branches, analogously to product obtain with Pd(II) complexes with Ar-BIAN and Ar-DAB ligands.

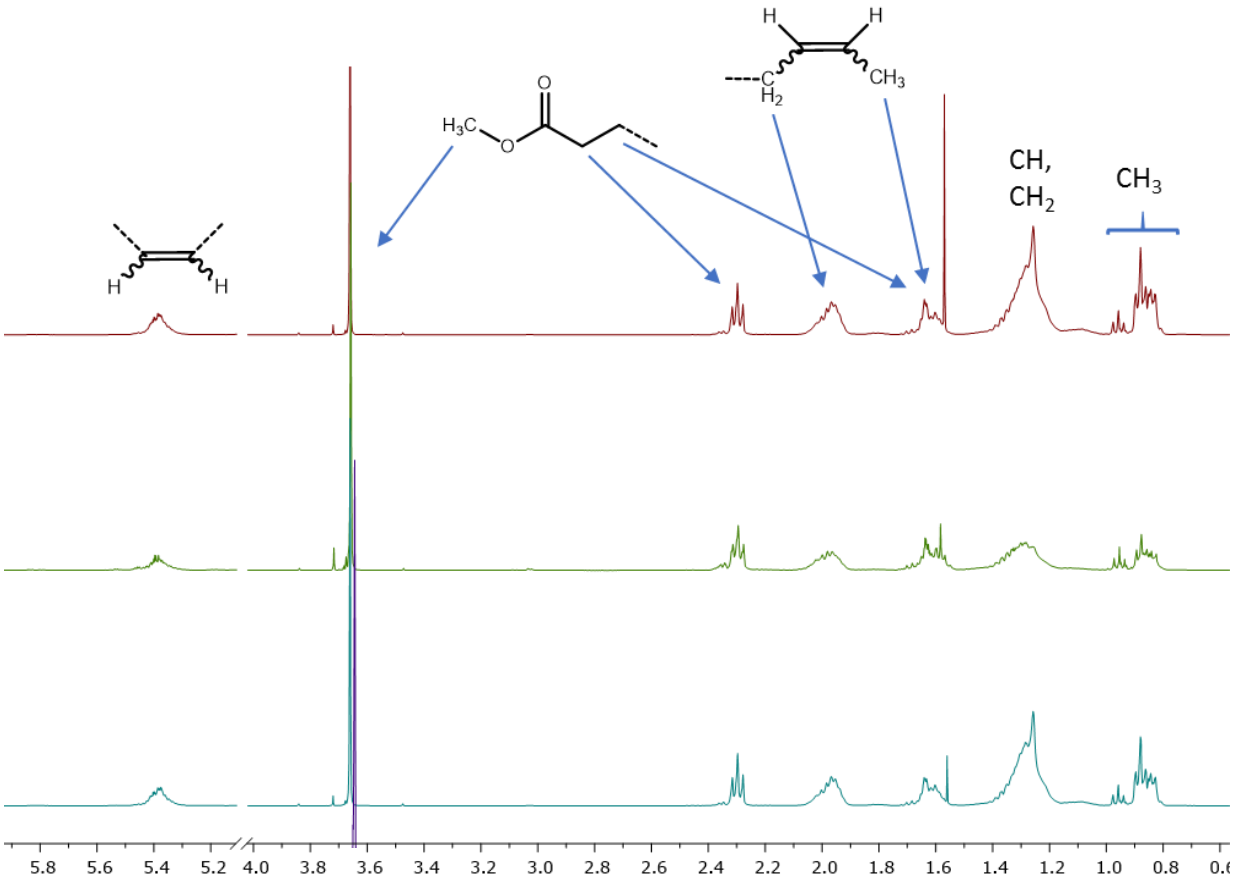

Figure 2.31. ^{1}H-NMR spectra ($CDCl_3$, 298 K) of the ethylene/methyl acrylate cooligomers obtained with precatalysts **1b** (top), **3b** (center), **4b** (bottom).

From the ^{13}C-NMR spectrum of the cooligomer obtained with precatalysts **1b** (Figure 2.32) some information about the structure of the cooligomers are obtained: the typical signals of branched oligomers are present (marked as brBn), with almost exclusively internal C-C double bonds (i, m, h vs n), with a *trans* geometry (g*E* vs g*Z*). Methyl acrylate is inserted only at the end of the branches, and the typical signal for the carbonyl of the ester group is visible at 174 ppm.

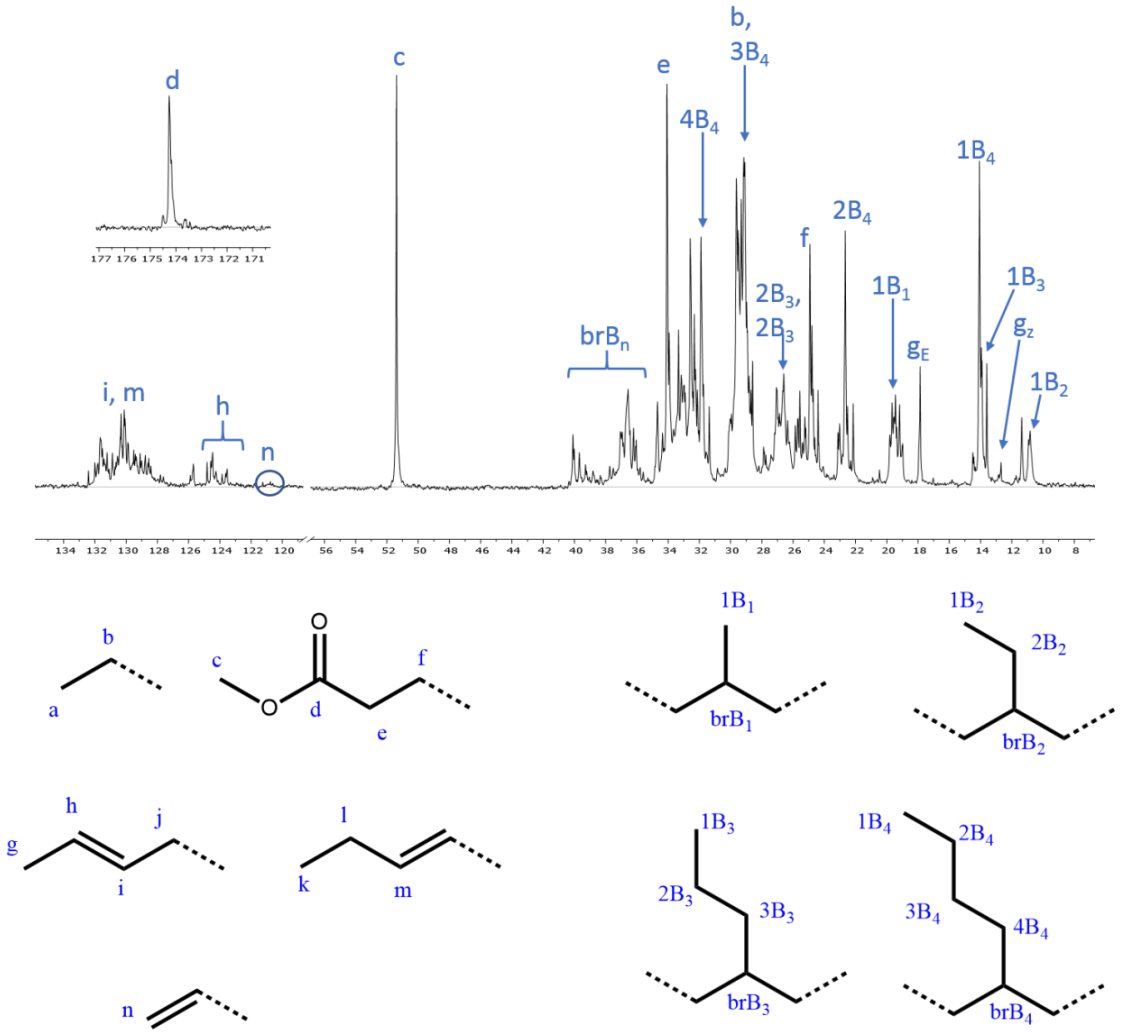

Figure 2.32. ^{13}C-NMR spectrum of the cooligomer obtained with **1b**.

Since the best results were obtained with complex **1b**, a more accurate study of its catalytic behaviour was performed.

The effect of the counteranion on the performance of the catalyst was firstly assessed, by testing **1b**, **1c** and **1d** in the cooligomerization reaction (Table 2.5).

Table 2.5. Ethylene/methyl acrylate cooligomerization: counteranion and solvent effect.[a] Precatalyst: [Pd(CH_3)($NCCH_3$)(**1**)][**X**].

Run	$\mathbf{X}^-$	solvent	Yield (g)	g P/g Pd[b]	MA (% mol)[c]	TON MA[d]	TON E[d]	M_n[c]
1	SbF_6^-	TFE	1.1243	503.1	14.8	217	1247	316
2	PF_6^-	TFE	1.7387	777.8	12.8	298	2041	293
3	OTf	TFE	2.4186	1085.0	7.1	255	3340	256
4	PF_6^-	DCM	0.1164	52.1	20.7	29	110	381
5	OTf	DCM	0.6607	295.7	15.9	134	711	284

[a] Reaction conditions: see Table 2.4; [b] Productivity, grams product per gram of Pd, calculated on the isolated products; [c] Based on ^{1}H NMR spectroscopy on isolated product; [d] Turnover number = mol of substrate converted per mol of catalyst.

When the solvent of choice is trifluoroethanol, there is a remarkable increase in the productivity going from **1c**, the precatalyst with hexafluoroantimonate as counteranion, to **1d**, that is the one with triflate (Table 2.5, runs 1-3). This trend is in contrast with what is usually reported in literature for analogous cationic catalysts, for which the productivity decreases with increasing the coordinating capability of the counteranion, due to the formation of the inner sphere ion pair.[20] The trend reported here suggests that this might not be related to the coordinating capability of the counteranion, and thus to the strength of the ion pair, but rather to the stability of the counteranion itself. It is known from literature that both hexafluoroantimonate and hexafluorophosphate, in the presence of traces of water and transition metals, can be hydrolysed;[17,21] in particular, for hexafluorophosphate, the obtained anion $PO_2F_2^-$ can coordinate to the palladium center, leading to the formation of inactive polynuclear species.[22] Actually, the hydrolysis of PF_6^- to $PO_2F_2^-$ was observed in the ^{19}F NMR spectrum of **1b** in CD_2Cl_2 after 15 h from dissolution (Figure 2.21). Moreover, the fact that this counteranion effect is visible in trifluoroethanol, a polar solvent with a high dielectric constant that disfavours the formation of ion pairs,[23] further supports our hypothesis. The counteranion effect is even more evident when dichloromethane is the solvent of choice. The productivity is more than one order of magnitude lower than that observed in trifluoroethanol, with evident decomposition to inactive palladium black. This data confirms the beneficial effect of the fluorinated solvent due to its capability of stabilizing the Pd-hydride intermediate.[18b,20d,24] In

addition, even in dichloromethane the productivity of the catalyst having the triflate as counteranion is higher than that of the active species with PF_6^-, thus supporting the hypothesis that the pyridylimines-based complexes might also catalyse the reaction of hydrolysis of PF_6^-. The nature of the solvent also affects the amount of polar monomer incorporated that is lower when the reaction is carried out in trifluoroethanol.

To further investigate this peculiar effect, different batches of **1b** were synthesized and obtained, with different amounts of acetonitrile of crystallization as determined by ^{1}H NMR spectroscopy. The presence of an excess of the labile ligand could help to highlight if it has an inhibiting ability on the catalytic process and if it is somehow linked to the counteranion effect. On increasing the amount of free acetonitrile the productivity decreases with the contemporary increase in the amount of formed Pd(0).

Table 2.6. Ethylene/methyl acrylate cooligomerization: effect of the acetonitrile excess.[a] Precatalyst: [Pd(CH_3)($NCCH_3$)(**1**)][PF_6], **1b.**

Run	Eq CH_3CN[b]	Yield (g)	g P/g Pd[c]	MA (% mol)[d]	Higher alkenes[e]
1	0.05	1.9235	863.8	13.1	C4-C12, C5-C11 esters
2	0.24	1.6537	739.7	10.0	C4-C12, C5-C11 esters
3	1.01	1.4458	645.6	14.6	C4-C12, C5-C11 esters

[a] Reaction conditions: see Table 2.4; [b] Productivity, grams product per gram of Pd, calculated on the isolated products; [c] Based on ^{1}H NMR spectroscopy on isolated product; [d] Turnover number = mol of substrate converted per mol of catalyst; [e] Evaluated with GC-MS analysis.

.

The inhibiting effect of acetonitrile can be explained by taking into consideration the need to have a free coordination site *cis* to the organometallic fragment, where the coordination of the incoming monomer can occur, followed by migratory insertion and chain growth of the cooligomer/copolymer (Scheme 2.7). The acetonitrile, the labile ligand commonly used for these complexes, when in excess, competes with the comonomers for the coordination to the palladium center, thus slowing down the growth of the cooligomer. The higher quantity of Pd(0) that is observed with the increasing amount of acetonitrile can be directly related to its inhibiting effect. The termination of the growing oligomeric chain (GOC) is due to the β-H elimination that leads to the Pd-H intermediate. From this intermediate, either decomposition to palladium black or a new coordination/insertion of ethylene can occur (Scheme 2.7). These two reactions are in competition

and depend on their relative rates. If coordination of ethylene is hampered by the presence of competing acetonitrile, the Pd-H decomposition prevails leading to inactive Pd black.

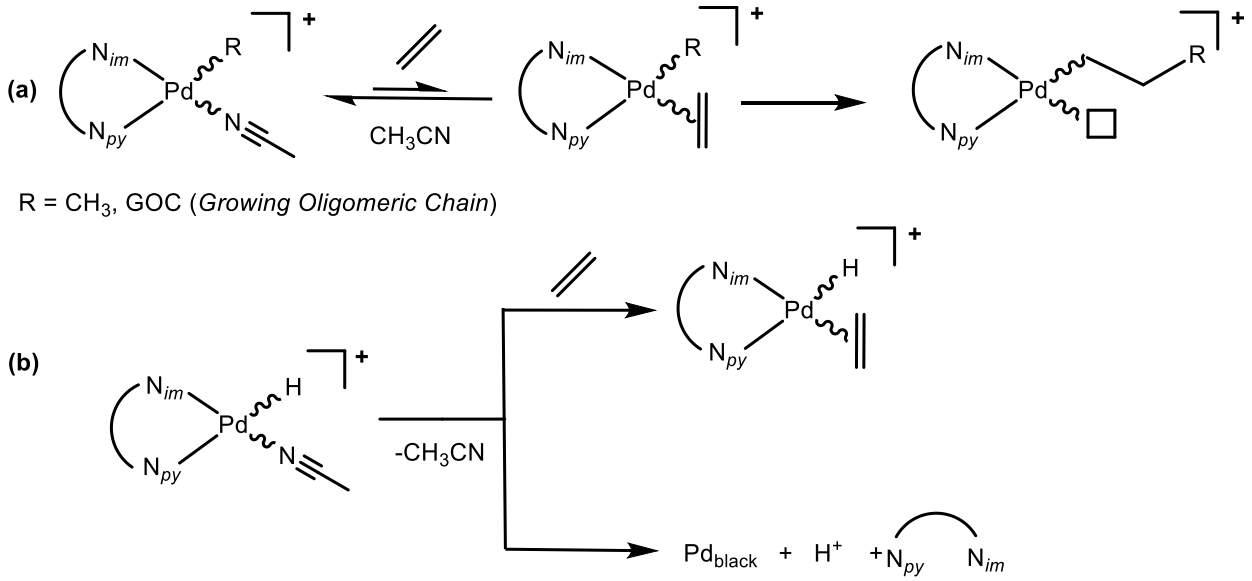

Scheme 2.7. Inhibiting effect of acetonitrile: a) cooligomer growth; b) start of a new chain.

The presence of more coordinating anions can thus be more favourable for the cooligomerization: the anion competes itself for the coordination site, but it does not bond directly with the palladium center, as also showed in paragraph 2.2.3. The proximity of the anion to the *cis* coordination site protects the latter from the "attack" of acetonitrile, favouring instead the coordination of ethylene.
At the end of all the catalytic runs, the formation of a double layer in the glass vessel (Figure 2.33).

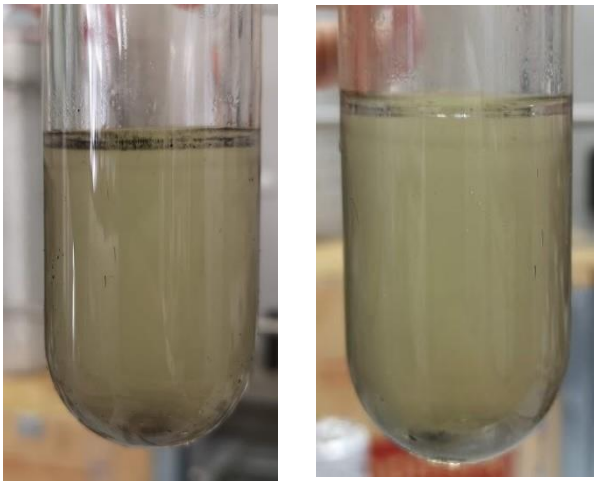

Figure 2.33. Double layer formation after 18 h of reaction (left), and after the recycling test (right).

The upper layer consists of the cooligomeric fraction only, whereas in the bottom one both the cooligomers and the catalyst are present, as determined by ^{1}H NMR spectroscopy. A preliminary recycling test was run upon separation of the cooligomeric layer formed after 18 h of reaction. Methyl acrylate was added,
the reactor pressurized again, and the cooligomerization reaction run for another 8 h. At the end, again a double layer was formed (with some formation of palladium black). The total yield at the end of the recycling trial is of 1.922 g, comparable to those obtained with the standard catalytic runs (Table 2.4, run 1), and of 2.2388 g if also the first separated fraction is considered. Even though this preliminary test is quite rudimental, it represents a promising first approach to the recycle of the homogeneous catalyst.

To further investigate the activity of complex **1b**, other acrylates were tested in the cooligomerization reaction, and precisely *tert*-butyl acrylate (tBA) and methyl methacrylate (MMA) (Table 2.7). Yields and productivities decrease going from MA to the other polar vinyl monomers. The ^{1}H NMR spectra of the isolated catalytic products (Figure 2.34) confirm the insertion of the polar comonomer and the formation of cooligomers. It is interesting to notice how the incorporation of the polar vinyl monomer is influenced by the steric hindrance of the employed monomer. When methyl methacrylate is used, a very low content of incorporation is achieved (Table 2.7, run 3), whereas with *tert*-butyl acrylate a content of 35% is reached, suggesting that the steric hindrance on the ester group is more tolerated rather than that on the carbon-carbon double bond.

Table 2.7. Ethylene/acrylic esters cooligomerization: comonomer effect.[a]
Precatalyst: [Pd(CH_3)($NCCH_3$)(**1**)][PF_6] **1b.**

Run	A	yield (g)	g P/g Pd[b]	Acrylic ester (% mol)[c]	TON A[d]	TON E[d]	Higher alkenes[e]	M_n[c]
1	MA	1.9235	863.8	13.1	337	2232	C4-C12, C5-C11 esters	293
3	MMA	1.2766	571.9	1.3	27	2070	C4-C6	220
2	*t*BuA	0.4601	205.5	35.6	123	222	Traces C4-C6	444

[a] Reaction conditions: see Table 2.4; [b] Productivity, grams product per gram of Pd, calculated on the isolated products; [c] Based on ^{1}H NMR spectroscopy on isolated product; [d] Turnover number = mol of substrate converted per mol of catalyst; [e] Evaluated with GC-MS analysis.

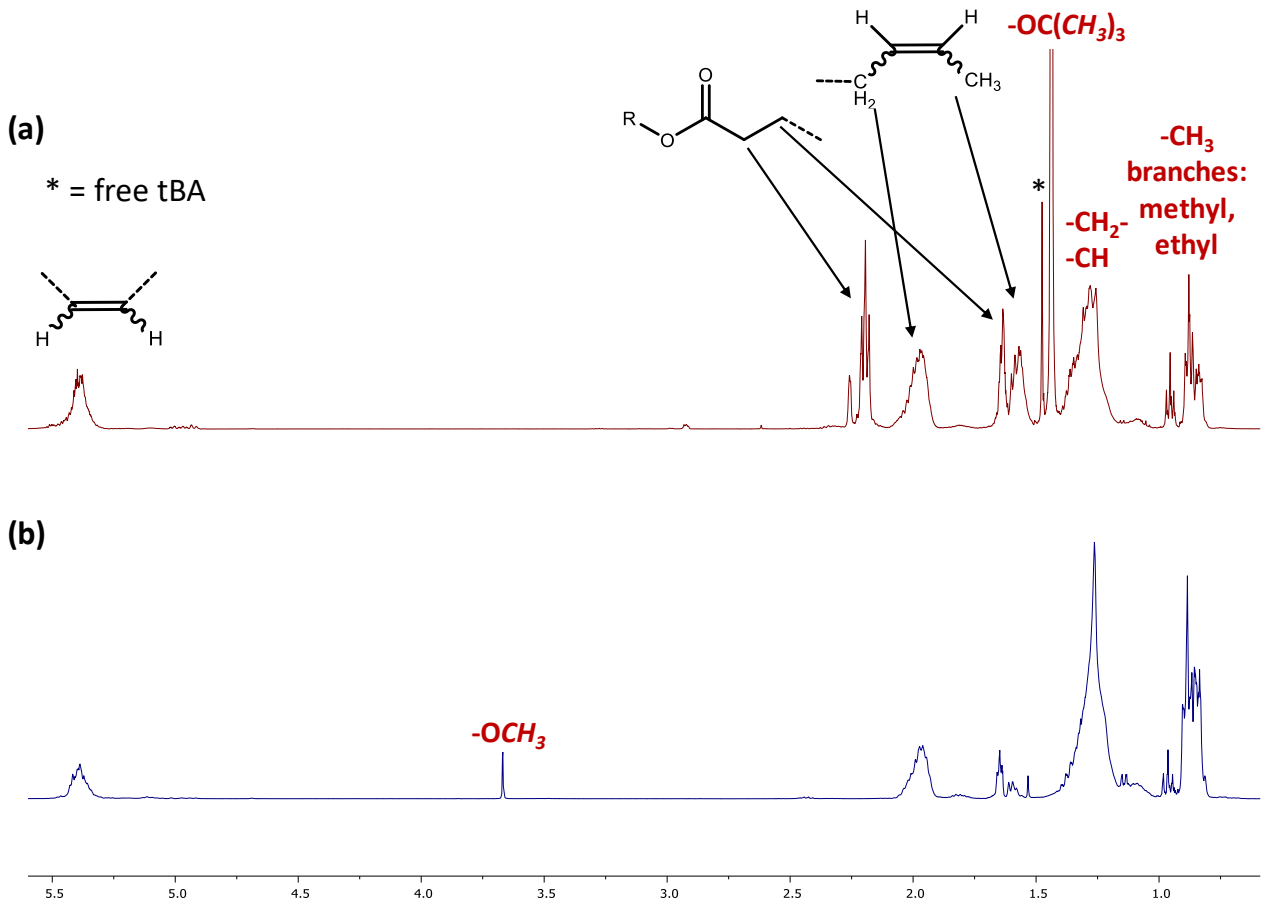

Figure 2.34. ^{1}H-NMR spectra ($CDCl_3$, 298 K) of cooligomerization products of **1b** and ethylene with: a) *tert*-butyl acrylate, b) methyl methacrylate.

*2.2.5. Reactivity of **1b** and **2b** with methyl acrylate*

The reactivity of precatalysts **1b**, the most productive, and **2b**, the inactive compound, towards methyl acrylate was studied by *in situ* NMR spectroscopy in CD_2Cl_2, at 298 K, adding 2 eq of the polar monomer to a 10 mM solution of the complex under investigation.

For symmetrical Pd-(α-diimine) precatalysts, the established mechanism for the reaction with MA is based on the migratory insertion of the polar monomer into the Pd-CH_3, that can occur with either primary or secondary regiochemistry. The latter is favoured by the chain walking process that leads to the intermediate C", a six membered metallacycle that is the catalyst resting state.[25] Typical intermediates can be recognized by ^{1}H NMR signals that can help us trace the reaction pathway. In the case of the studied pyridylimine complexes, we can assume that this mechanism is still valid, but we have to take into consideration that it can occur on both *cis* and *trans* isomers (Scheme 2.8).

.

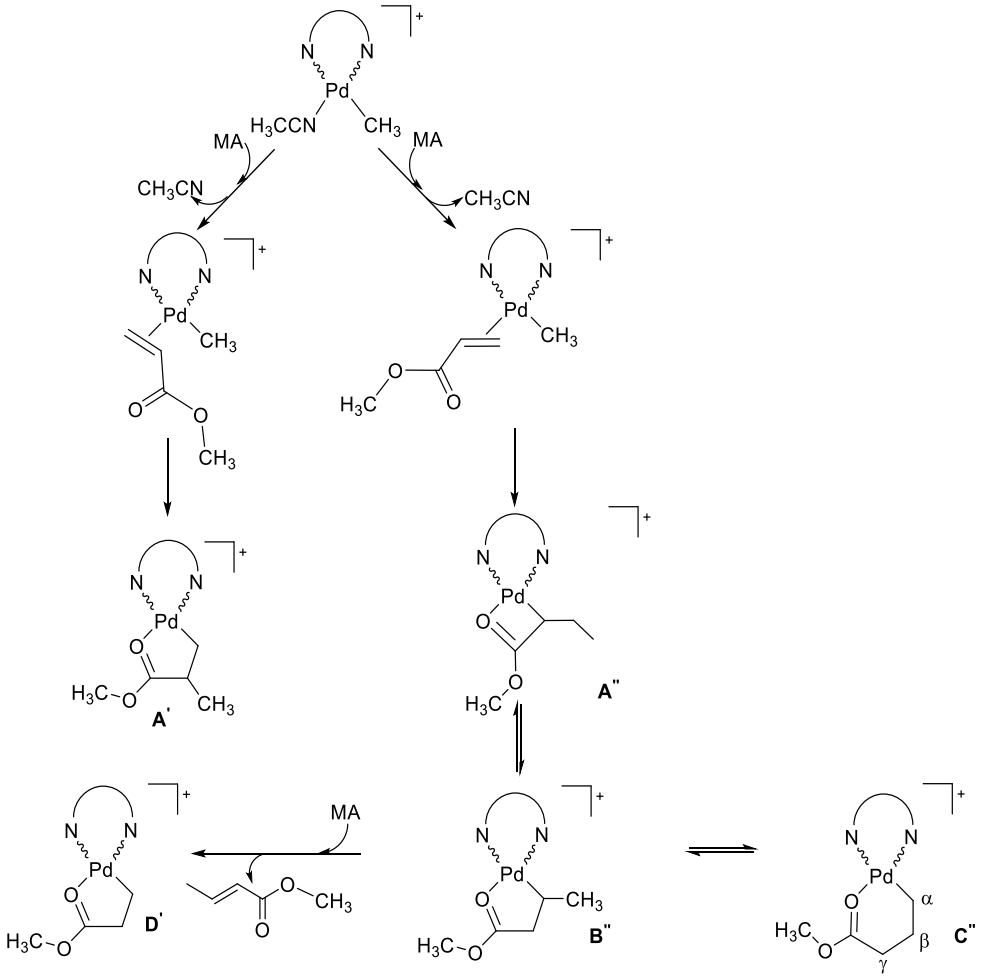

Scheme 2.8. Accepted mechanism for the reaction of Pd-(α-diimine) complexes with MA.

For **1b**, at the beginning of the reaction, both the *cis* and *trans* isomers are present in solution (Figure 2.35a). After the addition of methyl acrylate, the *cis* isomer is the first one that reacts with it, whereas the *trans* isomer starts to react at 15 min. This is in agreement with the rate of chain walking being faster than that of isomerization. After 3 h both isomers have reacted. In the first NMR spectrum recorder after the addition (Figure 2.35), three sets of signals start to appear, with the one that has the -OCH_3 peak at 3.04 ppm being the prevailing species, followed by the one at 3.58 ppm, and finally the one at 4.08 ppm.

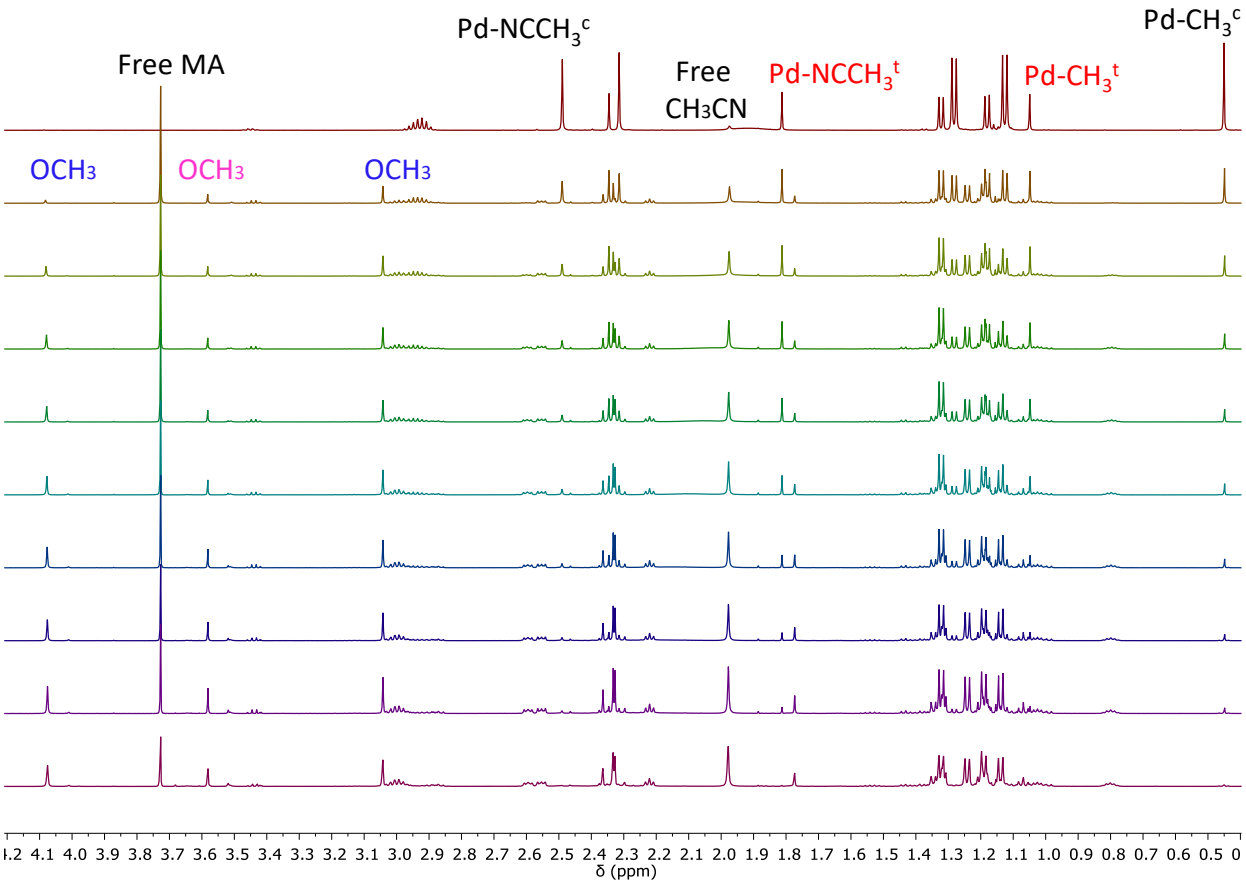

Figure 2.35. ^{1}H NMR spectra (CD_2Cl_2, 298 K) of the reactivity of **1b** with 2 equiv MA, aliphatic region, evolution with time.

The formation of new defined species is also visible in the aromatic region, in particular by looking at high frequencies, where usually the signals that are related to the protons in the sixth position of the pyridine ring appear (Figure 2.36).

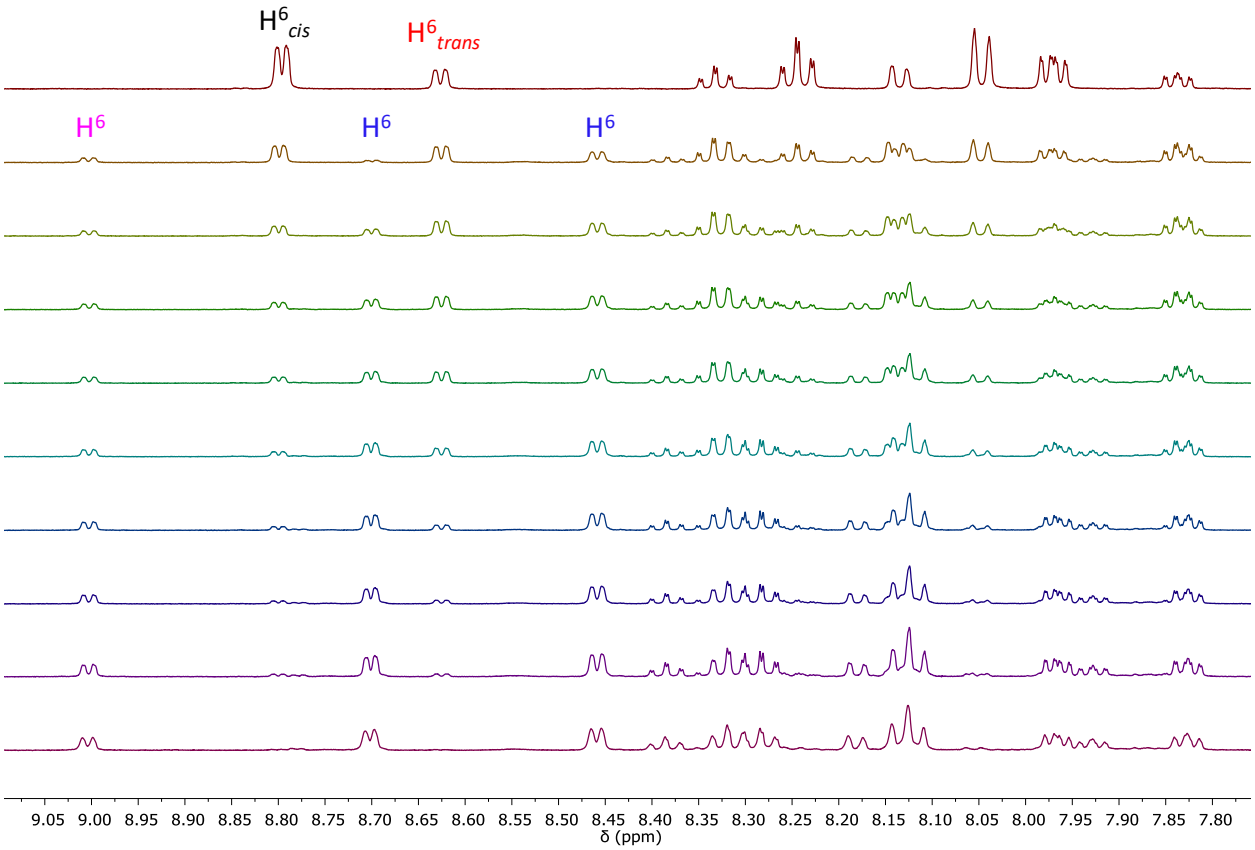

Figure 2.36. ^{1}H NMR spectra (CD_2Cl_2, 298 K) of the reactivity of **1b** with 2 equiv MA, aromatic region, evolution with time.

With a careful NMR characterization, the species that appear at the beginning of the reaction are assigned to i. C_{trans}'', that arises from the insertion of methyl acrylate with secondary regiochemistry into the Pd-CH_3 and that has the newly formed Pd-C bond trans to the N_{imino}, that is also the prevailing species; ii. C_{cis}'', the species that comes from the same reaction pathway as C_{trans}'' but has the Pd-C bond *cis* to the N_{imino} and iii. the open species O_{trans} that comes from the opening of the 4-membered metallacycle (Scheme 2.8, A'') that is the product of the migratory insertion with secondary regiochemistry. At the end of the reaction the three species are still present and are the prevailing ones, with an almost 1 : 1 ratio between the two C''isomers (42 % for C_{trans}'', 37 % for C_{cis}''), and a 2 : 1 ratio between the C''isomers and the open species (20 %).

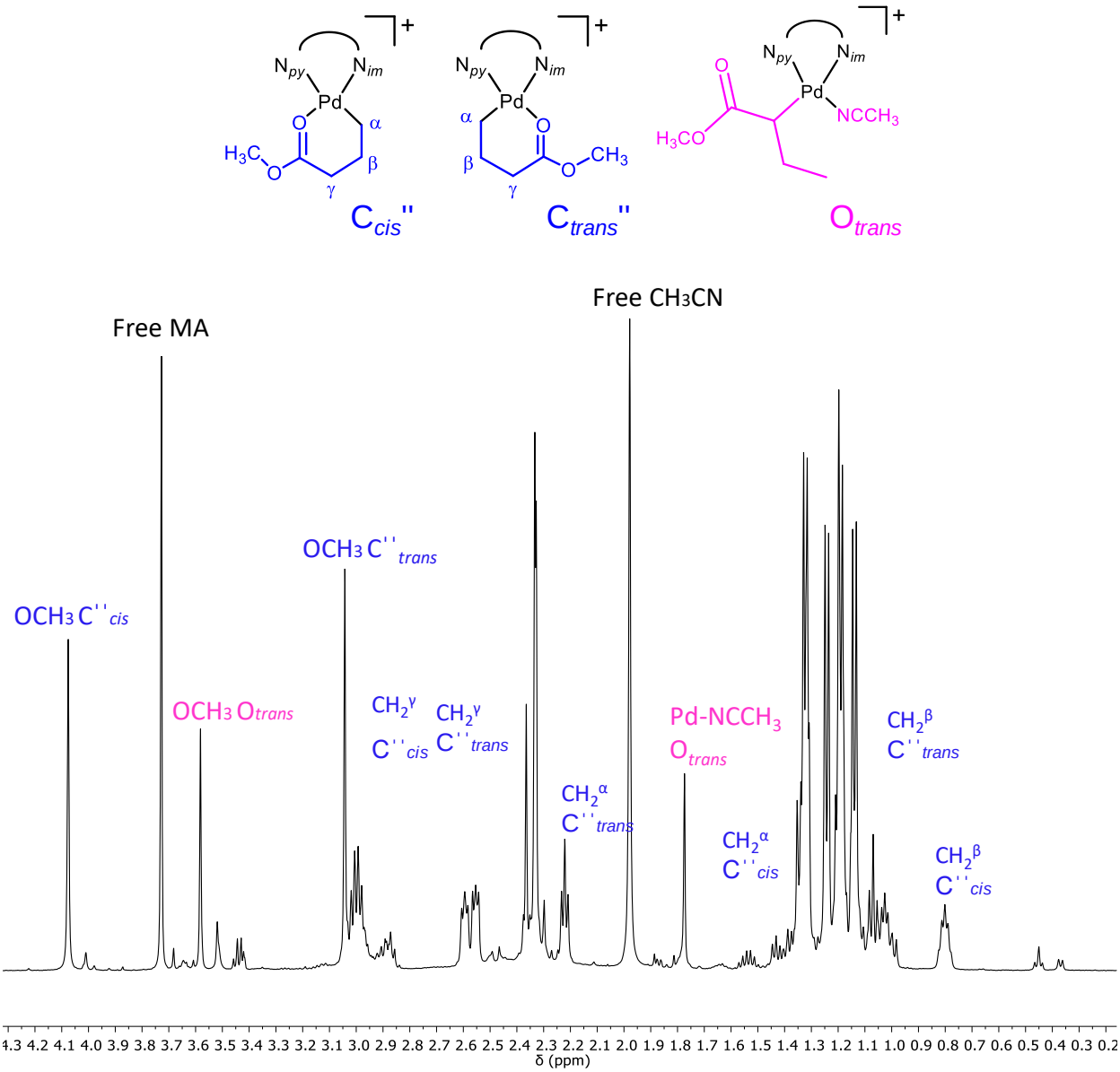

Figure 2.37. ^{1}H NMR spectra (CD_2Cl_2, 298 K) of the reactivity of **1b** with 2 equiv MA, aliphatic region, t = 3 h.

In particular, we assign the major species C_{trans}'' thanks to the NOE peak between the H^6 at 8.46 ppm, and the $CH_2\alpha$ at 2.21 ppm, that is clearly visible when the NOESY experiment was run after 3 h from the start of the reaction (Figure 2.38). A NOE peak is also visible between the H^6 at 9.00 ppm and the multiplet at 2.87 ppm, which allows to assign those signals to the O_{trans} species. The fact that H^6 of the latter falls at 9.00 ppm agrees with the fact that, with the open species, a hydrogen bond interaction can occur between the C=O of the inserted methyl acrylate and the proton on the pyridine rings, thus making it more deshielded with respect to those of the other intermediates. The relevant signal for the C_{cis}'' species was not detected.

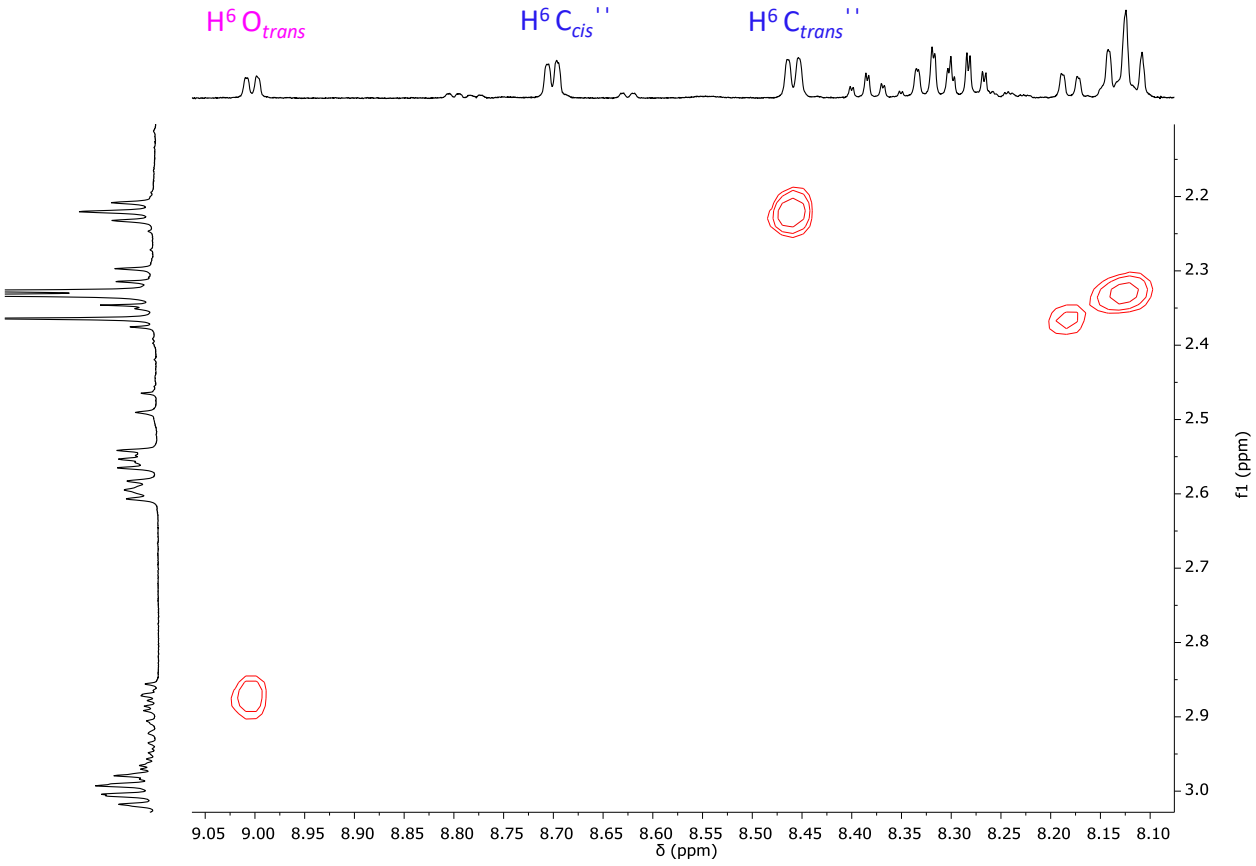

Figure 2.38. NOESY NMR spectra (CD_2Cl_2, 298 K) of the reactivity of **1b** with 2 equiv MA, magnification of the aromatic H^6 region, t = 3 h.

These data represent the first time that an open intermediate such as O_{trans} was detected in this kind of reactivity.

The reactivity of **2b** with MA is slower than that of **1b**, after 3 h only 23% has reacted, and even after 18 h from the beginning of the reaction there is no complete conversion of the starting material (Figure 2.39). However, the appearance of new species is evident after just 10 minutes of reaction: the signals at 0.44 ppm and at 1.51 ppm belong to the 5-membered metallacycle originated by the secondary insertion of methyl acrylate into the Pd-CH_3 bond, followed by chain walking (B''). After 3 h, it is possible to see also the signals that belong to the 6-membered metallacycle C'' that derives from B'' after the chain walking process. Methyl crotonate is also present after 1 h of reaction, and it is individuated by its common peaks at 1.88, 3.67, 5.76, 6.90 ppm. Alongside these signals, also those that can be attributed to the 5-membered metallacycle that is produced after the elimination of methyl crotonate and the insertion of a new molecule of methyl acrylate into the Pd-H bond are visible (D'), in agreement also with the outcome of the catalysis discussed in the

previous paragraph. Intermediate D' represents a dead-end of the catalytic cycle under the applied reaction conditions. It cannot be ruled out that by carrying out the catalytic tests at higher ethylene pressure the opening of the metallacycle occurs leading to the growth of cooligomers. At t = 18 h, the main species in solution other than the palladium precursor is methyl crotonate, followed by D'; B'' and C'' are present in traces, meaning that they are consumed over the course of the reaction. Also in this case the insertion of MA into the Pd-CH_3 appears to be highly regioselective, since it occurs always in a secondary fashion.

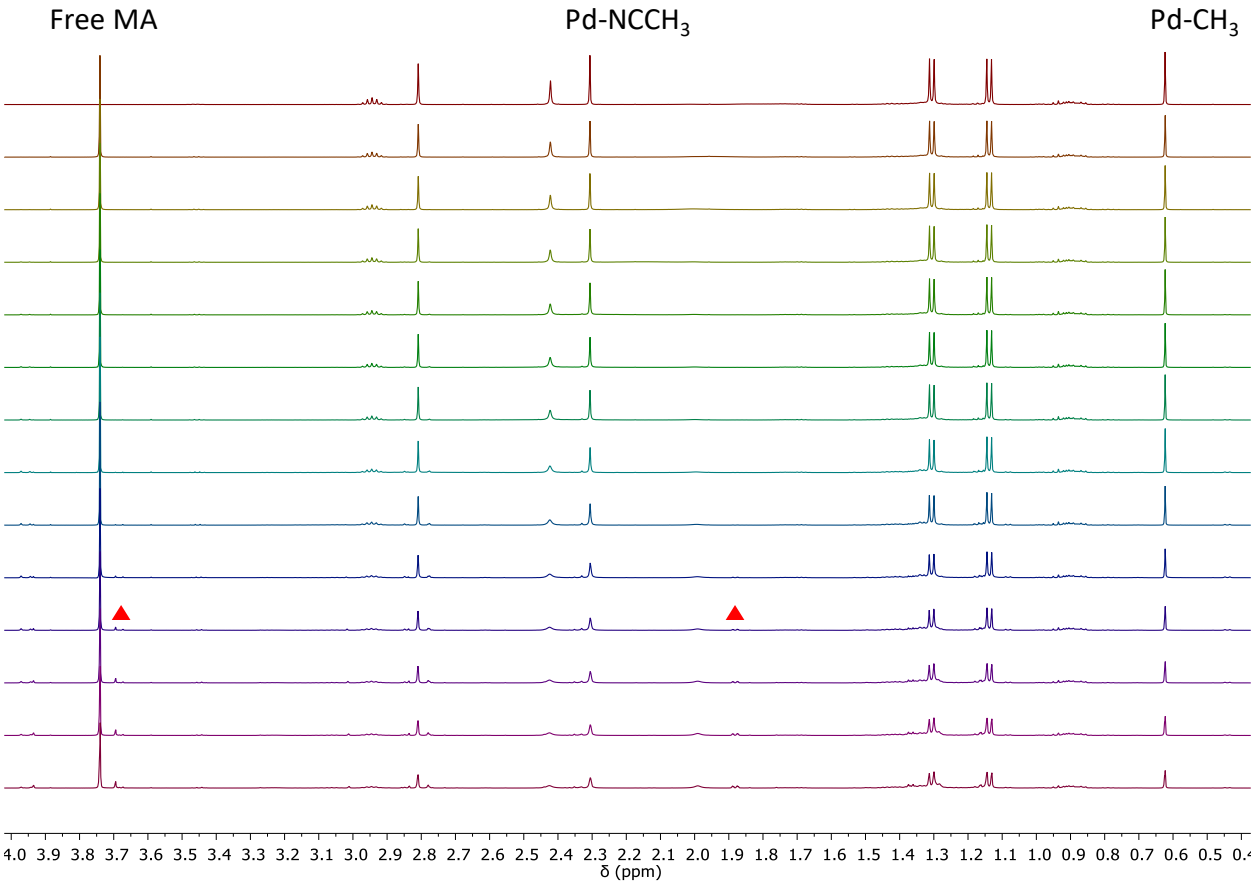

Figure 2.39. ^{1}H NMR spectra (CD_2Cl_2, 298 K) of the reactivity of **2b** with 2 equiv MA, evolution with time. ▲= methyl crotonate,

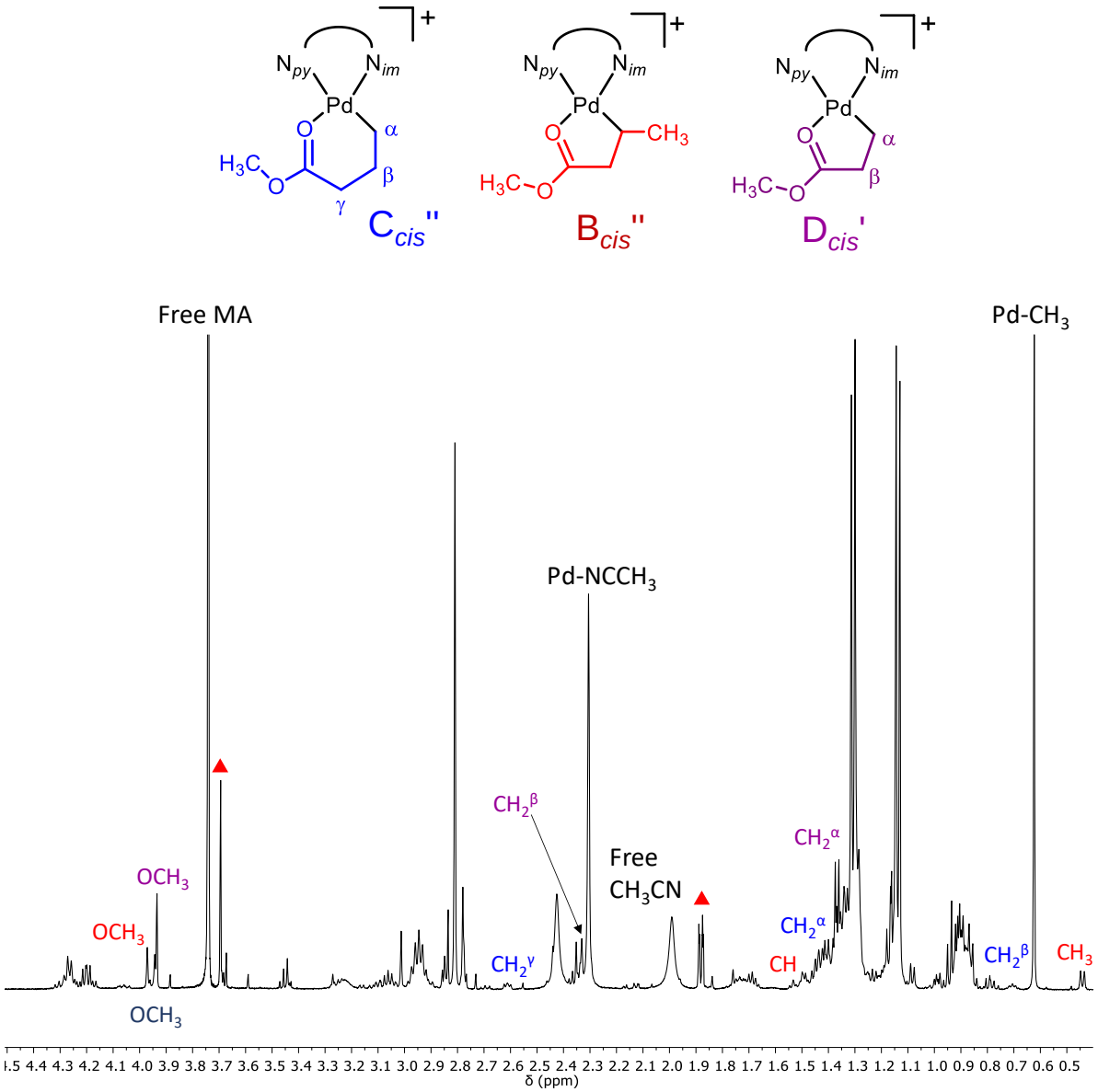

Figure 2.40. ^{1}H NMR spectra (CD_2Cl_2, 298 K) of the reactivity of **2b** with 2 equiv MA, t = 18 h, aliphatic region. ▲= methyl crotonate.

2.3. Conclusion

Pyridylimine Pd(II) complexes of the series [Pd(CH_3)Cl(N–N')] **1a-4a** and [Pd(CH_3)($NCCH_3$)(N–N')][X] **1b**–**4b** (X = PF_6^-), **1c** (X = SbF_6^-), **1d** (X = OTf) were synthesized and characterized in solution by NMR spectroscopy and, where possible, also in the solid state with X-ray diffraction.

The *cis/trans* isomeric distribution was analysed for both series of complexes, highlighting a prevalence of the *cis* isomer for the neutral complexes, and a general loss in the stereoselectivity of the coordination for the monocationic complexes. In particular, complexes of the series **1b-1d** showed that the rate of isomerization depends on the different counteranion employed.

The monocationic complexes **1b**-**4b**, **1c**, **1d** were tested in the copolymerization of ethylene and methyl acrylate. Furthermore, **1b**, taken as a reference compound, was tested also with other acrylic esters, such as methyl methacrylate and *tert*-butyl acrylate. Some general considerations can be made on the basis of the catalysis data:

- Cationic complexes with ligand **1** resulted to be the most productive (up to 1.1 kg of product/g Pd), whereas complex **2b** resulted to be inactive.
- The products, characterized with ^{1}H and ^{13}C NMR spectroscopy, have the polar monomer inserted at the end of the branches with a degree of incorporation that goes from 10.5 to 36 %; these values can be interesting for potential industrial applications.
- There is a remarkable counteranion effect on the catalysis: the more coordinating the anion, the more productive is the corresponding catalyst. This effect seems to be linked also to the presence of free acetonitrile in the starting material, and not in relation with the formation of ion pairs, but more likely it is related to the stability of the counteranion in solution.
- Complex **1b** is also active in the copolymerization of ethylene with other acrylic esters.

Overall, it is possible to state that the best catalytic results are the one obtained where a balance in the Lewis basicity of the two nitrogen donor atoms, Nimino and Npy, is present, that is the case of complex **1b** (*vs* **3b**, **4b**).

The possibility of recycling the homogeneous catalysts, which was assessed in a preliminary recycling test, opens up new interesting possibilities for this kind of systems.

Preliminary reactivity studies of complexes **1b** and **2b** shows the formation of metallacycles that are typical in the reactivity of Pd(II) complexes with α-diimines with methyl acrylate, but also there is evidence of the presence of an open species that was here reported for the first time.

2.4. Experimental

All complex manipulations were performed using standard Schlenk techniques under argon. Deuterated solvents (Cambridge Isotope Laboratories, Inc. (CIL)) were stored as recommended by CIL. 2-acetylpyridine, 2-acetyl-6-methylpyridine, 2-benzoylpyridine and 2,6-diisopropylaniline, TFE and the acrylic esters were purchased from Sigma-Aldrich and used without further purification for synthetic, spectroscopic and catalytic purposes. Ethylene (purity ≥ 99.9%) was purchased from SIAD and used as it is. Ligands 1, 2, 4 were synthesized according to literature procedures. Palladium(II) neutral complexes were synthesized using [Pd(cod)(CH_3)Cl], synthesized from [Pd($OCOCH_3$)$_2$] (Engelhard Italia), Benzonitrile (Sigma-Aldrich), HCl 37% (Fluka) and *cis*–*cis*–1,5–cyclooctadiene (Fluka) without further purification. The cationic complexes were synthesized from the appropriate AgX salt and anhydrous acetonitrile (Sigma-Aldrich). Dichloromethane (Sigma-Aldrich) used in the synthesis of Pd complexes was distilled over CaH_2 under argon atmosphere. Mono- and bidimensional NMR spectra were recorder on a Varian 500 spectrometer (500 MHz for ^{1}H, 125.68 MHz for ^{13}C), or on a Varian400 (400 MHz for ^{1}H, 100.55 MHz for ^{13}C, 376.3 MHz for ^{19}F and 161.9 MHz for ^{31}P), using the residual solvent peak as reference (CD_2Cl_2: 5.32 ppm for^{1}H NMR, 54.00 ppm for ^{13}C NMR; $CDCl_3$: 7.26 ppm for ^{1}H NMR, 77.16 ppm for ^{13}C NMR).

*2.4.1. Synthesis and characterization of ligands **1-4.***

Procedure for the synthesis of ligand **3**: To 1.0 mmol of 2-benzoylpyridine dissolved in 3 mL of methanol 1 equiv of aniline and 1 drop of sulphuric acid were added. The mixture was reacted in the microwave for 4.5 h at 373 K under stirring. The solvent was then removed under reduced pressure, obtaining a brown oil. Hexane was added and the mixture was left at 253 K for 18 h. Yellow crystal were obtained, then filtered and washed with cold n-hexane, and dried under vacuum. Yield: 16 %

1. ^{1}H NMR (400 MHz, $CDCl_3$, 298 K) δ 8.68 (ddd, *J* = 4.9, 1.8, 0.9 Hz, 1H), 8.36 (dt, *J* = 8.0, 1.1 Hz, 1H), 7.82 (ddd, *J* = 8.0, 7.5, 1.8 Hz, 1H), 7.39 (ddd, *J* = 7.5, 4.8, 1.2 Hz, 1H), 7.19 – 7.13 (m, 2H), 7.09 (dd, *J* = 8.6, 6.5 Hz, 1H), 2.75 (hept, *J* = 6.9 Hz, 2H), 2.21 (s, 3H), 1.15 (d, *J* = 6.9 Hz, 12H).

2. ^{1}H NMR (500 MHz, CD_2Cl_2) δ 8.13 (d, *J* = 7.8 Hz, 1H), 7.70 (t, *J* = 7.7 Hz, 1H), 7.26 (d, *J* = 7.6 Hz, 1H), 7.15 (d, *J* = 7.8 Hz, 2H), 7.09 – 7.03 (m, 1H), 2.73 (p, *J* = 6.8 Hz, 2H), 2.59 (s, 3H), 2.16 (s, 3H), 1.13 (dd, *J* = 11.1, 6.9 Hz, 12H). ^{13}C NMR (125.68 MHz, CD_2Cl_2, 298 K): δ 136.44 (H^4), 124.13 (H^5), 123.35 (H^m), 122.89 (H^p), 118.05 (H^3), 28.18 (CH-iPr), 24.19

(CH_3^6), 22.94, 22.69 (CH_3-iPr), 16.94 (CH_3^{im}) ppm; ESI-MS (m/z) : 295.2 $[M+H]^+$, 317.2 $[M+Na]^+$.

3. ^{1}H NMR (500 MHz, CD_2Cl_2, 298 K) δ 8.60 (d, J = 3.8 Hz, 1H), 8.56 (d, J = 4.1 Hz, 1H), 8.31 (d, J = 7.9 Hz, 1H), 7.88 (t, J = 7.5 Hz, 1H), 7.77 (d, J = 7.5 Hz, 1H), 7.50 (q, J = 7.3 Hz, 1H), 7.43 (t, J = 7.5 Hz, 1H), 7.40 (dd, J = 7.3, 5.5 Hz, 1H), 7.29 – 7.15 (m, 2H), 7.09 (d, J = 7.5 Hz, 1H), 7.04 – 6.89 (m, 4H), 2.95 (hept, J = 7.2 Hz, 1H), 2.87 (hept, J = 7.3 Hz, 1H), 1.12 (d, J = 6.7 Hz, 6H), 1.00 (d, J = 6.8 Hz, 3H), 0.94 (d, J = 6.9 Hz, 3H). ^{13}C NMR (125.68 MHz, CD_2Cl_2, 298 K): δ 148.97 (H^{6E}), 148.49 (H^{6Z}), 136.51 (H^{4E}), 135.36 (H^{4Z}), 130.41 ($H^{p'Z}$), 129.20 ($H^{o'E}$), 129.12 ($H^{o'Z}$), 128.75 ($H^{p'E}$), 128.06 ($H^{m'Z}$), 127.19 ($H^{m'E}$), 124.39 (H^{5E}), 123.50 ($H^{mZ,E}$, H^{pE}, H^{3Z}), 123.37 (H^{pZ}), 123.32 (H^{3E}) 123.28 (H^{5Z}), 122.51 ($H^{mZ,E}$, H^{pE}, H^{3Z}), 28.31 (CH-iPr^Z, CH-iPr^E), 23.52 (CH_3-iPr^Z, CH_3-iPr^E), 21.50 (CH_3-iPr^Z, CH_3-iPr^E) ppm; ESI-MS (m/z): 343.2 $[M+H]^+$.

4. ^{1}H NMR (500 MHz, CD_2Cl_2, 298 K) δ 8.74 – 8.63 (m, H^6), 8.32 – 8.21 (m, H^i + H^3), 7.96 – 7.71 (m, H^4), 7.42 (ddd, *J* = 7.5, 4.8, 1.2 Hz, H^5), 7.25 – 7.02 (m, H^m + H^p), 2.96 (hept, *J* = 6.9 Hz, CH-iPr), 1.16 (d, *J* = 6.8 Hz, CH_3-iPr) ppm; ^{13}C NMR (125.68 MHz, CD_2Cl_2, 298 K): δ 163.75 (H^i), 150.02 (H^6), 136.99 (H^4), 125.73 (H^5), 124.76, 123.40 (H^m, H^p), 121.43 (H^3), 28.31 (CH-iPr), 23.56 (CH_3-iPr) ppm; ESI-MS (*m/z*): 267.2 $[M+H]^+$, 289.1 $[M+Na]^+$.

2.4.2. Synthesis and characterization of [Pd(CH_3)Cl(N–N')] ***1a–4a.***

General procedure: To 1 equiv. of [Pd(cod)(CH_3)Cl] dissolved in 10 mL of distilled dichloromethane, 1.2 equiv. of ligand were added. The solution was left to stir at room temperature for 3 h. The solution was then concentrated under reduced pressure and diethyl ether was added to favour the precipitation of the product. The yellow precipitates were then filtered and washed with additional cold diethyl ether, then dried under vacuum.

1a. Yield = 97.5%; ^{1}H NMR (500 MHz, CD_2Cl_2, 298 K) δ 9.21 (ddd, J = 5.1, 1.7, 0.8 Hz, 1H), 8.09 (td, J = 7.8, 1.7 Hz, 1H), 7.91 (dt, J = 7.8, 1.0 Hz, 1H), 7.76 (ddd, J = 7.7, 5.1, 1.2 Hz, 1H), 7.39 – 7.19 (m, 3H), 3.07 (hept, J = 6.9 Hz, 2H), 2.21 (s, 3H), 1.29 (d, J = 6.8 Hz, 6H), 1.11 (d, J = 6.9 Hz, 6H), 0.30 (s, 3H).

2a. Yield = 87.5%; ^{1}H NMR (500 MHz, CD_2Cl_2, 298 K) δ 7.89 (d, J = 7.9 Hz, 1H), 7.76 (d, J = 7.8 Hz, 1H), 7.54 (d, J = 7.9 Hz, 1H), 7.33 – 7.24 (m, 3H), 3.11 (s, 1H), 3.10 (hept, J = 6.8 Hz, 2H), 2.17 (s, 1H), 1.30 (d, J = 6.8 Hz, 6H), 1.10 (d, J = 6.9 Hz, 6H), 0.52 (s, 3H). ^{13}C NMR (500 MHz, CD_2Cl_2, 298 K): δ 138.01, 130.25, 127.29, 123.88, 122.82, 27.98, 26.27, 23.70, 23.03, 20.19, 4.60; Elemental analysis, calcd for $C_{21}H_{29}N_2$ (%): C = 55.88, H = 6.48, N = 6.21; found: experimental: C = 55.52, H = 6.79, N = 6.59.

3a. Yield = 86.3%; ^{1}H NMR (500 MHz, CD_2Cl_2, 298 K) *cis* = 93.3% *trans* = 6.7%. *Cis*: δ 9.28 (ddd, J = 5.1, 1.7, 0.8 Hz, 1H), 7.94 (td, J = 7.8, 1.7 Hz, 1H), 7.75 (ddd, J = 7.7, 5.1, 1.2 Hz, 1H), 7.46 – 7.39 (m, 2H), 7.37 – 7.31 (m, 2H), 7.20 – 7.12 (m, 3H), 7.08 (d, J = 7.4 Hz, 2H), 3.10 (hept, J = 6.8 Hz, 2H), 1.31 (d, J = 6.7 Hz, 6H), 0.97 (d, J = 6.8 Hz, 6H), 0.37 (s, 3H). *Trans*: δ 8.82 (d, J = 5.6 Hz, 1H), 7.99 (td, J = 7.9, 1.6 Hz, 1H), 7.70 (ddd, J = 7.4, 5.5, 1.4 Hz, 1H), 7.46 (d, J = 7.9 Hz, 1H), 7.08 (1H), 7.02 (d, J = 7.7 Hz, 2H), 3.02 (hept, J = 6.8 Hz, 2H), 1.39 (d, J = 6.7 Hz, 6H), 1.08 (s, 3H), 0.96 (6H). ^{13}C NMR (500 MHz, CD_2Cl_2, 298 K): δ 149.22, 148.94, 138.42, 130.59, 128.49, 128.45, 128.31, 128.22, 12.32, 127.30, 123.61, 28.21, 23.65, 22.88, 2.04. Elemental analysis, calcd for $C_{25}H_{29}N_2$ (%): C = 60.13, H = 5.85, N = 5.61; found: C = 60.44, H = 5.79, N = 5.37.

4a. Yield = 77.0%; ^{1}H NMR (500 MHz, CD_2Cl_2, 298 K) δ 9.14 (d, J = 4.6 Hz, 1H), 8.36 (s, 1H), 8.11 (t, J = 7.7 Hz, 1H), 7.85 (d, J = 7.7 Hz, 1H), 7.81 (dd, J = 7.6, 5.2 Hz, 1H), 7.37 – 7.32 (m, 1H), 7.28 (d, J = 7.6 Hz, 2H), 3.26 (hept, J = 6.8 Hz, 2H), 1.32 (d, J = 6.8 Hz, 6H), 1.14 (d, J = 6.9 Hz, 6H), 0.49 (s, 3H). ^{13}C NMR (500 MHz, CD_2Cl_2, 298 K): δ 167.77, 149.50, 138.86, 129.03, 127.77, 126.74, 124.18, 27.88, 24.45, 22.29, -0.46. Elemental analysis, calcd for $C_{19}H_{25}N_2$ (%): C = 53.91, H = 5.95, N = 6.62; found: C = 54.00, H = 5.72, N = 6.46.

2.4.3. Synthesis and characterization of [Pd(CH$_3$)(NCCH$_3$)(N–N')][X] ***1b–4b, 1c, 1d.***

General procedure: To 1 equiv. of the neutral precursor dissolved in 6 mL of distilled dichloromethane, 1.2 equiv. of the desired AgX salt dissolved in 1.5 mL of dry acetonitrile were added. The reaction mixture was left to stir in the dark for 2.5 h. The suspension of AgCl was filtered over Celite® and washed with dichloromethane. The solution was then concentrated under reduced pressure and diethyl ether was added to favour the precipitation of the product. The bright yellow solids were then filtered under reduced pressure, washed with cold diethyl ether and dried under vacuum.

1b. Yield = 99.9%; ^{1}H NMR (500 MHz, CD_2Cl_2) *cis* = 56.5% *trans* = 43.5%. *Cis*: δ 8.82 (d, *J* = 5.1 Hz, 0H), 8.27 (td, *J* = 7.9, 1.4 Hz, 1H), 8.07 (d, *J* = 7.9 Hz, 1H), 7.99 (dd, *J* = 7.3, 5.6 Hz, 1H), 7.39 (dd, 1H), 7.32 (d, *J* = 7.5 Hz, 2H), 2.95 (hept, *J* = 6.5 Hz, 2H), 2.51 (s, 3H), 2.34 (s, 3H), 1.31 (d, *J* = 6.8 Hz, 6H), 1.15 (d, *J* = 6.8 Hz, 6H), 0.48 (s, 3H). *Trans*: δ 8.65 (d, *J* = 5.4 Hz, 1H), 8.36 (td, *J* = 7.9, 1.6 Hz, 1H), 8.17 (d, *J* = 7.9 Hz, 1H), 7.86 (ddd, *J* = 7.7, 5.5, 1.4 Hz, 1H), 7.36 (1H). 7.35 (2H), 2.97 (hept, *J* = 6.8 Hz, 2H), 2.37 (s, 3H), 1.84 (s, 3H), 1.35 (d, *J* = 6.8 Hz, 6H), 1.20 (d, *J* = 6.9 Hz, 6H), 1.07 (s, 3H). ^{13}C NMR (500 MHz, CD_2Cl_2): δ 149.73, 149.68, 141.29, 140.43, 130.55, 129.30, 128.31, 128.28, 127.88, 127.77, 126.57, 124.22, 124.07, 28.38, 23.61, 23.48, 23.37, 22.89, 19.37, 18.03, 4.89, 3.41, 2.89, 1.91, 1.72.

Elemental analysis, calcd for $C_{22}H_{30}N_3$ (%): C = 44.95 %, H = 5.14 %, N = 7.15 %; found: C = 45.05 %, H = 5.12 %, N = 6.95 %.

1c. Yield = 71.4%; ^{1}H NMR (500 MHz, CD_2Cl_2) *cis* = 56.5% *trans* = 43.5%. *Cis:* δ 8.93 (d, *J* = 4.7 Hz, 1H), 8.28 (t, *J* = 7.6 Hz, 1H), 8.10 (d, *J* = 7.9 Hz, 1H), 8.05 (dd, *J* = 7.5, 5.5 Hz, 1H), 7.39 (dd, *J* = 8.6, 6.9 Hz, 1H), 7.32 (d, *J* = 7.2 Hz, 2H), 2.96 (hept, *J* = 6.8 Hz, 2H), 2.56 (s, 3H), 2.34 (s, 3H), 1.31 (d, *J* = 6.8 Hz, 6H), 1.15 (d, *J* = 6.9 Hz, 6H), 0.47 (s, 3H). *Trans:* δ 8.63 (d, *J* = 6.1 Hz, 1H), 8.37 (td, *J* = 7.9, 1.6 Hz, 1H), 8.21 (d, *J* = 8.0 Hz, 1H), 7.85 (ddd, *J* = 7.3, 5.4, 1.4 Hz, 1H), 7.38 – 7.27 (m, 3H), 2.92 (hept, *J* = 6.8 Hz, 2H), 2.36 (s, 3H), 1.82 (s, 3H), 1.32 (d, *J* = 6.8 Hz, 6H), 1.18 (d, *J* = 6.9 Hz, 6H), 1.05 (s, 3H). Elemental analysis, calcd for $C_{22}H_{30}N_3$ (%): C = 38.93 %, H = 4.46 %, N = 6.19 %; found: C = 39.00 %, H = 4.76%, N = 6.57 %.

1d. Yield = 96.0%; ^{1}H NMR (500 MHz, CD_2Cl_2) *cis* = 56.5% *trans* = 43.5%. *Cis:* δ 8.76 (d, *J* = 4.4 Hz, 1H), 8.28 (t, *J* = 7.8 Hz, 1H), 8.08 (d, *J* = 7.9 Hz, 1H), 7.98 (dd, *J* = 7.8, 5.1 Hz, 1H), 7.43 – 7.27 (m, 3H), 2.94 (hept, *J* = 6.8 Hz, 2H), 2.50 (s, 3H), 2.34 (s, 3H), 1.31 (d, *J* = 6.7 Hz, 6H), 1.15 (d, *J* = 6.8 Hz, 6H), 0.48 (s, 3H). *Trans:* δ 8.65 (d, *J* = 5.1 Hz, 1H), 8.35 (t, *J* = 7.9 Hz, 1H), 8.14 (d, *J* = 7.9 Hz, 1H), 7.86 (dd, *J* = 7.8, 5.3 Hz, 1H), 7.47 – 7.24 (m, 3H), 2.96 (hept, *J* = 6.9 Hz, 2H), 2.37 (s, 3H), 2.28 (s, 3H), 1.35 (d, *J* = 6.6 Hz, 6H), 1.20 (d, *J* = 6.8 Hz, 6H), 1.07 (s, 3H). Elemental analysis, calcd for $C_{22}H_{30}N_3$ (%): C = 46.66 %, H = 5.11 %, N = 7.10 %; found: C = 46.91 %, H = 5.10 %, N = 6.80 %.

2b. Yield = 89.6%; ^{1}H NMR (500 MHz, CD_2Cl_2) δ 8.12 (t, *J* = 7.9 Hz, 1H), 7.94 (d, *J* = 7.8 Hz, 1H), 7.74 (d, *J* = 7.9 Hz, 1H), 7.39 (dd, *J* = 8.5, 7.0 Hz, 1H), 7.32 (d, *J* = 7.4 Hz, 2H), 2.96 (hept, *J* = 6.8 Hz, 2H), 2.82 (s, 3H), 2.43 (s, 3H), 2.32 (s, 3H), 1.32 (d, *J* = 6.8 Hz, 6H), 1.15 (d, *J* = 6.9 Hz, 6H), 0.63 (s, 3H). ^{13}C NMR (500 MHz, CD_2Cl_2): δ 140.04, 131.01, 128.30, 128.24, 124.56, 124.32, 28.22, 25.92, 23.64, 22.92, 20.22, 8.67, 3.44.

3b. Yield = 99.9%; ^{1}H NMR (500 MHz, CD_2Cl_2) *cis* = 24.8% *trans* = 75.2%. *Cis:* δ 8.91 (d, *J* = 5.1 Hz, 1H), 8.11 (td, *J* = 7.9, 1.6 Hz, 1H), 8.00 (ddd, *J* = 7.8, 5.1, 1.2 Hz, 1H), 7.53 (d, *J* = 7.9 Hz, 1H), 7.49 (t, *J* = 7.5 Hz, 1H), 7.39 (t, *J* = 7.8 Hz, 2H), 7.25 – 7.21 (m, 1H), 7.18 (d, *J* = 8.2 Hz, 2H), 7.12 (d, *J* = 7.7 Hz, 2H), 3.02 (hept, *J* = 6.7 Hz, 2H), 2.54 (s, 3H), 1.32 (d, *J* = 6.7 Hz, 6H), 1.00 (d, *J* = 6.8 Hz, 6H), 0.55 (s, 3H). *Trans:* δ 8.72 (d, *J* = 5.4 Hz, 1H), 8.21 (td, *J* = 7.9, 1.5 Hz, 1H), 7.88 (ddd, *J* = 7.8, 6.3, 1.4 Hz, 1H), 7.69 (d, *J* = 7.9 Hz, 1H), 7.53 (t, *J* = 6.9 Hz, 1H), 7.46 (d, *J* = 7.2 Hz, 2H), 7.29 – 7.14 (m, 5H), 3.01 (hept, *J* = 7.0 Hz, 2H), 1.82 (s, 3H), 1.38 (d, *J* = 6.8 Hz, 6H), 1.19 (s, 3H), 1.02 (d, *J* = 6.8 Hz, 6H). ^{13}C NMR (500 MHz, CD_2Cl_2): δ 150.19, 150.08, 140.72, 139.85, 131.63, 131.33, 138.58, 130.37, 129.70, 129.28,

128.86, 128.48, 128.47, 128.43, 128.11, 127.53, 123.98, 123.97, 28.44, 24.37, 23.49, 22.84, 22.60, 7.16, 3.46, 3.33, 2.01, 1.90.

4b. Yield = 86.4%; ^{1}H NMR (500 MHz, CD_2Cl_2) *cis* = 91.0% *trans* = 9.0%. *Cis:* δ 8.83 (d, *J* = 5.0 Hz, 1H), 8.32 (s, 1H), 8.23 (t, *J* = 7.8 Hz, 1H), 8.02 – 7.93 (m, 2H), 7.37 (t, *J* = 7.9 Hz, 1H), 7.28 (d, *J* = 7.6 Hz, 2H), 3.08 (hept, 2H), 2.50 (s, 3H), 1.29 (d, *J* = 6.8 Hz, 6H), 1.13 (d, *J* = 6.9 Hz, 6H), 0.61 (s, 3H). *Trans:* δ 8.62 (s, 1H), 8.40 (s, 1H), 8.32 (1H), 8.10 (d, *J* = 7.7 Hz, 1H), 7.86 (t, *J* = 6.8 Hz, 1H), 7.42 – 7.23 (m, 3H), 3.14 (hept, *J* = 6.3 Hz, 2H), 1.89 (s, 3H), 1.32 (d, *J* = 6.9 Hz, 6H), 1.24 – 1.16 (m, 9H). ^{13}C NMR (500 MHz, CD_2Cl_2): δ 171.98, 151.09, 140.91, 131.53, 129.01, 128.84, 124.28, 28.51, 24.66, 24.36, 23.10, 22.58, 5.05, 3.67.

*2.4.4. In situ isomerization kinetics of cationic complexes **1b, 1c, 1d**.*

A 10 mM solution in CD_2Cl_2 (vial) was prepared, and a first ^{1}H NMR spectrum recorded. The reaction was followed over time, at T = 298 K, to monitor the evolution of the *cis/trans* isomeric composition, until the equilibrium was reached. The time necessary to record every ^{1}H NMR spectrum (60 s) is taken into account when analysing the kinetic data.

2.4.5. Ethylene/acrylic esters cooligomerization reactions. All catalytic experiments were carried out in a Büchi "tinyclave" reactor equipped with an interchangeable 50 mL glass vessel. The liner was loaded with the complex of choice (21 μmol), TFE (21 mL) or distilled CH_2Cl_2 (22 mL) and the desired acrylic ester (ratio [A]/[Pd] = 600). The vessel was then placed in a preheated oil bath (308 K), connected to the ethylene tank, and then ethylene was bubbled for 10 min. The reactor was pressurized, and the reaction mixture stirred at constant temperature and pressure. After the proper time, the reactor was cooled to room temperature and vented. 200 μL of the reaction mixture were withdrawn and diluted in MeOH for GC-MS analysis. The reaction mixture was poured in a 50 mL flask with dichloromethane (3 x 2 mL) used to clean the glass vessel. In some cases, it was possible to observe the formation of Pd black. Volatile products were removed under reduced pressure and the residual oil was left to dry at constant weight, then analysed with NMR spectroscopy.

2.4.6. General procedure for the in situ 1H NMR reactivity of the cationic complexes with methyl acrylate. A 10 mM solution in CD_2Cl_2 (vial) of the desired complex was prepared and a first 1H NMR spectrum recorded. 2 equiv. of methyl acrylate were added. The reaction was followed over time, at T = 298 K to monitor the disappearing of Pd-CH_3. The time necessary

to record every ^{1}H NMR spectrum (60 s) is taken into account when analysing the kinetic data.

2.5. Bibliography

1. a) Small, B. L.; Brookhart, M.; Bennett, A. M. A. *J. Am. Chem. Soc.* 1**998**, *120*, 4049; b) Britovsek, G. J. P.; Gibson, V. C.; Kimberley, B. S.; Maddox, P. J.; McTavish, S. J; Solan, G. A.; White, A. J. P.; Williams, D. J. *Chem. Commun.* 1**998**, 849; c) Ittel, S. D.; Johnson, L.K.; Brookhart, M. *Chem. Rev.* **2000**, *100*, 1169; Gibson, V. C.; Spitzmesser, S. K. *Chem. Rev.* **2003**, *103*, 283.

2. a) Bianchini, C.; Giambastiani, G.; Luconi, L.; Meli, A. *Coord. Chem. Rev.* **2010,** *254*, 431; b) Boudier, A., Breuil, P. R., Magna, L., Olivier-Bourbigou, H., Braunstein, P. *Chem. Commun*. **2014**, *50*, 1398.

3. Chen, Z., Allen, K. E., White, P. S., Daugulis, O., Brookhart, M. *Organometallics* **2016,** *35*, 1756.

4. Chen, X. L., Gao, J., Liao, H., Gao, H. Y., Wu, Q. *Chin. J. Polym. Sci*. **2018**, *36*, 176.

5. Yorke, J., Dent, C., Decken, A., Xia, A. B. *Inorganic Chem. Commun.* **2010,** *13*, 54.

6. Cao, Y., Zhang, Y., Zhang, L., Zhang, D., Leng, X., Huang, Z. *Org. Chem. Front.* **2014,** *1*, 1101.

7. a) Elantabli, F. M., Radebe, M. P., Motswainyana, W. M., Owaga, B. O., El-Medani, S. M., Ekengard, E., Haukka, M., Nordlander, E., Onani, M. O. *J. Organomet. Chem.* **2017,** *843*, 40; b) Chen, W., Xi, C., Yang, K. *Appl. Organometal. Chem*. **2007**, *21*, 641.

8. a) Reddy, E. R., Trivedi, R., Sarma, A. V. S., Sridhar, B., Anantaraju, H. S., Sriram, D., Yogeeswari, P., Nagesh, N. *Dalton T.* **2015,** *44*, 17600; b) Li, J., Guo, L., Tian, Z., Tian, M., Zhang, S., Xu, K., Qian, Y., Liu, Z. *Dalton Trans.* **2017**, *46*, 15520; c) Nomoto, A., Sakamoto, N., Sakai, Y. *Res. Chem. Intermed.* **2019**, *45*, 3.

9. a) Nitschke, J. R. *Acc. Chem. Res.* **2007**, *40*, 2; b) Castilla, A. M., Ramsay, W. J., Nitschke, J. R. *Acc. Chem. Res.* **2014**, *47*, 2063; c) Hardy, M., Struch, N., Topic, F., Schnakenburg, G., Rissanen, K., Lützen, A. *Inorg. Chem.* **2018**, *57*, 3507.

10. a) Canil, G., Rosar, V., Dalla Marta, S., Bronco, S., Fini, F., Carfagna, C., Durand, J., Milani, B. *Chem. Cat Chem* **2015,** *7*, 2255; b) Rosar, V., Dedeic, D., Nobile, T., Fini, F., Balducci, G., Alessio, E., Carfagna, C., Milani, B. *Dalton Trans.* **2016,** *45*, 14609.

11. a) Nakamura, A., Ito, S., Nozaki, K. *Chem. Rev*. **2009**, 109, 5215; b) Ito, S., Nozaki, K. *Chem. Rec*. **2010**, 10, 315; c) Nakamura, A., Anselment, T. M. J., Claverie, J., Godall, B., Jordan, R. F., Mecking, S., Rieger, B., Sen, A., van Leeuwen, P. W. N. M., Nozaki, K. *Acc. Chem. Res*. **2013**, 46, 1438; d) Rünzi, T., Mecking, S. *Adv. Funct. Mat*. **2014**, 24, 387; e) Carrow, B. P., Nozaki, K. *Macromolecules* **2014**, 47, 2541; f) Si, G., Na, Y., Chen, C. *Chem Cat Chem* **2018**, *10*, 5135.

12. Meneghetti, S. P., Lutz, P. J., Kress, J. *Organometallics* **1999,** *18*, 2734.

13. Dai, Q., Jia, X., Yang, F., Bai, C., Hu, Y., Zhang, X. *Polymers* **2016,** *8*, 12.

14. Rulke, R. E., Ernsting, J. M., Spek, A. L., Elsevier, C. J., van Leeuwen, P. W. N. M., Vrieze, K. *Inorg. Chem.* **1993,** *32*, 5769.

15. Durand, J., Zangrando, E., Stener, M., Fronzoni, G., Carfagna, C., Binotti, B., Kamer, P. C. J., Müller, C., Caporali, M., van Leeuwen, P. W. N. M., Vogt, D., Milani, B. *Chem. Eur. J.* **2006,** *12*, 7639.

16. a) Groen, J. H., de Jong, B. J., Ernsting, J. M., van Leeuwen, P. W. N. M., Vrieze, K., Smeets, W. J. J., Spek, A. L. *J. Organomet. Chem.* **1999**, *573*, 3; b) Milani, B., Marson, A., Zangrando, E., Mestroni, G., Ernsting, J. M., Elsevier, C. J. *Inorg. Chim. Acta* **2002**, *327*, 188.

17. Fernandezgalan, R., Manzano, B. R., Otero, A., Lanfranchi, M., Pellinghelli, M. A. *Inorg. Chem.* **1994,** *33*, 2309.

18. a) Milani, B., Vicentini, L., Sommazzi, A., Garbassi, F., Chiarparin, E., Zangrando, E., Mestroni, G. *Dalton Trans.* **1996,** *14*, 3139; b) Milani, B., Anzilutti, A., Vicentini, L., Santi, A. S. O., Zangrando, E., Geremia, S., Mestroni, G. *Organometallics* **1997,** *16*, 5064; c) Milani, B., Corso, G., Mestroni, G., Carfagna, C., Formica, M., Seraglia, R. *Organometallics* **2000,** *19*, 3435; d) Amoroso, F., Zangrando, E., Carfagna, C., Müller, C., Vogt, D., Hagar, M., Ragaini, F., Milani, B. *Dalton Trans* **2013**, 42, 14583.

19. Britovsek, G. J. P., Bruce, M., Gibson, V. C., Kimberley, B. S., Maddox, P. J., Mastroianni, S., McTavish, S. J., Redshaw, C., Solan, G. A., Stromberg, S., White, A. J. P., Williams, D. J. *J. Am. Chem. Soc.* **1999,** *121*, 8728.

20. a) Macchioni, A. *Chem. Rev.* **2005,** *105*, 2039; b) Macchioni, A., Bellachioma, G., Cardaci, G., Travaglia, M., Zuccaccia, C., Milani, B., Corso, G., Zangrando, E., Mestroni, G., Carfagna, C., Formica, M. *Organometallics* **1999**, *18*, 3061; c) Chen, E. Y., Marks, T. *Chem. Rev.* **2000**, *100*, 1391; d) Rosar, V., Meduri, A., Montini, T., Balducci, G., Zangrando, E., Fornasiero, P., Milani, B. *Chem cat Chem* **2017**, *9*, 3402.

21. a) Dermitzaki, D., Raptopoulou, C. P., Psycharis, V., Escuer, A., Perlepes, S. P., Stamatatos, T. C. *Dalton Trans* **2014**, 43, 14520; b) Konidaris, K. F., Polyzou, C. D., Kostakis, G. E., Tasiopoulos, A. J., Roubeau, O., Teat, S. J., ManessiZoupa, E., Powell, A. K., Perlepes, S. P. *Dalton Trans* **2012**, *41*, 2862; c) Ponikvar, M., Zemva, B., Liebman, J. F. *J. Fluorine Chem.* **2003,** *123*, 217.

22. Dall'Anese, A., Rosar, V., Cusin, L., Montini, T., Balducci, G., D'Auria, I., Pellecchia, C., Fornasiero, P., Felluga, F., Milani, B. *Organometallics* **2019**, *38*, 3498.

23. Eckstrom, H. C., Berger, J. E., Dawson, L. R. *J. Phys. Chem.* **1960**, *64*, 1458.

24. Sirbu, D., Consiglio, G., Milani, B., Kumar, P. G. A., Pregosin, P. S., Gischig, S. *J. Organomet. Chem.* **2005,** *690*, 2254.

25. Mecking, S., Johnson, L. K., Wang, L., Brookhart, M. *J. Am. Chem. Soc.* **1998,** *120*, 888.

CHAPTER 3

Palladium Catalyzed Ethylene/Methyl Acrylate Copolymerization: Moving from the Acenaphthene to the Phenanthrene Skeleton of α-Diimine Ligands

Overview

Palladium(II) complexes with α-diimine ligands having a phenanthrene skeleton and 2,6-disubstituted aryl rings (Ar-BIP) were synthesized, characterized and tested as precatalysts in the copolymerization of ethylene with methyl acrylate. X-ray characterization in solid state and NMR analysis in solution of both neutral, [Pd(Ar-BIP)(CH_3)Cl], and monocationic [Pd(Ar-BIP)(CH_3)(CH_3CN)][PF_6] complexes, indicate that the Ar-BIP ligands have a higher Lewis basicity and are more strongly coordinated to the metal center than the Ar-BIAN counterparts previously reported in literature. Therefore, the Pd-(Ar-BIP) cationic complexes can be regarded as electron-rich metal cations. The monocationic species generate active catalysts for the ethylene/methyl acrylate copolymerization leading to copolymers with M_n values up to 37000 and a content of polar monomer of 5.3 mol %. The detailed study of the catalytic behavior points out that Pd-(Ar-BIP) catalysts show a good affinity for the polar monomer, a good thermal stability and favor the cleavage of the catalyst resting state, leading to copolymer with M_w values higher than that of the macromolecules produced with the corresponding Pd-(Ar-BIAN) under the same reaction conditions. NMR characterization of the produced copolymers points out that the polar monomer is inserted both at the end of the branches and into the main chain, with a more selective enchainment than that achieved when the copolymerization is carried out in dichloromethane. In situ NMR investigations allowed us to detect relevant intermediates of the catalytic cycle and shed light on the nature of possible deactivation species.

Part of this Chapter was published in the work:
Dall'Anese, A., Rosar, V., Cusin, L., Montini, T., Balducci, G., D'Auria, I., Pellecchia, C.; Fornasiero, P., Felluga, F., Milani, B., *Organometallics* **2019**, *38*, 3498.

3.1. Introduction

As previously mentioned in Chapter 1, most of the studies on Pd(II) catalysts with α-diimine ligands are focused on the variation of the aryl ring substituents, whereas the effect of the variation of the ligand backbone is less investigated. Phenanthrene based α-diimines (Ar-BIP) were reported for the first time in 1996 by Elsevier,[1] and have been recently reconsidered as ancillary ligands for catalysts for ring-opening polymerization of *rac*-lactides,[2] ethylene polymerization,[2b] and isoprene polymerization.[2c]

In this Chapter the catalytic behavior of organometallic Pd(II) complexes with Ar-BIP ligands in the ethylene/methyl acrylate copolymerization reaction will be presented; the studied ligands have either an isopropyl group or a methyl on the *ortho* positions of the aryl rings (Ligands **5-6** in Figure 3.1). The molecule with the simple phenyl and the 2,6-dimethyl substituted acenaphthene-based α-diimine were considered as reference compounds (Ligands **6-7** in Chart 3.1).

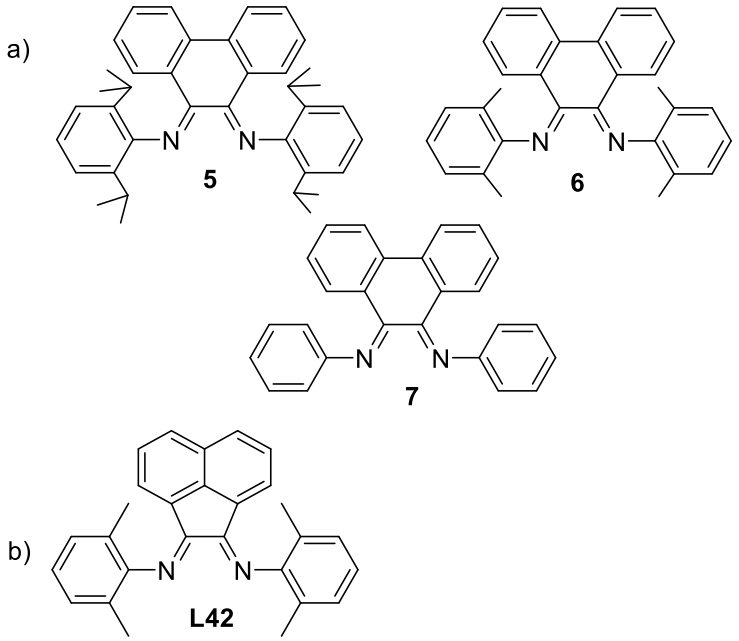

Figure 3.1. α-diimines under investigation: Ar-BIP molecules; b) already reported α-diimine.

The coordination chemistry of ligands **5-7** to Pd(II) has been investigated in detail, and remarkable differences with respect to the behavior the corresponding Ar-BIAN molecules were found. All of the ligands were already reported in literature, but not yet applied to this particular field of organometallic chemistry and catalysis. Neutral, [Pd(Ar-BIP)(CH_3)Cl], and monocationic, [Pd(Ar-BIP)(CH_3)($NCCH_3$)][PF_6], complexes were studied, and the latter were

also used as precatalysts in the ethylene/methyl acrylate copolymerization reaction. The reactivity of [Pd(Ar-BIP)(CH_3)($NCCH_3$)][PF_6] complexes with methyl acrylate was investigated by *in situ* NMR spectroscopy, allowing us to highlight a new possible deactivation pathway for the catalyst.

3.2. Results and discussion

3.2.1. Synthesis and characterization of ligands **5-7**.

For the synthesis of ligands **5-7**, of the three different synthetic methodologies present in the literature,[1,2] only the one based on the reaction of 9,10-phenanthrenequinone with the desired aniline, at room temperature, in the presence of $TiCl_4$, resulted to be successful in our hands.[3]

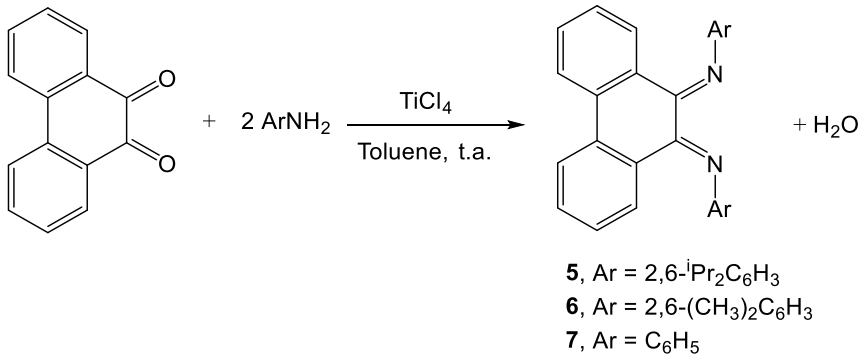

Scheme 3.1. Condensation synthesis of the BIP ligands at room temperature

Ligands **5-7**, isolated in moderate yields (40 – 60 %) as solids of orange (**5**, **6**) or red (**7**) color, were characterized by mass spectrometry and NMR spectroscopy in solution. In analogy to Ar-BIAN molecules, also for Ar-BIPs *E,Z*, *E,E*, and *Z,Z* isomers are possible depending on the relative configuration of the aryl rings with respect to the C=N imine bonds (Figure 3.2). In agreement with literature, in the ^{1}H NMR spectra of **5** and **6**, recorded in $CDCl_3$ at 298 K, the number of signals and their integration indicated the presence in solution of the nonsymmetrical *E,Z* isomer (Figure 3.3),[2a,2b,3] whereas for **7** the symmetrical *Z,Z* isomer was present (Figure 3.4).[1,2]

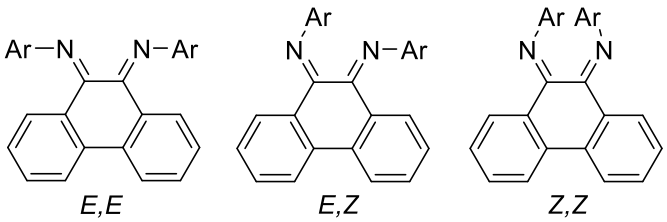

Scheme 3.2. *E,E*, *E,Z*, and *Z,Z* isomers for Ar-BIP ligands.

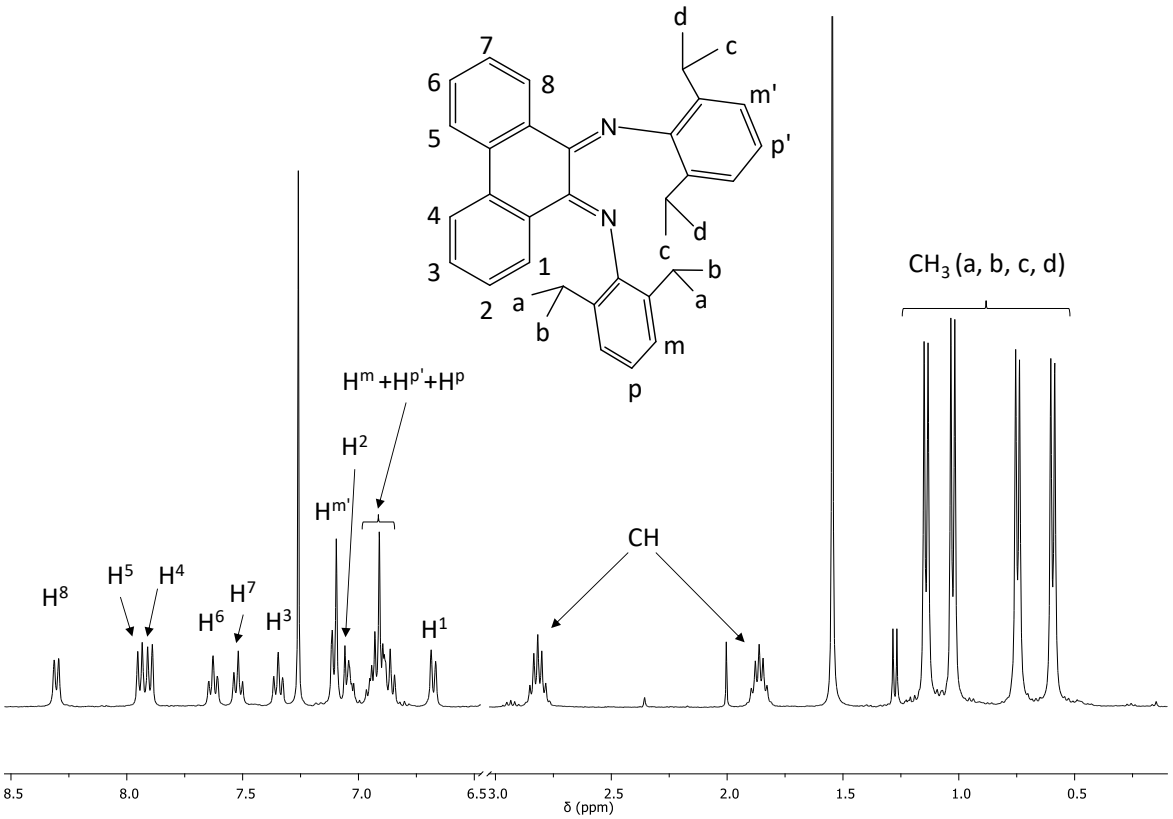

Figure 3.3. ^{1}H NMR ($CDCl_3$, 298 K) spectrum of **5**.

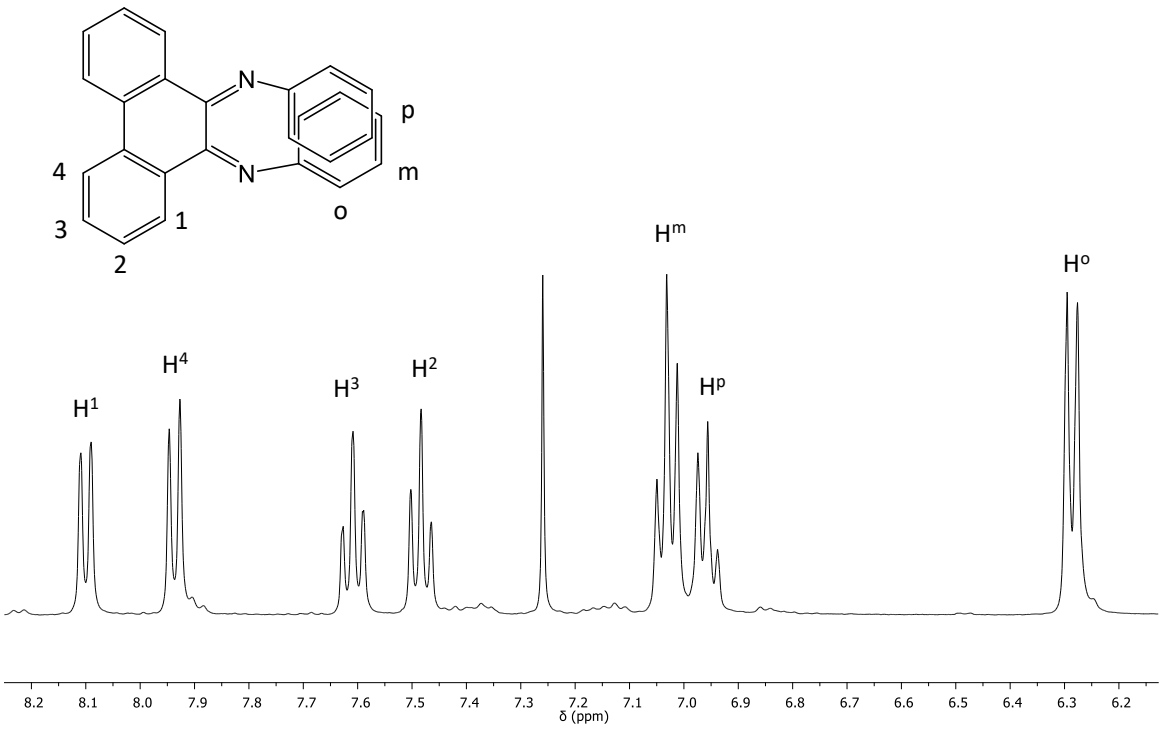

Figure 3.4. ^{1}H NMR ($CDCl_3$, 298 K) spectrum of **7**.

This represents a first main difference with respect to Ar-BIANs: these latter are always present in solution as a mixture of *E,Z* and *E,E* isomers, in equilibrium at slow rate on the NMR timescale. The *Z,Z* isomer was never observed up to now.[1,4]

The structure in solid state of ligands **5-7** is reported in literature.[1,2c,3] For ligand **7**, in agreement with the characterization in solution, the unit cell only the *Z,Z* isomer was found (Figure 3.5).[1] This configuration is stabilized by the π stacking interaction of the phenyl groups on the iminic nitrogens, which is made possible by the flexibility of the phenanthrene backbone. Actually, differently from Ar-BIANs, the skeleton of the Ar-BIP is not planar, and the central ring possess a twist-boat type geometry. The length of the iminic bonds C=N (Table 3.1) is typical for C(sp^2)=N(sp^2) type bonds of organic molecules in non-conjugated systems. Moreover, the bond distances between iminic carbon atoms and between the other two carbons of the central ring indicate that there is no conjugation between those the iminic bonds and the phenyl groups on the backbone. The lack of conjugation can be attributed to the torsion angle between the diiminic fragments (44.75°).

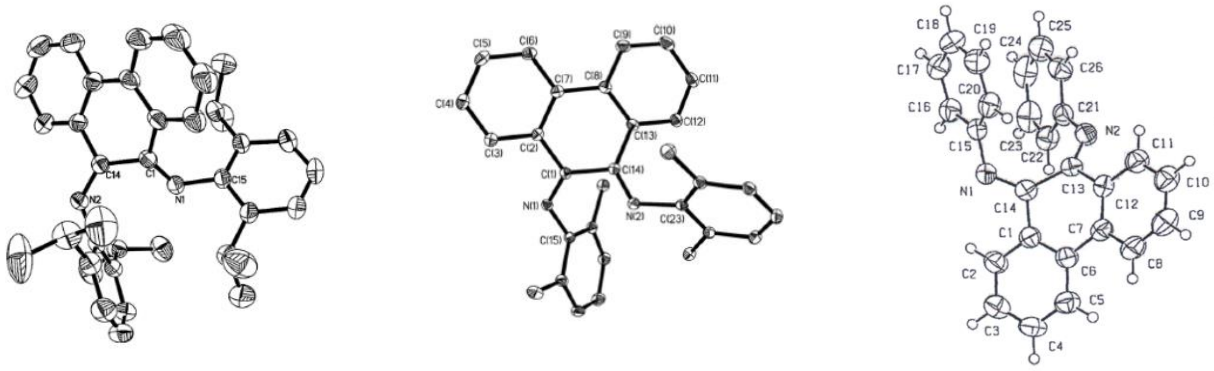

Figure 3.5. Solid state structure of ligands **5** (left), **6** (centre), **7** (right).[1,2c,3]

For ligands **5** and **6**, instead, in the unit cell only the *E,Z* isomer is present and so no kind of π stacking is observed. The values for the C=N bonds are similar to those of ligand **7**, whereas the bond distances between the iminic carbon atoms and those two carbons of the central ring are shorter for **5** and **6**, indicating a higher conjugation than in ligand **7**.

Table 3.1. Selected bond distances (Å) and torsion angles (°) for Ar-BIP ligands.

	Bond length (Å)			Torsion angles (°)		
Ar-BIP	C=N	C-C (i)[a]	C-C (f)[b]	N=C-C=N	C=C-C=C[c]	Ref.
5	1.275(4) (*Z*) 1.271(4) (*E*)	1.502(4)	1.478(5)	44.3(4)	16.9(5)	2c
6	1.278(1) (*Z*) 1.277(1) (*E*)	1.503(1)	1.484(1)	45.0(1)	12.0(2)	3
7	1.278(4) (*Z*) 1.267(4) (*Z*)	1.524(5)	1.494(6)	44.7(5)	14.5(5)	1

[a] C-C bond between the iminic carbons. [b] C-C bond between the two carbons of the phenanthrene backbone. [c] Torsion angle between the phenyl groups in the backbone.

For all the ligands, the results of the analysis in solution and in the solid state are in agreement with each other.

*3.2.2. Synthesis and characterization of Pd-neutral complexes **5a-7a** and Pd-cationic complexes **5b-7b**.*

Ligands **5-7** were used to synthesize the corresponding neutral, [Pd(Ar-BIP)(CH_3)Cl] **5a – 7a**, and monocationic, [Pd(Ar-BIP)(CH_3)($NCCH_3$)][PF_6] **5b – 7b**, organometallic Pd(II) complexes. To obtain the neutral derivatives, **5a –7a**, the procedure applied was based on the well-known substitution reaction of cyclooctadiene with α-diimine on the palladium precursor [Pd(cod)(CH_3)Cl] (cod = 1,5-*cis,cis*-cyclooctadiene).[5] Unlike the effortless synthesis of the corresponding (Ar-BIAN)-Pd(II) complexes,[5b] with Ar-BIP ligands much longer reaction times (up to 15 days) and larger excess of ligands with respect to palladium (up to 15 equiv.) were required to obtain **5a – 7a** (Scheme 3.2).

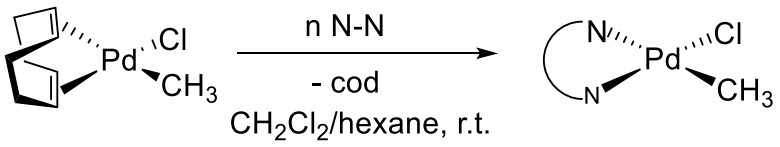

	N-N	n N-N	t	yield (%)
5a	**5**	15	15 d	83
6a	**6**	6	6 d	84
7a	**7**	1.5	6 d	70

Scheme 3.3. Synthesis of Pd(II) neutral complexes.

A similar behavior was found for the synthesis of the analogous palladium(II) derivatives with the 8-*p*-tolylnaphthyl or 2,6-bis(diphenylmethyl)-4-methyl substituted Ar-BIAN or Ar-DAB imines,[6] and it was explained as caused by the bulkiness of the ligands. For Ar-BIPs, the difficult coordination to palladium(II) can be ascribed to two main factors: first, the isomer required for the coordination of Ar-BIP to the metal center is the *E,E* one, that for **5-7** is not present in solution. An isomerization process is then required for the coordination to occur: this process in solution is easy for Ar-BIANs,[4e] but apparently this is not the case for Ar-BIPs. Second, for this class of ligands, the phenanthrene skeleton and the iminic fragment NCCN are not planar, and in particular for the latter the torsion angles are of 44.3(4), 45.0(1) and 44.7(5)°, for **5**,[2c] **6**,[3] and **7**,[1] respectively (Table 3.1). This angle hampers the coordination of the Ar-BIP since it has to decrease remarkably to have a square planar complex. Additionally, for ligands **5** and **6**, the steric hindrance of the substituents in *ortho* positions of the aryl rings might also disfavor the coordination. Nevertheless, complexes **5a – 7a** were isolated as dark purple solids in good to high yields (70 - 84 %). The complexes were all characterized in solution by mono- and bidimensional NMR spectroscopy, recording the spectra in CD_2Cl_2 at 263 K. In the ^1H NMR spectra the number of signals and their integration are in agreement with the coordination of the ligand in a nonsymmetric chemical environment.

Single crystals suitable for X-ray analysis of **6a** and **7a** were obtained by slow diffusion of *n*-hexane into a dichloromethane solution at 277 K (Figure 3.6).

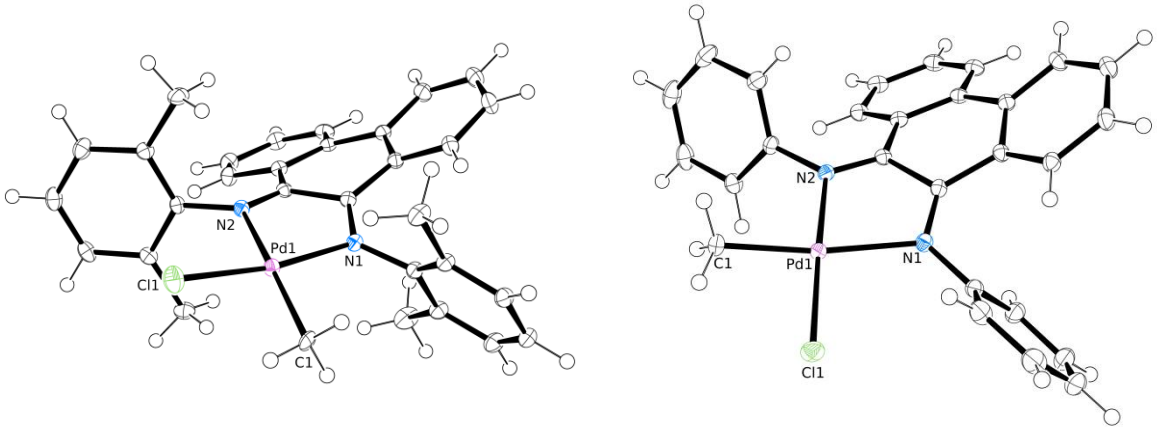

a) b)

Figure 3.6. ORTEP drawing (50 % probability ellipsoids) for complexes: a) **6a**; b) **7a**. Selected bond lengths (Å) and angles (°) for: **6a** Pd(1)-N(1) 2.064(1), Pd(1)-N(2) 2.122(1), Pd(1)-C 2.087(2), Pd(1)-Cl(1) 2.2821(5), N(1)-Pd(1)-N(2) 77.38(5), C(1)-Pd(1)-Cl(1) 85.64(6), N(1)-Pd(1)-C(1) 99.41(7), N(2)-Pd(1)-Cl(1) 98.73(4); **7a** Pd(1)-N(2) 2.043(1), Pd(1)-N(1) 2.171(1), Pd(1)-C(1) 2.035(1), Pd(1)-Cl(1) 2.2924(5), N(2)-Pd(1)-N(1) 76.99(4), C(1)-Pd(1)-Cl(1) 86.29(4), C(1)-Pd(1)-N(2) 96.08(5), N(1)-Pd(1)-Cl(1) 100.93(3).

The analysis of the structures points out the decrease in conformational freedom induced by the coordination to the Pd center and the constrain in the square planar geometry. This can also be seen in the values of the NCCN and CCCC torsion angles as well as the NCC angles of the diiminic fragment, that both diminish upon coordination (Table 3.2).

Table 3.2. NCC angles, NCCN and CCCC torsion angles (in degrees, as defined by the schematic drawing) for free and coordinated **6** and **7** ligands; for comparison purposes, the data for the Ar-BIAN counterpart of complex **6a**, **L42a**, have also been included; standard deviations (where available) are in parentheses.

Cmpnd	$N_1C_2C_3$	$N_2C_3C_2$	$N_1C_2C_3N_2$	$C_1C_2C_3C_4$
6	115.8	126.11	45.0(1)	41.3
6a	115.1(1)	113.6(1)	22.0(2)	29.6(2)
L42a	118.4	119.0	4.1	0.7
7	117.2	126.33	44.7(5)	47.4
7a	114.3(1)	115.1(1)	21.3(1)	32.9(2)

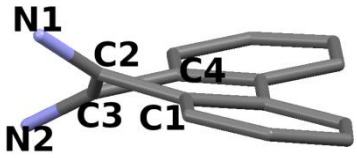

It is possible to compare the solid state structure of **6a** to that of its Ar-BIAN counterpart, [Pd(**L42**)(CH_3)Cl], **L42a**.[23] The Pd-N bond distances are shorter for **6a** (2.064(1) and 2.122(1) Å in **6a** *vs* 2.088(6) and 2.203(5) Å in **L42a**), thus indicating a stronger coordination of the Ar-BIP ligand in comparison with the Ar-BIAN one. This trend is reflected by the value of the Pd-C bond length that is longer in **6a** (2.087(2) Å) than in **L42a** (2.039(6) Å). As mentioned before, another difference lies in the degree of planarity of the diiminic moiety, the Ar-BIAN ligand being almost perfectly planar, while the Ar-BIP molecule being markedly twisted (Table 3.2, Figure 3.7a). The NCC angles also indicate a greater strain in the Ar-BIP derivative; they are nearly ideal for **L42a**, while substantially lower than 120° for **6a** (Table 3.2). Therefore, the N-Ph bonds in **6a** are bent away from the diazo ligand compared to **L42a**. The angle between the N-Ph bond and the line passing through the Pd atom and bisecting the opposite C-C bond (Figure 3.7b) can be an effective tool to measure this effect: the values for each N-Ph bond in **6a** and **L42a** are 80.3°, 80.8° and 88.1°, 86.7°, respectively.

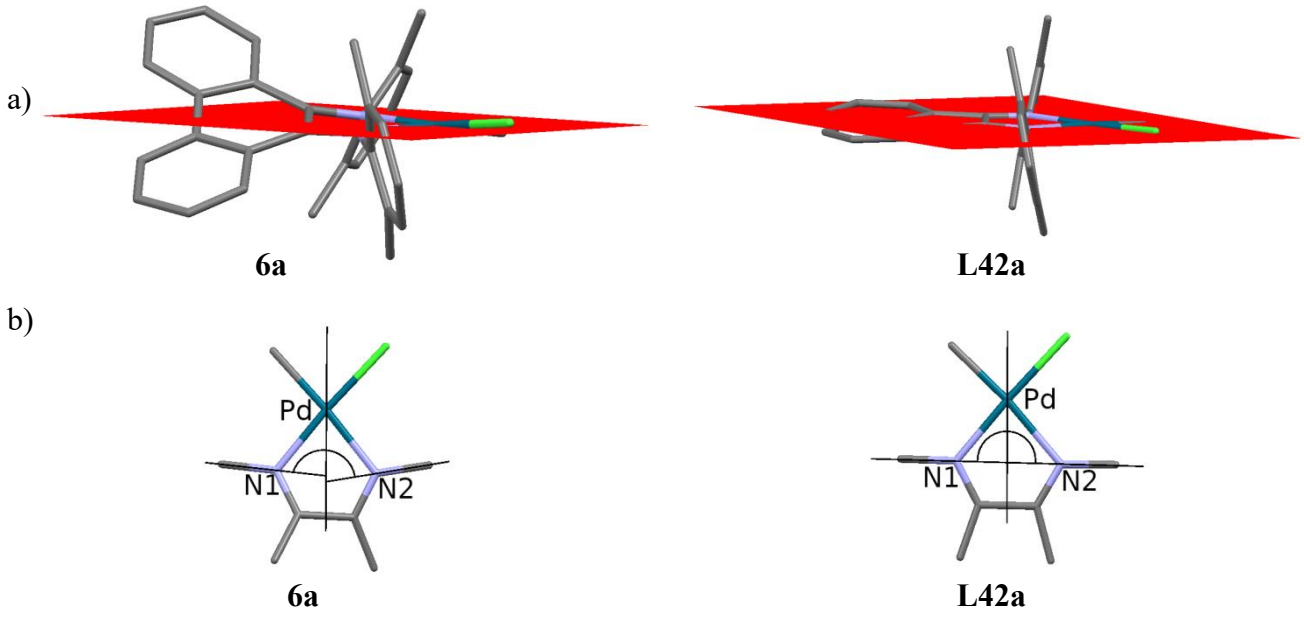

Figure 3.7. a) Average plane through the Pd and the four atoms directly bonded to it in complex **6a** and **L42a** to evidence the different degree of planarity of the diiminic ligand; b) Schematic drawing showing the bending effect on the N-Ph bonds in **6a** as compared to **L42a**.

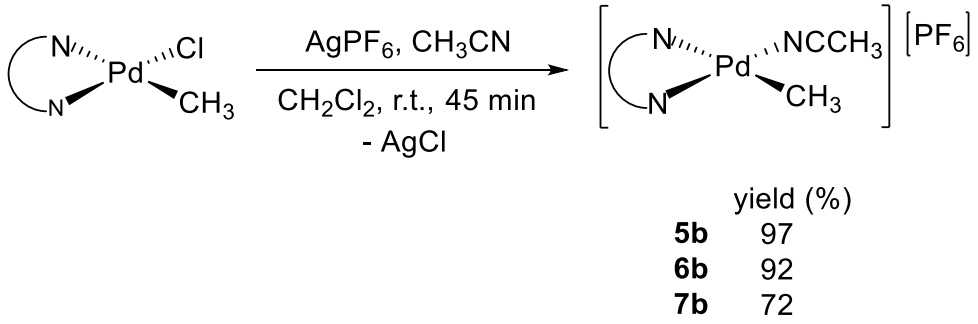

	yield (%)
5b	97
6b	92
7b	72

Scheme 3.4. Synthesis of Pd(II) cationic complexes.

The monocationic complexes [Pd(Ar-BIP)(CH_3)(CH_3CN)][PF_6] were synthesized using a dehalogenation reaction employing $AgPF_6$, in the presence of dry acetonitrile (Scheme 3.3). In this case the synthesis was very straightforward, as reported in literature for the corresponding cationic complexes with Ar-BIANs,[5b] confirming that the bottleneck in the synthesis of the neutral complexes is the coordination of Ar-BIPs to palladium. **5b-7b** were characterized in solution by NMR spectroscopy recording the spectra in $CDCl_3$ at 298 K. Again, the spectra show that the ligands are coordinated in a non-symmetrical environment, and the signal of Pd-$NCCH_3$ fragment is present.

Taking in consideration the resonances of the Pd-CH_3 fragment, its singlet falls between 0.78 and 0.41 ppm for the neutral complexes and between 0.88 and 0.50 ppm for the monocationic derivatives. In particular, for **6a** and **6b** the Pd-CH_3 moiety resonates at 0.32 and 0.42 ppm, respectively, that is at lower frequencies than the same signal for **L42a** and **L42b** (0.61 and 0.73 ppm). In the hypothesis that this signal could be considered as a good probe for assessing the electron density given by the ligand to the metal center,[4a-b,7,8] the variation in its chemical shift moving from Ar-BIAN to Ar-BIP complexes indicates that **6** is a stronger Lewis base than **L42**. This observation follows the trend of the Pd-N bond distances determined in from the solid state structures (Figure 3.4) and could be related to the lack of conjugation between the two C=N bonds in the free ligand.[1] The data of characterization of Ar-BIP complexes, both in solution and in solid state, suggest that Ar-BIPs are stronger ligands with respect to Ar-BIANs, and, in analogy with Pd-PDAP ligand reported in literature,[9] Pd-(Ar-BIP) cationic complexes can be considered as electron-rich metal cations.

*3.2.3. Ethylene/methyl acrylate copolymerization with **5b-7b**.*

Complexes **5b – 7b** were tested as precatalysts for the ethylene/methyl acrylate copolymerization (Scheme 3.4, Table 3.3). The catalytic reactions were carried out in 2,2,2-trifluoroethanol, at mild reaction conditions of temperature and ethylene pressure, and with no addition of any cocatalyst. The same reaction conditions were applied for **L42b**, in order to have a direct comparison of data.

A sample for GC-MS was taken before the work up, in order to analyze the presence of higher alkenes. The catalytic products were isolated as brown oils and, after removal of the volatile fraction at reduced pressure, characterized by NMR spectroscopy. The molecular weight of the produced macromolecules was determined by GPC analysis at the University of Salerno in the group of Prof. Claudio Pellecchia.

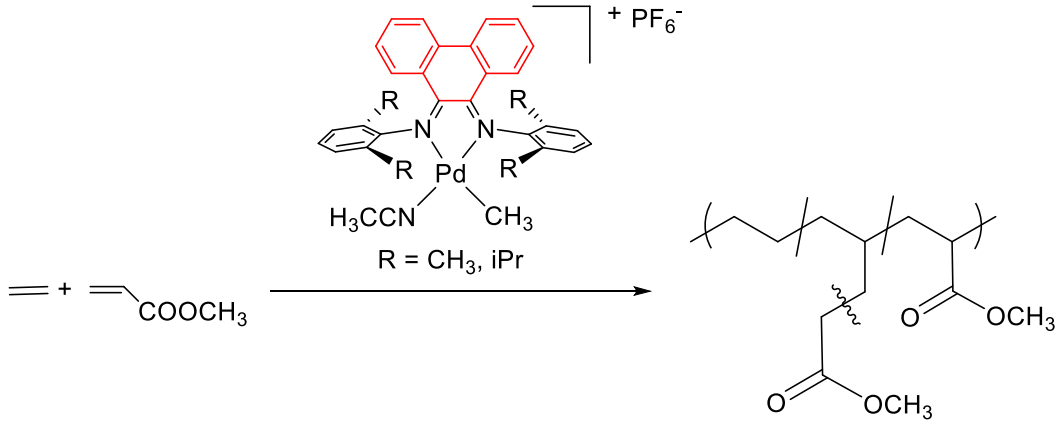

Scheme 3.5. Ethylene/methyl acrylate copolymerization.

Table 3.3. Ethylene/methyl acrylate copolymerization: effect of the ancillary ligand.[a]
Precatalyst: $[Pd(CH_3)(NCCH_3)(Ar\text{-}BIP)][PF_6]$,

Run	PreCat	Yield (mg)	g CP/ mol Pd[b]	MA (mol %)[c]	TON[d] E	TON[d] MA	M_n (M_w/M_n)[e]	Alkenes /esters[f]	Bd[c, g]
1	**5b**	436.4	20781	0.3	734	2.21	33000 (1.54)	none	83
2	**6b**	156.6	7443	2.4	248	6.08	10000 (1.60)	none	103
3	**7b**	-	-	-	-		-	C_4	-
4	**L42b**	379.3	18062	4.4	564	26.0	3200 (2.06)	none	111
5[h]	**5b**	452.1	21529	-	767		22600 (2.66)	none	90
6[h]	**6b**	181.7	8652	-	308		7800 (1.80)	none	114

[a] Reaction conditions: $n_{Pd} = 2.1 \cdot 10^{-5}$ mol, V_{TFE} = 21 mL, V_{MA} = 1.130 mL, [MA]/[Pd] = 594, T = 308 K, $P_{ethylene}$ = 2.5 bar, t = 18 h; [b] isolated yield, productivity as g CP/mol Pd = grams of copolymer per mol of palladium; [c] calculated by ^{1}H NMR spectroscopy on isolated product; [d] Turnover number = mol of substrate converted per mol of catalyst (E = ethylene); [e] determined by GPC at 30 °C, using THF as the solvent, an eluent flow rate of 1 mL min−1, and 19 narrow polystyrene standards as the reference; [f] determined by GC/MS; [g] Bd = degree of branching as branches per 1000 carbon atoms; [h] Reaction conditions: $n_{Pd} = 2.1 \cdot 10^{-5}$ mol, V_{TFE} = 21 mL, T = 308 K, $P_{ethylene}$ = 2.5 bar, t = 18 h.

The N-donor ligand has a remarkable effect on the catalytic behavior of the precatalysts, both when phenanthrene-based ligands bearing different substituents on the aryl ring and ligands with a different backbone are considered (Table 3.3). Complex **7b** resulted to be inactive in the copolymerization reaction, yielding just a mixture of butenes (Table 3.3, run 3). Instead, **5b** and **6b**, that are the complexes with *ortho*-substituted Ar-BIPs, generate active catalysts that produce ethylene/methyl acrylate copolymers. Going from the catalyst with methyl-substituted Ar-BIP, **6**, to that with the isopropyl substituted ligand, **5**, an increase in productivity is observed, and the top value of productivity is reached with **5b** (almost 21 kg CP/mol Pd, Table 3.3, run 1). The substituent on the aryl rings has an effect also on the content of inserted polar monomer, molecular weight and branching degree of the products. In particular, the content of methyl

acrylate and the branching degree decrease going from **6b** to **5b**, whereas the molecular weight increases by three times in the same order, reaching the value of 33000 when **5b** is used (Table 3.3, run 1, 2). No formation of higher alkenes was observed, as it can be expected for catalysts with steric hindrance around the axial position.[10] These trends observed for **5b** and **6b** are similar for the ones reported for Ar-DAB catalysts, even though the reaction conditions are different. The shared point between these two different systems is the steric hindrance around the catalytic center.[11] There is a difference instead for what concerns the catalysts TON: for the Ar-DAB systems the TON decreases for both comonomers when moving from isopropyl to methyl substituted ligands,[11] whereas for the Ar-BIP catalysts the TON for methyl acrylate increases. **5b** and **6b** are also active in ethylene homopolymerization (Table 3.3, run 5, 6); the increase in the productivity with respect to the ethylene/MA copolymerization is not as pronounced as that reported in the literature for Ar-DAB catalysts (where the difference is of one order of magnitude).[12] The lower productivity in the copolymerization with respect to ethylene homopolymerization is attributed to the formation of the stable six-membered palladacycle (species C" in Chapter 2, Scheme 2.8), which represents the catalyst resting state.[11] In the case of the Ar-BIP catalysts, the narrow difference in the productivity of the two polymerizations suggests a lower stability of the metallacycle C", that can be easily cleaved, thus favoring the growth of the polymeric chain. This is in agreement with the higher Lewis basicity of Ar-BIPs: since the metal center is made less oxophilic, the formation of C" is disfavored. Another factor that has to be considered in this comparison is the solvent of the catalytic reaction: in literature, the Ar-DAB systems are usually applied in dichloromethane, whereas here the reaction is carried out in trifluoroethanol, a solvent never used before for the synthesis of polyolefins. Due to the remarkable difference between the two solvents it cannot be ruled out that they might affect the outcome of the catalytic reaction.

The comparison between the Ar-BIAN catalyst **L42b** and the corresponding Ar-BIP counterpart, **6b,** shows that the first system is more productive and yields a copolymer with a higher content of methyl acrylate, but with a three times lower molecular weight and a slightly higher branching degree (Table 3.3, run 2, 4). For the active species with ligand **6**, the lower content of inserted polar monomer in the products and their higher molecular weight values can be related to the additional bulkiness of the phenanthrene backbone, as highlighted by the X-ray analysis (Figures 3.6a, 3.7a). In addition, as recently reported for the Pd-PDAP catalysts,[9] also the higher Lewis basicity of Ar-BIP ligands with respect to the corresponding Ar-BIAN derivatives can play a positive role in enhancing the length of polymer chains.

The effect of temperature, ethylene pressure, methyl acrylate to palladium ratio and reaction time has been evaluated for **5b** and **6b**, in order to find the optimal reaction conditions for the system. Generally speaking, in the investigated ranges the active species generated by **6b** is more influenced by catalytic parameters than **5b**.

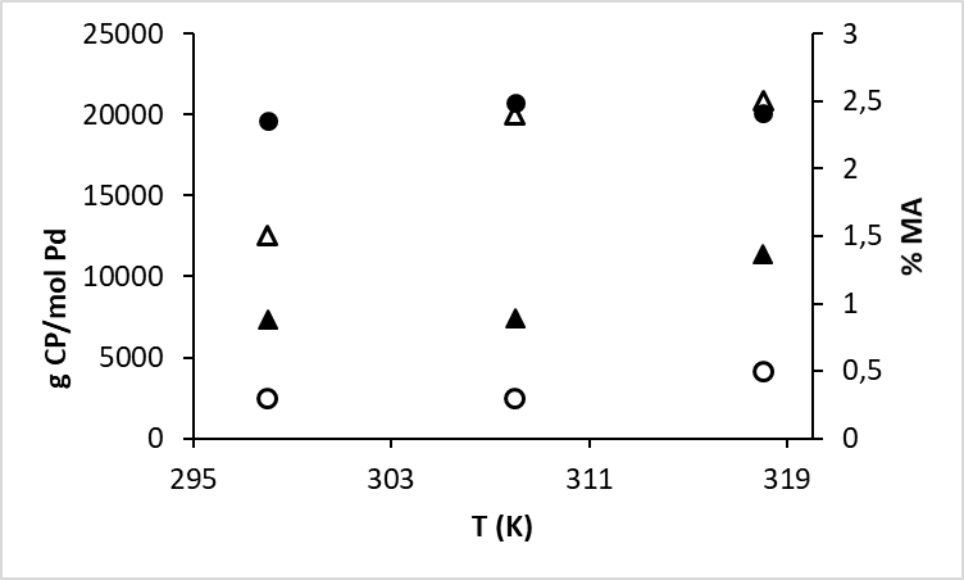

Figure 3.8. Ethylene/methyl acrylate copolymerization: effect of temperature. Precatalyst: [Pd(Ar-BIP)(CH$_3$)(CH$_3$CN)][PF$_6$] (Ar-BIP = **5, 6**). Reaction conditions: see Table 3.3. Filled symbols: productivity data; open symbols: content of MA in mol %; **5b** (●,○), **6b** (▲,△).

The temperature influence was investigated in the range 298 - 318 K (Figure 3.8, Table S3.3). The results obtained with **5b** are almost unaffected by the temperature variation, instead for **6b** an increase in both the productivity and the content of MA, alongside with a decrease in the molecular weight, were found going from 298 to 318 K (Table S3.3, runs 4-7). The effect on M_w indicates that the raise of productivity is related to an increase in the number of produced macromolecules rather than in their length, thus suggesting that the decrease in the propagation to chain transfer rate ratio is due to an increase in the rate of the chain transfer step. The effect of temperature on productivity is different for Ar-BIP systems than for the classical Ar-BIAN-based catalysts, whose productivity drops significantly at 318 K due to decomposition to inactive palladium metal.[4a,12] This improved thermal stability of the Ar-BIP catalysts agrees with both the stronger coordinating capability of Ar-BIP ligands with respect to Ar-BIANs and the increase in the bulkiness of the ligand. In particular, the latter strategy was already successfully applied in the Ni- and Pd-catalyzed ethylene homopolymerization,[6,13-15] and in one example of

ethylene/MA copolymerization, where a decrease in the productivity was achieved together with an increase in the content of inserted MA when the reaction temperature was raised from 293 to 333 K.[6a]

The effect of ethylene pressure was explored in the range 2.5 - 7.0 bar. Again the variation of ethylene pressure does not affect the performance of the catalyst obtained from **5b** (Table S3.4, runs 1 - 3), whereas for **6b** the productivity almost doubles when the ethylene pressure is increased from 2.5 to 5.0 bar, jointly with a drop in the content of the polar monomer (Table S3.4, run 4 *vs* 5). When the pressure is further increased up to 7 bar, a remarkable decrease in the productivity was obtained (Table S4, run 7). The molecular weight of the obtained macromolecules is marginally affected by the ethylene pressure. An analogous effect of the ethylene pressure on productivity was reported by our group in the ethylene/MA cooligomerization catalyzed by Pd-complexes with the nonsymmetric Ar-BIAN **L24**, also carried out in trifluoroethanol.[4a] In the case of Ar-BIP precatalysts, the effect is even more pronounced, and it might be connected with the fact that these kind of systems are not so good homopolymerization catalysts.

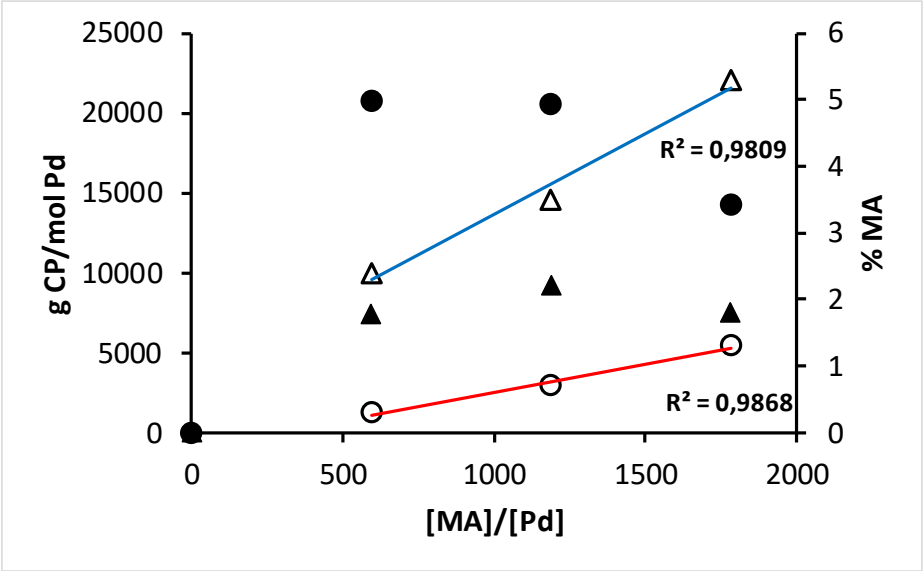

Figure 3.9. Ethylene/methyl acrylate copolymerization: effect of [MA]/[Pd] ratio. Precatalyst: [Pd(Ar-BIP)(CH_3)(CH_3CN)][PF_6] (Ar-BIP = **5, 6**). Reaction conditions: see Table 3.3. Filled symbols: productivity data; open symbols: mol % MA; **5b** (●,○), **6b** (▲,△).

The effect of methyl acrylate to palladium ratio was examined in the range [MA]/[Pd]= 594-1782, by increasing the amount of the polar monomer and keeping constant the amount of

precatalyst used. Similarly to what is reported on Ar-DAB catalysts,[11,12] the content of inserted acrylic ester linearly increases with MA concentration (Figure 3.9, Table S3.5), with a concomitant decrease in the M_n values (Table S3.5). Different Ar-BIP ligands give different results for what concerns the productivity of the systems: for precatalyst **5b** a decrease in productivity is found due to a drop in ethylene turnover number; whereas for **6b** initially there is an increase in productivity associated with an increase in the values of TON for both comonomers, followed by a decrease when [MA]/[Pd] ratio is further increased (Table S3.5, Figure 3.9). Differently from the Ar-DAB catalysts,[11,12] for both Ar-BIP precatalysts the TON for methyl acrylate increases with its concentration, suggesting a higher affinity of these systems for the polar monomer than classical Ar-BIAN or Ar-DAB derivatives. This might be related to the higher Lewis basicity of the phenanthrene-based α-diimines, indicating the positive effect of having electron-rich metal cations as catalysts. This agrees also with reported DFT calculations showing that anionic Pd(II) catalysts are highly tolerant toward polar monomers.[16]

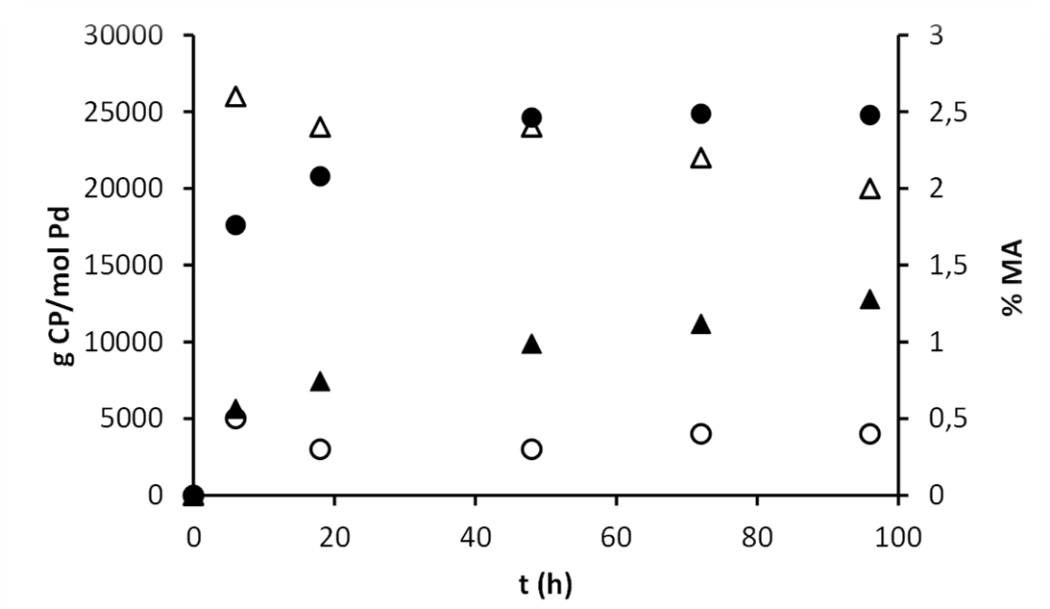

Figure 3.10. Ethylene/methyl acrylate copolymerization: effect of reaction time. Precatalyst: [Pd(Ar-BIP)(CH_3)(CH_3CN)][PF_6] (Ar-BIP = **5, 6**). Reaction conditions: see Table 3.3. Filled symbols: productivity data; open symbols: mol % MA; **5b** (●,○), **6b** (▲,△).

The catalytic behavior of precatalysts **5b** and **6b** was also assessed over time, in the range t = 6 - 96 hours, at a pressure of ethylene of 2.5 bar and temperature of 308 K. **5b** is active up to 48 h (achieving almost 25 kg CP/mol Pd of productivity), whereas **6b** is still working up to 96 h,

reaching a productivity value of 13 kg CP/mol Pd (Figure 3.10, Table S3.6). No formation of palladium black was evident in any of the catalytic tests, implying that catalyst deactivation does not follow the mechanism of ligand dissociation and decomposition to palladium metal. This also agrees with the hypothesis that Ar-BIP ligands are more strongly bonded to palladium than Ar-BIANs. The increase in productivity with reaction time is related to the increase in turnover numbers for both comonomers; however, for **6b**, there is a slight decrease in the content of inserted MA at longer reaction times (Figure 3.10, Table S3.6). Molecular weight values rise during the first 18 h, levelling off afterwards: the increase in productivity can so be associated to the formation of more polymer chains rather than longer macromolecules.

In order to measure ethylene consumption, two specific catalytic experiments were performed with both **5b** and **6b**, using a mass flow control device (Figure 3.11). The catalysts obtained from **5b** and **6b** have similar kinetic profiles: *i.* an induction period of 90 s is observed; *ii.* the rate of ethylene uptake (TOF) is the same up to 240 s; *iii.* Afterwards, catalyst with **6** slows down, whereas catalyst with **5** is very active up to 2 h. Monitoring the ethylene consumption for 18 h, the deactivation of catalyst with ligand **5** becomes evident, while catalyst with ligand **6** remains active.

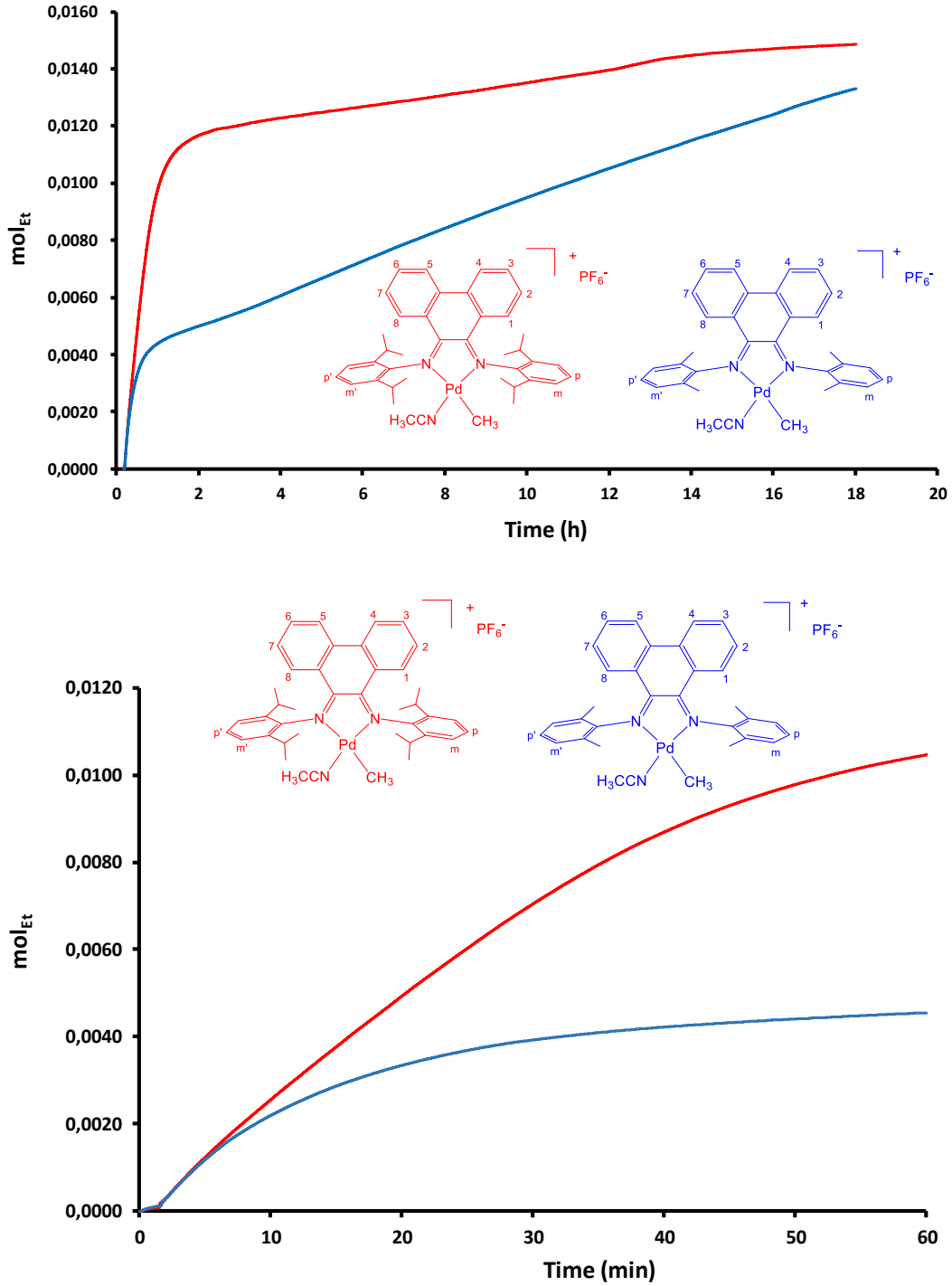

Figure 3.11. Ethylene/methyl acrylate copolymerization: kinetic profiles. Precatalyst: [Pd(Ar-BIP)(CH_3)(CH_3CN)][PF_6] (Ar-BIP = **5** (red curve), **6** (blue curve)). Reaction conditions: see Table 3.3; up) ethylene uptake for 18 h; bottom) magnification of ethylene uptake in the time range: 0 – 1 h.

3.2.4. Characterization of ethylene/methyl acrylate copolymers.

The isolated catalytic products were characterized with ^{1}H and ^{13}C NMR spectroscopy in $CDCl_3$, at room temperature. The signals in the ^{1}H NMR spectra were identified by comparison with literature data,[4a,12,17,18] and assigned as follows: the singlet at 3.66 ppm to the methoxy group, the signals between 2.50 and 1.50 ppm to allylic protons and to methylenic groups closer to the ester functionality, the broad signal centred at 1.25 ppm to the methylenic and methinic moieties of ethylene units, and the signals between 1.0 and 0.6 ppm to methyl groups at the end of branches (Figure 3.12).

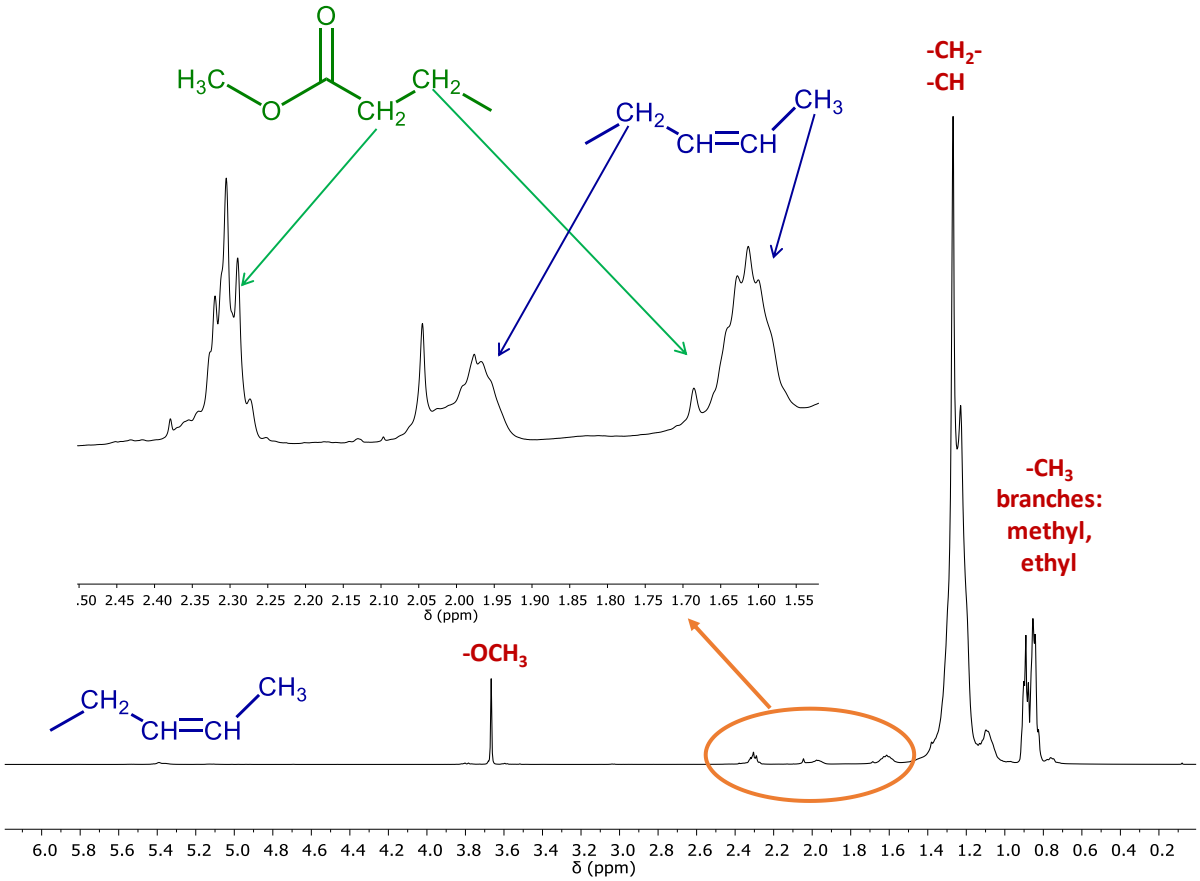

Figure 3.12. ^{1}H NMR spectrum ($CDCl_3$, 298 K) of ethylene/methyl acrylate copolymer obtained with **6b** (Table 3.3, run 2).

In agreement with the polymeric nature of the catalytic product no signals due to the vinylic protons are present in the spectrum of the copolymer produced with precatalyst **5b**, whereas very low intensity peaks are observed when **6b** was the precatalyst. In the ^{13}C NMR spectrum of the copolymers obtained with **5b** only the signals related to the polar monomer inserted at the end of the branches are evident (Figure S3.71). Considering the ^{13}C NMR spectra of the copolymers (Figure 3.13) obtained with either **6b** or **L42b** (Table 3.3, run 2 and 4, and Table S3.6, run 11),

other than the typical peaks of the methylenic and methyl groups, two overlapped signals for the methoxy (51.36 and 51.52 ppm) and one peak at 45.94 ppm are present; the latter has a methinic nature, as indicated by the $^{1}H,^{13}C$ HSQC spectrum (Figure S3.74, S3.75). In the carbonyl region three signals are present, at 174.37, 174.68 and 177.17 ppm. Accordingly to what is reported in literature,[12,19] the peak at 174.37 ppm is assigned to the acrylate inserted at the end of the branches as a $–CH_2–CH_2–C(O)OCH_3$ moiety. Matching our results with the ones presented by Osakada et al.,[19] the signals at 177.17 and 45.94 ppm unambiguously indicate that the polar monomer is inserted also into the main polymer chain (Figure 3.13). In the ^{13}C NMR spectrum of the copolymer obtained with **L42b** in CH_2Cl_2, instead of TFE, other than the signals discussed above, an additional two peaks for the carbonyl are present, at 177.23 and 167.07 ppm, that according to the literature,[20] are respectively attributed to the polar monomer inserted at the beginning of the copolymer chain as CH_3-CH-(CH_2COOCH_3)-CH_2- fragment and at the end of the chain as an unsaturated moiety –CH=CH-$COOCH_3$ (Figure 3.13c). In this last case also the peak for the methoxy group can be observed in the ^{1}H NMR spectrum, at 3.69 ppm (Figure S3.78, S3.79).

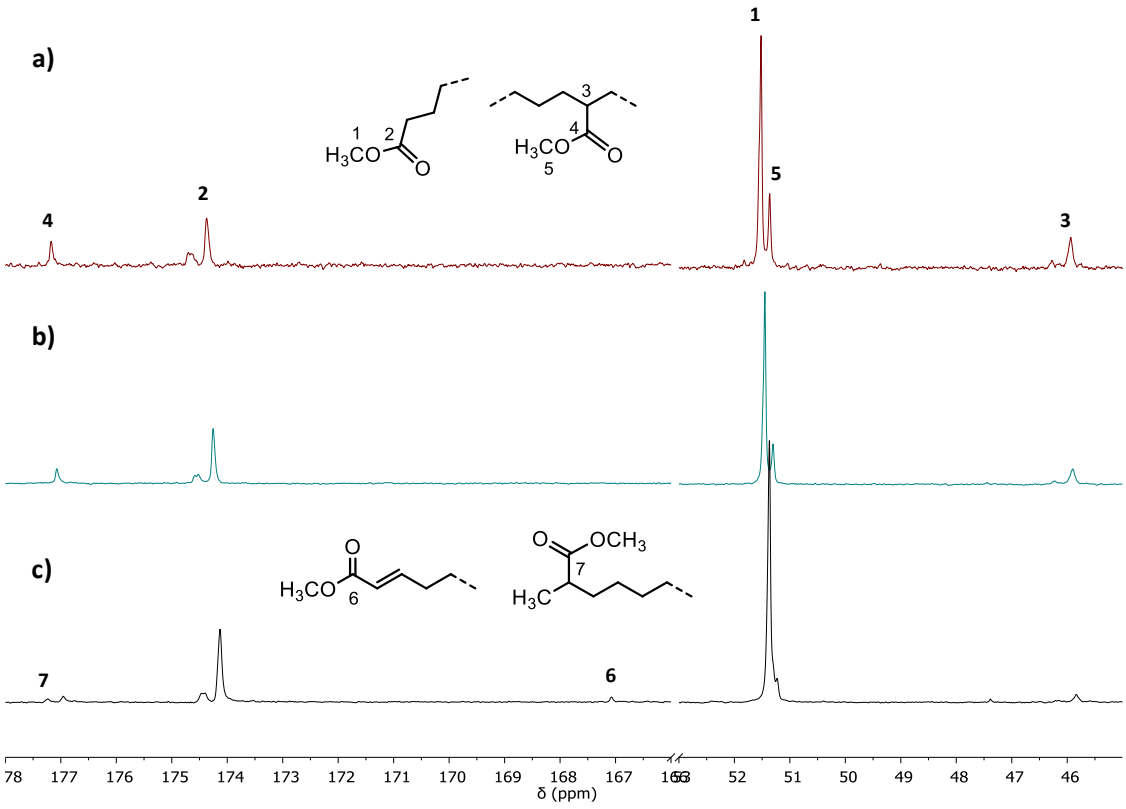

Figure 3.13. ^{13}C NMR spectra ($CDCl_3$, 298 K) of ethylene/methyl acrylate copolymers synthesized with: a) **6b** in TFE; b) **L42b** in TFE; c) **L42b** in CH_2Cl_2. Carbonyl region (left), methoxy and methinic region (right).

The NMR analysis points out that when trifluoroethanol is the solvent of choice, there is a more selective insertion of the polar vinyl monomer than when dichloromethane is used, where MA is found both into the main chain and at the end of the branches, with a preference for this latter kind of enchainment.

The beneficial effect of the fluorinated alcohol on the productivity was already reported by some of us in the ethylene/MA cooligomerization catalyzed by Pd complexes with nonsymmeric α-diimines,[4a-b,8] whereas the solvent effect on the microstructure of the macromolecules is highlighted here for the first time. Since trifluoroethanol has a higher coordinating capability with respect to dichloromethane, it could favourably compete for the fourth coordination site on palladium, that is necessary for β-hydrogen elimination to occur. If so, the latter process is disfavored and both termination and chain walking processes are inhibited consequently, leading to a more selective enchainment of the acrylic ester. This hypothesis is consistent with the molecular weight value of the copolymers synthesized in the two solvents with **L42b**: the M_n values estimated by integration of the signals in the ^{1}H NMR spectra is 3200 for the copolymer obtained in trifluoroethanol and 2500 for the one obtained in dichloromethane.

*3.2.5. In situ reactivity of **5b-7b** with ethylene and methyl acrylate.*

The mechanism of the ethylene/MA copolymerization reaction catalyzed by α-diimines-Pd(II) complexes is well established and based on three migratory insertion reactions: *i.* that of ethylene after the insertion of ethylene itself or *ii.* after that of methyl acrylate, *iii.* that of the polar monomer after the insertion of ethylene.[11]

Usually, as reported in literature,[4a,11] the migratory insertion of ethylene into Pd-C bonds in the Pd-(α-diimine) catalysts is very fast. The reactivity of **5b** with ethylene was investigated by ^{1}H NMR spectroscopy bubbling the gaseous monomer into a 10 mM solution of the complex in CD_2Cl_2 at 298 K. In the ^{1}H NMR spectrum recorded after 6 min from the bubbling, the formation of polyethylene is evident, the palladium precursor is present just in traces, with the almost complete consumption of ethylene (Figure 3.14), confirming also for our system the typical reactivity of the Pd-(α-diimine) catalysts.[4a,11] After 2 h, the peaks relevant to polyethylene are more defined and intense.

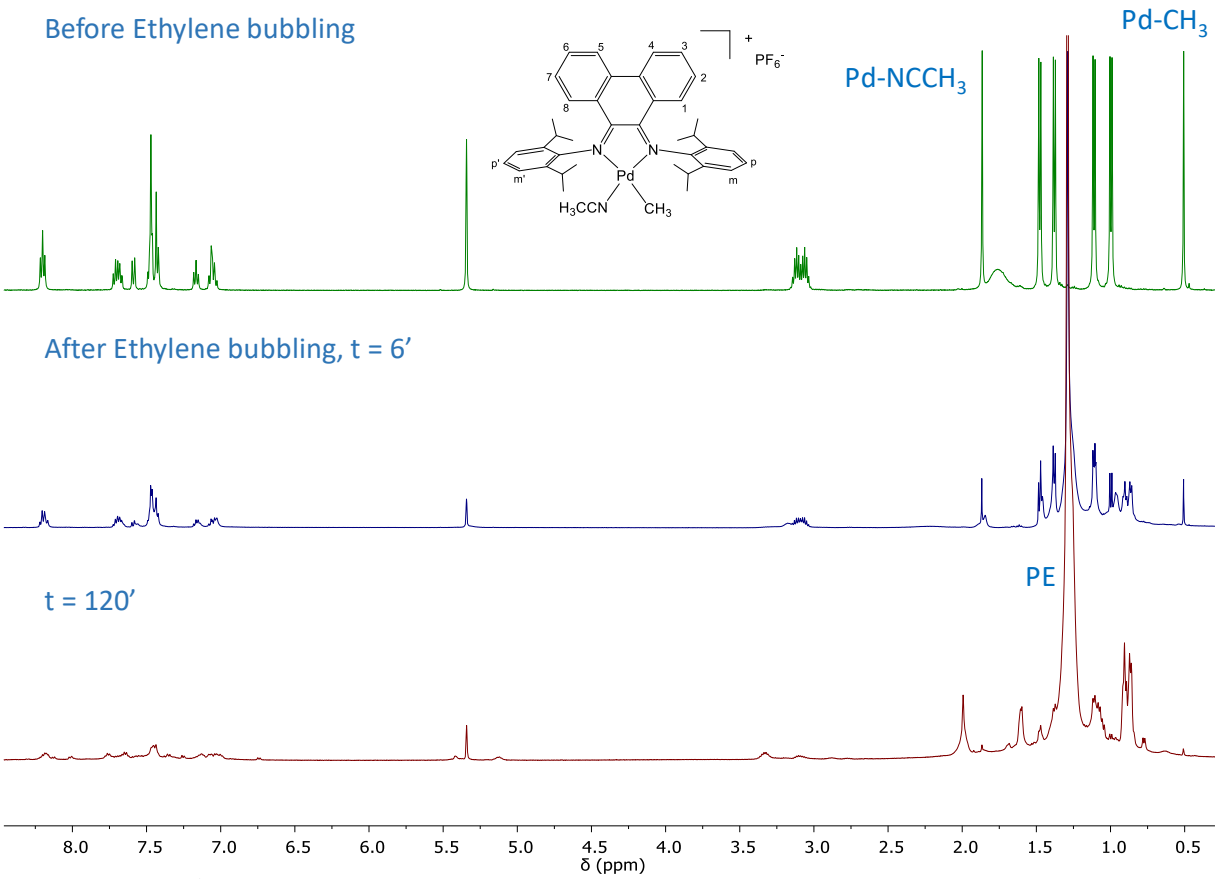

Figure 3.14. ^{1}H NMR spectra (CD_2Cl_2, 298 K) of reactivity of **5b** with ethylene; PE = polyethyelene.

The reactivity towards methyl acrylate was studied by adding 2 eq of the polar monomer to a 10 mM solution of **5b**, **6b** and **7b** in CD_2Cl_2, at 298 K. The three precatalysts exhibit different behaviours, starting from the remarkably different reaction rate: for complex **7b** all the precatalyst is consumed after 3 h, whereas for **5b** and **6b** at the same reaction time only the 29 and 86 % has reacted, respectively (Figures 3.15-3.17). The reaction of **6b** follows a second order kinetic (Figure S3.83b), unlike to what is usually reported for other Pd-(α-diimine) complexes.[4a] For the other two Ar-BIP complexes an appropriate kinetic profile is difficult to model (Figures S3.84a,c).

As already discussed in Chapter 2 (section 2.2.5), the mechanism for the reaction of the Pd-(α-diimine) precatalysts with methyl acrylate is based on the migratory insertion of the polar monomer into the Pd-CH_3 that can take place with either a primary or a secondary regiochemistry. The latter is usually favoured and followed by the chain walking process that leads to the intermediate C", the catalyst resting state (Scheme 3.5).[4a,11] The pathway followed by the specific precatalysts is recognized by the ^{1}H NMR signals of the typical intermediates. By

analysing the ^{1}H NMR spectra recorded during the reactivity experiments of **5b**, **6b** and **7b** with MA some differences both among the three complexes and between them and the behaviour of Pd-(Ar-BIAN) and Pd-(Ar-DAB) precatalysts are observed.

In the ^{1}H NMR spectrum of the reaction of **7b** recorded after 1 min from the addition of methyl acrylate the signals of the palladium precursor, of the 5-membered metallacycle **B''** and of **C''** are present. Following the reaction with time, the ^{1}H NMR spectra show that these species are progressively consumed leading to the formation of methyl crotonate, **D'** and **A'**, which are already observed after 15 min of reaction and become the main species after 3 h. **A'** derives from the insertion of MA into the Pd-CH_3 bond with primary regiochemistry. From these data it is possible to conclude that β-H elimination is fast and that the insertion of MA into the Pd-CH_3 bond is not highly regioselective (Figure 3.15).

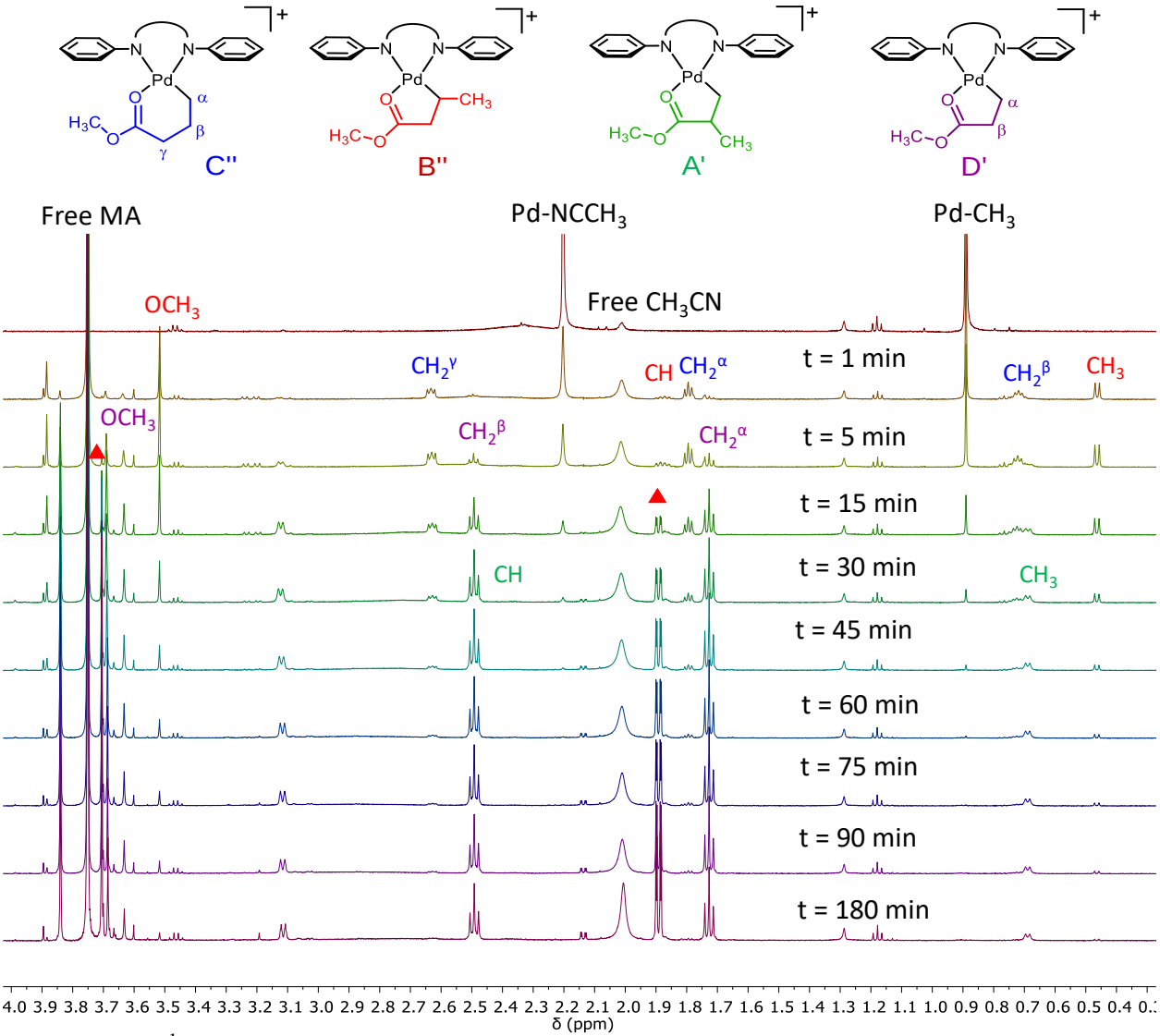

Figure 3.15. ^{1}H NMR spectra (CD_2Cl_2, 298 K) of reactivity of **7b** with MA, aliphatic region, evolution with time (min); ▲ = methyl crotonate.

When the reactivity of **6b** is taken into consideration, the signals of the metallacycles **B''**, **C''** and **A'** are observed after 5 min together with those of the cationic complex (Figure 3.16). These intermediates are also the main species, together with methyl crotonate and traces of residual **6b**, after 3 h. In this case, β-H elimination is slower than for **7b** and the data confirm the not highly regioselective insertion of MA into the Pd-CH_3 bond (Figure 3.16). Therefore, unlike the Pd-(Ar-BIAN) and Pd-(Ar-DAB) precatalsyts,[4a,11] for both **7b** and **6b** the migratory insertion reaction of the acrylic ester into the Pd-CH_3 bond is not regiospecific.

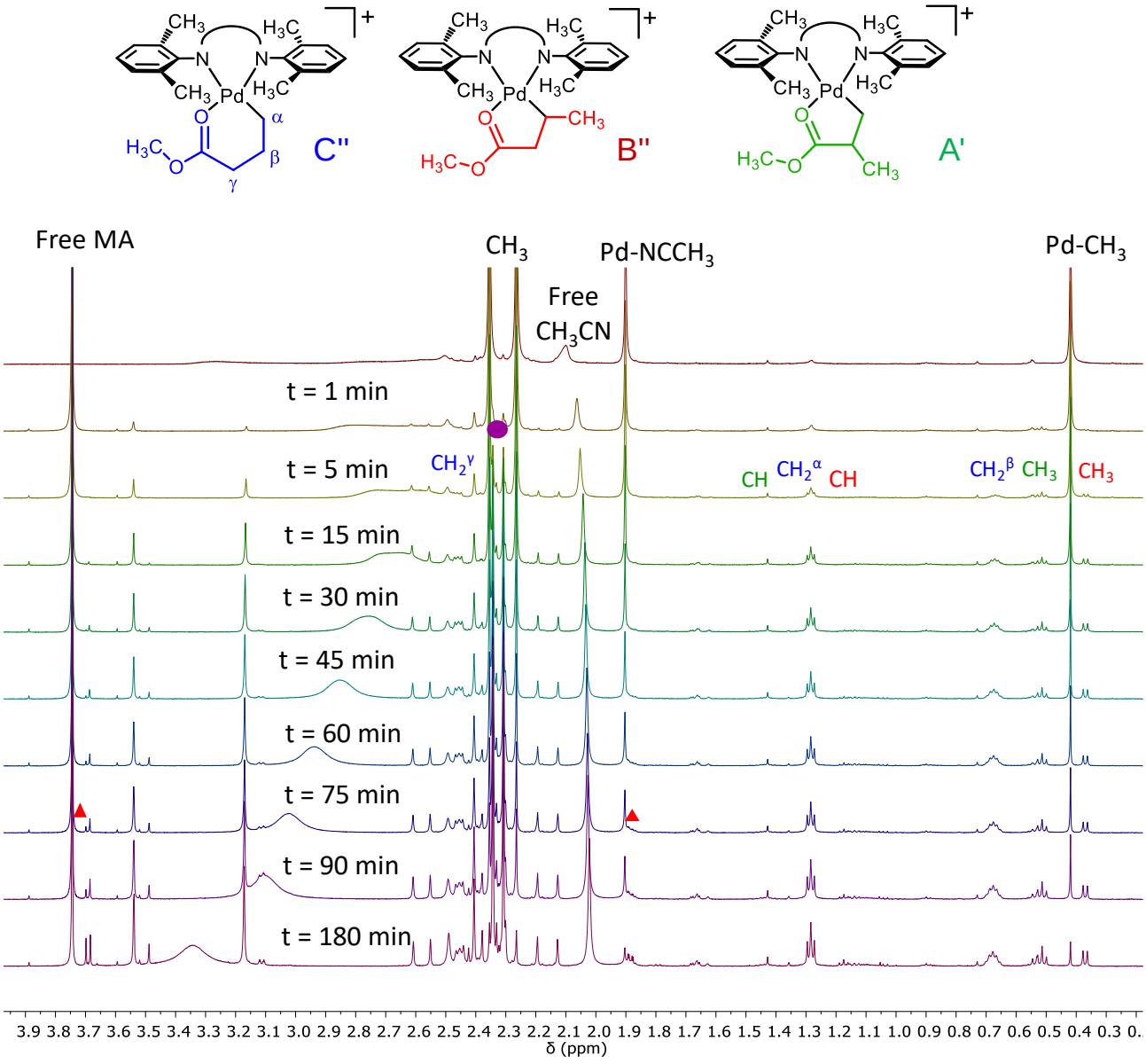

Figure 3.16. ^{1}H NMR spectra (CD_2Cl_2, 298 K) of reactivity of **6b** with MA, aliphatic region, evolution with time; ▲ = methyl crotonate, ● = trimer.

Consistently with the slow reaction rate, in the ^{1}H NMR spectra of the reactivity of **5b** the signals of methyl crotonate and **C''** appear only after 3 h. No signals belonging to the other intermediates are present. According to these data, for **5b** the migratory insertion reaction is very slow and, unlikely from the other two cationic Ar-BIP complexes, it is regiospecific (Figure 3.17).

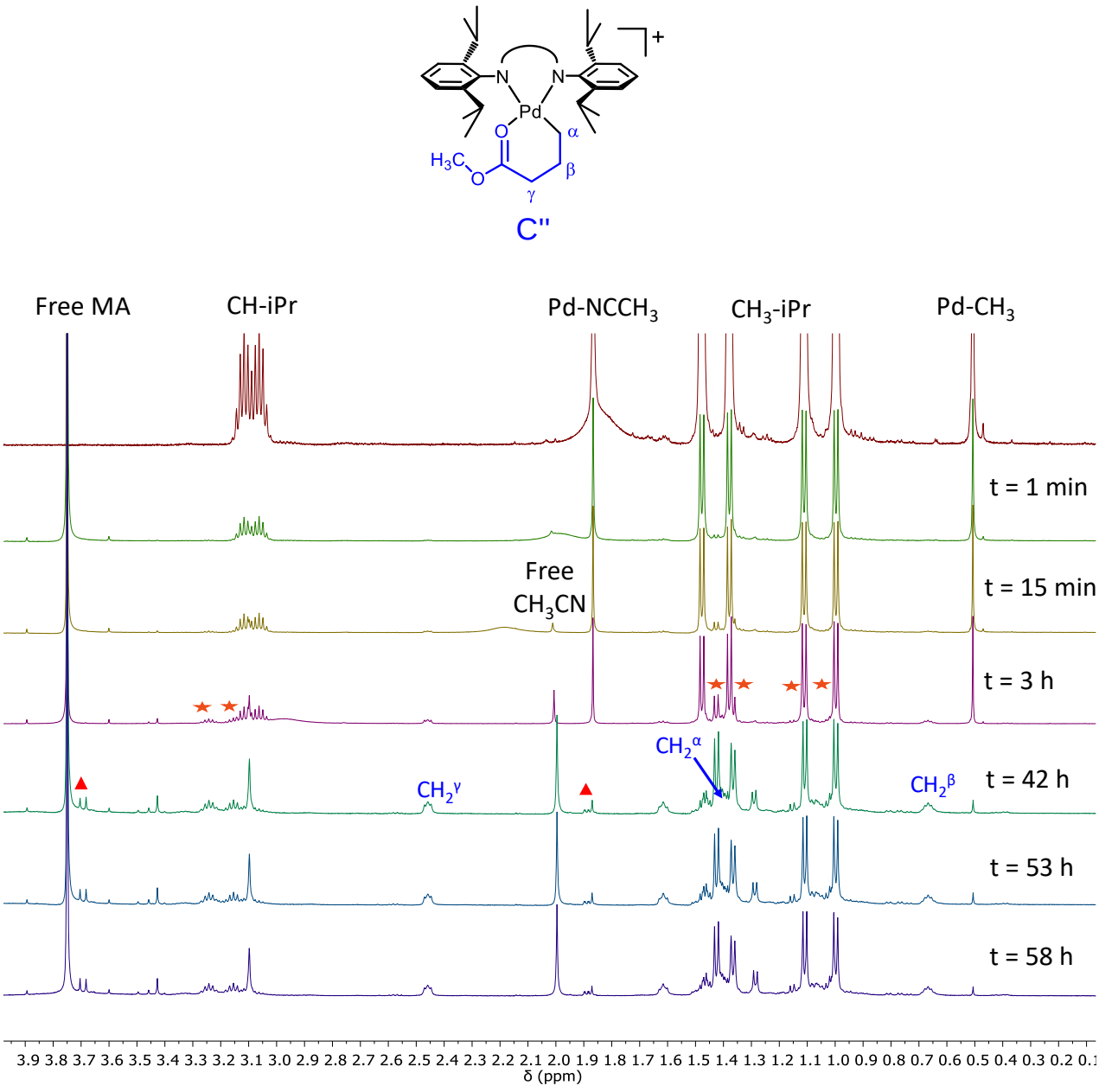

Figure 3.17. ^{1}H NMR spectra (CD_2Cl_2, 298 K) of reactivity of **5b** with MA, aliphatic region, evolution with time; ▲ = methyl crotonate, ★ = dimer.

Additionally, in the ^{1}H NMR spectra of the reactivity of **5b** and **6b**, other than the signals discussed above, new signals for the substituents on the aryl rings are clearly evident after 15 and

5 min, respectively. These results obtained with the study of the system in solution agree with the X ray analysis in solid state of crystals formed upon addition of *n*-hexane to these solutions kept at 277 K for two weeks.

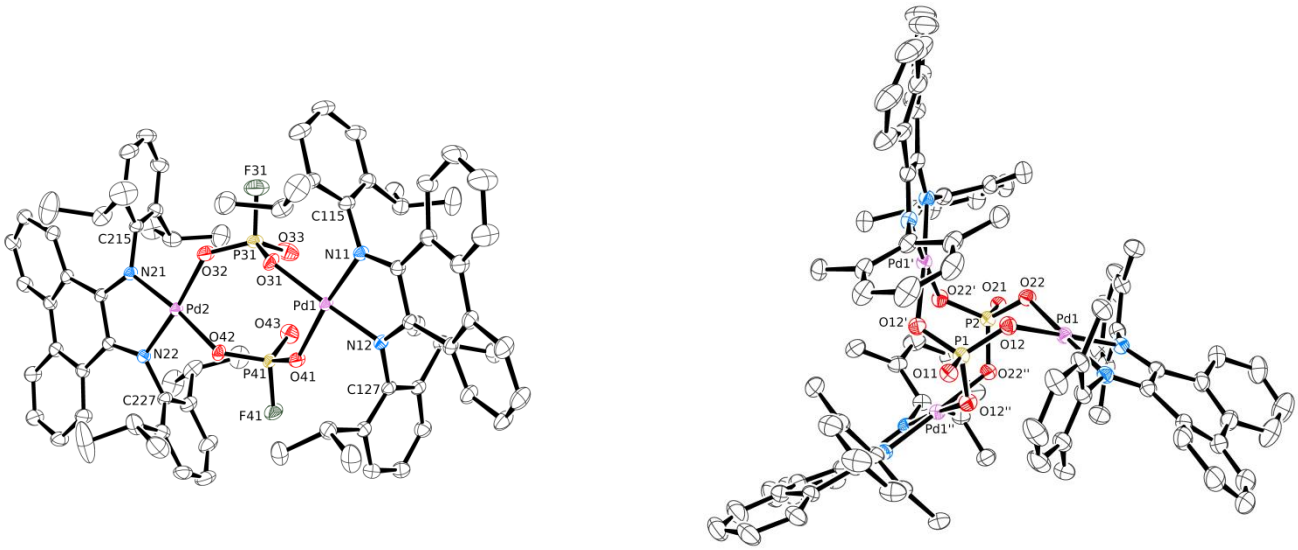

a) b)

Figure 3.18. ORTEP drawing (thermal ellipsoids at the 50 % of probability level) for complexes: a) dimer-**5c**; b) trimer-**6c**. Selected bond lengths (Å) for: **5c** Pd(1)-N(11) 1.969(21), Pd(1)-N(12) 1.968(2), Pd(1)-O(31) 2.013(2), Pd(1)-O(41) 2.007(2), Pd(2)-N(21) 1.970(2), Pd(2)-N(22) 1.968(2), Pd(2)-O(32) 2.017(2), Pd(2)-O(42) 2.014(2); **6c** Pd(1)-N 1.976(3), Pd(1)-N 1.973(3), Pd(1)-O(22) 2.024(2), Pd(1)-O(12) 2.021(2).

The crystals obtained from the reaction of **5b** with the monomer correspond to a dimeric species, **5c**, in which two tetrahedral PO_3F^{2-} ions bridge two Pd atoms (Pd---Pd distance: 5.227(2) Å; Figure 3.18a). The coordination sphere of each palladium is completed by the Ar-BIP ligand **5**. The crystals obtained from the reaction of **6b** with methyl acrylate are those of a trimeric species, **6c**, where two phosphate groups keep together the three Pd moieties. Also here the coordination sphere of each Pd is completed by one Ar-BIP ligand **2** (Figure 3.18b). Due to the increased rigidity of the trimeric molecule, the twisting of the Ar-BIP ligand is considerably reduced in **6c** with respect to the corresponding mononuclear complex **6a**, as shown in Figure 3.19. The Ar-BIP conformation in the dimer with ligand **5** is very similar to that in the trimer **6c** (Figure 3.19): however, no crystal structure is available for the corresponding **5a/b** complexes in order to make a direct comparison.

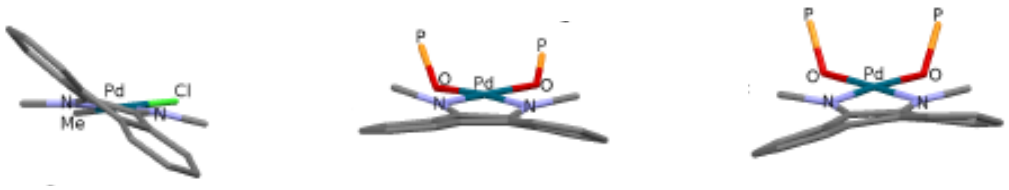

a) b) c)

Figure 3.19. Fragments cut out from the structures of a) **6a**; b) trimer **6c**; c) dimer **5c**. They put in evidence the decreased twisting of the Ar-BIP ligand on passing from the mononuclear to the multinuclear molecules.

The origin of the bridging ions, PO_3F^{2-} and PO_4^{3-}, can be traced to the partial or full hydrolysis of PF_6^- counteranions of the precatalyst. This is not a very common reaction pathway and only a few reports can be found in the literature about metal complexes with PO_3F^{2-} as bridging ligand, and even fewer where this anion connects just two metal centers.[21] Up to now, these are the first structurally characterized examples of Pd complexes of this kind.

Combining the NMR data about the reactivity with MA of the series of Ar-BIP complexes and the X-ray analysis, it is possible to suggest that the formation of the multinuclear species might represent a possible deactivation pathway for the Ar-BIP-catalysts, and that their formation is relevant when the catalytic reaction slows down.

3.3. Perspective: non-symmetrical Ar,Ar'-BIP ligands and the relevant Pd(II) complexes

In the group of Prof. Milani it was demonstrated that the introduction of a subtle steric and/or electronic unbalance in the substituents of the α-diimine ligand has a beneficial effect on the outcome of the catalysis.[4a,8] With the aim of moving forward in this direction and to evaluate if this outweigh in the properties of the two substituents on the nitrogen-donor atoms might result in some kind of cooperative effect with the properties related to the backbone of the ligand itself, two non-symmetric phenanthrene-based α-diimines were investigated. The studied Ar,Ar'-BIP ligands share one aryl ring substituted on 2,6-positions with the isopropyl group, and differ for the other aryl ring, having in one case the methyl substituent on both 2,6 positions (**8**) and in the other a CF_3 group on position 2 (**9**). Ligand **8** was already known in literature,[3] whereas **9** was synthesized here for the first time.

They were synthesized starting from the monoketimine with a 2,6-isopropyl substituted aryl ring, obtained through a condensation reaction between the phenanthrenequinone and the desired aniline, in the presence of formic acid, refluxing in methanol overnight (Scheme 3.6).[3,22]

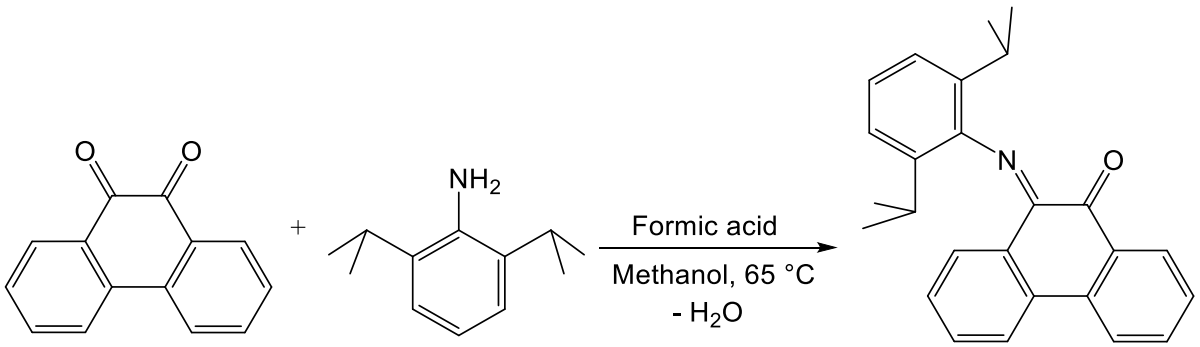

Scheme 3.6. Synthesis of the monoketimine.

From the ketimine, through a second condensation reaction carried out in toluene, in presence of $TiCl_4$ and the proper aniline, ligands **8** and **9** were obtained as orange or red solids, respectively, in acceptable yields (46 and 44%). The reaction was carried out at room temperature, to avoid the formation of sub- or scrambling products (Scheme 3.7).[3]

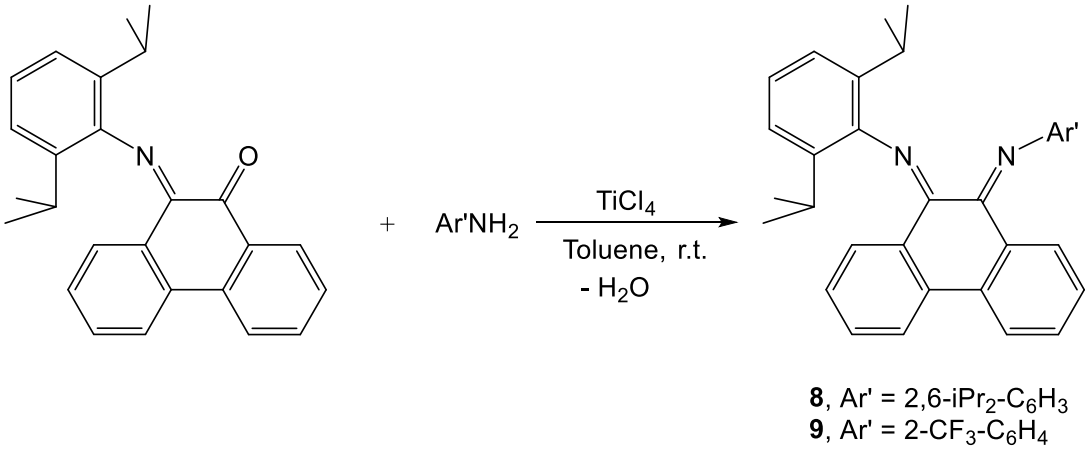

Scheme 3.7. Synthesis of the Ar,Ar'-BIP ligands **8** and **9**.

Ligands **8**, **9** were characterized both in solution and in solid state, evidencing the presence in solution of two different species, namely A, identified as the *E*,*Z* isomer with the C=N bond with the isopropyl group in *E* geometry, and B, identified as the *Z*,*E* isomer with the opposite configuration (Figures 3.20, 3.21). The two species were identified by mono- and bidimensional NMR spectroscopy. The ratio between the two isomers is different for the two ligands: for **8** is 1 : 0.74 for the A species, for **9** is 1 : 0.11 for the A species, thus suggesting a possible influence of the substituents in determining the preferred configuration. The presence of exchange peaks in the NOESY spectrum indicates that the two isomers are in slow equilibrium on the NMR time scale at room temperature.

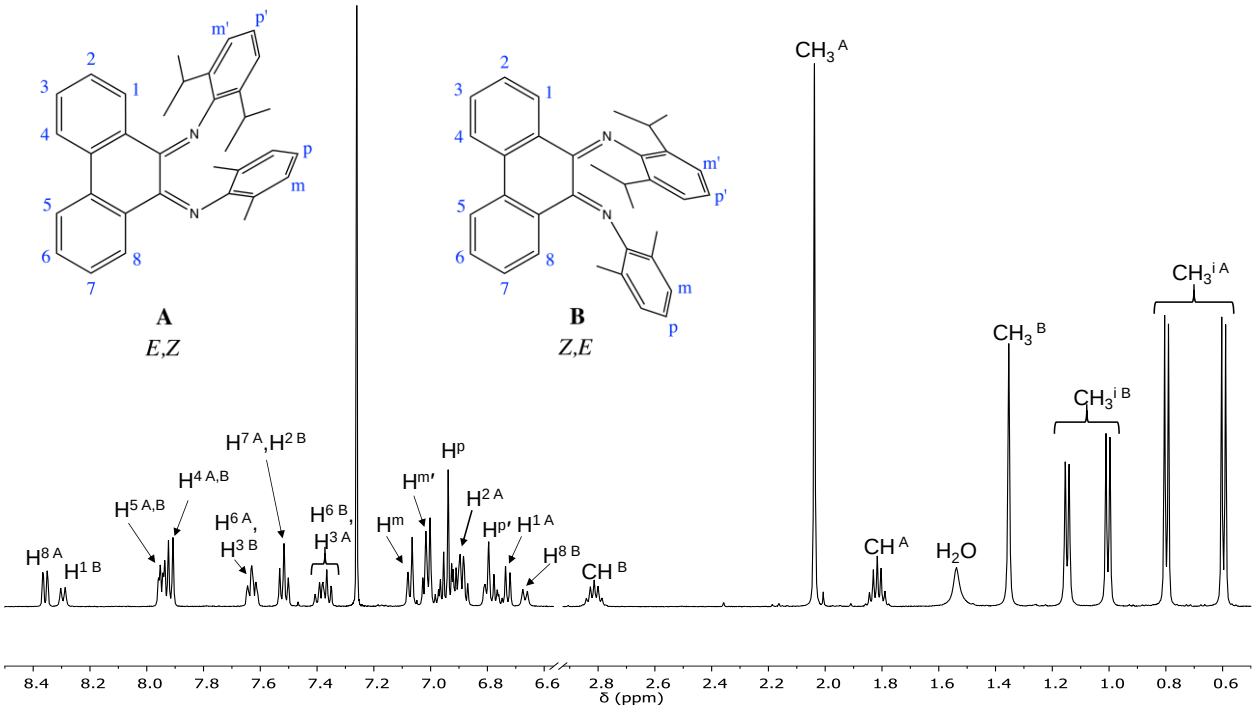

Figure 3.20. ^{1}H-NMR spectrum ($CDCl_3$, 298 K) of **8**.

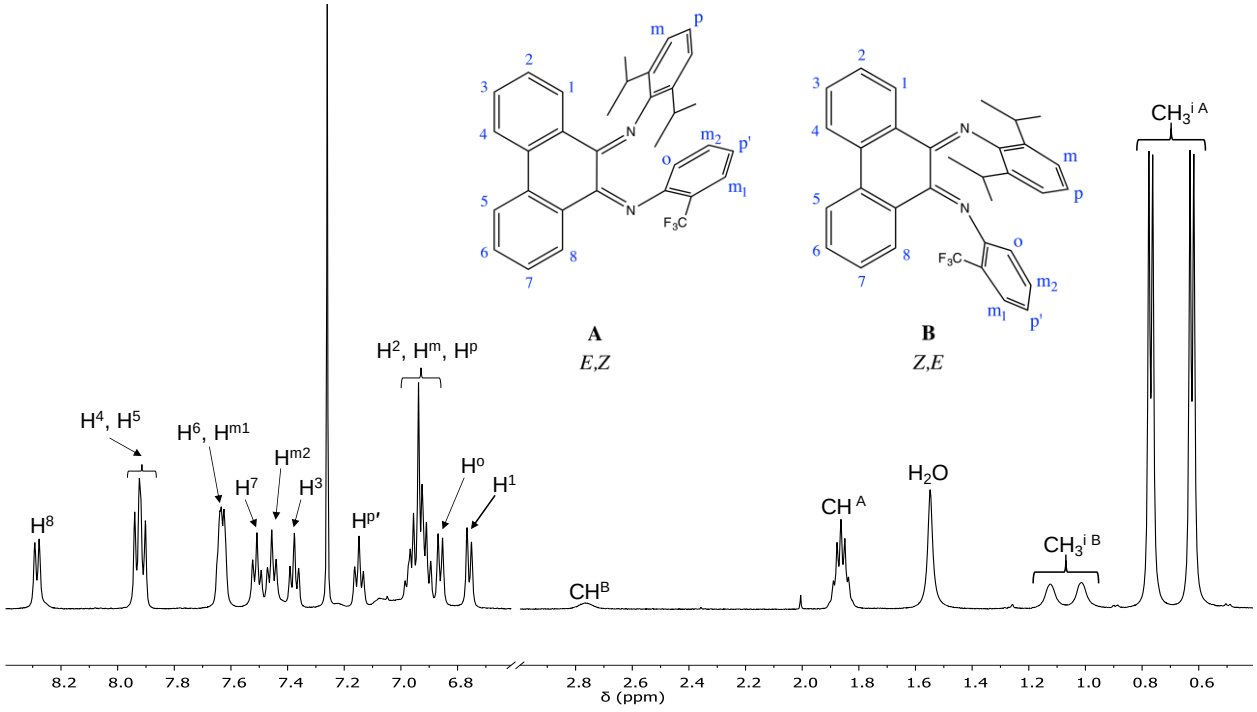

Figure 3.21. ^{1}H-NMR spectrum ($CDCl_3$, 298 K) of **9**.

Single crystals suitable for X-ray diffraction were obtained by layering n-hexane over a CD_2Cl_2 solution of **8** and **9**. For both ligands, the X-ray analysis shows the presence in the unit cell of just one isomer, the one in the *E,Z* configuration (A, Figure 3.22), that is also the prevailing one in solution. As for the symmetrical Ar-BIPs, the phenanthrene backbone is remarkably distorted from planarity, and the bond distances between the iminic carbon atoms and of the C=N bonds suggest a lack of conjugation in the molecules, similarly to the symmetrical Ar-BIP (Table 3.4).

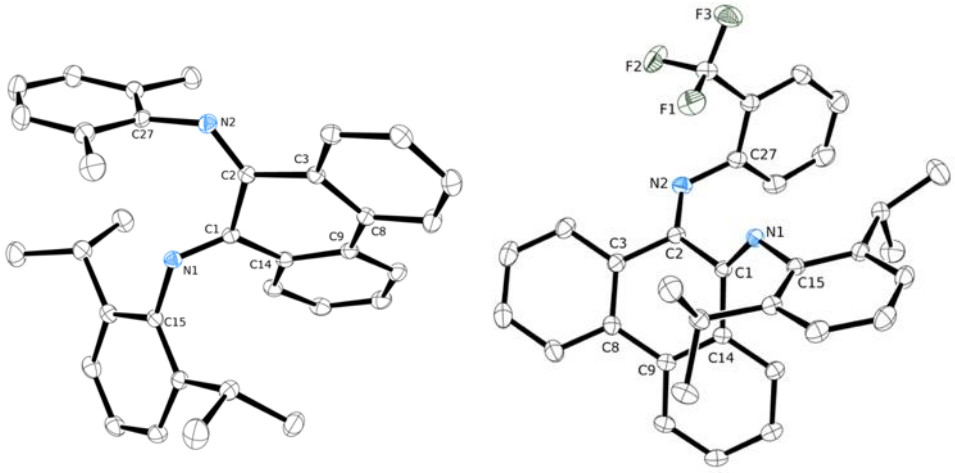

Figure 3.22. ORTEP drawing (thermal ellipsoids at the 50 % of probability level) for complexes: **8** (left), **9** (right).

Table 3.4. Distances, angles, torsion angles for ligands **8** and **9**.

Ligand	**8**	**9**
Distances (Å)		
N1-C1	1.2794(2)	1.2781(5)
N1-C15	1.4211(5)	1.4217(5)
N2-C2	1.277(2)	1.2774(5)
N2-C27	1.4172(9)	1.4077(2)
C1-C2	1.507(5)	1.5069(8)
C8-C9	1.4785(3)	1.4763(2)
C1-C14	1.4880(5)	1.4810(9)
C2-C3	1.4807(3)	1.4795(9)
Angles (°)		
C2-N2-C27	125.260(8)	122.727(6)
C1-N1-C15	122.644(5)	121.908(9)
Torsion angles (°)		
C1-C2=N2-C27	0.105(2)	11.317(5)
C14-C1-C2-C3	40.684(3)	45.024(9)
C2-C1=N1-C15	172.020(6)	166.978(5)
N1=C1-C2=N2	41.293(1)	46.456(3)

The synthesis of the neutral complexes [Pd(Ar,Ar'-BIP)(CH_3)Cl] **8a** and **9a** was performed by applying the same procedure used for the symmetrical counterparts (Scheme 3.2), and by using an excess of ligand of 6 and 9 equivalents with respect to palladium, and 19 and 30 days of reaction, with a yield of 54 and 48 %, respectively. Similarly to what is observed for complexes with pyridylimine ligands (see Chapter 2), for non-symmetrical ligands coordinated to palladium in a non-symmetrical chemical environment two different isomers are possible, both for neutral and cationic complexes, depending on the relative position of the Pd-CH_3 bond with respect to the two non-equivalent halves of the N-N' ligand. In this case, we define as the *cis* isomer the species with the Pd-CH_3 bond *cis* to the isopropyl-substituted aryl ring (Figure 3.23).

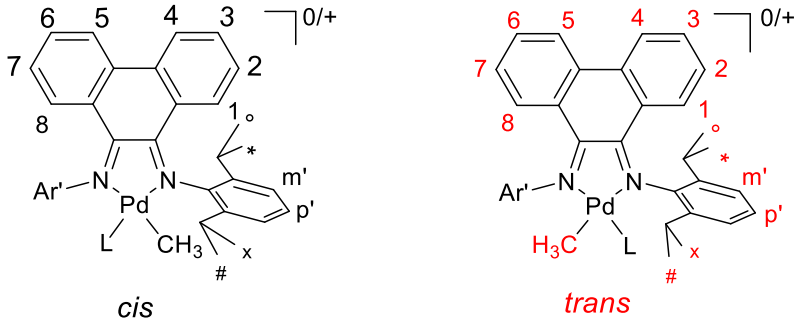

Figure 3.23. *Cis* and *trans* isomers for the neutral and cationic (Ar,Ar'-BIP)-Pd(II) complexes (L = Cl^- or labile ligand).

Both the neutral complexes were analysed in solution by mono- and bidimensional NMR spectroscopy, in CD_2Cl_2, at 298 K or 273 K. The ^1H NMR spectra of both **8a** and **9a** show the presence in solution of both *cis* and *trans* isomer, and in particular for the first, the ratio between the two species is *cis : trans* = 0.78 : 1, whereas for **9a** it is 10 : 1 (Figures 3.24, 3.25). The behaviour of **8a** does not agree with data reported in literature for other non-symmetrical complexes with Ar,Ar'-BIAN or Ar,Ar'-DAB ligands.[4a-b,8] Usually, for the neutral complexes, the difference in Lewis basicity of the two N-donor atoms determines the isomeric distribution, and the prevailing isomer is the one with the Pd-CH_3 bond *trans* to the iminic nitrogen with the lowest Lewis basicity that, for ligand **8**, is the nitrogen bearing the dimethyl-substituted aryl ring. This discrepancy could be due to the small difference in the donating capability of the two nitrogen-donor atoms in ligand **8**, that makes the steric effects more important in driving the coordination to palladium, thus directing it towards the isomer with the methyl *cis* to the less hindered aryl ring, that is the one with methyl groups in *ortho* positions. In addition, in the NOESY spectrum no exchange peaks are present indicating that the two isomers are not in equilibrium.

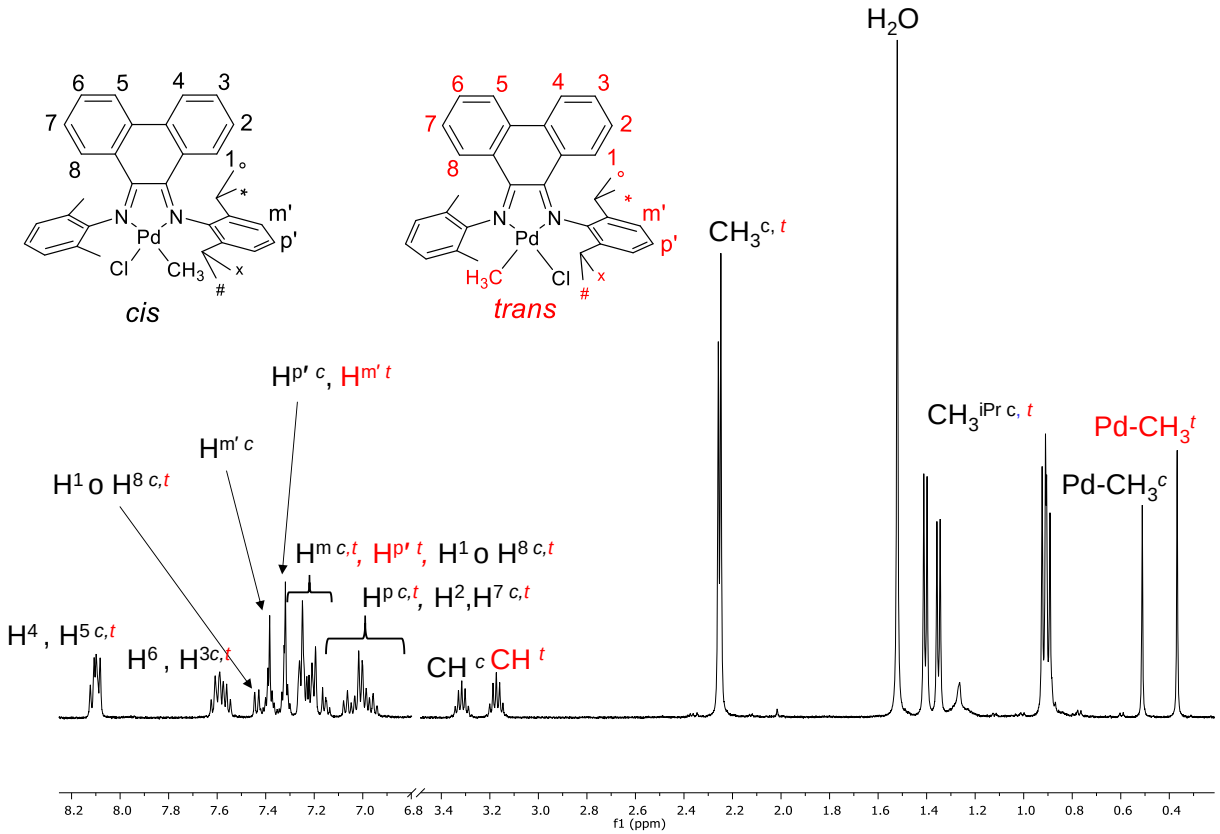

Figure 3.24. ^{1}H-NMR spectrum (CD_2Cl_2, 298 K) of **8a**.

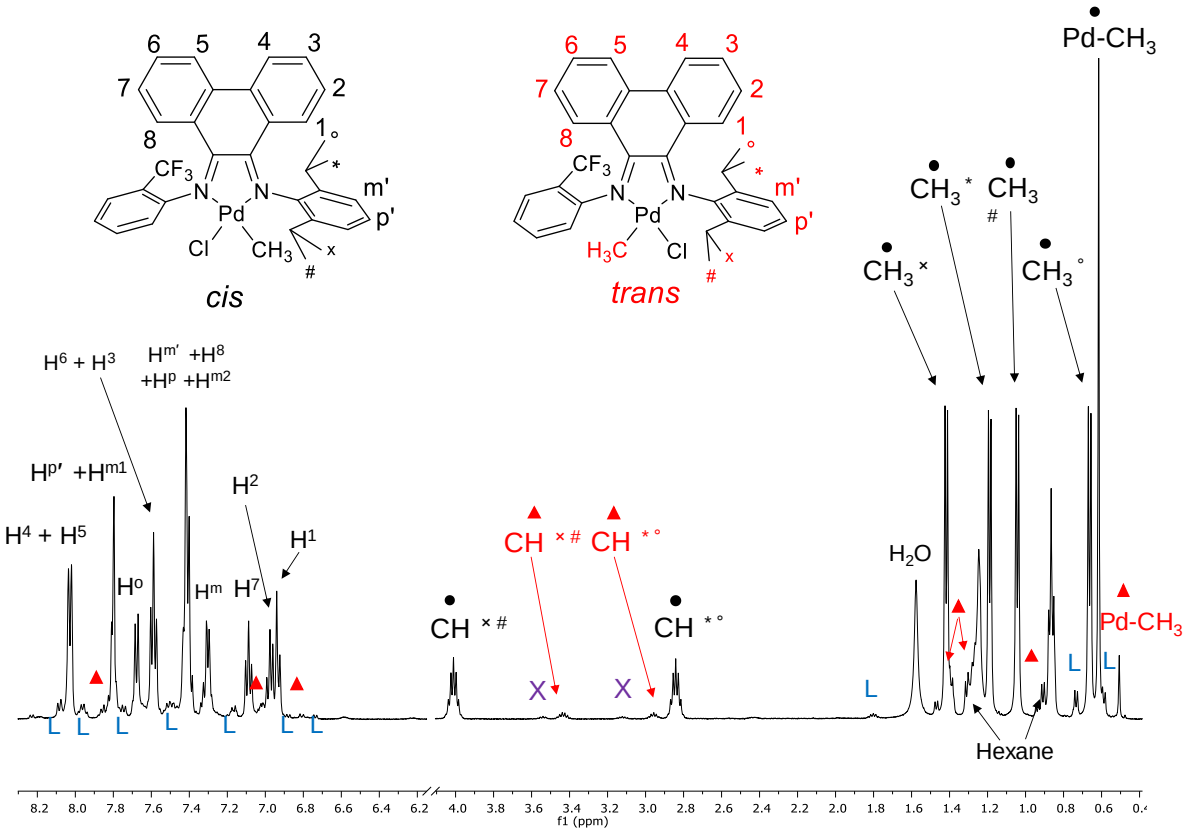

Figure 3.25. ^{1}H-NMR spectrum (CD_2Cl_2, 273 K) of **9a** (L= free ligand, X= unknown species).

In the ^{1}H NMR spectrum of **9a**, along with the signals relevant to the two isomers, the signals of the free ligand and of an unknown species with ligand **9** coordinated to the metal center are present in low intensity (Figure 3.25). The Pd-CH_3 resonate at 0.51 and 0.62 ppm respectively for the minor and the major species. Focusing on the latter, there are four doublets for the methyl of the isopropyl groups and two septets for the methinic protons: this differentiation is due to the fact that one of the aryl ring is mono-substituted in the *ortho* position, and consequently the square planar plane is no longer a symmetry plane. The NOESY NMR spectrum (Figure 3.26, dark green circles) confirms which is the prevailing species in solution and highlights a difference with respect to **8a**. For **9a** two different dynamic phenomena occur and are detectable in the NOESY spectrum: *i*. the rotation of the aryl rings around the C_{ipso}-N bond, resulting in the exchange between signals of the same groups in the same isomer (Figure 3.26, light blue circle), *ii*. the equilibrium between the isomers (Figure 3.26, brown peak). These phenomena are slow on the NMR time scale at 273 K.

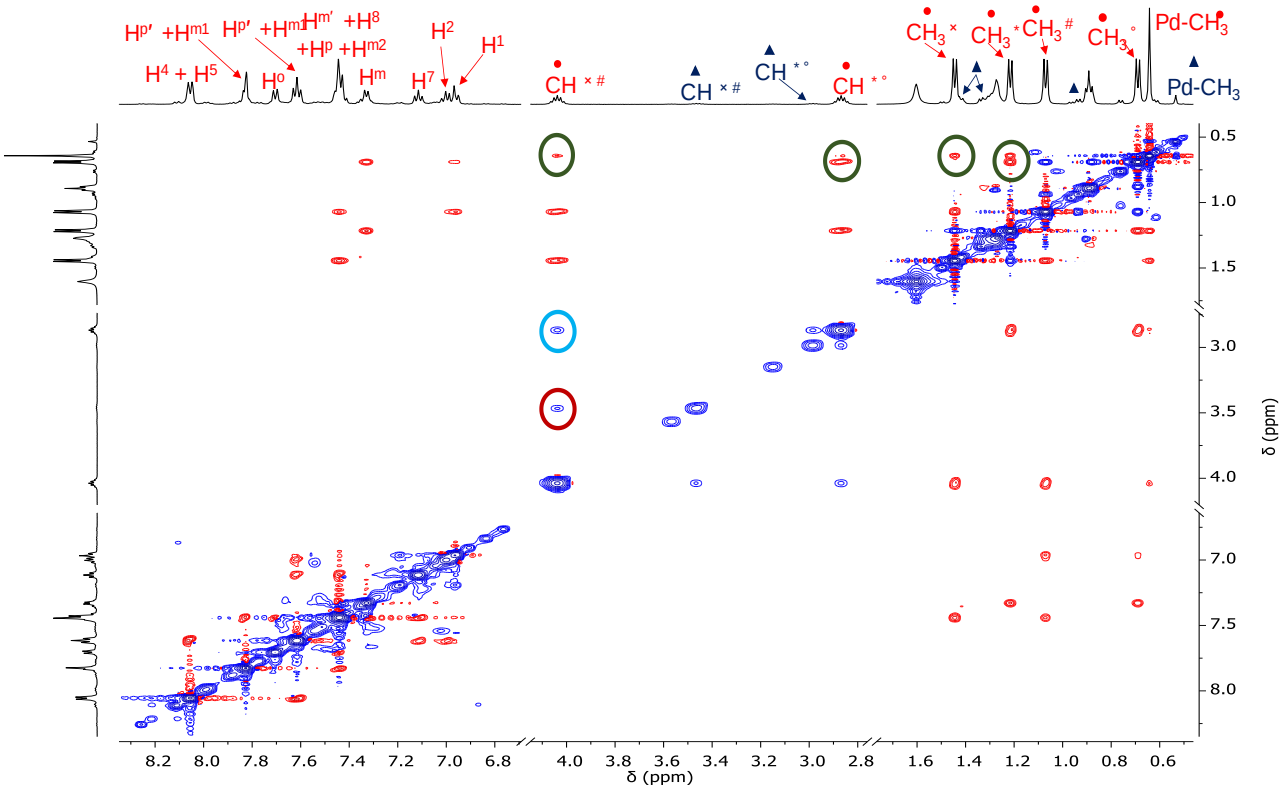

Figure 3.26. ^{1}H, ^{1}H-NOESY (CD_2Cl_2, 273 K) of complex **9a**. Dark green circles: NOE peaks between Pd-CH_3 and isopropyl groups; brown circles: exchange peak between *cis* and *trans* isomers; light blue circle: exchange peak between the methinic protons in the same isomer.

For complex **9a**, single crystals suitable for X-ray analysis were obtained by layering n-hexane over a solution of the complex in CD_2Cl_2. The complex crystalizes in a spatial group of the monoclinic system. In the unit cell only the *cis* isomer is present, featuring the Pd-CH_3 bond *trans* to the Pd-N atom bearing the aryl ring substituted with the CF_3 group, that is the major species in solution (Figure 3.27). The ligand coordinates to palladium in a *E,E* fashion and in a square planar environment, as expected. The two aryl substituents are projected outside the coordination plane, thus influencing the resonances of H^1 and H^8, for the diamagnetic anisotropic influence of the aryl rings.

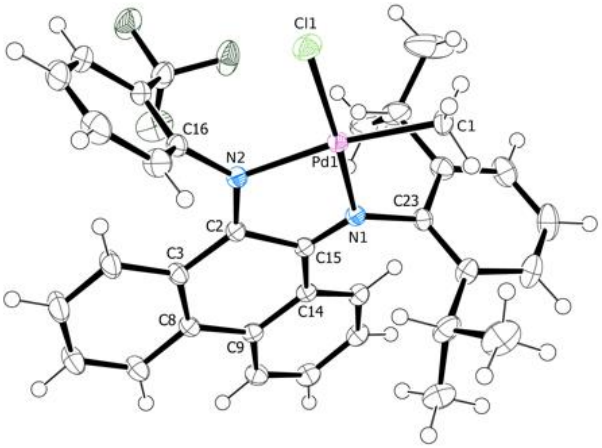

Figure 3.27. ORTEP drawing (thermal ellipsoids at the 50 % of probability level) for complex **9a.** Selected bond lengths (Å), angles and torsion angles (°) : Pd1-Cl1 2.2911(1), Pd1-C1 2.0642(8), Pd1-N1 2.0296(4), Pd1-N2 2.1182(2), N1-C15 1.3043(2), N2-C2 1.2985(2), C2-C15 1.5154(4), C8-C9 1.4809(3).

The Pd-N bonds are remarkably different, because of the methyl *trans*-influence: the length of the Pd-N2 *trans* to Pd-C1 is longer than that of Pd-N1 *trans* to Pd-Cl1 (2.1182(2) *vs* 2.0296(4) Å). The torsion angles between the iminic bond fragment N2C2-C15N1 and C3C2-C15C14 in the phenanthrene backbone significantly decreases upon coordination of **9** to palladium (from 46.456(3) to 12.704(6)° and from 20.595(3) to 5.887(7)°, respectively), thus imposing a higher planarity to the ligand skeleton. This behaviour is different from that of the symmetrical counterparts **6a** and **7a** (Figure 3.6), where upon coordination the iminic fragment becomes more planar, but as a consequence the phenanthrene backbone exhibits a higher distortion.[1,23] This higher planarity of the coordinated ligand might be induced by a favourable interaction between the proton of the isopropyl group and the fluorides in the trifluoromethyl substituent on the other

aryl ring. This interaction gets the two groups closer together, inducing a torsion in the two rings on the backbone. This is in agreement with the chemical shift of the methanic protons of one isopropyl group, that resonates at 4.01 ppm (Figure 3.25). Despite the planarity, there is still no conjugation between the rings in the phenathrene skeleton, as shown by the C2-C15 and C8-C9 bond distances, similar to those of the free ligand. The comparison between the crystal structures of **9a** and **6a** (Figure 3.27 *vs* 3.6a) points out that the Pd-CH_3 bond in **9a** is remarkably shorter than in **6a** (2.064(3) in **9a**, 2.087(2) Å in **6a**). This behaviour could be due to the fact that ligand **9**, having an electron-withdrawing substituent on the aryl ring *trans* to the methyl group, is a worse Lewis base, thus draining more charge density from palladium, with the consequence that in **9a** the coordinated methyl is a better σ-donor than in the other complexes. This is also in agreement with NMR data, where the resonance of the Pd-CH_3 moves to a deshielded direction going from **6a** to **9a** (0.39 and 0.61 ppm, respectively).[23]

The monocationic complexes [Pd(CH_3)(CH_3CN)(**8**)][X] (X = PF_6, **8b**; SbF_6, **8c**,) were synthesized from the neutral complex **8a**, following the usual synthetic procedure also employed for the symmetrical Ar-BIP cationic complexes (Scheme 3.3). Both $AgPF_6$ and $AgSbF_6$ were employed in the dehalogenation reaction, giving the desired complex with a yield of 95 and 92%, respectively. The complexes were characterized by mono- and bidimensional NMR spectroscopy in CD_2Cl_2 at 273 K and, as expected, they show the same signals in the ^{1}H NMR spectrum (Figures S3.63-65). For both complexes the *trans* isomer is the prevailing one, with a *cis : trans* ratio of 0.45 : 1. This is in agreement with the fact that for the monocationic complexes the isomeric distribution is determined also by steric hindrance. In fact, the acetonitrile, smaller than the methyl group, tends to occupy the position *cis* to the most hindered aryl ring, that is the one with isopropyl substituents. This is why the preference for the *trans* isomer is further enhanced in the monocationic complexes with respect to the neutral precursors. Unlike to **8a**, for **8b** and **8c** the two isomers are in equilibrium at 273 K, with a low rate on the NMR time scale.

The cationic complexes will be tested in the future in the ethylene/methyl acrylate copolymerization, and their performances compared to those of the precatalysts with the symmetrical Ar-BIP presented earlier in the chapter, to evaluate if the different substitution on the aryl rings has the same beneficial effect already observed for non-symmetrical α-diimines with the acenaphthene or the 1,4-diazabutadiene based backbone.[4a,8]

3.4. Conclusions

Organometallic palladium(II) complexes with α-diimine ligands having a phenanthrene skeleton and 2,6-disubstituted aryl rings (Ar-BIP) have now been investigated. The synthetic procedure applied to obtain the neutral complexes [Pd(Ar-BIP)(CH_3)Cl] was not as trivial as that typically applied to obtain the same compounds with the corresponding Ar-BIANs. This can be due to the lack in solution of the *E,E* isomer, to the remarkable distortion from planarity of the phenanthrene backbone and to the steric hindrance of the substituents in *ortho* positions on the aryl rings. The cationic [Pd(Ar-BIP)(CH_3)(CH_3CN)][PF_6] compounds were obtained from the neutral complexes with no difficulties.

From the characterization of the two series of complexes, both in solution and in solid state, it is clear that Ar-BIP ligands have a higher Lewis basicity than the corresponding Ar-BIAN counterparts and are more strongly bonded to the metal center. This makes the monocationic derivatives electron-rich metal cations.

The cationic compounds generated efficient catalysts for the ethylene/methyl acrylate copolymerization under mild reaction conditions of temperature and pressure leading to the corresponding copolymers. We carried out a detailed investigation of the catalytic behavior of the complexes, highlighting the main differences with catalysts having the Ar-BIANs. In particular, the Pd-(Ar-BIP) active species show a good affinity towards the polar monomer, a good thermal stability, lead to copolymers of higher molecular weight, and favor the cleavage of the 6-membered metallacycle, recognized as the resting state of the catalytic cycle. All these catalytic features are in agreement with the electron-rich metal cationic nature of the precatalysts.

The detailed NMR characterization of the produced macromolecules probed evidence that the polar vinyl monomer is inserted both at the end of the branches and into the main chain with a more selective enchainment of that achieved when the copolymerization is carried out in dichloromethane.

As a general conclusion this study points out the importance of the ligand backbone in the catalysts design for the ethylene/MA copolymerization and shows that moving from the acenaphthene to the phenanthrene skeleton has remarkable influence on both coordination chemistry and catalysis.

Moving forward into the design of the ligands for this kind of catalysts, Ar,Ar'-BIP were synthesized, and their coordination chemistry to Pd(II) was investigated. The non-symmetrical ligand should create a subtle steric and electronic unbalance around palladium, that can

favorably influence the catalytic outcomes. We are currently focusing on this aspect of the research.

3.4. Experimental

The synthesis of the ligands and of the neutral complexes were performed at room temperature; the cationic complexes were obtained using standard Schlenk techniques under argon. Anhydrous dichloromethane was obtained by distillation over CaH_2 under argon atmosphere. Deuterated solvents (Cambridge Isotope Laboratories, Inc. (CIL) and Sigma Aldrich) were stored as recommended by sellers. Ethylene (purity ≥ 99.9 %) supplied by SIAD and methyl acrylate (99.9%, with 0.02% of hydroquinone monomethyl ether) supplied by Aldrich were used as received. TFE and all the other reagents and solvents were purchased from Sigma-Aldrich/Merck and used without further purification for synthetic, spectroscopic and catalytic purposes. Ligands **5-9** and [Pd(cod)(CH_3)Cl], were synthesized according to literature procedures. [Pd($OAc)_2$] was a donation from BASF Italia and used as received.

NMR spectra of ligands, complexes and catalytic products were recorded on a Varian 500 spectrometer at 500 MHz (^{1}H) and 125.68 MHz (^{13}C). The resonances are reported in ppm (δ) and referenced to the residual solvent peak versus Si($CH_3)_4$: $CDCl_3$ at δ 7.26 (^{1}H and δ 77.0 (^{13}C), CD_2Cl_2 at δ 5.32 (^{1}H) and δ 54.0 (^{13}C). NMR experiments were performed employing the automatic software parameters. In the case of NOESY experiments a mixing time of 500 ms was used. IR spectra were recorded in Nujol on a Perkin Elmer System 2000 FT-IR. Elemental analyses were performed in the Department of Chemistry "G. Ciamician" of University of Bologna, on a Thermo Flash 2000 CHNS/O analyzer. Checking of low-molecular weight oligomers were performed by GC-MS analyses using an Agilent GC 7890 instrument equipped with a DB-225ms column (J&W, 60 m, 0.25 mm ID, 0.25 μm film, carrier He) and a 5975 MSD. Before analysis, samples were diluted with methanol and nonane was added as internal standard. The consumption of ethylene was monitored by using a Bronkhorst EL-Pressure e EL-Flow *select* mass flow control device. TLC were run on silica gel plates, eluting with petroleum ether: AcOEt mixtures. Mass spectra (ESI-MS) were recorded on a Perkin Elmer APII spectrometer at 5600 eV.

The average molecular weights (M_n and M_w) and polydispersity (M_w/M_n) values of copolymer samples were measured through gel permeation chromatography at 30 °C, using THF as the solvent, an eluent flow rate of 1 mL min^{-1}, and 19 narrow polystyrene standards as the reference.

The measurements were performed on a Waters 1525 binary system equipped with a Waters 2414 RI detector using four Styragel columns (range 1000–1 000 000 Å).

3.4.1. Synthesis and characterization of ligands ***5-7****.*

The ligands were synthesized by a slight modification of the procedure reported by Shavyrin et al.[1] To a solution of 9,10-phenanthrenequinone (2.4 mmol) in toluene (15 mL) the appropriate aniline was added (19.2 mmol, 8 equiv), followed by dropwise addition of $TiCl_4$ (2.4 mmol), dissolved in 0.5 mL of the same solvent The solution was left on stirring at r.t. for 24 h, until complete conversion of the starting material (TLC, eluent: petroleum ether : ethyl acetate = 6 : 1). The reaction mixture was then washed with H_2O to neutrality, the organic phase was separated, dried over $NaSO_4$ and filtered. The product obtained after removal of the solvent in vacuo was recrystallized from acetonitrile.

5. (Orange solid, yield 45%); ^{1}H NMR (400 MHz, $CDCl_3$, 298 K): δ 8.30 (d, *J* = 7.6 Hz, 1H, H^8), 7.94 (d, *J* = 7.9 Hz, 1H, H^5), 7.90 (d, *J* = 7.9 Hz, 1H, H^4), 7.63 (t, *J* = 7.3 Hz, 1H, H^6), 7.52 (t, *J* = 7.5 Hz, 1H, H^7), 7.35 (t, *J* = 7.5 Hz, 1H, H^3), 7.10 (m, 2H, $H^{m'}$), 7.04 (m, 1H, H^2), 6.99 – 6.81 (m, 4H, H^m, H^p, $H^{p'}$), 6.68 (d, *J* = 7.8 Hz, 1H, H^1), 2.82 (sept., 2H, Ar-*CH*$(CH_3)_2$), 1.86 (sept., 2H, Ar-*CH*$(CH_3)_2$), 1.14 (d, *J* = 6.8 Hz, 6H, Ar-CH(*CH*$_3)_2$), 1.03 (d, *J* = 6.9 Hz, 6H, Ar-CH(*CH*$_3)_2$), 0.75 (d, *J* = 6.7 Hz, 6H, Ar-CH(*CH*$_3)_2$), 0.59 (d, *J* = 6.8 Hz, 6H, Ar-CH(*CH*$_3)_2$); ^{13}C NMR (125.68 MHz, $CDCl_3$, 298 K): δ 131.61 (H^6), 130.76 (H^3), 128.16 (H^1), 127.19 (H^8), 126.67 ($H^{p,p'}$), 124.16 (H^4), 123.14 (H^m), 123.09 (H^5), 123.05 (H^2), 122.22 ($H^{m'}$), 28.62, 27.20 (Ar-*C*H$(CH_3)_2$), 24.63, 23.35, 22.56, 22.37 (Ar-CH(*C*$H_3)_2$) ppm. TLC (silica, petroleum ether : ethyl acetate = 6:1) Rf = 0.83. ESI-MS (*m/z*) : 527.4 $[M+H]^+$.

6. (Orange-red solid, yield 60%); ^{1}H NMR (500 MHz, $CDCl_3$, 298 K): δ8.33 (d, *J* = 7.6 Hz, 1H, H^8), 7.94 (d, *J* = 7.9 Hz, 1H, H^5), 7.91 (d, *J* = 8.0 Hz, 1H, H^4), 7.62 (t, *J* = 7.5 Hz, 1H, H^6), 7.51 (t, *J* = 7.4 Hz, 1H, H^7), 7.40 (t, *J* = 7.6 Hz, 1H, H^3), 6.98 (d, *J* = 7.5 Hz, 2H, $H^{m'}$), 6.92 (t, *J* = 7.5 Hz, 1H, H^2), 6.86 (t, *J* = 7.5 Hz, 1H, H^p), 6.84 – 6.76 (m, 3H, H^m, $H^{p'}$), 6.71 (d, *J* = 7.8 Hz, 1H, H^1), 2.04 (s, 6H, Ar-*CH*$_3$), 1.38 (s, 6H, Ar-*CH*$_3$); ^{13}C NMR (125.68 MHz, $CDCl_3$, 298 K): δ 131.70 (H^6), 131.26 (H^3), 128.94 (H^7), 127.72 (H^m), 127.59 (H^1), 127.41 ($H^{m'}$), 127.26 (H^2), 126.87 (H^8), 124.43, 123.45 ($H^{4,5}$), 122.98 ($H^{p'}$), 122.39 (H^p), 18.21, 17.04 (Ar-*CH*$_3$) ppm. TLC (silica, petroleum ether : ethyl acetate = 6 : 1) Rf = 0.60; ESI-MS (*m/z*) : 415.3 $[M+H]^+$.

7. (Red solid, yield 44 %) ^{1}H NMR (400 MHz, $CDCl_3$, 298 K): δ 8.10 (d, *J* = 7.6 Hz, 1H, H^1), 7.94 (d, *J* = 7.9 Hz, 1H, H^4), 7.61 (t, *J* = 7.6 Hz, 1H, H^3), 7.48 (t, *J* = 7.5 Hz, 1H, H^2), 7.03 (t, *J* = 7.5 Hz, 2H, H^m), 6.96 (t, *J* = 7.3 Hz, 1H, H^p), 6.29 (d, *J* = 7.6 Hz, 2H, H^o); ^{13}C NMR (100.54

MHz, $CDCl_3$, 298 K): δ 131.70 (H^3), 128.96 (H^2), 128.74 (H^m), 126.48 (H^1), 124.50 (H^p), 123.63 (H^4), 119.73 (H^o) ppm. TLC (silica, petroleum ether : ethyl acetate = 6 : 1) Rf = 0.49. ESI-MS (*m/z*) : 359.2 $[M+H]^+$.

*3.4.2. Synthesis and characterization of ligands **8-9**.*

The ligands were synthesized following a slightly modified literature procedure: 1.0 eq. (2.72 mmol, 1.01 g) of 2,6-isopropyl substituted monoketimine are dissolved in 4 mL of toluene in a round bottom flask. 3.0 equiv of the desired aniline are added (8.16 mmol, 1.01 mL of 2,6-dimethylaniline for **8** and 1.03 mL di 2-(trifluoromethyl)aniline per **9**) and 1.0 equiv of $TiCl_4$ (2.72 mmol, 0.52 mL) dissolved in 0.5 mL of toluene. The dark green solution turns immediately to dark red-brown and a precipitate forms. The reaction mixture is left under stirring for 2 h, and then washed with H_2O to neutrality. The organic phase was separated, dried over $NaSO_4$ and filtered. The product obtained after removal of the solvent in vacuo was recrystallized from acetonitrile.

8. (orange solid, yield 46%) ^{1}H-NMR (500 MHz, $CDCl_3$, 298 K) δ = 8.36 (d, *J* = 7.8, 1.4 Hz, 1H, $H^{8\ A}$), 8.30 (d, *J* = 7.7 Hz, 1H, $H^{1\ B}$), 7.95 (dd, *J* = 8.2, 3.4 Hz, 1H, H^4), 7.92 (d, *J* = 8.0 Hz, 1H, H^5), 7.63 (dd, *J* = 8.0, 2.1 Hz, 1H, H^6), 7.52 (t, *J* = 7.5 Hz, 1H, H^7), 7.42 – 7.34 (m, 1H, H^3), 7.07 (d, *J* = 7.6 Hz, 2H, H^m), 7.01 (d, *J* = 7.3 Hz, 1H, $H^{p\prime}$), 6.99 – 6.85 (m, 2H, H^p, H^2), 6.83 – 6.74 (m, 2H, $H^{m\prime}$), 6.73 (d, *J* = 8.0, 1.3 Hz, 1H, $H^{1\ A}$), 6.67 (d, *J* = 7.9 Hz, 1H, $H^{8\ B}$), 2.81 (hept, *J* = 7.0 Hz, 2H, Ar-$CH^{i\ B}$), 2.04 (s, 6H, Ar-$CH_3{}^A$), 1.82 (hept, *J* = 6.9 Hz, 2H, Ar-$CH^{i\ A}$), 1.35 (s, 6H, Ar-$CH_3{}^B$), 1.15 (d, *J* = 6.9 Hz, 6H, Ar-$CH_3{}^{i\ B}$), 1.00 (d, *J* = 6.9 Hz, 6H, Ar-$CH_3{}^{i\ B}$), 0.80 (d, *J* = 6.8 Hz, 6H, Ar-$CH_3{}^{i\ A}$), 0.60 (d, *J* = 6.8 Hz, 6H, Ar-$CH_3{}^{i\ A}$); ^{13}C-NMR (125.68 MHz, $CDCl_3$, 298 K) δ = 127.20, 127.40, 123.39, 124.47, 128.99, 131.18, 122.45, 123.15, 127.40, 123.39, 127.74, 128.68, 28.67, 18.42, 24.41, 12.43, 27.35, 17.21, 23.44, 22.57, 14.65, 30.41, 24.00, 22.74. ESI-MS (*m/z)* = 471.3 $[M+H]^+$.

9. (Red crystals, yield 44 %); ^{1}H-NMR (500 MHz, $CDCl_3$, 298 K) δ = 8.29 (d, *J* = 7.9 Hz, 1H, H^8), 7.92 (dd, *J* = 10.9, 7.9 Hz, 2H, H^5, H^4), 7.64 (dd, *J* = 7.7, 4.4 Hz, 2H, H^{m1}, H^6), 7.51 (t, *J* = 7.5 Hz, 1H, H^7), 7.46 (t, 1H, H^{m2}), 7.38 (t, *J* = 7.6 Hz, 1H, H^3), 7.15 (t, *J* = 7.7 Hz, 1H, H^p), 7.00 – 6.88 (m, 4H, H^2, $H^{m\prime}$, $H^{p\prime}$), 6.86 (d, *J* = 7.9 Hz, 1H, H^o), 6.76 (d, *J* = 7.9 Hz, 1H, H^1), 2.76 (s, 2H, Ar-CH^B), 1.86 (hept, *J* = 6.8 Hz, 2H, Ar-CH^A), 1.07 (d, *J* = 54.5 Hz, 12H, Ar-$CH_3{}^{i\ B}$), 0.77 (d, *J* = 6.7 Hz, 6H, Ar-$CH_3{}^{i\ A}$), 0.62 (d, *J* = 6.8 Hz, 6H, Ar-$CH_3{}^{i\ A}$); ^{13}C-NMR (125.68 MHz, $CDCl_3$, 298 K) δ = 127.95, 123.31, 124.44, 132.28, 126.20, 129.09, 131.98, 131.29, 122.48, 124.21, 123.41, 127.31, 119.88, 128.41, 27.52, 23.94, 31.82, 16.04, 22.59, 13.88, 31.25; ^{19}F-NMR (376 MHz, CD_2Cl_2, 298 K) δ = -61.78 (s, Ar-CF_3); ESI-MS (*m/z*) = 511.3 $[M+H]^+$.

3.4.3. Synthesis and characterization of [Pd(Ar-BIP)(CH_3)Cl] ***5a-9a****.*

To a stirred solution of [Pd(cod)(CH_3)Cl] (0.2 mmol) in dichloromethane (2 mg/ml of Pd complex) the Ar-BIP ligand (15 equiv for **5**, 6 equiv for **6**, 1.5 equiv for **7,** 6 equiv for **8,** 9 equiv for **9**) was added, at r.t.. Hexane (to a ratio dichloromethane : hexane = 3 : 4) was then slowly added, the reaction mixture was left on stirring protected from light until the appearance of a solid (15 days for **5,** 6 days for **6** and **7,** 20 days for **8**, 30 days for **9**), maintaining constant the volume of the solution by addition of hexane. The solid formed was filtered under reduced pressure and washed with cold hexane.

5a. (Dark brown-purple solid, yield 83%); ^{1}H NMR (500 MHz, CD_2Cl_2, 263 K): δ 8.12 (dd, *J* = 7.9, 2.9 Hz, 2H, $H^{4,5}$), 7.62 – 7.51 (m, 2H, $H^{3,6}$), 7.36 (m, 3H, $H^{m,p}$), 7.30 (m, 3H, $H^{m',p'}$), 7.23 (d, *J* = 8.4 Hz, 1H, H^8), 7.03 (d, *J* = 8.4 Hz, 1H, H^1), 6.99 (t, *J* = 7.8 Hz, 1H, H^7), 6.94 (t, *J* = 7.8 Hz, 1H, H^2), 3.28 – 3.15 (m, 2H, Ar-*CH*(CH_3)$_2$), 3.15 – 3.04 (m, 2H, Ar-*CH*(CH_3)$_2$), 1.40 (d, *J* = 6.8 Hz, 3H, Ar-CH(*CH_3*)$_2$), 1.34 (d, *J* = 6.8 Hz, 3H, Ar-CH(*CH_3*)$_2$), 0.89 (dd, *J* = 10.6, 6.9 Hz, 6H Ar-CH(*CH_3*)$_2$), 0.41 (s, 3H, Pd-CH_3); ^{13}C NMR (125.68 MHz, $CDCl_3$, 263 K): δ 133.60 ($H^{3,6}$), 131.13 (H^1), 130.83 (H^8), 128.45 (H^7), 128.26 (H^2), 127.34 ($H^{m,p}$), 126.49 ($H^{m,p}$), 124.91 ($H^{m,p}$), 124.81 ($H^{4,5}$), 124.19 ($H^{m,p}$), 29.98, 29.37 (Ar-*C*H(CH_3)$_2$), 23.43, 23.24, 22.85 (Ar-CH(*C*H_3)$_2$), 7.20 (Pd-*C*H_3) ppm. Elemental analysis, calcd for $PdClC_{39}H_{45}N_2$ (%): C = 68.52, H = 6.63, N = 4.10; found: C = 68.42, H = 6.49, N = 4.57.

6a. (Dark red-purple solid, yield 84%); ^{1}H NMR (500 MHz, CD_2Cl_2, 263 K): 8.08 (dd, *J* = 7.8, 2.3 Hz, 2H, $H^{4,5}$), 7.60 (dt, *J* = 10.5, 7.5 Hz, 2H, $H^{3,6}$), 7.37 (d, *J* = 8.3 Hz, 1H, H^8), 7.28-7.11 (m, 7H, $H^{m',1,m,p',p}$), 7.06 (t, *J* = 7.7 Hz, 1H, H^7), 7.01 (t, *J* = 7.8 Hz, 1H, H^2), 2.25 (s, 12H, Ar-*CH_3*), 0.32 (s, 3H, Pd-CH_3); ^{13}C NMR (125.68 MHz, $CDCl_3$, 263 K): δ 133.82 ($H^{3,6}$), 129.15 ($H^{7,2}$), 129.00 ($H^{7,2}$), 128.94 ($H^{m'}$), 128.78 (H^8), 128.40 (H^m), 126.47 (H^1), 125.80 ($H^{p'}$), 125.65 (H^p), 125.04 ($H^{4,5}$), 18.55 (Ar-*C*H_3), 5.60 (Pd-*C*H_3) ppm. Elemental analysis, calcd for $PdClC_{31}H_{29}N_2$ (%): C = 65.16, H = 5.11, N = 4.90; found: experimental: C = 65.21, H = 4.99, N = 4.69.

7a. (Dark red solid, yield 70%); ^{1}H NMR (500 MHz, CD_2Cl_2, 263 K): δ 7.89 (d, *J* = 8.1 Hz, 2H, $H^{4,5}$), 7.53 (ddd, *J* = 12.1, 6.4, 3.1 Hz, 2H, $H^{3,6}$), 7.48 (t, *J* = 7.9 Hz, 1H, H^m), 7.42 (t, *J* = 7.8 Hz, 1H, $H^{m'}$), 7.36-7.31 (m, 4H, $H^{p,o',p'}$), 7.21 (d, *J* = 7.4 Hz, 2H, H^o), 7.09 – 6.89 (m, 4H, $H^{8,7,1,2}$), 0.78 (s, 3H, Pd-CH_3); ^{13}C NMR (125.68 MHz, CD_2Cl_2, 263 K) δ = 133.75 ($H^{3,6}$), 131.14 (H^8), 130.98 (H^1), 129.99 (H^m), 129.32 ($H^{m'}$), 128.60 ($H^{7,2}$), 127.77 (H^p), 127.33 ($H^{p'}$), 125.80 ($H^{4,5}$),

123.28 (H^{o}), 123.11 ($H^{o'}$), 6.45 (Pd-CH_3) ppm. Elemental analysis, calcd for $PdClC_{27}H_{21}N_2$ (%): C = 62.93, H = 4.11, N = 5.44; found: C = 62.49, H = 3.84, N = 5.03.

8a. (Dark red solid, yield 54 %), ^{1}H-NMR (500 MHz, CD_2Cl_2, 298 K) δ = 8.10 (dd, *J* = 12.4, 7.9 Hz, 2H, H^4, H^5 *cis,trans*), 7.58 (dt, *J* = 14.6, 7.9 Hz, 2H, H^6, H^3 *cis,trans*), 7.44 (d, *J* = 8.4 Hz, 1H, H^8 o H^1 *cis,trans*), 7.41 – 7.36 (m, 2H, $H^{m\prime}$ *trans*), 7.36 – 7.29 (m, 2H, $H^{m\prime}$ *cis*), 7.26 (d, *J* = 6.6 Hz, 2H, H^m *cis,trans*, $H^{p\prime}$ *trans*), 7.23 (d, *J* = 4.6 Hz, 1H, H^1 o H^8 *cis,trans*), 7.06 (t, *J* = 8.6, 7.2 Hz, 1H, H^7 o H^2 *cis,trans*), 7.04 – 6.98 (m, 2H, H^p *cis,trans*), 6.96 (t, 1H, H^2 o H^7 *cis,trans*), 3.32 (hept, *J* = 6.8 Hz, 2H, Ar-*CH*^{i} *cis*), 3.17 (hept, *J* = 6.8 Hz, 2H, Ar-*CH*^{i} *trans*), 2.25 (d, *J* = 5.2 Hz, 12H, Ar-*CH*$_3$ *cis*, Ar-*CH*$_3$ *trans*), 1.41 (d, *J* = 6.8 Hz, 6H, Ar-*CH*$_3^{i^\circ}$ *trans*), 1.35 (d, *J* = 6.8 Hz, 6H, Ar-*CH*$_3^{i^\circ}$ *cis*), 0.91 (dd, *J* = 9.3, 6.9 Hz, 6H, Ar-*CH*$_3^{i*}$ *trans*, Ar-*CH*$_3^{i*}$ *cis*), 0.51 (s, 3H, Pd-*CH*$_3$ *cis*), 0.37 (s, 3H, Pd-*CH*$_3$ *cis*); ^{13}C-NMR (125.68 MHz, CD_2Cl_2, 298 K) δ = 124.94, 133.64, 124.94, 126.50, 124.15, 130.77, 129.02, 126.38, 126.50, 128.39, 129.02, 130.97, 128.66, 18.11, 23.41, 22.83, 31.47, 23.20, 14.90.

9a. (dark red solid, yield 48 %); ^{1}H-NMR (500 MHz CD_2Cl_2, 273 K) δ = 8.06 – 8.00 (d, 2H, H^4, H^5 *cis*), 7.84 – 7.76 (m, 2H, H^{m1}, $H^{p\prime}$ *cis*), 7.68 (d, *J* = 7.9 Hz, 1H, H^o *cis*), 7.59 (t, *J* = 7.7 Hz, 2H, H^6, H^3 *cis*), 7.46 – 7.36 (m, 4H, H^8, H^p, H^m, H^{m2} *cis*), 7.35 – 7.26 (m, 1H, $H^{m\prime}$ *cis*), 7.09 (t, *J* = 7.9 Hz, 1H, H^7 *cis*), 6.98 (t, *J* = 7.9 Hz, 1H, H^2 *cis*), 6.93 (d, 1H, H^1 *cis*), 4.01 (hept, *J* = 6.8 Hz, 1H, *CH*$^{\times\,\#}$ *cis*), 3.43 (hept, *J* = 6.9 Hz, 1H, *CH*$^{\times\,\#}$ *cis*), 2.96 (hept, 1H, *CH**° *cis*), 2.84 (hept, *J* = 6.8 Hz, 1H, *CH**° *trans*), 1.45 – 1.37 (m, 6H, *CH*$_3^{\times}$ *cis*, *trans*), 1.31 (d, *J* = 6.9 Hz, 3H *CH*$_3^{*}$ *trans*), 1.19 (d, *J* = 6.8 Hz, 3H, *CH*$_3^{*}$ *cis*), 1.04 (d, *J* = 6.8 Hz, 3H, *CH*$_3^{\#}$ *cis*), 0.91 (d, *J* = 6.9 Hz, 3H, *CH*$_3^{\#}$ *trans*), 0.66 (d, *J* = 6.8 Hz, 3H, *CH*$_3$° *cis*), 0.62 (s, 3H, Pd-*CH*$_3$ *cis*), 0.51 (s, 3H, Pd-*CH*$_3$ *trans*); ^{13}C-NMR (125.68 MHz, CD_2Cl_2, 273 K) δ = 125.35, 131.86, 125.93, 126.85, 133.99, 125.09, 125.93, 127.71, 130.49, 124.46, 125.09, 128.66, 128.66, 130.68, 29.34, 29.08, 28.99, 28.05, 22.55, 23.70, 23.42, 23.70, 23.70, 23.23, 23.42, 23.08, 6.37, 5.43.

3.4.4. Synthesis and characterization of [Pd(Ar-BIP)(CH$_3$)(NCCH$_3$)][PF$_6$] ***5b-9b****.*

All the synthetic procedures were performed according to the literature, using standard Schlenk techniques, under argon atmosphere at r.t. To a stirred solution of [Pd(Ar-BIP)(CH_3)Cl] (**5a-8a**) (0.1 mmol) in 5 mL of CH_2Cl_2 a solution of $AgPF_6$ (1.4 equiv) in anhydrous CH_3CN (1.2 mL) was added. The reaction was left under stirring for 45 minutes in exclusion of light, then filtered over Celite. The solvent was removed, and upon addition of hexane and sonication (5-30 minutes) a solid was obtained, that was filtered and washed with cold hexane; for **7b**, the CH_2Cl_2

solution was concentrated and upon addition of cold diethyl ether the product was precipitated. The same procedure was applied for **8c**, by using $AgSbF_6$ as dehalogenation reagent.

5b.- (Dark brown-purple solid, yield 97%); ^{1}H NMR (500 MHz, $CDCl_3$, 298 K): δ 8.12 (d, *J* = 8.2 Hz, 2H, H^4, H^5), 7.73 – 7.62 (m, 2H, H^3, H^6), 7.49 (d, *J* = 8.4 Hz, 1H, H^1 or H^8), 7.51-7.35 (m, 6H, Ar-*H*), 7.14 (t, *J* = 7.8 Hz, 1H, H^2 or H^7), 7.07-6.97 (m, 2H, H^1 or H^8, H^2 or H^7), 3.14-3.04 (m, 2H, Ar-*CH*$(CH_3)_2$), 3.04-2.94 (m, 2H, Ar-*CH*$(CH_3)_2$), 1.93 (s, 3H, Pd-NC*CH*$_3$), 1.46 (d, *J* = 6.8 Hz, 3H, Ar-CH(*CH*$_3$)$_2$), 1.36 (d, *J* = 6.8 Hz, 3H, Ar-CH(*CH*$_3$)$_2$), 1.08 (d, *J* = 6.8 Hz, 3H, Ar-CH(*CH*$_3$)$_2$), 0.97 (d, *J* = 6.8 Hz, 3H, Ar-CH(*CH*$_3$)$_2$), 0.50 (s, 3H, Pd-*CH*$_3$); ^{13}C NMR (125.68 MHz, $CDCl_3$, 298 K): δ 135.63 ($H^{3,6}$), 131.63 (H^1 or H^8, H^2 or H^7), 130.56 (H^1 or H^8), 129.44 (H^2 or H^7), 128.80 (H^1 or H^8, H^2 or H^7), 128.65, 128.13 ($H^{m,m'}$), 125.55 (H^3, H^6), 125.48, 125.41 (H^p or $H^{p'}$), 29.31, 29.11 (Ar-*CH*$(CH_3)_2$), 23.45, 23.31, 23.17, 22.67 (Ar-CH(*CH*$_3$)$_2$), 11.53 (Pd-*CH*$_3$), 1.68 (Pd-NC*CH*$_3$) ppm. IR: ν_{max} = 843 cm^{-1} (PF_6^-). Elemental analysis, calcd for $PdC_{41}H_{48}N_3PF_6$ (%): C = 59.03, H = 5.80, N = 5.04; found: experimental: C = 59.30, H = 5.73, N = 5.05.

6b.- (Dark brown-purple solid, yield 92%); ^{1}H NMR (500 MHz, $CDCl_3$, 298 K): δ 8.12 (d, *J* = 8.2, 2H, H^4, H^5), 7.67 (m, 2H, H^3, H^6), 7.49 (d, *J* = 8.4 Hz, 1H, H^1 o H^8), **7**.35 – 7.28 (m, 6H, Ar-*H*), 7.16 (t, 1H, H^2 or H^7), 7.11 (d, *J*= 8.4 Hz, 1H, H^1 or H^8), 7.04 (t, *J* = 7.8 Hz, 1H, H^2 or H^7), 2.34 (s, 6H, Ar-*CH*$_3$), 2.25 (s, 6H, Ar-*CH*$_3$*'*), 1.98 (s, 3H, Pd-NC*CH*$_3$), 0.42 (s, 3H, Pd-CH_3)**;** ^{13}C NMR (125.68 MHz, $CDCl_3$, 298 K): δ 135.71 ($H^{3,6}$), 130.18 (H^2 or H^7), 129.68 (H^2 or H^7), 129.65 (H^m or $H^{m'}$), 129.63 (H^1 or H^8), 129.60 (H^m or $H^{m'}$), 129.03 (H^1 or H^8), 127.63 (H^p or $H^{p'}$), 125.63 (H^p or $H^{p'}$), 18.03 (Ar-*CH*$_3$), 17.92 (Ar-*CH*$_3$*'*), 9.83 (Pd-*C*H_3), 1.80 (Pd-NC*C*H_3) ppm. IR: ν_{max} = 835 cm^{-1} (PF_6^-). Elemental analysis, calcd for $PdC_{33}H_{32}N_3PF_6$ (%): C = 54.90 %, H = 4.47 %, N = 5.82 %; found: C = 55.02 %, H = 3.97 %, N = 5.27 %.

7b.- (Bright red solid, yield 72%); ^{1}H NMR (500 MHz, $CDCl_3$, 298 K): δ 7.90 (d, *J* = 8.0 Hz, 2H, H^4, H^5), 7.65 – 7.48 (m, 6H, H^3, H^6, H^m, $H^{m'}$), 7.40 (td, *J*= 7.4, 3.3 Hz, 2H, H^p, $H^{p'}$), 7.24 (b, 2H, H^o or $H^{o'}$), 7.20 – 7.12 (m, 3H, H^o or $H^{o'}$, H^1 or H^8), 7.09 (t, *J*= 7.6 Hz, 1H, H^2 or H^7), 7.02 (t, *J*= 7.6 Hz, 1H, H^2 or H^7), 6.93 (m, 1H, H^1 or H^8), 2.26 (s, 3H, Pd-NC*CH*$_3$), 0.88 (s, 3H, Pd-CH_3); ^{13}C NMR (125.68 MHz, $CDCl_3$, 298 K) δ = 134.82 ($H^{3,6}$), 131.47 (H^1 or H^8), 131.27 (H^1 or H^8), 130.33 (H^m or $H^{m'}$), 130.08 (H^m or $H^{m'}$), 128.93 (H^2 or H^7), 128.55 (H^2 or H^7), 128.01 ($H^{p,p'}$), 125.60 ($H^{4,5}$), 122.30 (H^o or $H^{o'}$), 120.57 (H^o or $H^{o'}$), 11.30 (Pd-*C*H_3), 2.83 (Pd-NC*C*H_3) ppm. IR: ν_{max} = 839 cm^{-1} (PF_6^-). Elemental analysis, calcd for $PdC_{29}H_{24}N_3PF_6$ (%): C = 52.31 %, H = 3.63 %, N = 6.31 %; found: C = 52.59 %, H = 3.57 %, N = 6.46 %.

8b/c. (Brown-purple solid, yield 94.5 %); ^{1}H-NMR (500 MHz, CD_2Cl_2, 273 K) δ = 8.16 (dd, *J* = 14.4, 8.4, 1.7 Hz, 2H, H^4, H^5 *cis,trans*), 7.72 – 7.62 (m, 2H, H^6, H^3 *cis,trans*), 7.51 (dd, *J* = 13.9, 8.5, 1.2 Hz, 2H, H^8 o H^1 *cis,trans*), 7.47 – 7.39 (m, 3H, $H^{p\prime}$, $H^{m\prime}$ *cis,trans*), 7.35 – 7.24 (m, 3H, H^p, H^m *cis,trans*), 7.15 – 7.11 (m, 1H, H^2 o H^7 *cis,trans*), 7.05 (t, *J* = 8.5, 7.2, 1.3 Hz, 1H, H^2 o H^7 *cis,trans*), 7.02 (d, *J* = 8.5, 1.3 Hz, 1H, H^8 o H^1 *cis,trans*), 6.98 (t, *J* = 8.5, 1.4 Hz, 1H, H^2 o H^7 *cis,trans*), 3.16 (hept, *J* = 13.7, 6.7 Hz, 2H, Ar-*CH cis*), 3.06 (hept, *J* = 7.1 Hz, 2H, Ar-*CH trans*), 2.33 (s, 6H, Ar-CH_3 *cis*), 2.23 (s, 6H, Ar-CH_3 *trans*), 1.89 (s, 3H, NC-CH_3 *cis*), 1.85 (s, 3H, NC-CH_3 *trans*), 1.45 (d, *J* = 6.8 Hz, 6H, Ar-$CH_3^{i\,\circ}$ *trans*), 1.36 (d, *J* = 6.8 Hz, 6H, Ar-$CH_3^{i\,\circ}$ *cis*), 1.07 (d, *J* = 6.9 Hz, 6H, Ar-$CH_3^{i\,*}$ *trans*), 0.95 (d, *J* = 6.9 Hz, 6H, Ar-$CH_3^{i\,*}$ *cis*), 0.53 (s, 3H, Pd-CH_3 *cis*), 0.37 (s, 3H, Pd-CH_3 *trans*); ^{13}C-NMR (125.68 MHz, CD_2Cl_2, 273 K) δ = 125.58, 135.65, 130.58, 129.01, 128.64, 125.24, 127.73, 129.54, 127.73, 126.82, 129.62, 129.54, 129.01, 131.52, 29.27, 29.33, 17.77, 17.77, 2.14, 2.14, 1.94, 23.54, 22.67, 23.17, 22.18, 23.30, 11.43, 8.65; ^{19}F NMR (376 MHz, CD_2Cl_2, 273 K) δ = -73.57 (d, *J* = 710.0 Hz, PF_6^-); ^{31}P NMR (162 MHz, CD_2Cl_2, 273 K) δ = -131.09 – -158.18 (m, 1P, PF_6^-).

3.4.5. General procedures for in situ NMR reactivities.

General procedure for the *in situ* ^{1}H NMR reactivity of the cationic complexes 5b-7b with methyl acrylate (MA)

A 10 mM solution of the desired cationic complex (**5b-7b**) in CD_2Cl_2 is prepared, and a first ^{1}H NMR spectrum is recorded. 2 equivalents of methyl acrylate are then added to the solution. The reaction is followed with time, at T = 298 K, to monitor the disappearance of the Pd-CH_3 signal. The required time to record each ^{1}H NMR spectrum (60 s) is taken into account when analysing the kinetic data.

General procedure for the *in situ* ^{1}H NMR reactivity of the cationic complex 5b with ethylene.

A 10 mM solution of **5b** in CD_2Cl_2 is prepared, and a first ^{1}H NMR spectrum is recorded. Ethylene is bubbled into the NMR tube for 10 min. The reaction is followed with time, at T = 298 K, by monitoring the disappearance of the Pd-CH_3 signal. The required time to record each ^{1}H NMR spectrum (60 s) is taken in account when analyzing the kinetic data.

3.4.6. Ethylene/methyl acrylate Copolymerization Reactions. All catalytic experiments are carried out in a Büchi “tinyclave” reactor equipped with an interchangeable 50 mL glass vessel.

The vessel is loaded with the desired complex (21 μmol), TFE (21 mL) or distilled CH_2Cl_2 (22 mL) and methyl acrylate (1.13 mL). The reactor is placed in a preheated oil bath and connected to the ethylene tank. The ethylene is bubbled for 10 min, then the reactor is pressurized. The reaction mixture is stirred at constant temperature and pressure. After the proper time (from 4 up to 96 h), the reactor is cooled to room temperature and vented. An aliquot (200 μL) of the reaction mixture is withdrawn and diluted in CH_3OH (1 mL) for GC-MS analyses. The reaction mixture is poured in a 50 mL round flask, together with dichloromethane (3 x 2 mL) used to wash the glass vessel. No formation of Pd black is observed. Volatiles were removed under reduced pressure and the residual gum or oil is dried at constant weight and analyzed by NMR spectroscopy.

The ethylene uptake was measured by performing the catalysis in the same Büchi "tinyclave" reactor connected to a thermal mass flow meter (Bronkhorst EL-FLOW Select model F-111B) and forward pressure controller device (Bronkhorst EL-PRESS model P-602). Gas flow needed to feed the reactor at a constant pressure was computer-recorded using the FlowPlot interface. The reaction procedure was the same as above.

3.5. Bibliography

1. van Belzen, R., Klein, R. A., Smeets, W. J. J., Spek, A. L., Benedix, R., Elsevier, C. J. *Rec.Trav. Chim. Pays-Bas* **1996,** *115,* 275.

2. a) Gao, B., Zhao, D., Li, X., Cui, Y., Duan, R., Pang, X., *RSC Adv.* **2015,** *5*, 440; (b) Li, L., Jeon, M., Kim, S. Y. *J. Mol. Cat. A: Chemical* **2009,** *303*, 110; (c) Gao, B., Luo, X., Gao, W., Huang, L., Gao, S.-m., Liu, X., Wu, Q., Mu, Y. *Dalton Trans.* **2012,** *41* (9), 2755-2763.

3. Cherkasov, V. K., Druzhkov, N. O., Kocherova, T. N., Shavyrin, A. S., Fukin, G. K. *Tetrahedron* **2012,** *68,* 1422.

4. a) Meduri, A., Montini, T., Ragaini, F., Fornasiero, P., Zangrando, E., Milani, B. *ChemCatChem* **2013,** *5*, 1170; b) Rosar, V., Meduri, A., Montini, T., Fornasiero, P., Zangrando, E., Milani, B. *Dalton Trans.* **2018,** *47*, 2778; c) Hill, N. J., Vargas-Baca, I., Cowley, A. H. *Dalton Trans.* **2009,** 2, 240; d) Rosar, V., Meduri, A., Montini, T., Fini, F., Carfagna, C., Fornasiero, P., Balducci, G., Zangrando, E., Milani, B. *ChemCatChem* **2014,** *6*, 2403; e) van Asselt, R., Elsevier, C. J., Smeets, W. J. J., Spek, A. L., Benedix, R. *Rec. Trav. Chim. Pays-Bas* **1994,** *113*, 88.

5. a) Rülke, R. E., Ernsting, J. M., Spek, A. L., Elsevier, C. J., Van Leeuwen, P. W. N. M., Vrieze, K. *Inorg. Chem.* **1993,** *32*, 5769; b) Durand, J., Zangrando, E., Stener, M., Fronzoni, G.,

Carfagna, C., Binotti, B., Kamer, P. C. J., Muller, C., Caporali, M., van Leeuwen, P. W. N. M., Vogt, D., Milani, B. *Chem. Eur. J.* **2006,** *12*, 7639.

6. a) Dai, S., Sui, X., Chen, C. *Angew. Chem. Int. Ed.* **2015,** *54*, 9948; b) Allen, K. E., Campos, J., Daugulis, O., Brookhart, M. *ACS Catal.* **2015,** *5*, 456.

7. Rosar, V., Dedeic, D., Nobile, T., Fini, F., Balducci, G., Alessio, E., Carfagna, C., Milani, B. *Dalton Trans.* **2016,** *45*, 14609.

8. Rosar, V., Montini, T., Balducci, G., Zangrando, E., Fornasiero, P., Milani, B. *ChemCatChem* **2017,** *9*, 3402.

9. Zhang, W., Waddell, P. M., Tiedemann, M. A., Padilla, C. E., Mei, J., Chen, L., Carrow, B. P. *J. Am. Chem. Soc.* **2018,** *140*, 8841.

10. a) Ittel, S. D., Johnson, L. K., Brookhart, M. *Chem. Rev.* **2000,** *100*, 1169; b) Johnson, L. K., Killian, C. M., Brookhart, M. *J. Am. Chem. Soc.* **1995,** *117*, 6414.

11. Mecking, S., Johnson, L. K., Wang, L., Brookhart, M. *J. Am. Chem. Soc.* **1998,** *120*, 888.

12. Johnson, L. K., Mecking, S., Brookhart, M. *J. Am. Chem. Soc.* **1996,** *118*, 267.

13. Zhong, L., Li, G., Liang, G., Gao, H., Wu, Q. *Macromolecules* **2017,** *50*, 2675.

14. Popeney, C. S.; Camacho, D. H.; Guan, Z. *J. Am. Chem. Soc.* **2007,** *129*, 10062.

15. Guo, L., Gao, H., Guan, Q., Hu, H., Deng, J., Liu, J., Liu, F., Wu, Q. *Organometallics* **2012,** *31*, 6054.

16. Szabo, M. J., Jordan, R. F., Michalak, A., Piers, W. E., Weiss, T., Yang, S.-Y., Ziegler, T. *Organometallics* **2004,** *23*, 5565.

17. Drent, E., van Dijk, R., van Ginkel, R., van Oort, B., Pugh, R. I. *Chem. Commun.* **2002,** 7, 744.

18. a) Berkefeld, A., Drexler, M., Moller, H. M., Mecking, S. *J. Am. Chem. Soc.* **2009,** *131*, 12613; b) Usami, T., Takayama, S. *Macromolecules* **1984,** *17*, 1756; c) Axelson, D. E., Levy, G. C., Mandelkern, L. *Macromolecules* **1979,** *12*, 41; d) McCord, E. F., McLain, S. J., Nelson, L. T. J., Arthur, S. D., Coughlin, E. B., Ittel, S. D., Johnson, L. K., Tempel, D., Killian, C. M., Brookhart, M. *Macromolecules* **2001,** *34*, 362; e) McCord, E. F., McLain, S. J., Nelson, L. T. J., Ittel, S. D., Tempel, D., Killian, C. M., Johnson, L. K., Brookhart, M. *Macromolecules* **2007,** *40*, 410.

19. Takano, S., Takeuchi, D., Osakada, K., Akamatsu, N., Shishido, A. *Angew. Chem. Int. Ed.* **2014,** *53*, 9246.

20. Contrella, N. D., Sampson, J. R., Jordan, R. F. *Organometallics* **2014,** *33*, 3546.

21. a) Dermitzaki, D., Raptopoulou, C. P., Psycharis, V., Escuer, A., Perlepes, S. P., Stamatatos, T. C. *Dalton Trans.* **2014,** *43*, 14520; b) Konidaris, K. F., Polyzou, C. D., Kostakis, G. E., Tasiopoulos, A. J., Roubeau, O., Teat, S. J., Manessi-Zoupa, E., Powell, A. K., Perlepes, S. P. *Dalton Trans.* **2012,** *41*, 2862; c) Fernandez-Galan, R., Manzano, B. R., Otero, A., Lanfranchi, M., Pellinghelli, M. A. *Inorg. Chem.* **1994,** *33*, 2309.

22. Abakumov, G. A., Cherkasov, V. K., Druzhkov, N. O., Kurskii, Y. A., Fukin, G. K., Abakumova, L. G., Kocherova, T. N. *Synth. Commun*. **2006**, 36, 3241.

23. Dall'Anese, A., Rosar, V., Cusin, L., Montini, T., Balducci, G., D'Auria, I., Pellecchia, C., Fornasiero, P., Felluga, F., Milani, B. *Organometallics* **2019**, *38*, 3498.

CHAPTER 4

MAin Chain: in-chain incorporation of acrylic esters in homogenously-catalyzed copolymerization reactions.

Overview

In this Chapter, hydrogen-substituted and 1,4-diaza-2,3-butadiene-based ligands with a butoxy-pyrene tag (pyr-DAB) and the relevant palladium complexes of the general formula [Pd(CH_3)Cl(pyr-DAB)] and [Pd(CH_3)(CH_3CN)(pyr-DAB)][SbF_6] are presented. A detailed study of the catalytic properties of the monocationic complexes is reported, highlighting the high activity of the system and the peculiarity of the produced functionalized macromolecules. When the catalytic tests are run in 2,2,2-trifluoroethanol, the produced copolymers have the polar monomer incorporated prevailingly into the main polymeric chain, which represents a remarkable difference with all of the α-diimine-based catalysts reported up to now. Moving from trifluoroethanol to dichloromethane, a loss in productivity is found, along with an opposite selectivity for the enchainment of the incorporated methyl acrylate. The precatalysts employed have proven to be also active in the copolymerization of ethylene with other acrylic esters, such as *tert*-butyl acrylate and *n*-butyl acrylate. The reactivity of the most productive precatalyst with methyl acrylate, investigated by NMR spectroscopy in both deuterated trifluoroethanol and dichloromethane is also discussed.

Dall'Anese, A., Souleymanou, M. Y., Godard, C., Milani, B.

Patent pending

4.1. Introduction

In the previous Chapters the effect of nitrogen-donor ligands diversity on the copolymerization of ethylene with polar vinyl monomers was assessed, in particular ligand desymmetrisation (Chapter 2) and ligand backbone variation (Chapter 3) were studied. Another aspect that can be considered when changing the ligand structure is the effect of the substituent on the *para* position of the aryl ring on the iminic nitrogen atoms. In 2005, Popeney and Guan reported a series of DAB ligands with electron donating or withdrawing substituents on the *para* position, in order to study the ligand electronic effect on the ethylene homo- and copolymerization with methyl acrylate.[1] For the latter, in particular, it was observed that catalysts with strong electron-donating ligands afforded copolymers with an increased content of inserted acrylate when the electron-donating capability of the *para* group was increased (Table 4.1, precatalysts **L47-49**) and exhibited a higher activity with respect to catalysts bearing weakly donating ligands (Table 4.1, **L43-46**). In this case, a deactivation of the catalyst was observed at higher concentrations of MA.

Table 4.1. Ethylene/methyl acrylate copolymerization with precatalysts **L43a-L49a** (in the figure underneath) under copolymerization conditions,[a] at varying initial concentrations of MA (mol/L).

Precatalyst	**TOF**[b]			**MA%**			**M_n (kg/mol)**		
	0.12	**0.58**	**1.67**	**0.12**	**0.58**	**1.67**	**0.12**	**0.58**	**1.67**
L43a	10	0	0	0.1	-[c]	-	6.4	-	-
L44a	40	<5	0	0.5	1.2	-	17	5.7	-
L45a	130	30	<5	0.7	2.4	-	33	2.0	-
L46a	130	10	<5	0.5	2.2	6.9	56	8.6	5.4
L47a	160	50	20	0.7	2.6	4.2	62	15	0.6
L48a	170	30	<5	0.6	2.9	6.1	41	12	4.7
L49a	180	60	20	0.9	3.6	8.4	66	10	2.4

[a] Copolymerization conditions: 10 μmol catalyst, CH_2Cl_2, P_E = 1 at, 298 K, 6.5 h reaction times with an added 0.5, 2.5, or 8.0 mL of MA. [b] TOF values of "<5" means a trace of recovered polymer (0.01 g or less), while "0" indicates negligible polymer; [c] Data not available.

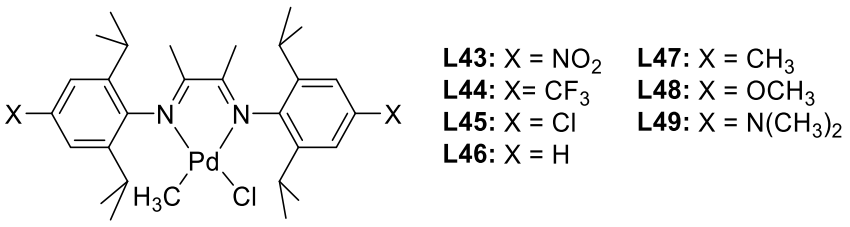

L43: X = NO_2 **L47:** X = CH_3
L44: X= CF_3 **L48:** X = OCH_3
L45: X = Cl **L49:** X = $N(CH_3)_2$
L46: X = H

Starting from this work, other efforts were made with respect of the substitution of the N-aryl moieties, as shown in Chapter 1.[2] Fewer examples of substitution on the *para* position of similar DAB systems are reported: Chen and co-workers investigated a ferrocenyl-substituted DAB ligand

(Figure 4.1, **L50**), and the effect of its different redox states in the homo and copolymerization of ethylene with other monomers, such as norbornene and 5-norbornene-2-yl acetate.[3]

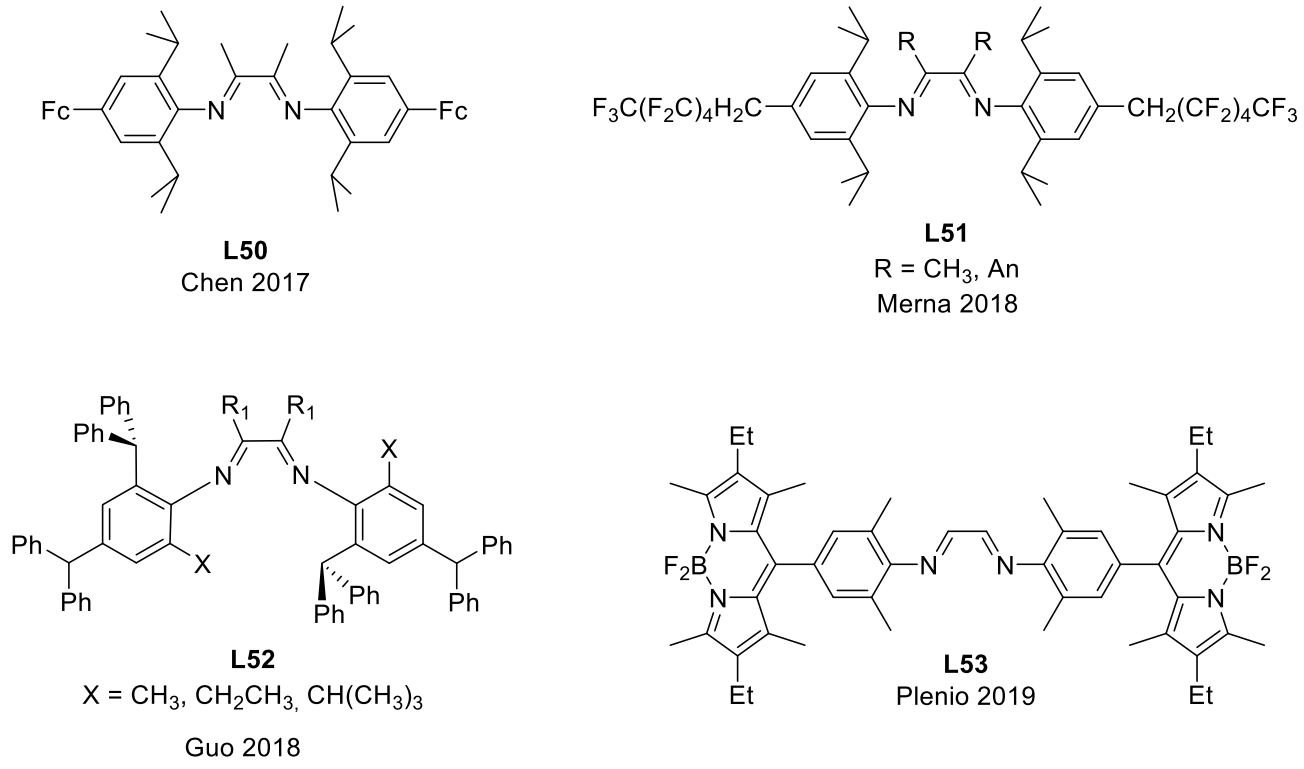

Figure 4.1. *Para* substituted DAB ligands (Fc = ferrocenyl).

The ferrocenyl groups on the monocationic palladium complex [Pd(CH_3)(CH_3CN)(Fc-DAB)][BArF] can be oxidized in a stepwise fashion upon addition of $AgBAr^F$, in order to evaluate the catalysts properties. The oxidation of the Fc decreases the electron donating ability of the ligand, making the palladium center more electrophilic. Looking at the copolymerization with methyl acrylate, good results in terms of activity are obtained when the ferrocenyl moiety is not oxidized (9.7 and 13 · 10^3 g/(mol Pd·h) for [MA] = 1 and 0.7 mol/L, respectively), with a high content of inserted polar monomer (5.5 and 7.2 %, respectively). The better activity of the non-oxidized species with respect to the mono- and di-oxidized one is in agreement with the fact that methyl acrylate could have a poisoning effect on the electron-poor palladium center. Guo and collaborators reported instead nonsymmetrical DAB ligands, bearing on *ortho* positions of the N-aryl rings a benzhydryl and and alkyl substituent (methyl, ethyl, isopropyl), and on the *para* position an additional benzhydryl moiety (Figure 4.1, **L52**).[4] The resultant bulky Pd(II) precatalysts were tested in the copolymerization of ethylene with methyl acrylate and acrylic acid, achievng activities in the range of 10.83 - 34.44 · 10^2 g/(mol_{Pd}·h), and a good degree of incorporation of the

polar monomer, even in the case of acrylic acid (4.7-1.0 % for methyl acrylate, 2.7-1.1 % for acrylic acid). More recently, 1,4-diazabutadiene ligands with methyl groups on the *ortho* position of the N-aryl rings and a bodipy (bodipy = boron-dipyrromethene) moiety in the *para* position were reported (Figure 4.1, **L53**).[5] These complexes, however, were not applied for co- or polymerization reactions, but instead for monitoring ligand substitution exploiting the fluorescence of the bodipy tags. In particular, the coordination of different molecules (pyridine, CO, acetonitrile, ethylene, 1-hexene, styrene, methyl acrylate) on the [Pd(CH_3)Cl(**L53**)] was followed by following the fluorescence evolution of the bodipy tag, that increases upon addition of such molecules, because of the increased electron density on the palladium center. Another interesting modification of the N-aryl *para* substituents of BIAN and DAB derivatives has been reported recently by Merna *et al*., where a fluorinated tail of formula -$CH_2(CF_2)_4CF_3$ has been introduced in the *para* position (Figure 4.1, **L51**). However, the relevant Pd(II) complexes have not been applied to ethylene/acrylic esters copolymerization yet, but instead just to ethylene homopolymerization.[6]

Taking as a reference the classical Brookhart-type ligand with the 1,4-diazabutadiene backbone and isopropyl substituents on the *ortho* position of the aryl rings, in this Chapter the effect of an increased steric bulk of the electron-donating moiety on the *para* position on the aryl substituents will be taken into consideration. In particular, ligands with a pyrene tag bonded to the N-aryl substituent with a -O(CH_2)$_4$- bridge will be investigated (pyr-DAB). This work is carried out in collaboration with the group of Dr. Cyril Godard of University Rovira i Virgili in Tarragona (Spain).

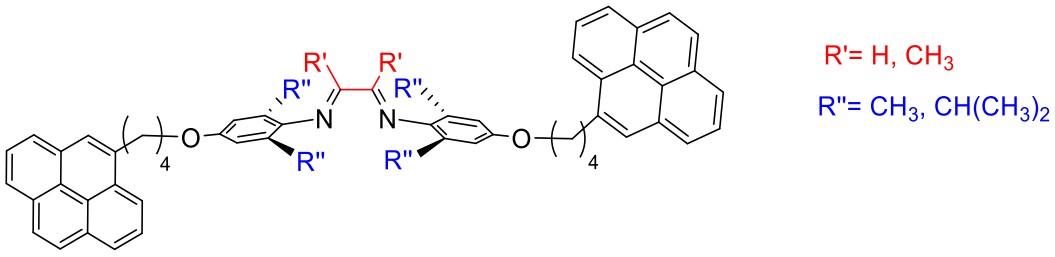

Figure 4.2. The studied pyr-DAB ligands.

The aim of the work would be the exploitation of the pyrene tags for the immobilization of the active palladium complexes to carbon-based materials via π-π stacking interactions. While supported early transition metal-based catalysts have been widely studied and applied and found also commercialization in the market,[7] the corresponding late transition metal-based systems have remained unexplored. Indeed, when looking at ethylene/polar vinyl monomer copolymerization, the first example of immobilized catalyst was reported in 2014 by Mecking and coworkers: the covalent

immobilization of phosphino-sulfonate palladium catalysts to inorganic substrates and polystyrene was assessed, alongside with their performances in ethylene homopolymerization and copolymerization with methyl acrylate (Figure 4.3). The polystyrene-immobilized systems shows an activity that is almost one order of magnitude lower than that of the relevant homogeneous Pd(II) catalyst (yields (g) in the range 0.14-0.29 for the immobilized systems, 0.65-6.81 for the relevant catalysts in solution), leading to the copolymer with an incorporation of MA and molecular weight that is similar or lower to that of the macromolecule obtained with the soluble Pd(II) catalyst.[7b,8] When the catalyst is immobilized on clay or silica, its activity is similar to that of the non-supported complex, and the resulting copolymer has the same content of MA (2.5-4.0%) and slightly lower Mn are achieved (2.1-3.7 kg/mol in the supported system vs 4.9 kg/mol in the non-supported one). The next step would be the use of weaker linkages of the metal complex to the surface of choice, in order to obtain an increased accessibility, mobility and electrophilic character of the catalytic centre. This aim was reached by Conley *et al*, by exploiting the electrostatic interaction between Ni(II) and Pd(II) catalysts with α-diimine ligands and partially dehydroxylated sulphated zirconium oxide. Again, the results obtained are worse with respect of those obtained with solution catalysts, but the activity is higher when compared to covalently-bonded Pd(II) systems (activities in the range of 5.0-14.9 kg/($mol_{active\ Pd}$·h), 0.25-0.46 % inserted methyl acrylate).[9] In this light, having weaker interactions between the catalytic systems and the substrate, such as π-π interactions, could lead to more productive catalysts.

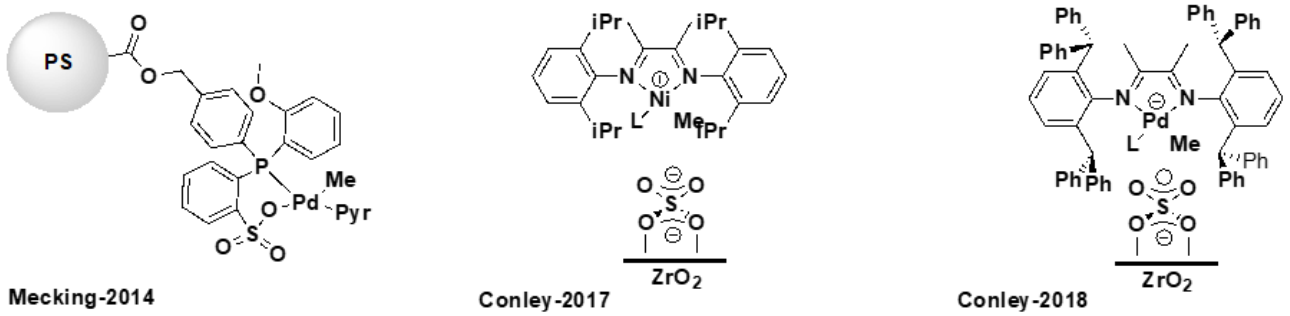

Figure 4.3. Examples of covalently and electrostatically bonded catalysts.

4.2. Results and discussion.

*4.2.1. Synthesis and characterization of ligands **10-13**.*

Ligands **10-13** have all been synthesized for the first time in the group of Prof. Cyril Godard at the University Rovira i Virgili in Tarragona. This kind of molecules are already known in literature and are often synthesized as intermediates for NHC ligands. Supported transition metal complexes with NHC ligands have a wide range of applications, going from Büchwald-Hartwig aminations,[10] to selective hydrogenolysis of arenols,[11] to the production of polyethylene.[12] The synthetic methodology for ligands **10-13**, designed in the Claver's and Godard's group, is based on a two-step reaction, the first one being the synthesis of the pyrene-tagged aniline. Starting from either 4-amino-3,5-dimethylphenol or 4-amino-3,5-diisopropylphenol, an etherification reaction using 2-(4-iodobutyl)pyrene was performed (Scheme 4.1), obtaining the desired pyrene-tagged anilines in good yields.

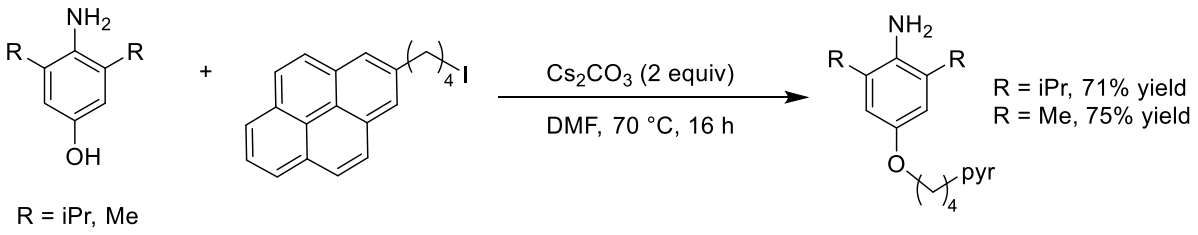

Scheme 4.1. Synthesis of the pyrene-tagged anilines; pyr = pyrene.

Afterwards, the desidered aniline was condensed with either 2,3-butanedione (Scheme 4.2a) or with 1,4-dioxane-2,3-diol (Scheme 4.2b) in dry ethanol, with formic acid as catalyst, yielding the desired α-diimine ligands in good yields (52-67 %).

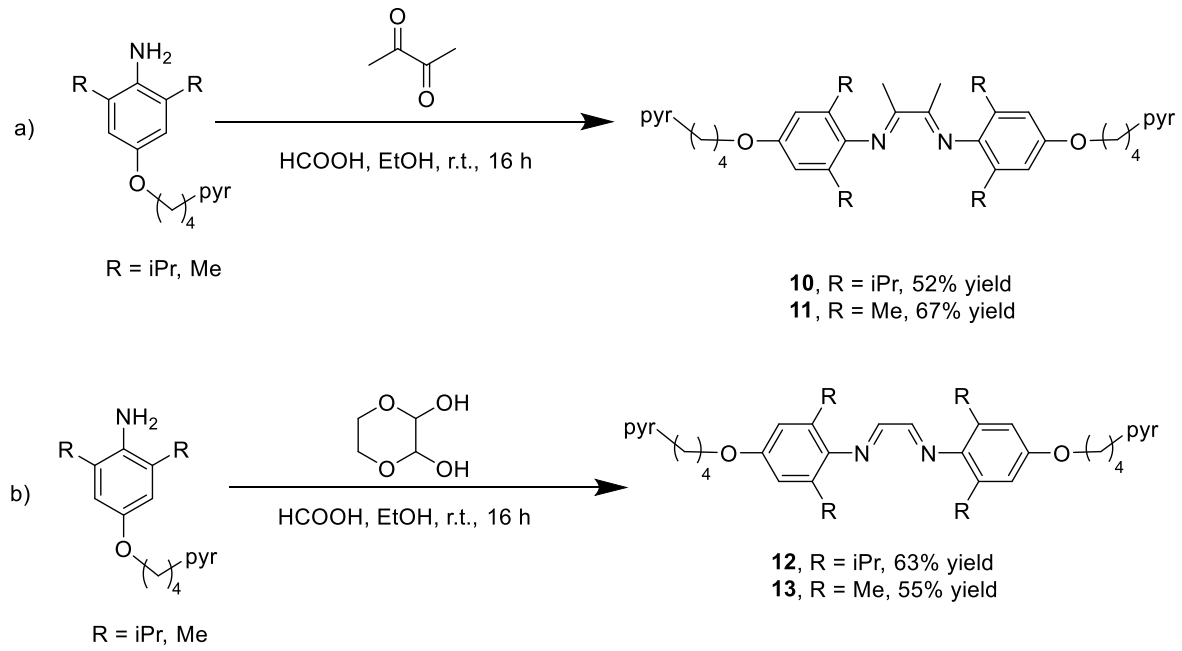

Scheme 4.2. Synthesis of ligands **10-13**; pyr = pyrene.

These new four pyrene-tagged ligands were characterized by NMR spectroscopy and mass spectrometry. The formation of the desired products is confirmed by the presence in the ^{1}H NMR spectra of the signals typical of the ligand backbone, that are found at 8.03 and 8.06 ppm respectively for the methyl and the isopropyl substituted ligand **12** and **13** (Figure S3, S5), whereas for the imino-methyl derivatives **10** and **11**, the most significant signals are those of the NC*CH$_3$*-*CH$_3$*CN protons at 2.01 and 1.97 ppm, respectively (Figure S1, S2).

*4.2.2. Synthesis and characterization of neutral Pd-complexes **10a-13a**.*

The synthesis of the neutral [Pd(CH$_3$)Cl(pyr-DAB)] complexes was performed by following the literature procedure employed also for similar complexes with Ar-BIAN derivatives.[13] **10a** and **11a** were synthesized in our laboratory, whereas **12a** and **13a** were synthesized in the group of Prof. Godard in Tarragona. The complexes were all obtained in good yields, as orange or purple solids. The complexes with isopropyl substituents **10a** and **12a** were characterized using NMR spectroscopy, both mono- and bidimensional, whereas for the methyl-substituted derivatives **11a** and **13a** the characterization in solution was not possible, due to their insolubility in common organic solvents. This could be related to the presence of π interactions between the pyrene moieties that induce π-π stacking between different molecules, that hampers their solubility.

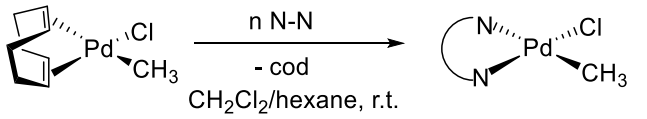

Scheme 4.3. Synthesis of the neutral [Pd(CH_3)Cl(pyr-DAB)] complexes.

Taking **10a** as an example, in the ^{1}H NMR spectrum the number of signals and the integrations are in agreement with ligand **10** being coordinated in a non-symmetrical chemical environment: the signals that are most affected are those relevant to the protons of the isopropyl groups, that are split in three doublets, whereas those belonging to the pyrene moiety, the butyl chain and the aryl ring on the iminic nitrogen are not affected so much by the coordination to the Pd(II) centre (Figure S1 *vs* S6).

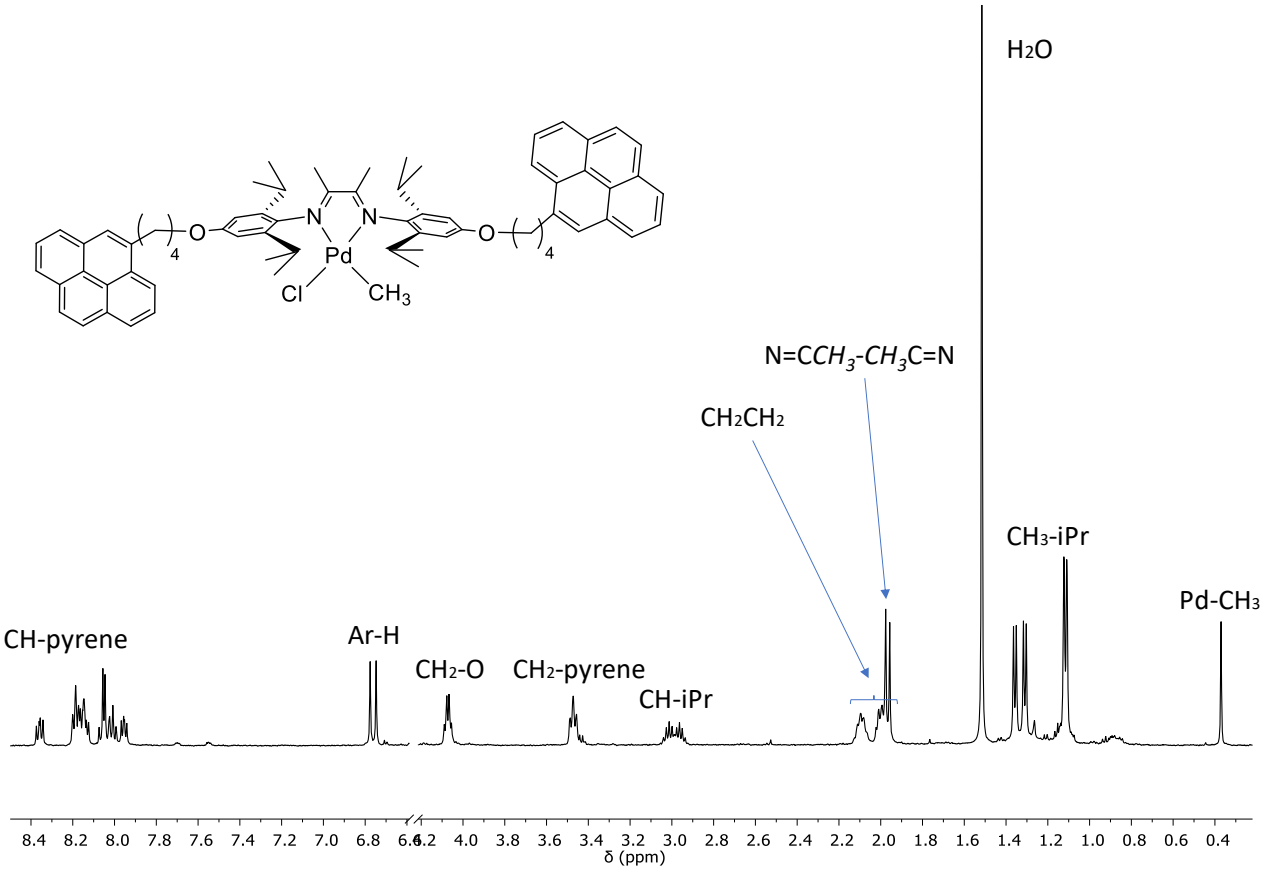

Figure 4.4. ^{1}H NMR spectrum (CD_2Cl_2, 298 K) of complex **10a**.

The coordination to the metal is confirmed by the presence of the singlet at 0.37 ppm that is due to the Pd-CH_3 group. When hydrogen-substituted derivative **12a** is considered, the same group gives a singlet at 0.67 ppm. The shift at lower frequencies going from the hydrogen-substituted skekelton to

1,4-diazabutadiene backbone agrees with the expected higher electron density on the N-donor atoms of ligand **10** that results in a higher electron density on palladium for **10a** than for **12a**, as it was previously reported for complexes with pyridylimines.[14]

*4.2.3. Synthesis and characterization of cationic Pd-complexes **10b-13b**.*

The cationic complexes were synthesized from the corresponding neutral complexes **10a-13a** following the well-established protocol that employs a silver salt (in this case, $AgSbF_6$) as a dehalogenating agent. The complexes were all obtained in good to excellent yields as dark solids and characterized by mono- and bidimensional NMR spectroscopy.

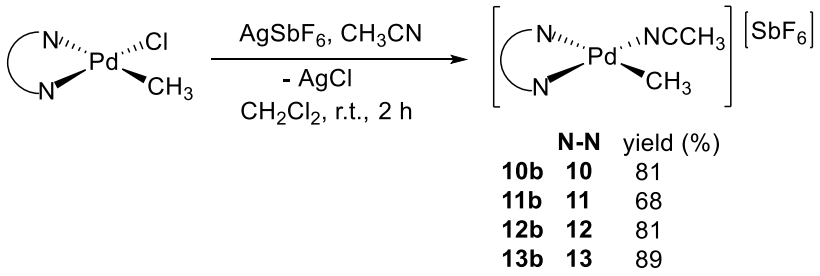

	N-N	yield (%)
10b	**10**	81
11b	**11**	68
12b	**12**	81
13b	**13**	89

Scheme 4.4. Synthesis of the cationic complexes [Pd(CH_3)(CH_3CN)(pyr-DAB)][SbF_6] **10b-13b**.

Unlike the corresponding neutral precursors, all the cationic complexes are soluble in CD_2Cl_2 at room temperature. Only for complex **13b** some solubility issues, likely due to interactions between pyrene moieties of different molecules that can occur at the concentrations used for preparing the NMR sample (10 mM), make the ^{1}H NMR peaks relevant to CH protons of the pyrene and CH_2 protons of the bridge close to it very broad and hard to properly integrate (Figure S4.19). As for the neutral derivatives, also for the monocationic complexes in the ^{1}H NMR spectra the signals of the protons belonging to the pyr-DAB are not much affected by coordination and by the change in the charge of the complex, as it is possible to observe in the ^{1}H NMR spectrum of **10b** (Figure 4.5). The signals that are affected by the change in the charge of the complex are those of the isopropyl group and the signal of the methyl on the backbone, that is deshielded with respect to complex **10a** (Figure 4.4).

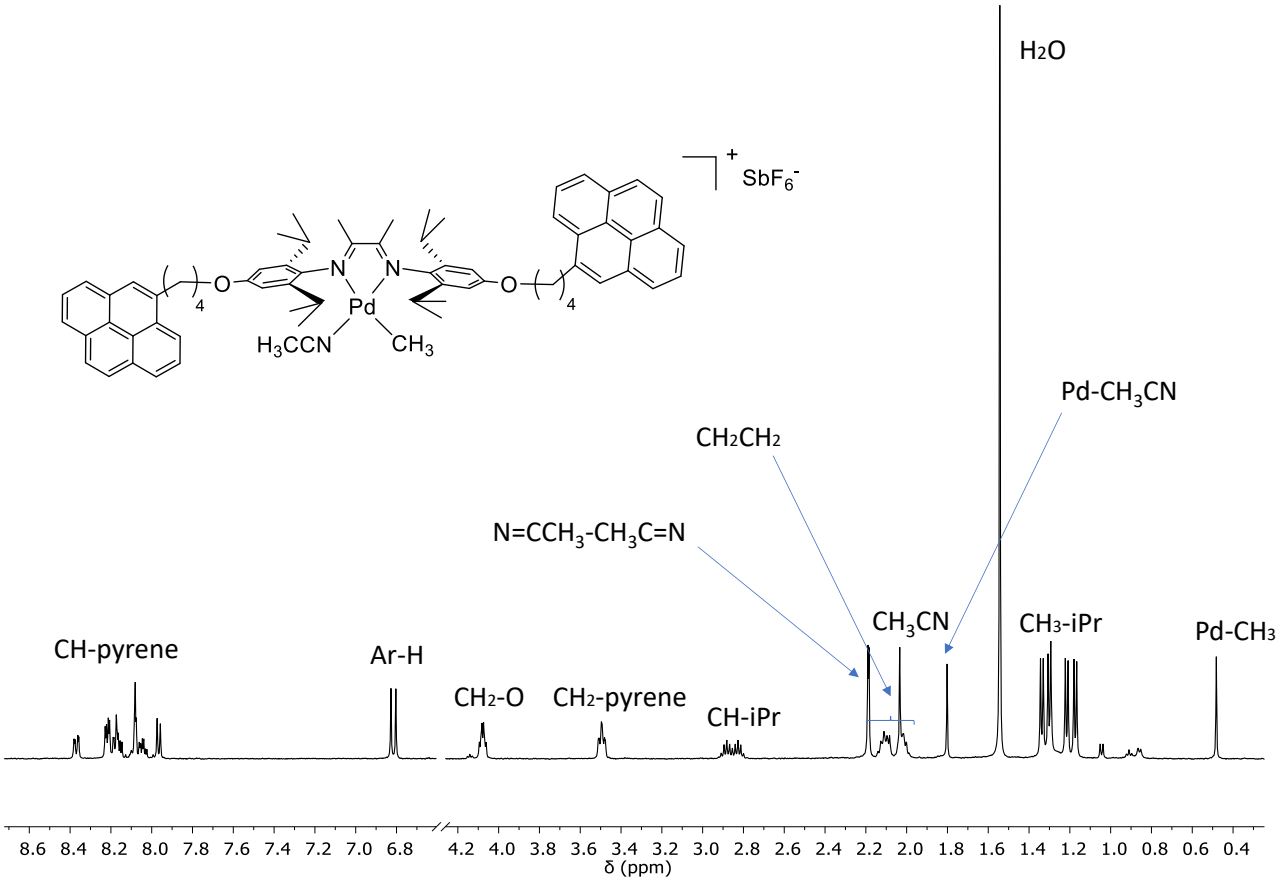

Figure 4.5. ^{1}H NMR spectrum (CD_2Cl_2, 298 K) of complex **10b**.

For all the complexes the singlet of the acetonitrile ligand (Pd-$NCCH_3$) is present between 1.78 and 1.93 ppm, thus confirming the substitution of the chlorido ligand. When the Pd-CH_3 peak is considered, a certain trend can be highlighted.

Table 4.2. Selected chemical shifts for complexes **10a-13a**, **10b-13b** (^{1}H NMR spectra, CD_2Cl_2, 298 K).

	Pd-CH_3 (ppm)	Pd-$NCCH_3$ (ppm)
10a	0.37	-
10b	0.45	1.78
11a	-	-
11b	0.33	1.79
12a	0.67	-
12b	0.73	1.92
13a	-	-
13b	0.63	1.93

The comparison of the chemical shift values for the Pd-CH_3 fragment for the complexes under investigation and for the classical Brookhart system with DAB ligands[15] points out that: for the isopropyl substituted pyr-DABs and the classical DAB, **L3**, the values are the same indicating that the electron-donating ability of the two types of ligand is the same; going from the 1,4-diazabutadiene to the H-substituted skeleton there is a shift at higher frequencies for both series of complexes, indicating that the electron-donating ability of the two types of ligand increases in the same order.

The careful analysis of the Pd-CH_3 chemical shift points out that moving from **10b** to **12b** or from **11b** to **13b** the shift at higher frequencies is of 0.30 ppm, whereas going from **10b** to **11b** or from **12b** to **13b** the shift is on the opposite direction and is smaller ($\Delta\delta$ = 0.10 ppm). Since going from **10b** to **12b** (or from **11b** to **13b**) means changing the ligand skeleton from CH_3 to H, whereas going from **10b** to **11b** (or from **12b** to **13b**) means changing the substituent on the aryl rings from isopropyl to methyl, the $\Delta\delta$ values suggest that the electron density on the N-donor atoms is mainly affected by the substituents on the ligand skeleton rather than by the groups on the aryl rings. For the latter, the fact that moving from **10b** to **11b** (or from **12b** to **13b**) the $\Delta\delta$ values are small and towards the opposite direction suggest that the Pd-CH_3 feels more the shielding cone of the methyl-substituted aryl rings than that of the isopropyl-substituted aryls. The variation of the ligand skeleton also affects the chemical shift of the acetonitrile bonded to palladium that is shifted at high frequencies ($\Delta\delta$ = 0.14 ppm) moving from **10b** to **12b** (or from **11b** to **13b**), supporting our hypothesis that the substituents on the ligand skeleton are the most important in terms of donating capability of the ligand itself.

In order to validate this hypothesis, several crystallization trials were made both for neutral and cationic complexes, to obtain single crystals suitable to X-ray diffraction. By leaving for one month a solution of **10b** in dichloromethane layered with n-hexane at 277 K crystals were obtained, but the recorded structure is different from the one expected: the species found is $[Pd_2(\mathbf{10})(\mu\text{-}OH)]_2[X]_2$ (**10c**).

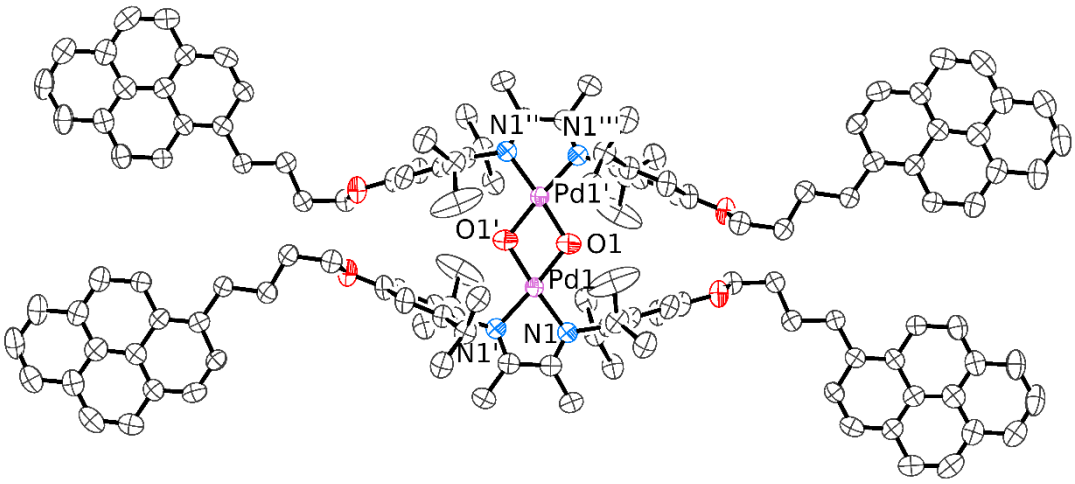

Figure 4.6. ORTEP representation of $[Pd_2(\mathbf{10})(\mu\text{-OH})]_2[X]_2$. Relevant bond distances and angles reported in Table S1.

The tentative refinement of the structure shows two palladium centers, at 3.158(2) Å from each other, connected by a hydroxy bridge, and they both possess the expected square planar coordination. The coordination sphere of each metal centre is completed by one ligand (**10**). The refinement of the counter anions for the dinuclear structure has not been made yet, since it presents some degree of disorder. The Pd-N and Pd-O distances are quite similar (1.965(6) vs 1.926(3) Å) and, as expected, the N-aryl rings are almost perpendicular to the square planar plane (86.7(2)°) and to the plane of the pyrene tags (90.0(2)°); the latter are consequently almost coplanar to the metal coordination plane (3.59(3)°) and to each other (4.64(4)°).

*4.2.4. Ethylene/acrylic esters copolymerization with complexes **10b-13b**.*

Complexes **10b-13b** were tested as precatalysts in the copolymerization of ethylene with methyl acrylate (Scheme 4.5). The catalytic reactions were performed under very mild reaction conditions (2.5 bar of ethylene pressure, 308-318 K), using either 2,2,2-trifluoroethanol or dichloromethane as a solvent. No cocatalyst was added. Other acrylic esters were also tested, such as *tert*-butyl acrylate and *n*-butyl acrylate.

The catalytic products, obtained as gummy off-white solids (Figure 4.7) or as brown oils, were characterized by NMR spectroscopy. The molecular weight of the produced macromolecules was determined by GPC analysis at the University of Salerno, in the group of Prof. Claudio Pellecchia.

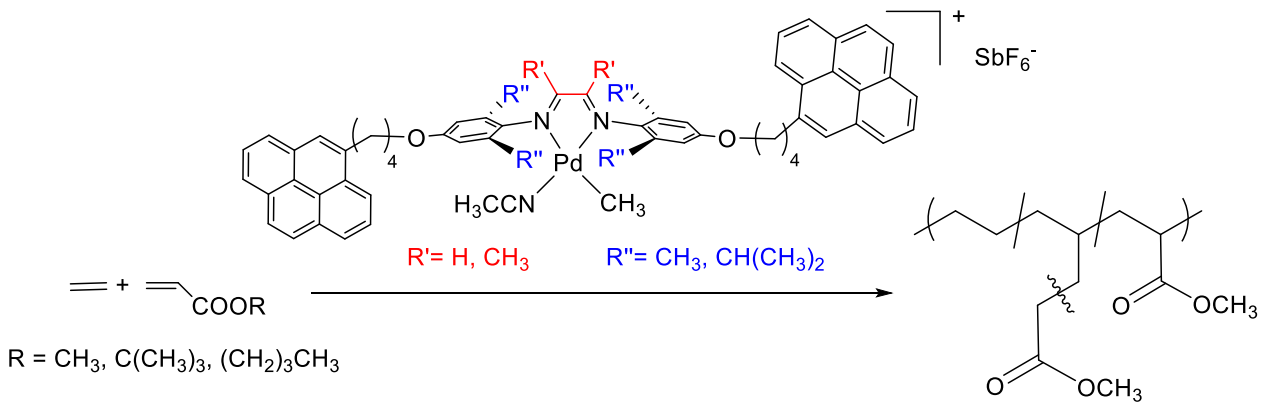

Scheme 4.5. Ethylene/acrylic esters copolymerization.

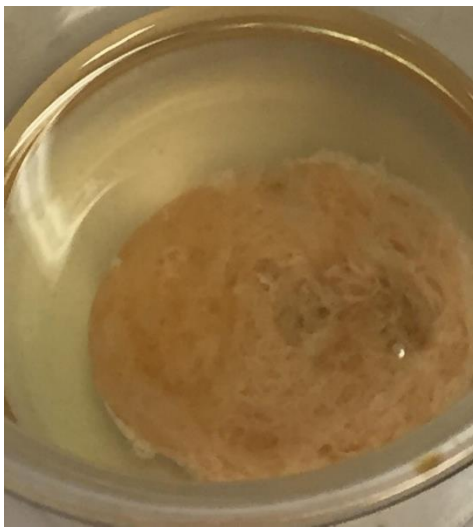

Figure 4.7. Ethylene/methyl acrylate copolymer obtained with **10b**.

Table 4.3. Ethylene/methyl acrylate copolymerization: effect of the ancillary ligand.[a]

Precatalyst: [Pd(CH_3)(CH_3CN)(**pyr-DAB**)][SbF_6]

Run	Pyr-DAB	Yield (g)	kg CP/g Pd[b]	kg CP/mol Pd	mol % MA[c]	TON[d] E	TON[d] MA	M_n[e] (M_w/M_n)	Bd[f]
1	**10**	1.5237	0.683	72.6	0.8	2521	20	260000 (1.55)	87
2	**11**	0.9223	0.414	43.9	3.0	1430	44	52000 (1.53)	73
3	**12**	0.2911	0.131	13.9	1.2	476	6	15000 (1.52)	100
4	**13**	0.2999	0.134	14.2	3.9	453	18	42000 (2.00)	92
5[g]	**10**	0.9494	0.426	45.2	-	1611	-	109000 (1.47)	96

[a] Reaction conditions: $n_{Pd} = 2.1 \cdot 10^{-5}$ mol, V_{TFE} = 21 mL, V_{MA} = 1.130 mL, [MA]/[Pd] = 594, T = 308 K, $P_{ethylene}$ = 2.5 bar, t = 18 h; [b] isolated yield, productivity as kg CP/g Pd = kilograms of copolymer per gram of Pd or kg CP/mol Pd = kilograms of copolymer per mol of Pd; [c] calculated by ^{1}H NMR spectroscopy on isolated product; [d] TON as mol comonomer/mol of Pd; [e] The molecular weights (M_n and M_w) and the molecular mass distribution (M_w/M_n) of polymer samples were measured by *gel permeation chromatography (GPC*) at 30 °C, using THF as the solvent, an eluent flow rate of 1 mL min^{-1}, and 19 narrow polystyrene standards as the reference. The measurements were performed on a Waters 1525 binary system equipped with a Waters 2414 RI detector using four Styragel columns (range 1000–1 000 000 Å); [f] Bd = degree of branches as branches per 1000 carbon atoms, calculated by ^{1}H NMR spectroscopy on isolated product; [g] $n_{Pd} = 2.1 \cdot 10^{-5}$ mol, V_{TFE} = 21 mL, T = 308 K, $P_{ethylene}$ = 2.5 bar, t = 6 h.

Precatalysts with different pyr-DAB ligands give remarkably different outcomes in the catalytic tests, in particular when the different substitution on the ligand backbone is considered (Table 4.3). The productivity rises of three times when going from ligand **13** to **11** (Table 4.3, runs 4-2; from 14.2 to 43.9 kg CP/mol Pd), and this effect is even more pronounced for the isopropyl-substituted system, where an increase of 5 times is observed (from 13.9 to 72.6 kg CP/mol Pd for **12b** and **10b**, respectively). **10b** generates the most productive catalyst of the series, whereas **13b** leads to the worst. The productivity data are strictly related to the ligand skeleton, indeed very similar values are obtained for catalysts with the ligands having the H atom on the backbone, and they are remarkably lower than the data obtained with catalysts with ligands with the butadiene skeleton. This might be related to catalyst stability: with precatalysts **12b** and **13b** the formation of a small amount of Pd black is observed at the end of the catalytic runs, thus indicating that ligand dissociation occurs,

whereas this is not the case for catalysts with **10** or **11**. This is in agreement with the difference in the ligand coordinating capability evidenced by NMR studies.

The trend of productivity is reflected in the TON values, which remarkably decrease going from the butadiene derived ligands **10** and **11** to those with the H in the skeleton, **12** and **13**. When the TON of MA is considered for both series of catalysts, it significantly increases going from the isopropyl to the methyl substituted ligand (Table 4.3, run 1 *vs* 2 and 3 *vs* 4). These values are in agreement with the content of MA that increases in the same order. Regardless of the ligand skeleton, the content of MA is three times higher for the macromolecules obtained with the methyl substituted ligands than for those obtained with the isopropyl derivatives, thus indicating that the amount of inserted methyl acrylate is mainly determined by the steric hindrance of the *ortho* substituents on the aryl rings, as already observed for catalysts with Ar-BIP ligands (Chapter 3).[16] Therefore, coordination-insertion of the polar monomer is disfavoured by increasing the steric hindrance around the palladium centre, and this is further evidenced moving from ligands with the H to those with methyl groups on the skeleton (Table 4.3, run 3 *vs* 1 and 4 *vs* 2).

The molecular weight of the produced macromolecules increases of more than one order of magnitude going from catalyst with ligand **12** to that with **10** (Table 4.3, run 3 *vs* 1), thus indicating that the increase in the productivity is due to an increase in the length of the polymeric chain and not in the number of the chains. This data suggests that the presence of the methyl groups in the skeleton in place of hydrogen atoms remarkably slows down the chain transfer step, that consists of two reactions, β-hydrogen elimination and associative displacement of the growing polymeric chain with vinylic termination, the latter being affected the most by the steric hindrance around palladium.[17] The experimental data of decrease in branching degree for the macromolecules obtained with ligand **10** with respect to those produced with ligand **12** indicates that for the catalytic system under investigation the ligand backbone also affects the β-hydrogen elimination.

One test of ethylene homopolymerization was run with complex **10b**, over the time of 6 h, resulting in an increase in the activity of almost two times going from the co- to the homopolymerization (4 and 7.5 kg CP·mol $Pd^{-1}\cdot h^{-1}$, respectively). This increase is expected, but it is not as pronounced as for the classic Ar-DAB system, where it is of one order of magnitude.[18] As for the Ar-BIP systems reported in Chapter 3, this effect might be attributed again to the solvent of choice, trifluoroethanol, that is not usually used for the homopolymerization of ethylene.

Indeed, a direct comparison of the catalytic data reported in literature is very difficult because remarkably different reaction conditions are applied. To overcome this limit, specific experiments were run with **11b** and a few catalysts already reported in literature, such as [Pd(**6**)(CH_3)(CH_3CN)][PF_6],[16] [Pd(**L42**)(CH_3)(CH_3CN)][PF_6],[13] and

[Pd(**L54**)(CH_3)(CH_3CN)][PF_6].[19] All of the used precatalysts have ligands with methyl substituents on the *ortho* positions of the aryl rings. A mass flow control device was used to measure the ethylene consumption during the course of 6 h (Figure 4.8).

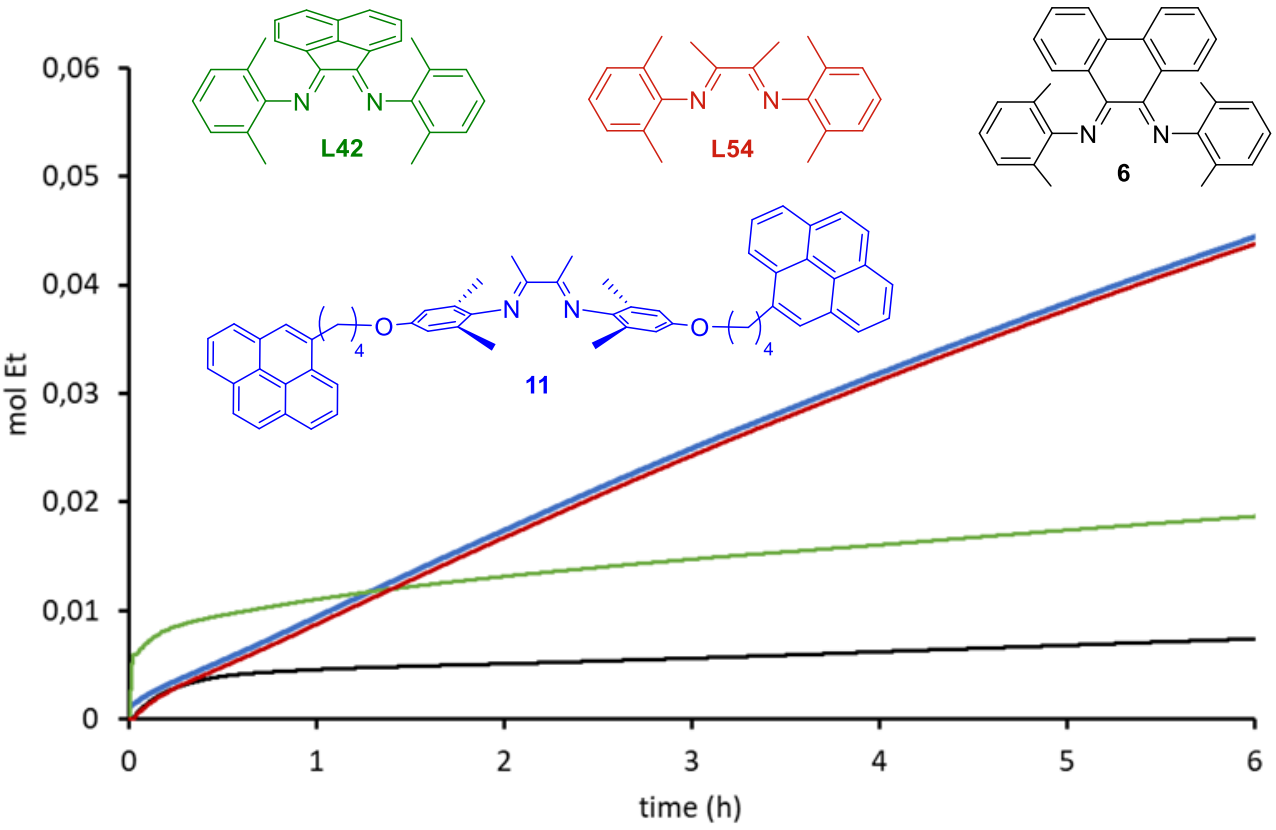

Figure 4.8. Ethylene/methyl acrylate copolymerization: kinetic profiles. Precatalyst: [Pd(**N-N**)(CH_3)(CH_3CN)][X] (**N-N** = **11**, X = SbF_6 (blue curve); **N-N** = **6**, X = PF_6 (black curve); **N-N** = **L42**, X = PF_6 (green curve); **N-N = L54**, X = PF_6 (red curve). Reaction conditions: see Table 4.3, t = 6 h.

The catalyst that forms from **11b** and the relevant Ar-DAB **L54b** complex show a similar kinetic profile: *i.* an induction period of 95 s is observed for **L54b**, but not for **11b**; *ii.* the rate of ethylene uptake (TOF) is slightly higher for **11b**; *iii.* both catalysts do not deactivate during the first 6 h of reaction. By comparing all the four catalysts under investigation it is clear that: the highest initial ethylene uptake is obtained by **L42b**, followed by **11b,** whereas **6b** and **L54b** have a similar profile up to 20 min; *iv*. both the catalysts with **L41** and **6** slow down after that time, deactivating over the course of the reaction, whereas the two systems with ligands **11** and **L54**, having the diazabutadiene backbone, remain active, and catalyst with **11** is the slightly most active between the two.

Since **10b** generated the most productive catalyst under the tested reaction conditions, a variation in the parameters such as temperature and methyl acrylate to palladium ratio was assessed, in order to optimize the system. For the latter parameter, the amount of catalyst employed was kept constant, and a larger quantity of acrylate was added to the reaction mixture, by keeping constant the total volume of the solution.

Table 4.4. Ethylene/methyl acrylate copolymerization: effect of [MA]/[Pd] and temperature.[a] Precatalyst: [Pd(CH_3)(CH_3CN)(**10**)][SbF_6]

Run	[MA]/[Pd]	Yield (g)	kg CP/g Pd[b]	kg CP/mol Pd	mol % MA[c]	TON[d]		M_n[e] (M_w/M_n)	Bd [f]
						E	MA		
1	594	1.5237	0.683	72.6	0.8	2521	20	260000 (1.55)	87
2	1188	1.4562	0.653	69.3	1.7	2347	41	159000 (1.25)	88
3[g]	1188	2.1412	0.960	102.0	1.6	3462	56	52000 (1.66)	85

[a] Reaction conditions: see Table 4.3, run 1: V_{MA} = 1.130 mL, run 2: V_{MA} = 2.260 mL; [b] isolated yield, productivity as kg CP/g Pd = kilograms of product per gram of Pd; [c] calculated by ^{1}H NMR spectroscopy on isolated product; [d] see Table 4.3; [e] see Table 4.3; [f] see Table 4.3; [g] Reaction conditions as [a], T = 318 K.

Doubling the [MA]/[Pd] ratio from 594 to 1188 resulted in a small loss in the productivity of the system, reflected by the decrease in the TON of ethylene (Table 4.4, run 1 *vs* 2, from 2521 to 2347), together with an increase in the amount of inserted methyl acrylate and in the TON for this comonomer, as expected based on previous reports, and similarly to what was obtained with catalysts with Ar-BIP ligands (Chapter 3).[17,18] The molecular weight of the macromolecule obtained with a doubled [MA]/[Pd] ratio is almost half of that of the macromolecule obtained under the standard reaction conditions.

Working at [MA]/[Pd] = 1188, the increase in the temperature from 308 K to 318 K resulted in an increase of nearly 1.5 times in the productivity (from 69.3 to 102.0 kg CP/mol Pd), that is in agreement with the increase in the TON of both ethylene and methyl acrylate. No effect of temperature on the content of the inserted polar monomer was observed. The molecular weight of the functionalized polyolefin produced at higher temperature is lower (Table 4.4, run 2 *vs* 3), thus indicating a higher chance of β-hydrogen elimination and chain walking, that also affects the

structure of the macromolecule, as it will be discussed in paragraph 4.2.5. The branching degree of the copolymer is not affected by the reaction conditions, and it has to be related more to the bulkiness of the ligand itself.

The activity of precatalysts **10b** and **11b** towards *tert*-butyl acrylate and *n*-butyl acrylate was assessed (Table 4.5).

Table 4.5. Ethylene/methyl acrylate copolymerization: effect of the acrylate.[a]

Precatalyst: [Pd(CH_3)(CH_3CN)(**pyr-DAB**)][SbF_6]

Run	**Pyr-DAB**	**Acrylate**	**Yield (g)**	**kg CP/g Pd[b]**	**kg CP/mol Pd**	**mol % MA[c]**	**TON[d]**		**M_n[e] (M_w/M_n)**	**Bd[f]**
							E	**A**		
1	**10**	MA	1.5237	0.683	72.6	0.8	2521	20	260000 (1.55)	87
2	**10**	*t*BuA	1.9465	0.873	92.7	0.2	3274	7	143000 (1.59)	88
3	**10**	*n*BuA	1.9481	0.923	98.0	0.6	3218	19	161000 (1.65)	84
4	**11**	MA	0.9223	0.414	43.9	3.0	1430	44	52000 (1.53)	73
5	**11**	*t*BuA	1.4575	0.654	69.4	0.5	2419	12	69000 (1.66)	79
6	**11**	*n*BuA	0.7652	0.343	36.4	3.2	1129	37	61000 (1.44)	84

[a] Reaction conditions: see Table 4.3, [A]/[Pd] = 594; [b] isolated yield, productivity as kg CP/g Pd = kilograms of product per gram of Pd; [c] calculated by ^{1}H NMR spectroscopy on isolated product; [d] see Table 4.3; [e] see Table 4.3; [f] see Table 4.3.

For precatalyst **10b**, the productivity increases on going from methyl acrylate to *tert*-butyl and *n*-butyl acrylate (Table 4.5, run 1 *vs* 2, 3), and this is reflected in the increase in the TON of ethylene from 2521 to 3274 for *tert*-butyl acrylate and 3218 for *n*-butyl acrylate. For precatalyst **11b** a similar trend with respect to *tert*-butyl acrylate is obtained, whereas when *n*-butyl acrylate is used a decrease in both the productivity and the TON of ethylene is found (Table 4.4, run 4 *vs* 5, 6). For both catalysts, the TON of the acrylate is only slightly decreased on going from MA to *n*BuA, thus indicating that the increase in the number of -CH_2- groups on the ester part of the comonomer has almost a negligible effect, whereas going from MA to *t*BuA a remarkable decrease in the TON of the acrylate was found, indicating that the increase in the steric hindrance of the ester group has a

negative effect on the rate of the migratory-insertion reaction of the polar monomer. The molecular weight of the macromolecules produced with **10b** and either *t*BuA or *n*BuA is half of that of the ethylene/methyl acrylate copolymer (Table 4.5, run 2, 3 *vs* 1), whereas all the copolymers obtained with **11b** have similar molecular weights. The branching degree is practically unaffected by the different acrylates, but it is more related to the nature of the catalyst itself, thus suggesting that the chain walking process is only slightly affected by the nature of the polar monomer.

Table 4.6. Ethylene/methyl acrylate copolymerization: effect of dichloromethane.[a]
Precatalyst: [Pd(CH_3)(CH_3CN)(pyr-DAB)][SbF_6]

Run	Pyr-DAB	Yield (g)	kg CP/g Pd[b]	kg CP/mol Pd	mol % MA[c]	TON[d] E	TON[d] MA	M_n[e] (M_w/M_n)	Bd[f]
1	**10**	2.4431	1.096	116.3	0.9	4035	37	180000 (1.56)	84
2	**11**	1.9356	0.868	92.2	4.0	2913	121	24000 (1.53)	95
3	**12**	0.1507	0.068	7.2	1.2	247	3	1200 (1.54)	100
4	**13**	0.0952	0.043	4.5	4.5	141	7	800 (1.27)	98

[a] Reaction conditions: see Table 4.3; [b] isolated yield, productivity as kg CP/g Pd = kilograms of copolymer per gram of Pd or kg CP/mol Pd = kilograms of copolymer per mol of Pd; [c] calculated by ^{1}H NMR spectroscopy on isolated product; [d] TON as mol comonomer/mol of Pd; [e] see Table 4.3; [f] see Table 4.3.

As presented in Chapter 3, a strong solvent effect on the catalytic outcome and on the copolymer microstructure has already been observed; therefore, complexes **10b**-**13b** were tested also in dichloromethane (Table 4.6). The different solvent has a remarkable effect on the productivity of the systems, and the trends are different depending on the substituent on the backbone of the ligand. For catalysts with ligands **10** and **11** an increase in the productivity was achieved moving from TFE to dichloromethane (Table 4.3, run 1 and 2 *vs* Table 4.6, run 1 and 2), whereas for those with **12** and **13** a pronounced decrease in the productivity was obtained (Table 4.3, run 3 and 4 *vs* Table 4.6, run 3 and 4), together with a decrease in the turnover number for both comonomers. The observed solvent effect confirms what we already reported for Ar-BIAN and Ar-BIP[16] catalysts: when the catalyst stability is low, as in the case of catalysts with **12** and **13**, the use of trifluoroethanol is mandatory thanks to its beneficial effect in stabilizing the Pd-H intermediate; whereas when catalyst

stability is not an issue, dichloromethane is a better solvent, likely for solubility reasons of both catalyst and comonomers. In addition, for catalysts with ligands **10** and **11** there is an increase in the TON of MA (from 20 in trifluoroethanol to 37 in dichloromethane, and from 44 to 121, respectively) and a concomitant increase in the amount of methyl acrylate inserted, that is more evident for **11** (from 0.8 to 0.9 % and from 3.0 to 4.0 % for **10** and **11**, respectively). For both series of catalysts, shorter macromolecules are produced in dichloromethane than in trifluoroethanol, thus suggesting that in the aprotic solvent the associative displacement of the polymeric chain with the vinylic termination is favoured with respect to trifluoroethanol. However, this effect is much more pronounced for catalysts with **12** and **13** than for those with **10** and **11** suggesting that also the β-hydrogen elimination is favoured in dichloromethane. The fact that the branching degree is very similar in both solvents supports this hypothesis.

For all the catalytic tests, the polydispersity values, indicated as M_w/M_n in the Tables, are around 1.5, indicating a deviation from the Flory-Schulz distribution for the coordination-insertion chain-growth polymerization, suggesting a partial *living* character for the copolymerization reaction with complexes **10b-13b**. To prove or disprove this hypothesis, copolymerization tests at different reaction times are needed in order to evaluate if the molecular weight of the produced macromolecules linearly increases with time.

4.2.5. Characterization of the produced functionalized polyolefins.

The macromolecules produced with different precatalysts have a different aspect: those obtained with catalysts with ligands with H-substituted backbone are brown oils, whereas those produced with catalysts with the 1,4-diaza-1,3-butadiene ligand skeleton are off-white solids (Figure 4.7).

The produced macromolecules were characterized by ^{1}H and ^{13}C NMR spectroscopy in $CDCl_3$ at room temperature. The signals in the ^{1}H NMR spectra were identified and assigned by comparison with literature data (Figure 4.9):[18,20-22] the singlet at 3.66 ppm is relevant to the methoxy group, the signals between 2.50 and 1.50 ppm belong to allylic protons and to methylenic groups closer to the ester functionality, the broad and intense signal centred at 1.25 ppm to the methylenic and methinic moieties of ethylene units, the signals between 1.0 and 0.6 ppm are assigned to methyl groups at the end of branches (Figure 4.9). No signal relevant to the vinylic termination is observed for the products obtained with **10b** and **11b**, whereas for the macromolecules produced with **12b** and **13b** these are present, in agreement with the lower molecular weight of these products (Figure S4.29, S4.31).

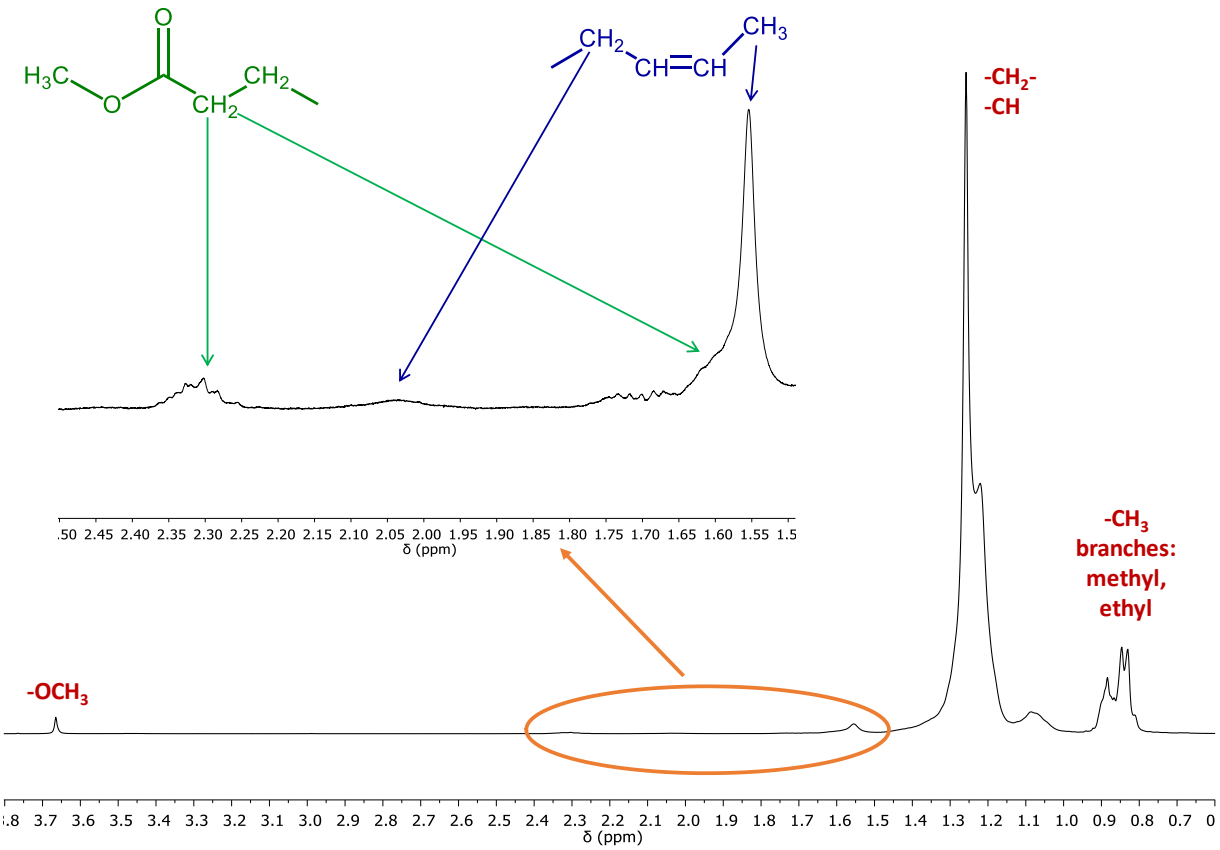

Figure 4.9. ^{1}H NMR spectrum ($CDCl_3$, 298 K) of the macromolecule obtained with **10b**.

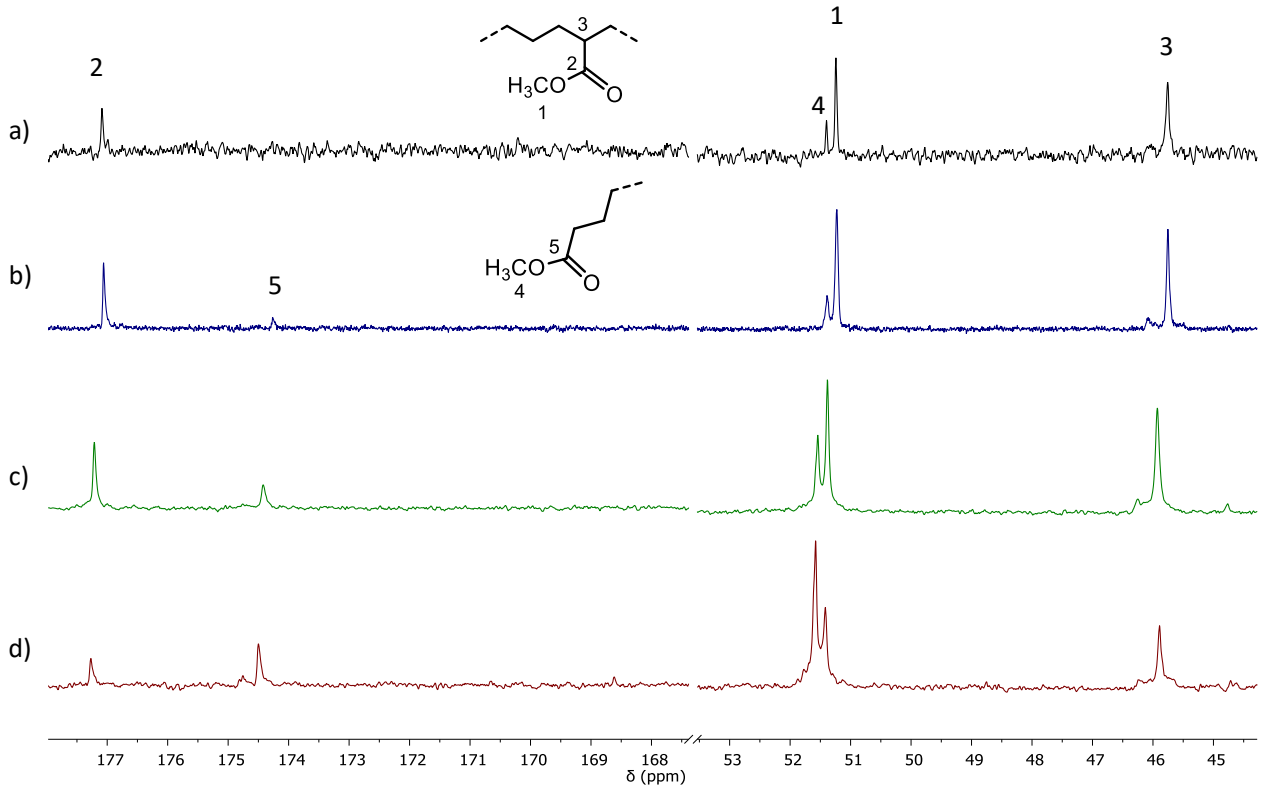

Figure 4.10. ^{13}C NMR spectra ($CDCl_3$, 298 K) of the catalytic products obtained with: a) **10b**, b) **11b**, c) **12b**, d) **13b**.

However, the proton spectrum itself is not enough to determine the exact microstructure of the macromolecule, and ^{13}C NMR spectra together with bidimensional experiments, such as $^{1}H,^{13}C$-HSQC and HMBC, are required to have a better understanding of the type of insertion of the acrylic ester. In particular, in the ^{13}C NMR spectrum of the copolymer synthesized with **10b**, in the carbonyl region only the signal at 177 ppm is present, whereas two signals for the methoxy group are observed at 51.41 and 51.57 ppm, together with signals at 45.92 ppm for the methinic group (Figure 4.10a). In the $^{1}H,^{13}C$-HSQC spectrum (Figure 4.11) the correlation peak between the singlet of the -OCH_3 groups at 3.66 ppm and the relevant carbon atoms at 51.41 and 51.57 ppm, and that between the signal of the methinic proton at 2.32 ppm and the relevant carbon at 45.92 ppm are present (black dashed circles, Figure 4.11).

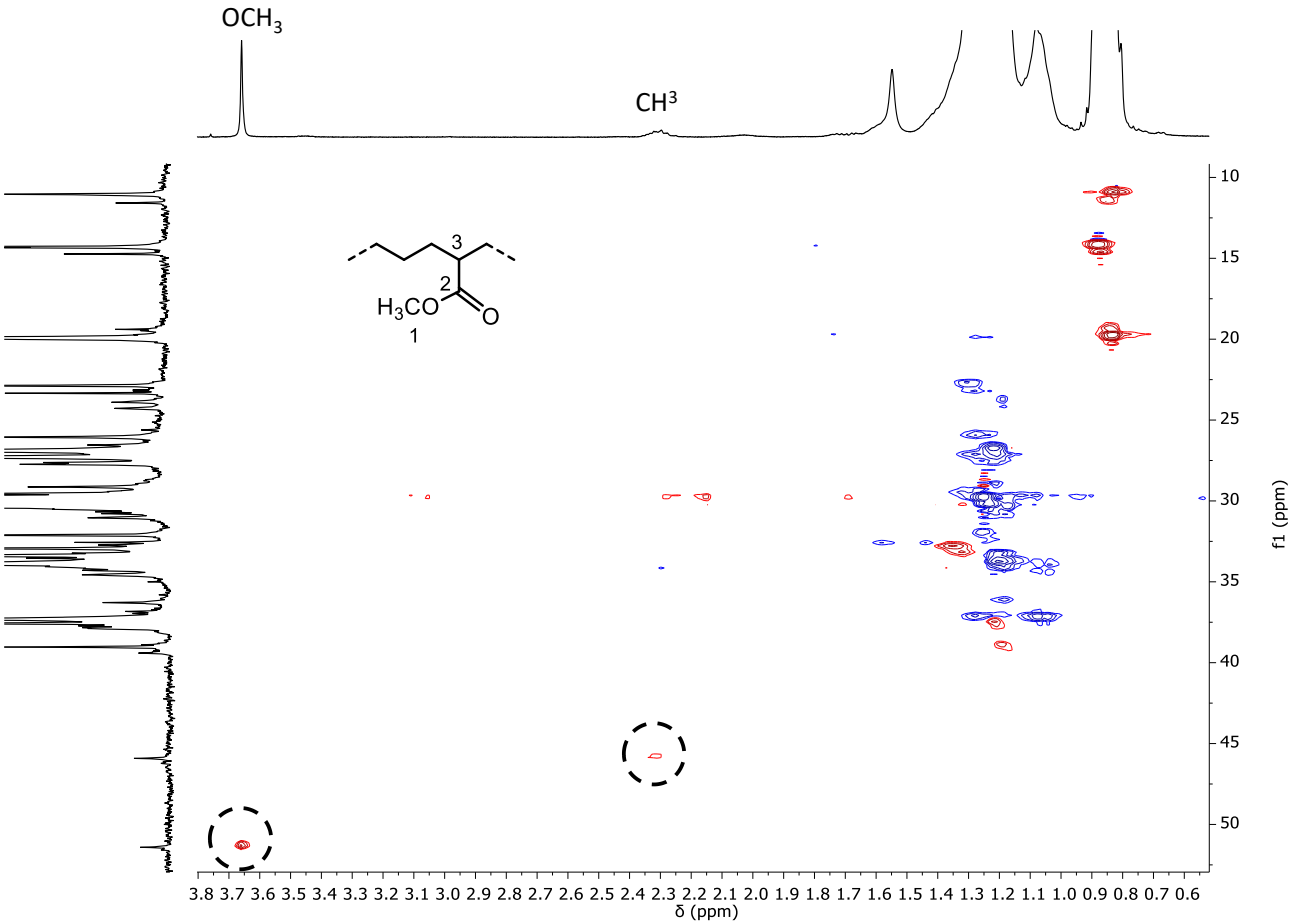

Figure 4.11. $^{1}H,^{13}C$-HSQC spectrum of the macromolecule obtained with **10b** ($CDCl_3$, 298 K); selected peak in black dashed circles, aliphatic region.

In the $^{1}H,^{13}C$-HMBC experiment (Figure 4.12), in the carbonyl region, cross peaks generated from the ^{3}J coupling between the methoxy group at 3.66 ppm and the carbonyl peak at higher frequency,

and from the ^{2}J coupling between the same carbonyl and a CH group are clearly visible. Moreover, the experiment is so sensitive that also the correlation peaks between the -OCH_3 and the CH_2 groups of the methyl acrylate inserted at the termination of the branches and the relevant carbonyl at 174 ppm are present, even though the latter is not visible in the ^{13}C monodimensional spectrum. This thorough NMR investigation and the comparison with literature data indicate that in these macromolecules methyl acrylate is inserted mainly into the main polymeric chain rather than at the end of the branches, as it usually happens for copolymers obtained with Pd(II) catalysts based on α-diimine ligands (Chapter 1).

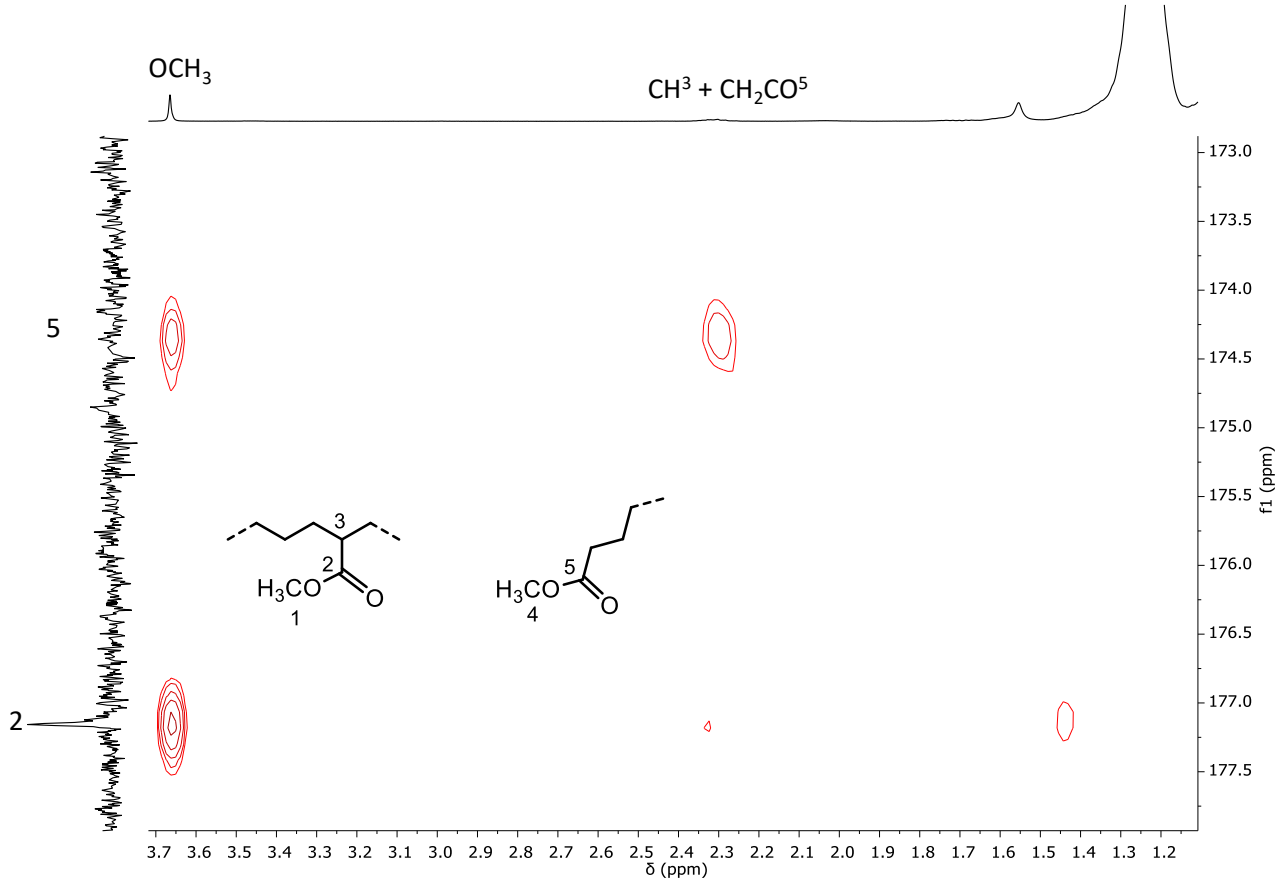

Figure 4.12. $^{1}H,^{13}C$-HMBC spectrum of the macromolecule obtained with **10b** ($CDCl_3$, 298 K); carbonyl region.

It is straightforward to note that moving from the product obtained with **10b**, which is the most hindered precatalyst (Figure 4.10a), to the one obtained with **13b**, the less hindered one (Figure 4.10d), there is an inversion in the selectivity of the enchainment of the polar monomer, going from a 98 % insertion into the main chain in the first case, to a 49 % in-chain insertion in the latter, as evaluated from the integration of carbonyl peaks in the ^{13}C NMR spectrum. This switch of the copolymer microstructure from the main chain to the termination of the branches is due to the

different nature of the ligand and, in particular, it appears to be mainly dictated by the ligand skeleton, methyl *vs* hydrogen. Such a remarkable effect of the α-diimine ligand architecture on the copolymer microstructure, in particular on the enchainment of the polar monomer, is observed for the first time with these catalysts.

When analysing the ^{13}C NMR spectrum (Figure S4.54, S4.56) of the macromolecules produced with an increased [MA]/[Pd] ratio and temperature (Table 4.4, runs 2, 3), an increase in the quantity of comonomer inserted in the termination of the branches was found, leading nearly to a 1:1 ratio between the two main types of enchainment for the copolymer synthesized with [MA]/[Pd] = 1188 and at T = 318 K. This effect is in agreement with the fact that the higher temperature increases the rate of β-hydrogen elimination, leading to a higher chance of chain walking.

In the ^{1}H NMR spectra of the ethylene/*tert*-butyl acrylate copolymers obtained with **10b** (Figure S4.41) or **11b** (Figure 4.13a), the signal of the inserted -OC(CH_3)$_3$ group is present at 1.45 ppm. In the corresponding ^{13}C NMR spectra the signals are assigned as follows: those in the region between 10 and 40 ppm are due to the CH and CH_2 and CH_3 groups; the peak at 46.60 ppm is assigned to the CH in the main polymer chain close to the carbonyl group, and the one at 79.65 ppm to the quaternary carbon of the *tert*-butyl group (Figure 4.14a). The signal of the carbonyl group at 176.00 ppm further confirms the insertion into the main polymeric chain.

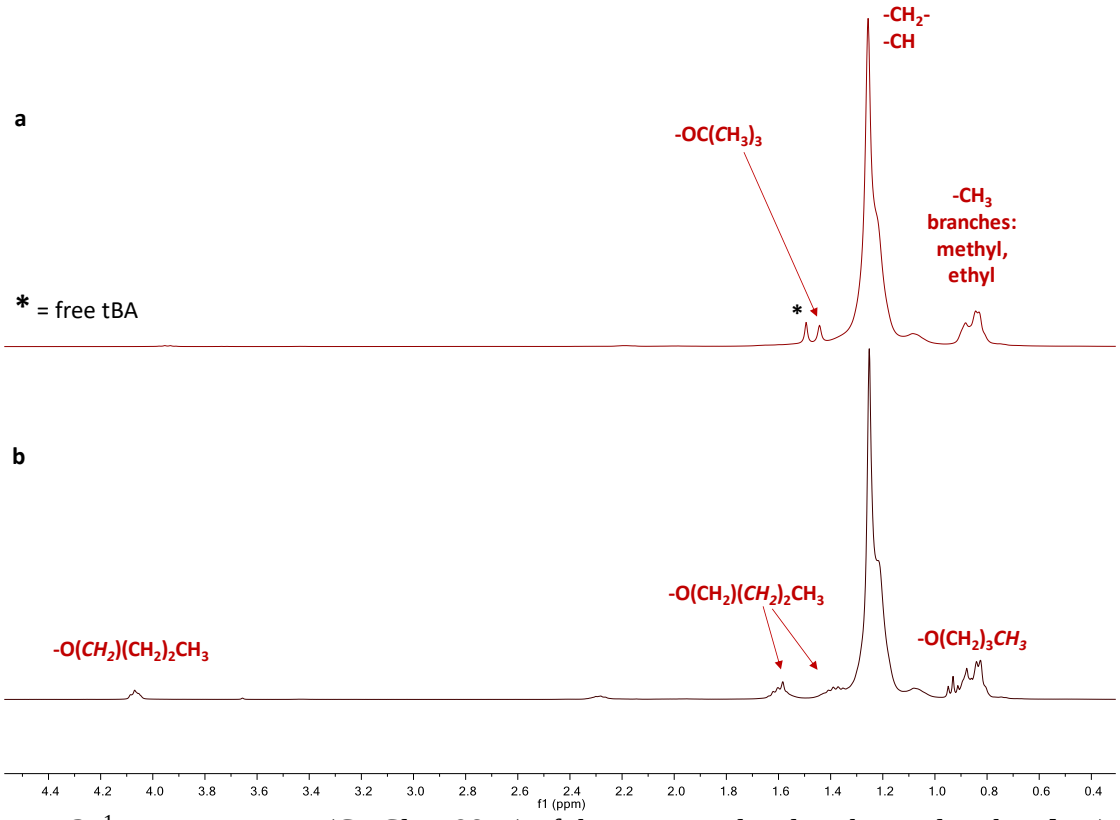

Figure 4.13. ^{1}H NMR spectra ($CDCl_3$, 298 K) of the macromolecules obtained with **11b**: a) ethylene/*tert*-butyl acrylate copolymer; b) ethylene/*n*-butyl acrylate copolymer.

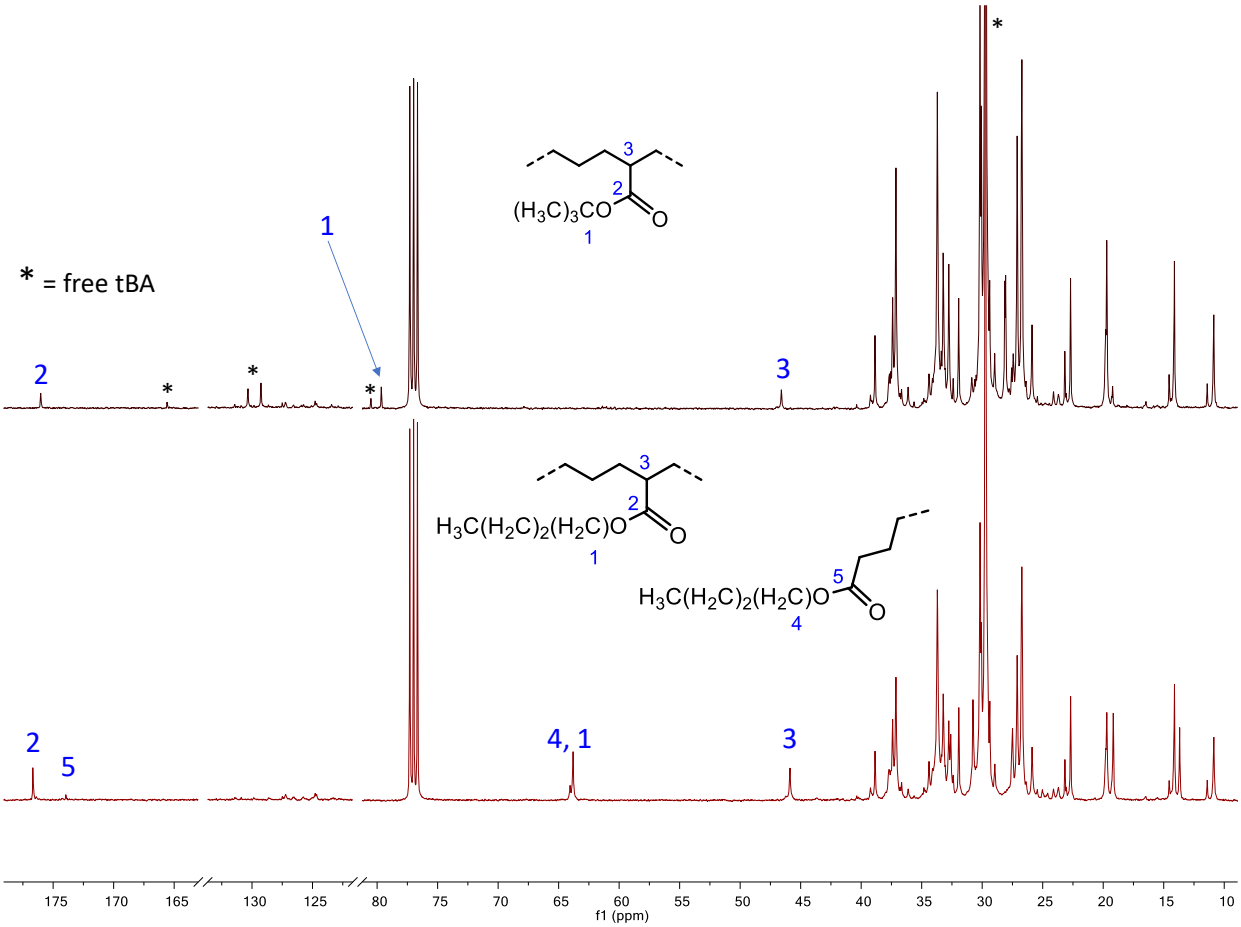

Figure 4.14. ^{13}C NMR spectra ($CDCl_3$, 298 K) of the macromolecules obtained with **11b**: a) ethylene/*tert*-butyl acrylate copolymer; b) ethylene/*n*-butyl acrylate copolymer.

When the copolymerization of ethylene with *n*-butyl acrylate is considered, no significant differences in the ^1H NMR spectra of the macromolecules obtained with **10b** and **11b** is observed (Figure S47, Figure 4.13b, respectively). In the ^{13}C NMR spectra of the two different products, in the region between 10 and 40 ppm the same signals are present, though with a different distribution in intensity (Figure S48 and 4.14b for **10b** and **11b**, respectively). By comparing these spectra to those of the ethylene/methyl acrylate copolymers, the signals at 176.68 ppm and 173.96 ppm in the carbonyl region are assigned to the *n*-butyl acrylate inserted into the main chain and in the termination of the branches, respectively, and those around 64 ppm to the -O(CH_2)$(CH_2)_2CH_3$ group (63.81 ppm for the in chain insertion, 64.06 ppm for the branch end insertion). The peak at 45.93 ppm is assigned to the CH in proximity of the carbonyl group into the main polymeric chain.

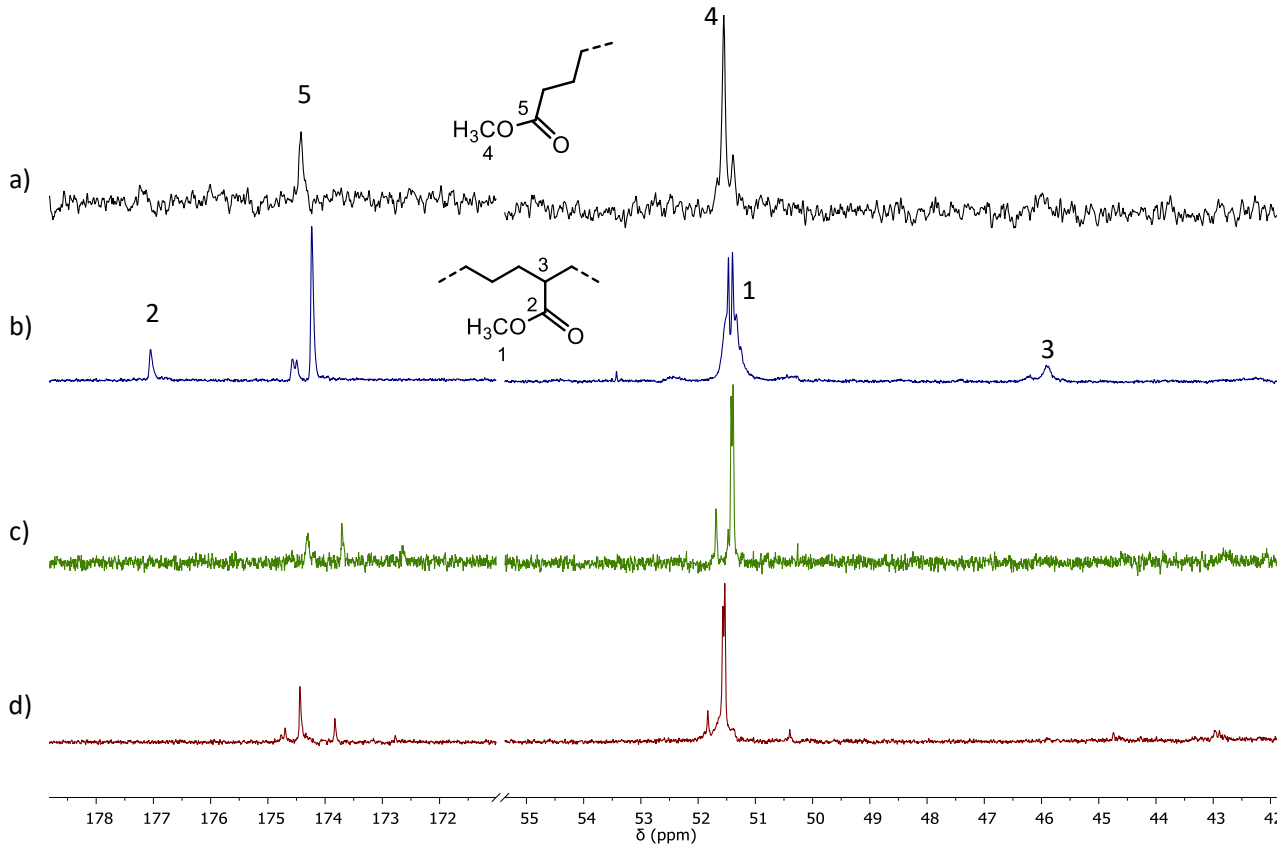

Figure 4.15. ^{13}C NMR spectra ($CDCl_3$, 298 K) of the macromolecules obtained in DCM from: a) **10b**, b) **11b**, c) **12b**, d) **13b**.

The analysis of the ^{13}C NMR spectra of the functionalized polyolefins produced in dichloromethane highlights that changing the reaction media from trifluoroethanol to dichloromethane results in a different enchainment of the polar vinyl comonomer. The carbonyl peak at 177 ppm, belonging to the comonomer inserted into the main chain, is present only in the macromolecules obtained by using **11b**. For the copolymers synthesized with all the other catalysts, only C=O peaks around 174 ppm are observed, indicating that the polar monomer is inserted at the end of the branches. An additional proof of the change in the selectivity, when the copolymerization is carried out in DCM, is the presence of more than one peak around 174 ppm, that might belong to slightly different kind of enchainment in the branches.

As for Ar-BIP complexes discussed in Chapter 3, the effect of the solvent on the copolymer microstructure might be due to the coordinating capability of trifluoroethanol with respect to dichloromethane. Its possible coordination disfavours the chain-walking process leading to the macromolecules with the polar monomer into the main chain. The molecular weight values, lower for the macromolecules produced in dichloromethane with respect to those obtained with trifluoroethanol, support this hypothesis.

The NMR analysis of the obtained macromolecules and the recorded GPC traces (see Figures S4.57-4.60) allow us to state that the products obtained with precatalysts **10b-13b** are indeed real ethylene/acrylic ester copolymers, and not a mixture of polyethylene and polymethylacrylate homopolymers.

*4.2.6. Reactivity of **10b** with ethylene and methyl acrylate.*

As discussed in the previous Chapters, the catalytic cycle of the Pd(II) complexes with α-diimine ligands in the ethylene/polar vinyl monomer copolymerization is well known and generally accepted.[17,23] The interesting results obtained with the ligands under investigation suggest that the relevant active species might follow different reaction pathways, due to the ligand peculiarity itself. To clarify this aspect, the *in situ* reactivity of the most productive precatalyst, **10b**, with both methyl acrylate and ethylene, was studied by using NMR spectroscopy and both CD_2Cl_2 and TFE-d_3 as solvents.

To a 2.5 mM solution of **10b**, in CD_2Cl_2 or in TFE-d_3, two equivalents of the acrylic ester were added at 298 K, and the reaction was followed with time, by recording NMR spectra during the first 3 h. Afterwards, ethylene was bubbled in the solution for 10 minutes, and additional spectra were registered.

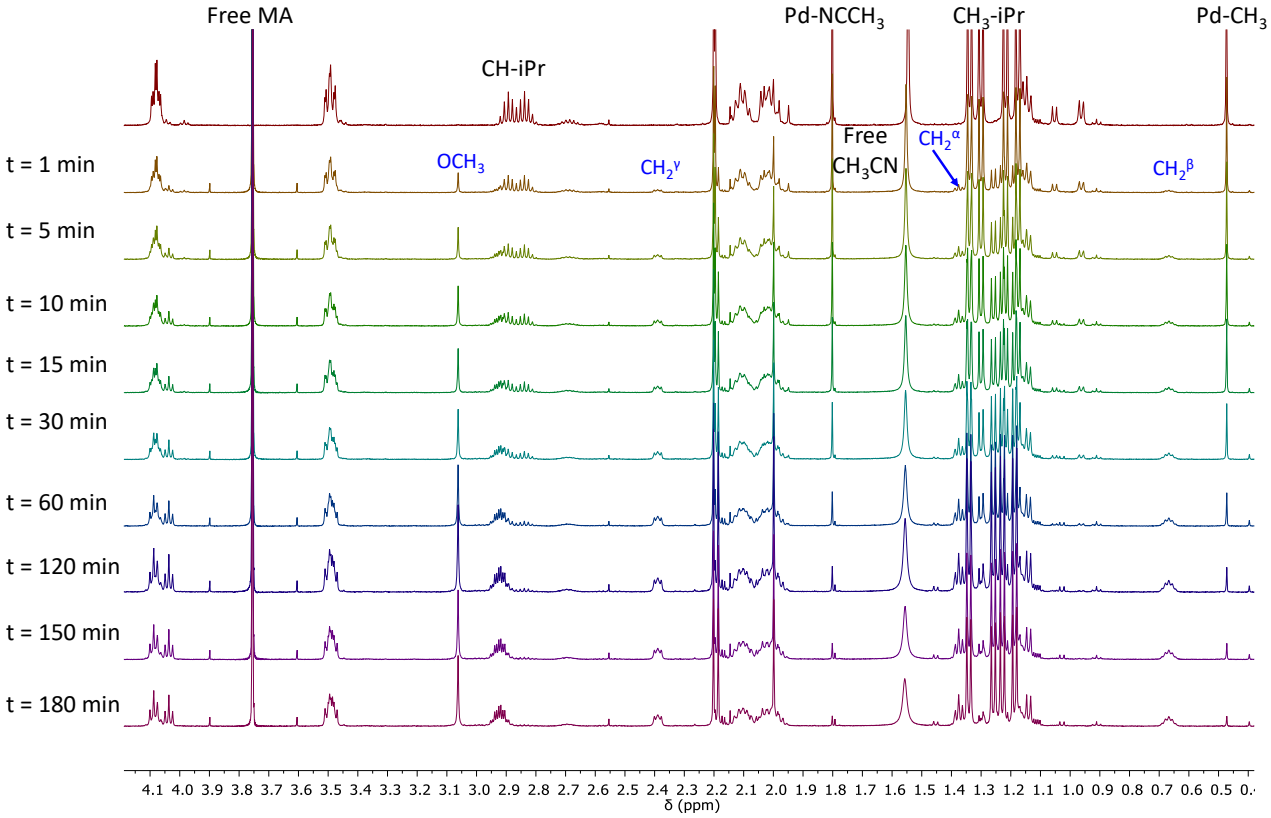

Figure 4.16. ^{1}H NMR spectra in CD_2Cl_2 at T= 298 K of the reactivity of **10b** with MA, aliphatic region, evolution with time (min); in blue signals of the C'' intermediate (Scheme 3.5).

When deuterated dichloromethane is used, **10b** slowly reacts with MA and it is almost completely consumed over the course of the 3 h (87 %), following a second order kinetic (Figure S68), analogous to that previously observed for Pd(II) complexes with Ar-BIP ligands (see Chapter 3).

The analysis of the ^{1}H NMR spectra evidences, already in the first spectrum recorded after the addition of methyl acrylate, the presence of the metallacycle C'', the catalyst resting state (Scheme 2.8; Figure 4.16, Figure S61-63). The -OCH_3 moiety of this molecule resonates at 3.07 ppm, probably due to the shielding cone of the bulky ligand. No other intermediates can be clearly detected.

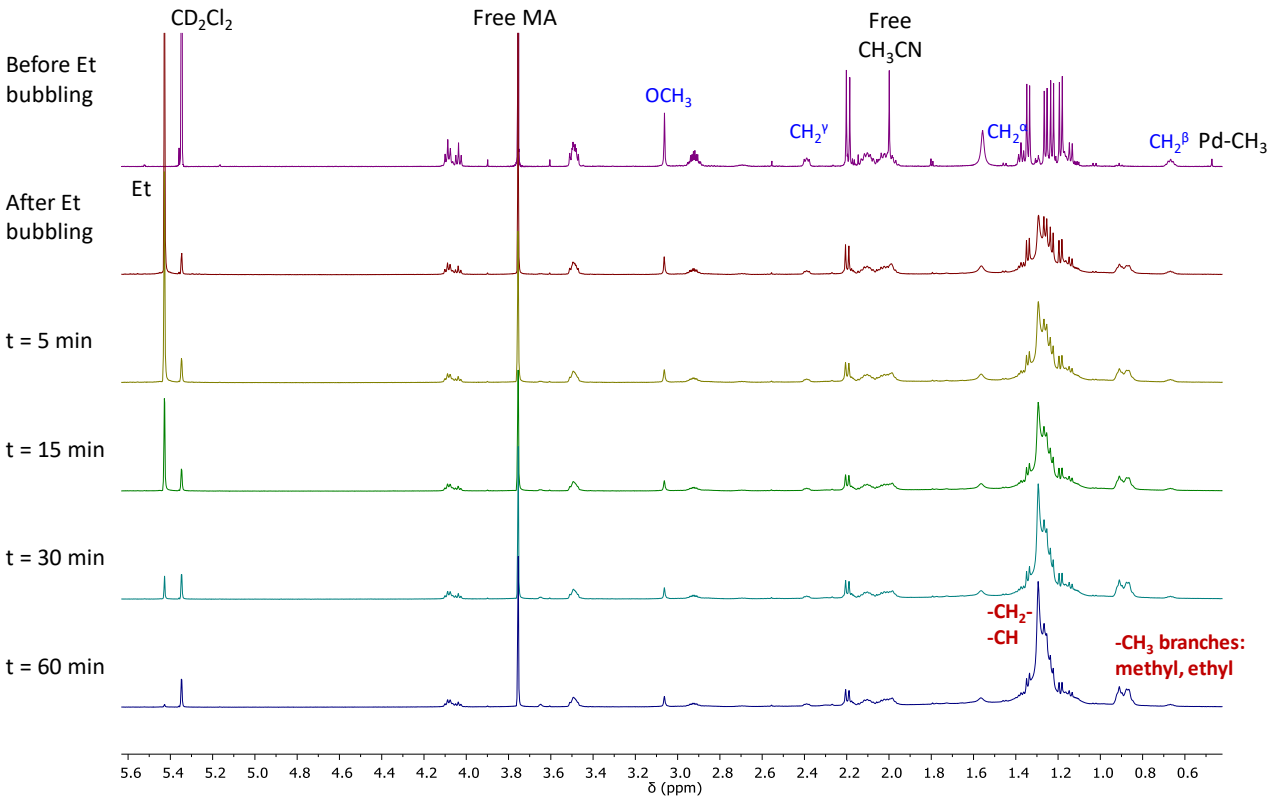

Figure 4.17. ^{1}H NMR spectra in CD_2Cl_2 at T= 298 K of reactivity of **10b** with MA, aliphatic region, evolution with time (min); in blue signals of the C'' intermediate (Scheme 3.5).

Ethylene was then bubbled in the CD_2Cl_2 solution containing C''(Scheme 2.8): the residual traces of **10b** are readily consumed with the concomitant formation of some kind polymeric species, as indicated by the broad peak centered at 1.30 ppm (Figure 4.17). At 3.66 ppm the resonance characteristic for the methoxy group inserted at the end of the branches starts to be visible in the spectrum recorded at 5 min, and it is clearly visible in the spectrum at 1 h. During this time almost all the ethylene is consumed. In addition only traces of the 6-membered palladacycle are still present.

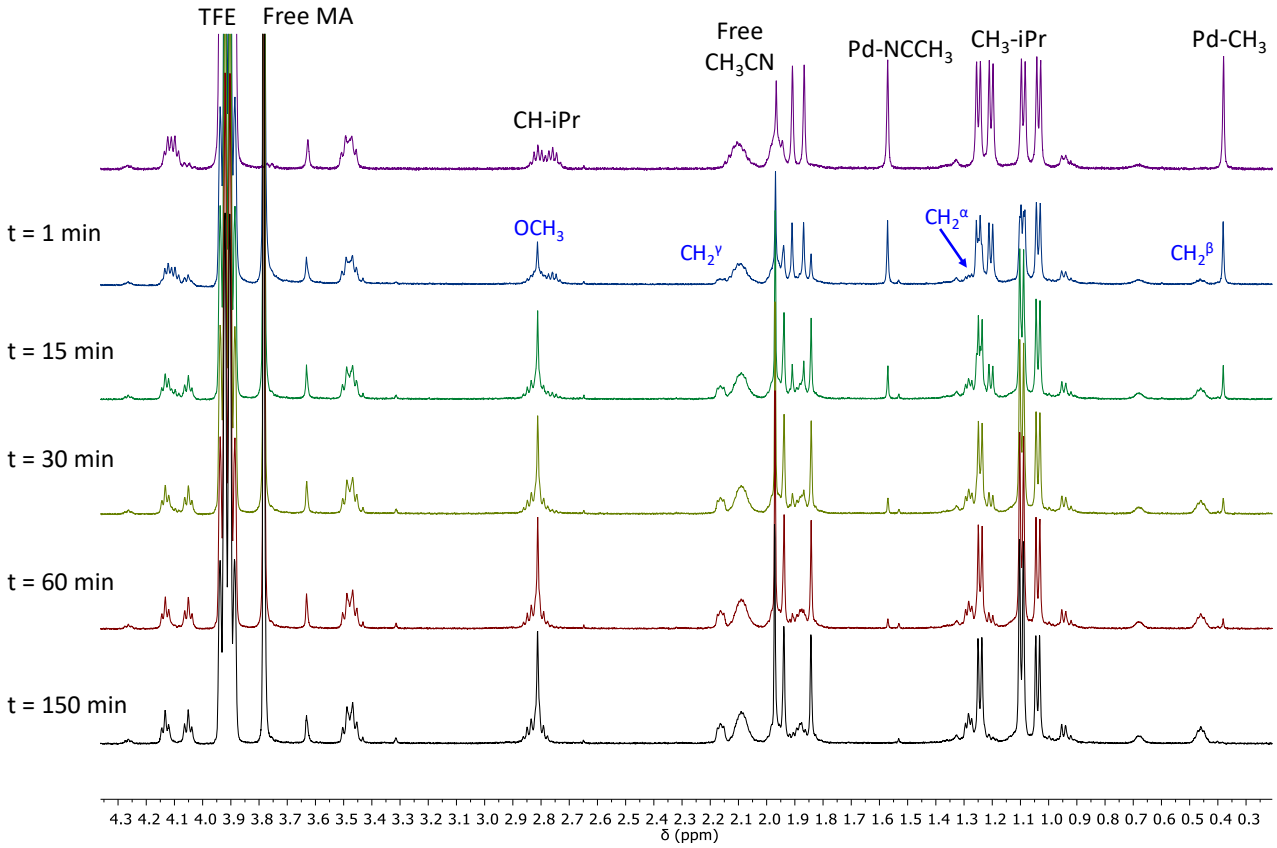

Figure 4.18. ^{1}H NMR spectra in TFE-d3 at T= 298 K of reactivity of **10b** with MA, aliphatic region, evolution with time (min); in blue signals of the C'' intermediate (Scheme 3.5).

When the reaction is performed in deuterated TFE the cationic complex reacts more rapidly than in CD_2Cl_2 (94% after 1 h, 100% after 2 h 30 minutes), and again, the signals of the C'' intermediate appear right after the addition of MA. In this case, the kinetic profile is not trivial to model (Figure S4.69), probably due to the small number of points taken. Also in this case the methoxy group of the palladacycle is found at lower frequency (2.82 ppm) than for complexes without any pyrene tag, as confirmed also by ^{1}H-^{13}C-HSQC analysis. After 3 h from the beginning of the reaction, ethylene was bubbled inside the NMR tube: after 5 minutes of ethylene bubbling a white film starts to appear at the solution interphase and the formation of a precipitate is visible after 8 minutes (Figure 4.19). In the ^{1}H NMR spectra recorded after the ethylene bubbling, a broad peak in the aliphatic region appears, alongside with the peaks belonging to the 6-membered metallacycle (Figure S4.67).

Figure 4.19. Reactivity of **10b** with methyl acrylate in deuterated TFE after ethylene bubbling.

Precatalyst **10b** exhibits a similar reactivity in the two different solvents, even though the reaction is faster in TFE than in CD_2Cl_2. The main product of the reaction is in both cases the six membered metallacycle C'' (Scheme 2.8, also indicated as *ii.* in Scheme 4.6) that is originated by the migratory insertion of MA into the Pd-CH_3 bond with a secondary regiochemistry, followed by chain walking, indicating that for the active species with ligand **10** the migratory insertion reaction is regiospecific. The difference between the behaviour in the two solvents arises when ethylene is added: in dichloromethane the polymeric product that is formed is soluble, whereas in deuterated TFE it precipitates (Figure 4.19), as it also happens in the case of the catalytic experiments. This suggests that the different architecture of the produced macromolecules by using the same precatalyst has to be mainly attributed to the nature of the reaction medium. Trifluoroethanol and dichloromethane are remarkably different in terms of coordinating capability, polarity and acidity: trifluoroethanol is considered as a coordinating solvent, whereas dichloromethane is not; trifluoroethanol is a polar, protic solvent (pK_a = 12.37) having a strong hydrogen bonding capability,[24] whereas dichloromethane is slightly polar and aprotic. To connect these differences to the macromolecule microstructure the main steps involved in the growth of the polymer chain should be taken into consideration. In particular, the kind of enchainment of the polar monomer in the polymer chain is originated by both its migratory insertion reaction into the Pd-alkyl bond and the reactions that take place afterwards (Scheme 4.6).

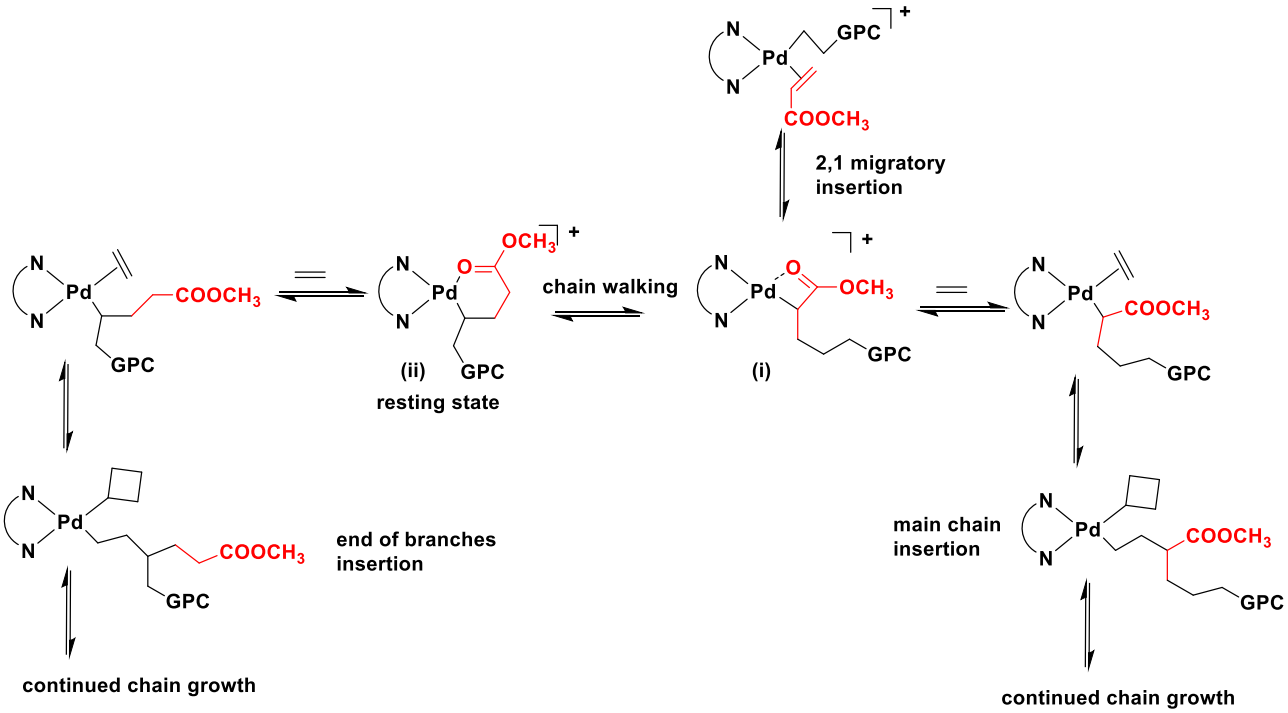

Scheme 4.6. Proposed pathways for the migratory insertion of methyl acrylate into the growing polymer chain (GPC = growing polymeric chain).

Generally speaking, it is reasonable to assume that, during the chain growth, methyl acrylate is always inserted into the main polymeric chain as the result of a 2,1-migratory insertion reaction into the Pd-alkyl bond, leading to the four-membered metallacycle *i* (Scheme 4.6). The latter can follow two competitive reaction pathways, that were also proposed for systems based on Pd(II) and amine-imine ligands:[25] *a*. the chain walking process, usually observed for Pd(II) catalysts based on α-diimine ligands, leading to copolymers with the polar monomer at the end of the branches (Scheme 4.6, left); *b*. the coordination/insertion of ethylene, typically observed for Pd(II) catalysts based on phosphino sulfonate ligands, leading to copolymers with the polar monomer into the main chain (Scheme 4.6, right). These two reactions compete with each other and their occurrence is driven by the relevant rate constants. The chain walking process consists in a series of β-hydrogen elimination/reinsertion reactions that lead to the six-membered metallacycle *ii.*, the catalyst resting state. This process requires a readily available coordination site *cis* to the growing polymeric chain. The catalytic data obtained in the two solvents suggest that the coordinating capability of trifluoroethanol is enough to favourably compete with the β-agostic interaction, prelude to the β-hydrogen elimination, disfavouring the chain walking process. In addition, it cannot be ruled out that the protic nature of TFE destabilizes the four-membered metallacycle *i.* through protonation of the oxygen atom bonded to palladium, favouring its cleavage and the coordination/insertion of ethylene leading to the growth of the copolymer chain. Therefore, it is reasonable to propose that in

the fluorinated alcohol the ethylene coordination/insertion overcomes the chain walking process leading to the functionalized polyethylene with MA inserted into the main chain.
Some specific experiments are now in progress in Milani's research group to validate or not the proposed mechanism.

4.3. Conclusions

α-diimine ligands bearing pyrene tags and the relevant neutral [Pd(pyr-DAB)(CH_3)Cl] and cationic [Pd(pyr-DAB)(CH_3)(CH_3CN)][SbF_6] complexes were investigated. Some solubility issues were encountered, in particular with neutral complexes bearing methyl substituents on the *ortho* position of the N-aryl rings and with the cationic complex with a 1,4-diazabutadiene skeleton and isopropyl substituents. These issues could derive from π-π stacking interactions that can occur between the pyrene moieties of different molecules of the complexes. In the ^{1}H NMR spectra, the Pd-CH_3 chemical shifts for the isopropyl-substituted pyr-DAB neutral complexes are the same as those reported for "classical" Brookhart-type catalysts, suggesting that the introduction of a -$O(CH_2)_4$-pyrene group does not affect the overall donating ability of the ligand. For the pyr-DAB monocationic Pd(II) complexes bearing the same substituent on the *ortho* position but having a different skeleton, the Pd-CH_3 NMR peak shifts at higher frequencies going from **10b** to **12b** and from **11b** to **13b** in agreement with the expected variation of the Lewis basicity of the ligand.
The cationic complexes generate very efficient catalysts for the ethylene/acrylic esters copolymerization under mild reaction conditions of temperature and pressure leading to the corresponding copolymers. A detailed catalytic investigation was carried out, testing different solvents (TFE, DCM), temperatures, [MA] to [Pd] ratios and acrylic esters different from the reference methyl acrylate. The detailed NMR characterization of the produced macromolecules highlighted that, when trifluoroethanol is the reaction medium, the polar vinyl monomer is mainly (or almost exclusively) inserted into the main polymeric chain rather than at the end of the branches, as it is always found out for catalytic systems based on α-diimines. This trend is reversed when dichloromethane is applied as solvent for the catalysis. The different enchainment obtained in trifluoroethanol must then be related to the combination of the peculiar ligand and the nature of the solvents.
These promising results prompt us to further investigate the catalytic system based on pyrene-tagged α-diimines to unravel the role played by the ligand tail and to develop a second generation of better performing catalysts. In addition, the results obtained with precatalysts with both Ar-BIP ligands and pyr-DAB indicate that the active species containing such ligands are not good catalysts for ethylene homopolymerization, while they efficiently catalyze the copolymerization reaction,

suggesting that the route to follow when designing new and efficient copolymerization catalysts is to move towards catalysts that promote the homopolymerization of polar vinyl monomers.

4.4. Experimental

The synthesis of the ligands and of the neutral complexes were performed at room temperature; the cationic complexes were obtained using standard Schlenk techniques under argon. Anhydrous dichloromethane was obtained by distillation over CaH_2 under argon atmosphere. Deuterated solvents (Cambridge Isotope Laboratories, Inc. (CIL) and Sigma Aldrich) were stored as recommended by sellers. Ethylene (purity ≥ 99.9 %) supplied by SIAD and methyl acrylate (99.9%, with 0.02% of hydroquinone monomethyl ether) supplied by Aldrich were used as received. TFE and all the other reagents and solvents were purchased from Sigma-Aldrich/Merck and used without further purification for synthetic, spectroscopic and catalytic purposes. [Pd(cod)(CH_3)Cl] was synthesized according to literature procedures. [$Pd(OAc)_2$] was a donation from BASF Italia and used as received.

NMR spectra of ligands, complexes and catalytic products were recorded on a Varian 500 spectrometer at 500 MHz (^{1}H) and 125.68 MHz (^{13}C). The resonances are reported in ppm (δ) and referenced to the residual solvent peak versus $Si(CH_3)_4$: $CDCl_3$ at δ 7.26 (^{1}H and δ 77.0 (^{13}C), CD_2Cl_2 at δ 5.32 (^{1}H) and δ 54.0 (^{13}C). NMR experiments were performed employing the automatic software parameters. In the case of NOESY experiments a mixing time of 500 ms was used. Elemental analyses were performed in the Department of Chemistry "G. Ciamician" of University of Bologna, on a Thermo Flash 2000 CHNS/O analyzer. The consumption of ethylene was monitored by using a Bronkhorst EL-Pressure e EL-Flow *select* mass flow control device.

The average molecular weights (M_n and M_w) and polydispersity (M_w/M_n) values of copolymer samples were measured through gel permeation chromatography at 30 °C, using THF as the solvent, an eluent flow rate of 1 mL min^{-1}, and 19 narrow polystyrene standards as the reference. The measurements were performed on a Waters 1525 binary system equipped with a Waters 2414 RI detector using four Styragel columns (range 1000–1 000 000 Å).

*4.4.1. Synthesis and characterization of ligands **10-13**.*

The α-diimine ligands were prepared according to the following procedure: the appropriate aniline and 2,3-butandienone or 1,4 dioxane-2,3-diol (0.5 eq) were dissolved in ethanol in a flame-dry schlenk flask. With stirring, the mixture was gently heated with a hot-air gun until all material had dissolved. Next, formic acid (3-5 drops) was added resulting in the formation of precipitated product (starting a few min after addition and/or overnight). The reaction mixture was stirred

overnight, then cooled in an ice bath. The precipitate was collected on a fritter filter, washed with cold ethanol and dry under vacuum.

10. (Pale yellow solid, yield 63%) ^{1}H NMR (400 MHz, CD_2Cl_2): δ 8.36 (d, J = 9.3 Hz, 2H), 8.21 – 8.12 (m, 8H), 8.07 – 7.98 (m, 6H), 7.95 (d, J = 7.8 Hz, 2H), 6.71 (s, 4H), 4.04 (t, J = 6.3 Hz, 4H), 3.49 – 3.44 (m, 4H), 2.68 (dq, J = 13.7, 6.7 Hz, 4H), 2.11 – 1.94 (m, 14H), 1.12 (dd, J = 10.3, 6.9 Hz, 24H).^{13}C NMR (100 MHz, CD_2Cl_2): δ 169.71, 156.45, 140.30, 137.55, 137.03, 132.00, 131.50, 130.35, 129.21, 128.05, 127.91, 127.68, 127.05, 126.40, 125.36, 125.21, 124.09, 109.77, 68.38, 54.00, 33.74, 30.11, 29.17, 28.96, 23.29, 22.89, 16.75. HRMS (ESI): calc for $C_{68}H_{72}N_2O_2$ $[M+H]^+$ = 949.56, found 949.5603.

11. (Pale yellow solid, yield 55%) ^{1}H NMR (400 MHz, CD_2Cl_2): δ 8.34 (d, *J* = 9.3 Hz, 2H), 8.23 – 8.10 (m, 8H), 8.08 – 7.98 (m, 6H), 7.94 (d, *J* = 7.8 Hz, 2H), 6.64 (s, 4H), 4.01 (t, *J* = 6.3 Hz, 4H), 3.48 – 3.41 (m, 4H), 2.11 – 1.90 (m, 26H).^{13}C NMR (100 MHz, CD_2Cl_2): δ 169.48, 155.64, 142.59, 137.56, 132.00, 131.50, 130.34, 129.20, 128.04, 127.91, 127.67, 127.05, 126.45, 126.40, 125.36, 125.21, 124.09, 114.45, 68.45, 54.00, 33.71, 30.01, 28.92, 18.33, 16.08.HRMS (ESI): calc for $C_{60}H_{57}N_2O_2$ $[M+H]^+$ = 837.43, found 837.4404.

12. (Pale yellow solid, yield 52%); ^{1}H NMR (400 MHz, CD_2Cl_2): δ 8.35 (d, *J* = 9.3 Hz, 2H), 8.26 – 7.97 (m, 18H), 7.94 (d, *J* = 7.8 Hz, 2H), 6.70 (s, 4H), 4.04 (t, *J* = 6.3 Hz, 4H), 3.49 – 3.43 (m, 4H), 2.94 (sept, *J* = 6.8 Hz, 4H), 2.12 – 2.04 (m, 4H), 2.01 – 1.94 (m, 4H), 1.15 (d, *J* = 6.9 Hz, 24H). ^{13}C NMR (100 MHz, CD_2Cl_2): δ 164.17, 157.28, 142.24, 139.14, 137.48, 131.98, 131.48, 130.34, 129.18, 128.03, 127.89, 127.67, 127.05, 126.39, 125.36, 125.21, 124.06, 109.82, 68.33, 33.70, 30.00, 28.89, 28.66, 23.69. HRMS (ESI): calc for $C_{66}H_{69}N_2O_2$ $[M+H]^+$ = 921.53, found 921.5342.

13. (Pale yellow solid, yield 67%); ^{1}H NMR (400 MHz, CD_2Cl_2) δ 8.34 (d, *J* = 9.3 Hz, 2H), 8.23 – 8.10 (m, 8H), 8.10 – 7.97 (m, 8H), 7.93 (d, *J* = 7.8 Hz, 2H), 6.64 (s, 4H), 4.02 (t, *J* = 6.3 Hz, 4H), 3.44 (t, *J* = 6.3 Hz, 4H), 2.15 (s, 12H), 2.08 – 2.01 (m, 4H), 2.00 – 1.93 (m, 4H). ^{13}C NMR (100 MHz, CD_2Cl_2): δ 164.04, 156.64, 143.96, 137.49, 131.97, 131.47, 130.33, 129.17, 128.99, 128.03, 127.90, 127.66, 127.05, 126.39, 125.53, 125.46, 125.35, 125.21, 124.06, 114.69, 68.35, 33.67, 29.90, 28.84, 18.96. HRMS (ESI): calc for $C_{58}H_{53}N_2O_2$ $[M+H]^+$ = 809.40, found 809.4083.

4.4.3. Synthesis and characterization of [Pd(pyrDAB)(CH_3)Cl] ***10a-13a****.*

To a stirred solution of [Pd(cod)(CH_3)Cl] (1.0 eq) in dry CH_2Cl_2, a solution of 1.1 equiv of the appropriate α-diimine ligand (**10-13**) in dry CH_2Cl_2 was added. After 22 h at room temperature, the reaction mixture was concentrated in a *vacuo* and the resulting mixture precipitated and washed upon addition of cold diethyl ether.

10a. (Red solid, yield 75%); ^{1}H NMR (500 MHz, CD_2Cl_2, 298 K): δ 8.42 – 7.87 (m, 18H, CH-Py), 6.80 (s, 2H, Ar-CH), 6.77 (s, 2H, Ar-CH), 4.07 (m, J = 5.8 Hz, 4H, CH_2-O), 3.47 (t, J = 7.3 Hz, 4H, CH_2-Py), 3.02 (m, J = 19.6, 6.2 Hz, 4H, CH-iPr), 2.12 (m, 4H, CH_2CH_2), 2.05 – 1.83 (m, 10H, CH_2CH_2 and Me-C=N), 1.38 (d, J = 19.0, 6.7 Hz, 6H, Me-iPr), 1.34 (d, J = 19.0, 6.7 Hz, 6H, Me-iPr), 1.14 (m, 12H, Me-iPr), 0.40 (s, 3H, Pd-Me). ^{13}C NMR (125.68 MHz, CD_2Cl_2, 298 K): δ = 127.84 (CH-Py), 127.66 (CH-Py), 127.43 (CH-Py), 126.83 (CH-Py), 126.16 (CH-Py), 125.08 (CH-Py), 123.85 (CH-Py), 110.04 (Ar-CH), 109.36 (Ar-CH), 68.08 (CH_2-O), 33.48 (CH_2-Py), 29.77 (CH_2CH_2), 29.41 (CH-iPr), 28.98 (CH-iPr), 28.68 (CH_2CH_2), 23.68 (Me-iPr), 23.44 (Me-iPr), 23.20 (Me-iPr), 21.29 (Me-C=N), 19.87 (Me-C=N), 2.09 (Pd-Me) ppm.

11a. (Red solid, yield 78%); the characterization in solution of this complex was not possible due to its insolubility.

12a. (Red solid, yield 44%); ^{1}H NMR (400 MHz, CD_2Cl_2) δ 8.37 – 7.93 (m, 20H, CH-Py and H-C=N), 6.76 (s, 2H, Ar-CH), 6.75 (s, 2H, Ar-CH), 4.07 (q, J = 6.0 Hz, 4H, CH_2-O), 3.47 (t, J = 7.4 Hz, 4H, CH_2-Py), 3.20 (m, J = 13.6, 6.8 Hz, 4H, CH-iPr), 2.04 (br, J = 33.6, 6.8 Hz, 8H, CH_2CH_2), 1.32 (m, J = 11.1, 6.8 Hz, 12H, Me-iPr), 1.12 (dd, J = 6.8, 2.2 Hz, 12H, Me-iPr), 0.67 (s, 3H, Pd-Me).

13a. (Orange-red solid, yield 46%), the characterization in solution of this complex was not possible due to its insolubility.

4.4.4. Synthesis and characterization of [Pd(pyrDAB)(CH_3)(NCCH_3)][PF_6] ***10b-13b****.*

All the synthetic procedures were performed according to the literature, using standard Schlenk techniques, under argon atmosphere at room temperature. To a stirred solution of [Pd(pyrDAB)(CH_3)Cl] (**10a-13a**) (0.1 mmol) in 5 mL of CH_2Cl_2 a solution of $AgSbF_6$ (1.2 equiv) in anhydrous CH_3CN (1.2 mL) was added. The reaction was left under stirring for 2 h in exclusion of light, then filtered over Celite. The solvent was removed, and upon addition of hexane and sonication (5-30 minutes) a solid was obtained, that was filtered and washed with cold hexane.

10b.- (Red-brown solid, yield 81%); ^{1}H NMR (500 MHz, CD_2Cl_2): δ 8.37 (dd, J = 9.3, 2.7 Hz, 2H, CH-Py), 8.27 – 8.12 (m, 8H), 8.10 – 8.02 (m, 6H), 7.97 (d, J = 7.8 Hz, 2H), 6.80 (s, 2H, Ar-CH), 6.78 (s, 2H, Ar-CH), 4.08 (m, 4H, CH_2-O), 3.59 – 3.27 (m, 4H, CH_2-Py), 3.02 – 2.77 (m, 4H, CH-iPr), 2.19 (s, 3H, Me-C=N), 2.18 (s, 3H, Me-C=N), 2.10 (m, 4H, CH_2CH_2), 2.02 (m, 7H, CH_2CH_2 and free MeCN), 1.80 (s, 3H, Pd-NCMe), 1.30 (d, 6H, Me -iPr), 1.28 (d, 6H, Me -iPr), 1.19 (d, 6H, Me -iPr), 1.15 (d, 6H, Me -iPr), 0.48 (s, 3H, Pd-Me). ^{13}C NMR (125.68 MHz, CD_2Cl_2, 298 K): δ 127.48 (CH-Py), 127.32 (CH-Py), 127.07 (CH-Py), 126.62 (CH-Py), 125.92 (CH-Py), 124.79 (CH-

Py), 123.36 (CH-Py), 110.14 (Ar-CH), 109.84 (Ar-CH), 67.95 (CH_2-O), 32.99 (CH_2-Py), 29.35 (CH_2CH_2), 29.27 (CH-iPr), 29.03(CH-iPr), 28.36 (CH_2CH_2), 23.31 (Me-iPr), 23.21 (Me-iPr), 22.99 (Me-iPr), 22.61 (Me-iPr), 21.23 (Me-C=N), 19.59 (Me-C=N), 6.33 (Pd-Me), 2.12 (Pd-NCMe) ppm. Elemental analysis, calcd for $C_{71}H_{78}N_3$ (%): C = 62.98, H = 5.81, N = 3.10; found: experimental: C = 63.21, H = 5.57, N = 3.47

11b.- (Orange solid, yield 68%); ^{1}H NMR (500 MHz, CD_2Cl_2, 298 K): δ 8.33 (d, J = 9.2 Hz, 2H, CH-Py), 8.16 (d, J = 23.4 Hz, 8H, CH-Py), 8.11 – 8.01 (m, 6H, CH-Py), 7.93 (d, J = 7.8 Hz, 2H, CH-Py), 6.73 (s, 2H, Ar-CH), 6.71 (s, 2H, Ar-CH), 4.03 (d, J = 1.6 Hz, 4H, CH2-O), 3.45 (br, 4H, CH2-Py), 2.19 (s, 6H, Ar-Me), 2.14 (s, 3H, Me-C=N), 2.13 (s, 3H, Me-C=N), 2.11 (s, 6H, Ar-Me) 2.09 – 1.84 (m, 8H, CH2CH2), 1.78 (s, 3H, Pd-NCMe), 0.33 (s, 3H, Pd-Me). 13C NMR (125.68 MHz, CDCl3, 298 K): δ 127.88 (CH-Py), 127.73 (CH-Py), 127.51 (CH-Py), 126.94 (CH-Py), 126.31 (CH-Py), 125.19 (CH-Py), 123.82 (CH-Py), 114.59 (Ar-CH), 68.47 (CH2-O), 33.47 (CH2-Py), 29.62 (CH2CH2), 28.66 (CH2CH2), 20.21 (Me-C=N), 19.21 (Me-C=N), 18.33 (Me-Ar), 18.19 (Me-Ar), 4.52 (Pd-Me), 2.51 (Pd-NCMe) ppm.

12b.- (Red-purple solid, yield 92%); ^{1}H NMR (500 MHz, CD_2Cl_2, 298 K): δ 8.71-7.79 (br, 18H, CH-Py) 8.18 (s, 2H, H-C=N), 6.79 (s, 2H, Ar-CH), 6.77 (s, 2H, Ar-CH), 4.07 (br, 4H, CH_2-O), 3.69-3.30 (br, 4H, CH_2-Py), 3.14 (sept, 2H, CH-iPr), 3.00 (sept, 2H, CH-iPr), 2.24 (s, 3H, free MeCN), 2.07 – 1.95 (br, 8H, CH_2CH_2), 1.92 (s, 3H, Pd-NCMe), 1.31 (d, 6H, Me-iPr), 1.29 (d, 6H, Me-iPr), 1.20 (d, 6H, Me-iPr), 1.16 (d, 6H, Me-iPr), 0.73 (s, 3H, Pd-Me); ^{13}C NMR (125.68 MHz, CD_2Cl_2, 298 K): δ 169.95 (H-C=N), 162.75 (H-C=N), 110.13 (Ar-CH), 110.09 (Ar-CH), 68.43 (CH_2-O), 29.60 (CH_2CH_2), 29.43 (CH-iPr), 29.19 (CH-iPr), 24.16 (Me-iPr), 23.85 (Me-iPr), 23.10 (Me-iPr), 22.49 (Me-iPr), 8.02 (Pd-Me), 2.84 (Pd-NCMe), 2.65 (free MeCN) ppm.

13b. (Red-purple solid, yield 89 %); ^{1}H-NMR (500 MHz, CD_2Cl_2, 298 K) δ 8.33 (d, J = 8.1 Hz, 2H, CH-Py), 8.27 – 7.97 (m, 14H, CH-Py + H-C=N), 7.93 (m, 2H, CH-Py), 6.71 (s, 2H, Ar-H), 6.68 (s, 2H, Ar-H), 4.03 (br, 4H, CH_2-O), 3.45 (br, 4H, CH_2-Py), 2.30 (s, 6H, Me-Ar), 2.19 (s, 6H, Me-Ar), 2.11 – 1.89 (m, 8H, CH_2CH_2 and Pd-NCMe), 0.63 (s, 3H, Pd-Me). ^{13}C-NMR (125.68 MHz, CD_2Cl_2, 298 K): δ 127.71 (CH-Py), 127.57 (CH-Py), 127.36 (CH-Py), 126.78 (CH-Py), 126.14 (CH-Py), 125.03 (CH-Py), 125.01 (CH-Py), 123.65 (CH-Py), 114.65 (Ar-CH), 114.35 (Ar-CH), 68.27 (CH_2-O), 33.29 (CH_2-Py), 29.37 (CH_2CH_2), 28.41 (CH_2CH_2), 18.68 (Me-Ar), 18.34 (Me-Ar), 6.14 (Pd-Me), 2.76 (Pd-NCMe) ppm.

4.4.5. General procedures for in situ NMR reactivities.

General procedure for the *in situ* ^{1}H NMR reactivity of the cationic complex 10b with methyl acrylate (MA) and ethylene.

A 10 mM solution of the desired cationic complex (**10b**) in CD_2Cl_2 is prepared, and a first ^{1}H NMR spectrum is recorded. 2 equivalents of methyl acrylate are then added to the solution. The reaction is followed with time, at T = 298 K, to monitor the disappearance of the Pd-CH_3 signal. The required time to record each ^{1}H NMR spectrum (60 s) is taken into account when analysing the kinetic data. After 3 h from the beginning of the reaction, ethylene is bubbled into the NMR tube for 10 min. The evolution of the reaction is followed with time, at T = 298 K. The required time to record each ^{1}H NMR spectrum (60 s) is taken in account when analyzing the kinetic data.

4.4.6. Ethylene/methyl acrylate Copolymerization Reactions.

All catalytic experiments are carried out in a Büchi "tinyclave" reactor equipped with an interchangeable 50 mL glass vessel. The vessel is loaded with the desired complex (21 μmol), TFE (21 mL) or distilled CH_2Cl_2 (22 mL) and methyl acrylate (1.13 mL). The reactor is placed in a preheated oil bath and connected to the ethylene tank. The ethylene is bubbled for 10 min, then the reactor is pressurized. The reaction mixture is stirred at constant temperature and pressure. After the proper time, the reactor is cooled to room temperature and vented. The reaction mixture is either poured in a 50 mL round flask, together with dichloromethane (3 x 2 mL) used to wash the glass vessel or in a 150 mL beaker with methanol to favor the precipitation of the products. No formation of Pd black is observed. Volatiles were removed under reduced pressure and the residual gum or oil is dried at constant weight and analyzed by NMR spectroscopy.

The ethylene uptake was measured by performing the catalysis in the same Büchi "tinyclave" reactor connected to a thermal mass flow meter (Bronkhorst EL-FLOW Select model F-111B) and forward pressure controller device (Bronkhorst EL-PRESS model P-602). Gas flow needed to feed the reactor at a constant pressure was computer-recorded using the FlowPlot interface. The reaction procedure was the same as above.

Formula for calculating the %MA inserted.

$$\%MA = \frac{\frac{1}{3}B}{[\frac{1}{4}(A + C + D - B) + \frac{1}{3}B]} \cdot 100$$

4.5. Bibliography

1. Popeney, C., Guan, Z. *Organometallics* **2005**, *24*, 1145.

2. a) Dai, S., Sui, X., Chen, C. *Angew. Chem. Int. Ed*. **2015**, *54*, 9948; b) Liao, Y., Zhang, Y., Cui, L., Mu, H., Jian, Z. *Organometallics* **2019**, *38*, 2075; c) Kanai, Y., Foro, S., Plenio, H. *Organometallics* **2019**, *38*, 544.

3. Zhao, M., Chen, C. *ACS Catal.* **2017**, *7*, 7490.

4. Guo, L., Liu, Y., Sun, W., Du, Q., Yang, Y., Kong, W., Liu, Z., Chen, D. *Journal of Organometallic Chemistry* **2018**, *877*, 12.

5. Halter, O., Spielmann, J., Kanai, Y., Plenio, H. *Organometallics* **2019**, *38*, 2138.

6. Mundil, R., Sokolohorskyj, A., Hošek, J., Cvačka, J., Císařová, I., Kvičala, J., Merna, J. *Polym. Chem*. **2018**, *9*, 1234.

7. a) Stalzer, M. M., Delferro, M., Marks, T. J. *Catal. Lett.* **2015**, *145*, 3; b) Baier, M. C., Zuideveld, M. A., Mecking, S. *Angew. Chem. Int. Ed*. **2014**, 53, 9722.

8. Wucher, P., Schwaderer, J. B., Mecking, S. *ACS Catal*. **2014**, 4, 2672.

9. a) Tafazolian, H., Culver, D. B., Conley, M. P. *Organometallics* **2017**, *36*, 2385; b) Culver, D. B., Tafazolian, H., Conley, M. P. *Organometallics* **2018**, *37*, 1001.

10. Krinsky, J. L., Martínez, A., Godard, C., Castillón, S., Claver, C. *Adv. Synth. Catal.* **2014**, *356*, 460.

11. Ohgi, A., Nakao, Y. *Chem. Lett*. **2016**, *45*, 45.

12. Kimiaghalam, M., Isfahani, H. N., Zohuri, G. H., Keivanloo, A. *Inorg. Chim. Acta* **2017**, *464*, 99.

13. Scarel, A., Axet, M. R., Amoroso, F., Ragaini, F., Elsevier, C. J., Holuigue, A., Carfagna, C., Mosca, L., Milani, B. *Organometallics* **2008,** *27*, 1486.

14. Rosar, V., Dedeic, D., Nobile, T., Fini, F., Balducci, G., Alessio, E., Carfagna, C., Milani, B., *Dalton Trans.*, **2016**, *45*, 14609.

15. Johnson, L. K., Killian, C. M., Brookhart, M. *J. Am. Chem. Soc.* **1995,** *117*, 6414.

16. Dall'Anese, A., Rosar, V., Cusin, L., Montini, T., Balducci, G., D'Auria, I., Pellecchia, C., Fornasiero, P., Felluga, F., Milani, B. *Organometallics* **2019**, *38*, 3498.

17. Mecking, S., Johnson, L. K., Wang, L., Brookhart, M. *J. Am. Chem. Soc.* **1998,** *120*, 888.

18. Johnson, L. K., Mecking, S., Brookhart, M. *J. Am. Chem. Soc.* **1996,** *118*, 267.

19. Rosar, V., Montini, T., Balducci, G., Zangrando, E., Fornasiero, P., Milani, B. *ChemCatChem* **2017,** *9*, 3402.

20. Drent, E., van Dijk, R., van Ginkel, R., van Oort, B., Pugh, R. I. *Chem. Commun.* **2002,** *7*, 744.

21. Meduri, A., Montini, T., Ragaini, F., Fornasiero, P., Zangrando, E., Milani, B. *ChemCatChem* **2013,** *5*, 1170.

22. a) Berkefeld, A., Drexler, M., Moller, H. M., Mecking, S., *J. Am. Chem. Soc.* **2009,** *131*, 12613; b) Usami, T., Takayama, S. *Macromolecules* **1984,** *17*, 1756; c) Axelson, D. E., Levy, G. C., Mandelkern, L. *Macromolecules* **1979,** *12*, 41; d) McCord, E. F., McLain, S. J., Nelson, L. T. J., Arthur, S. D., Coughlin, E. B., Ittel, S. D., Johnson, L. K., Tempel, D., Killian, C. M., Brookhart, M. *Macromolecules* **2001,** *34*, 362; e) McCord, E. F., McLain, S. J., Nelson, L. T. J., Ittel, S. D., Tempel, D., Killian, C. M., Johnson, L. K., Brookhart, M. *Macromolecules* **2007,** *40*, 410.

23. Carrow, B. P., Nozaki, K. *Macromolecules* **2014,** *47*, 2541.

24. Samanta, S. R., Levere, M. E., Percec, V. *Polym. Chem*. **2013**, *4*, 3212.

25. Hu, H., Chen, D., Gao, H., Zhong, L., Wu, Q. *Polymer Chem.* **2016**, *7*, 529.

CHAPTER 5

Pd(II)-catalyzed copolymerization of CO and styrene derivatives: effect of the vinyl arene comonomer

Overview

Pyridylimine ligands (N-N', **14-22**) featured by a polycyclic aromatic fragment on the iminic nitrogen atom and differing for the presence of hydrogen, methyl or phenyl group on the iminic carbon atom were synthesized and used to obtain the corresponding neutral [Pd(N-N')(CH_3)Cl] and monocationic [Pd(N-N')(CH_3)(CH_3CN)][PF_6] (where N-N' = **14-22**) palladium(II) complexes. The latter were tested as precatalysts for the CO/vinyl arene copolymerization reaction, using styrene, 4-methyl styrene and 4-*tert*-butyl styrene as comonomers, under mild reaction conditions of temperature and pressure. The microstructure of the produced copolymers was studied by ^{13}C NMR spectroscopy, highlighting an effect of the vinyl arene on the stereochemistry of the polyketones produced with aldimine-derived precatalysts. The control of the macromolecule stereochemistry is also connected to the *cis*/*trans* isomer distribution in the precatalysts, that was investigated by NMR spectroscopy.

Part of this Chapter will result in a future publication:

Dall'Anese, A., Fiorindo, M., Dedeic, D., Rosar, V., Balducci, G., Carfagna, C., Durand, J., Milani, B., manuscript in preparation.

5.1. Introduction

Among the group of copolymers that contain functional groups with heteroatoms, polyketones stand out: these macromolecules are obtained from the direct, homogeneously catalysed copolymerization of carbon monoxide with terminal alkenes (Scheme 5.1),[1] very cheap and abundant comonomers, have a perfectly alternating microstructure, and present unique properties, including the fact that the reactivity of the carbonyl groups can be further exploited leading to different macromolecules, such as polyalcohols.[2]

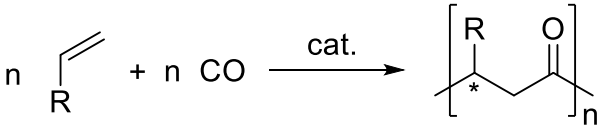

Scheme 5.1. CO/terminal alkene copolymerization.

Based on the nature of the terminal alkene, it is possible to recognize two main classes of polyketones: those obtained from CO and aliphatic alkenes, and those obtained with vinyl arenes.

The synthesis of the first class of polyketones, in particular that of carbon monoxide and ethylene, was reported for the first time in 1950 in the group of Reppe and Magin, by using $K_2[Ni(CN)_4]$ as catalyst, under very harsh reaction conditions (230 °C and 2000 atm), yielding CO/ethylene cooligomers, along with propionic acid and penthan-3-one as side products.[3] Other example were later reported, and in particular in 1967 Gough described a catalytic system based on a Pd(II) complex, stabilized by a tertiary phosphine ligand, that allowed to obtain the actual CO/ethylene copolymer, again under harsh conditions and in low yield.[4] Sen and coworkers reported in 1984 the synthesis of a perfectly alternating CO/ethylene copolymer by using an *in situ* system based on $[Pd(NCCH_3)_4][BF_4]_2$, triphenyl phosphine, at 298 K and 20 atm, even though with low yields and molecular weights.[1a,5] The major breakthrough in this field is represent by the use of bidentate phosphines instead of monodentate ones, and it was reported by Drent *et al.* in 1984. The use of relatively mild reaction conditions (363 K, 40-60 bar) and a productivity high enough to satisfy the needs of industry led to a patent by Shell Chemicals, in which an *in situ* system based on a palladium(II) salt (acetate or triflate), a chelating diphosphine ligand, a Brønsted acid as cocatalyst and methanol as solvent is reported. In particular, the best results were obtained with 1,3-bis-(di-anisol)phosphino propane (DAPP, Figure 5.1) as chelating ligand and *p*-toluensulphonic acid as cocatalyst.[1b,6] In the presence of 1,4-benzoquinone (BQ), the activity reached values of 6 kg CP/g Pd h^{-1}.

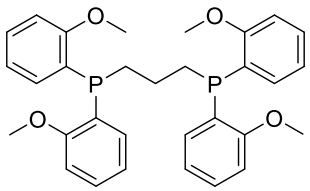

Figure 5.1. The DAPP ligand.

The weak point of the CO/ethylene copolymer is the decomposition temperature being too close to its melting point, that makes impossible to manufacture it as a thermoplastic material. The introduction of propylene as additional comonomer led to a CO/ethylene/propylene terpolymer, where propylene units randomly substitute ethylene along the polymeric chain. This feature lowers the melting point of the terpolymer with respect to the copolymer, keeping the decomposition temperature constant and thus allowing its use as a thermoplastic material.[7] The terpolymer was commercialized in the '90 by Shell and BP under the name of Carilon® and Ketonex®, respectively. The commercialization was stopped at the beginning of the 2000's, essentially for the high cost of the catalyst. Nevertheless, this hasn't stopped the research in the field of polyketone synthesis, both in academia and in industry, and in 2015 Hyosung, a Korean company, started again to sell the CO/ethylene/propylene terpolymer (under the trademark of Poketone™), that is produced in quantities around 50 kt/year.[8]

When the comonomer belongs to the class of vinyl arenes (such as styrene or its derivatives), the catalysts with diphosphine are not efficient, since they lead to the formation of the product of monocarbonylation of styrene, E-1,5-diphenyl-pent-1-en-3-one (Scheme 5.2).[6,9]

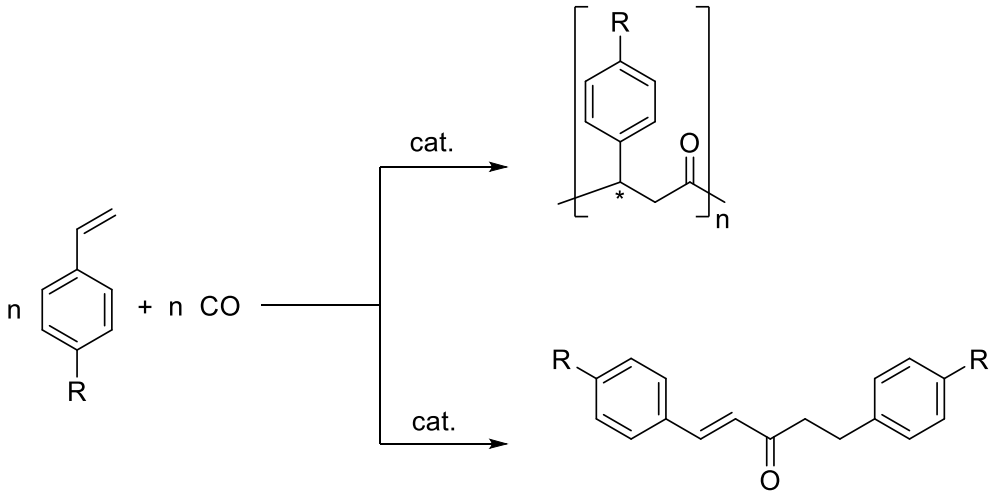

Scheme 5.2. Copolymerization *vs* monocarbonylation of CO/vinyl arenes.

In order to obtain the desired copolymer the use of bidentate nitrogen-donor ligands (N-N) is required. Three main classes of precatalysts can be individuated: *i*. dicationic complexes of general formula $[Pd(N–N)(OH_2)_2][X]_2$ or $[Pd(N–N)_2][X]_2$,[9,10] *ii*. monocationic complexes of general formula $[Pd(N–N)(CH_3)(L)][X]$,[11] *iii*. neutral complexes $[Pd(N–N)(Y)_2]$;[12,13] in all cases X is a weakly coordinating anion such as OTf, BF_4^- or PF_6^-, L is a labile ligand (usually acetonitrile or diethyl ether) and Y a more coordinating anion, such as acetate or trifluoroacetate. Systems with P-N hybrid ligands,[14] or the P-PO phosphino-phosphito derivatives, like BINAPHOS, have been also reported.[15]

The use of terminal alkenes like the vinyl arenes implies the possibility of having products with different regio- and/or stereochemistry, that influences the chemical, physical and mechanical properties of the macromolecule, determining also its potential applications.

When looking at the regiochemistry, three different regiosequences are possible, depending on the regioregularity of the insertion of the terminal alkene into the growing polymeric chain (GPC). If the insertion is regiospecific, occurring with either a primary or a secondary regiochemistry, the resulting polymer will be regioregular and will possess a “head-tail” regiosequences (Figure 5.2a). Errors in the regiochemistry of the insertion lead to either “head-head” or “tail-tail” sequences (Figure 5.2b, 5.2c).

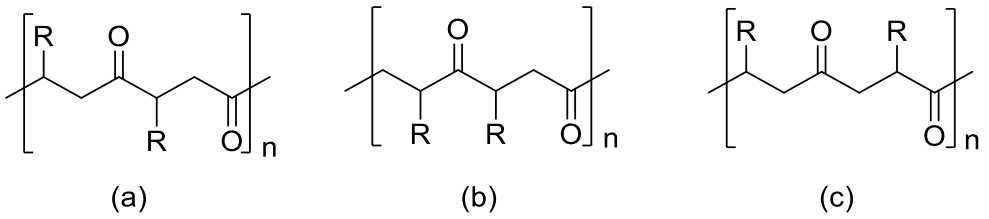

Figure 5.2. Possible regiosequences: (a) *head-tail*; (b) *head-head*; (c) *tail-tail*.

When styrene is the comonomer, regioregular polyketones are usually obtained, with either a primary or a secondary regiospecific insertion, depending on the catalyst that is used.[9,15e-f]

In addition, each insertion of the prochiral alkene into the growing polymer chain generates a stereogenic center, and the control of the stereochemistry is an important goal in polyketone synthesis. As far as stereochemistry is concerned, three main situations can be individuated: *i.* if the stereogenic centers have all the same relative configuration, the resulting polymer is isotactic, and when it is obtained with a chiral catalyst, it is also optically active; *ii*. if the stereogenic center have

an alternating *R* or *S* relative configuration, the copolymer is syndiotactic; *iii.* if the sequence of configuration is random, the copolymer is atactic.

The stereochemistry of CO/vinyl arenes polyketones is studied in terms of microtacticity, that is the relationship between the relative configurations of the stereogenic centers in short repetitive units. When the two adjacent stereogenic centers have the same configuration, the corresponding diad is marked as *l* (like), instead if it is different, the diad is indicated as *u* (unlike) (Figure 5.3). For the CO/vinyl arenes copolymers the stereogenic centers of three repetitive units (triads) are considered.

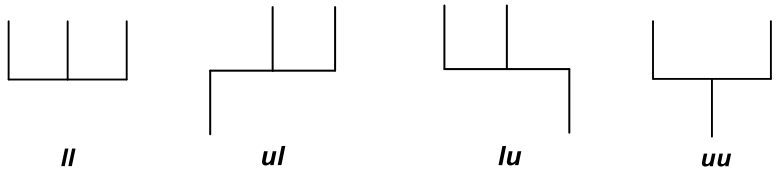

Figure 5.3. Modified Fischer representation of the possible triads.

To study the stereochemistry of macromolecules, the technique of choice is ^{13}C NMR spectroscopy, and in the case of CO/vinyl arene polyketones the signal of the *ipso* carbon atom is considered, since its resonance frequency is affected by the closest stereogenic center configuration with respect to the configuration of the two adjacent stereogenic centers (Figure 5.4). The *ipso* carbon resonates at different frequencies with respect to the triad it belongs to, making it a good probe for the polyketone tacticity. The presence, in the ^{13}C NMR spectrum, for the *ipso* carbon atom, of four signals of the same intensity indicates that in the copolymer all the four triads are present with a statistical distribution, and so the copolymer is atactic (Figure 5.4a). The prevalence of the signal at lower frequencies indicates a predominance of the *uu* triad, and the copolymer is prevailingly syndiotactic (Figure 5.5b); instead the presence of the signal at higher frequencies only, due to the *ll* triad, indicates the formation of an isotactic copolymer (Figure 5.4c).[16,17]

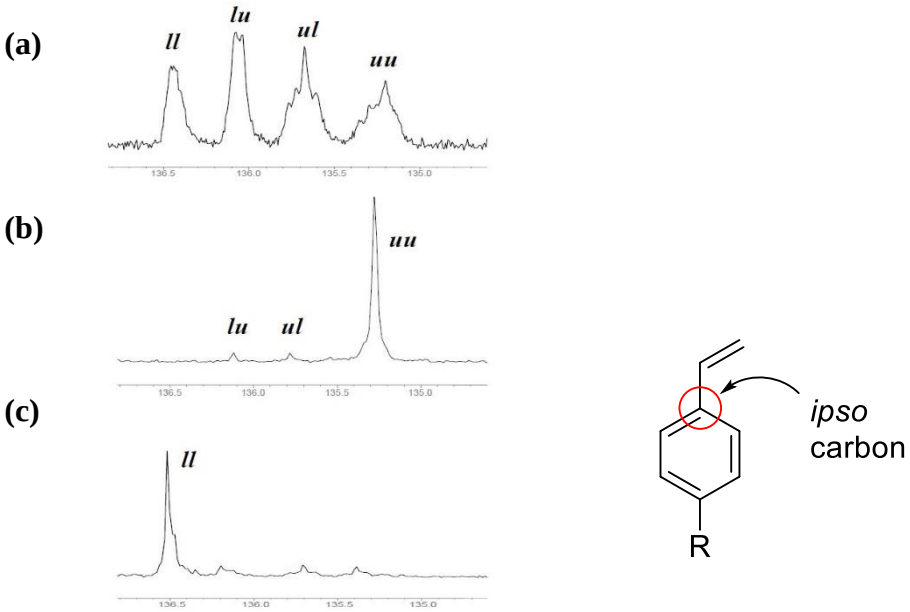

Figure 5.4. ^{13}C NMR spectra in 1,1,1,3,3,3–hexafluoroisopropanol (HFIP) + $CDCl_3$ of the CO/styrene copolymer: (a) atactic, (b) syndiotactic, (c) isotactic; *ipso* carbon atom region.

The possibility of obtaining stereoregular polymers in asymmetric catalysis depends on whether the catalyst can discriminate between the two enantiotopic faces of the alkene, that can occur with two different mechanisms: the *enantiomorphic site control*, that is the control imposed by the coordination sphere around the metal center, and the *chain end control*, that is the control of the last stereogenic center in the last repetitive unit in the growing polymeric chain.[18] In 1992, Consiglio and coworkers demonstrated that syndiotactic polyketones derive from *chain–end control*.[17] The high stereoregularity (80% of *uu* triad) is due to the 6-membered metallacycle that forms after the insertion of CO into the growing polymeric chain, where the carbonyl group in the second-last unit coordinates to palladium, thus approaching the stereogenic center to the active polymerization site, that makes it more efficient in the differentiation of the two enantiofaces of the incoming vinyl arene (Figure 5.5). This mechanism and the formation of the intermediate was proven by NMR spectroscopy.[1b,19]

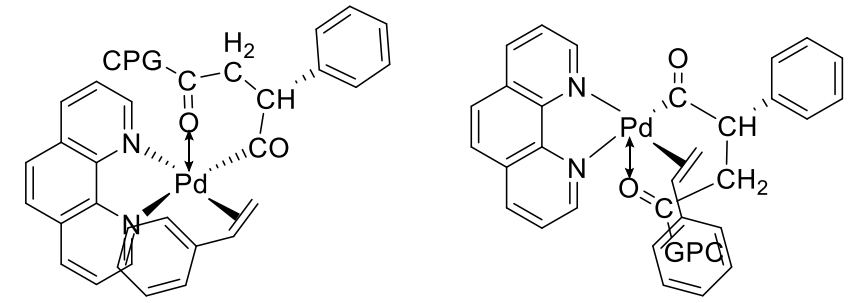

GPC= growing polymeric chain

Figure 5.5. Metallacycle in the propagation step of CO/styrene copolymerization. GPC = growing polymeric chain.

Further research allowed to establish a relationship between the symmetry of the ancillary N-N donor ligand and the stereochemistry of the synthesized polyketones.[18] For example, if the catalyst bears a ligand of C_{2v} symmetry, such as 2,2'–bipyridyl (bpy) or 1,10-phenanthroline the produced copolymer is syndiotactic with a content of *uu* triad from 80 to 96 %,[11c,12,17,20] according to the ligand substituents; isotactic CO/vinyl arene copolymers with a content of *ll* triad over 90 % are obtained with catalysts with ligands of C_2 symmetry, like bisoxazolines (Figure 5.6a), bioxazolines (Figure 5.6b), diketimines (Figure 5.6c) and azabisoxazolines (Figure 5.6d).[23-26] In this case, the stereochemistry of the product is driven by the *enantiomorphic site control*.

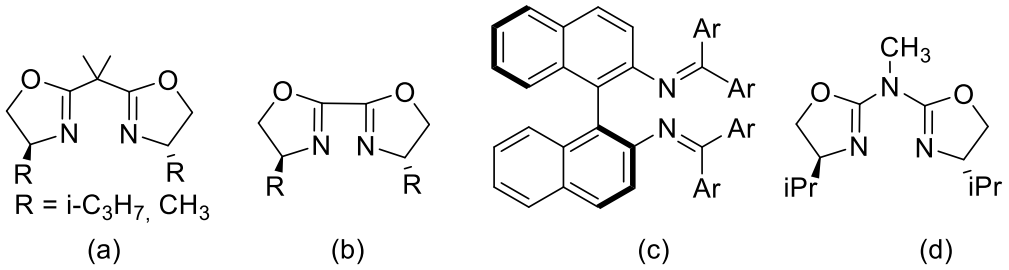

Figure 5.6. Examples of ligands with C_2 symmetry: (a) bisoxazolines; (b) bioxazoline; (c) diketimines; (d) azabisoxazolines.

Ligands with lower symmetry (C_s o C_1) yield polyketones with a different tacticity that varies upon the specific ligand used. For ligands with a C_S symmetry the content of *uu* triad decreases going from 5-nitro-1,10-phenanthroline (Figure 5.7a),[27] to pyridyl-pyrazolyl ligands (Figure 5.7b),[28] to P-N hybrid ligands (Figure 5.7c),[15a,29] also yielding an atactic CO/styrene copolymer.

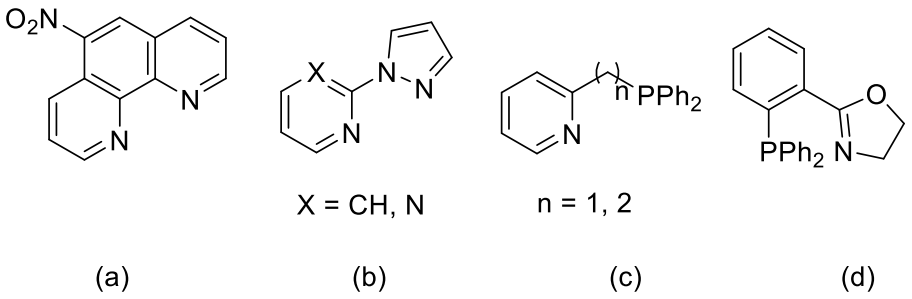

Figure 5.7. Ligands with a C_S symmetry: (a) 5–nitro–1,10–phenanthroline; (b) pyridyl-pyrazolyl ligands; (c) P-N ligands.

When ligands of C_1 symmetry are used, it is impossible to predict the stereochemistry of the obtained copolymer. For instance, pyridyl-imidazolyl based ligands yield copolymers with different stereochemistry according to the substituent on the sp^3 nitrogen atom of the imidazolyl moiety.[16] Pyridyl-oxazolines, instead, generate catalysts that yield both cooligomers and copolymers with a content of *uu* triad over 99% (Figure 5.8).[30] The BINAPHOS ligand (Figure 5.8c) gives a CO/styrene isotactic copolymer, with the peculiarity of generating a system that copolymerizes the reaction a *living* fashion.[15e-f,31]

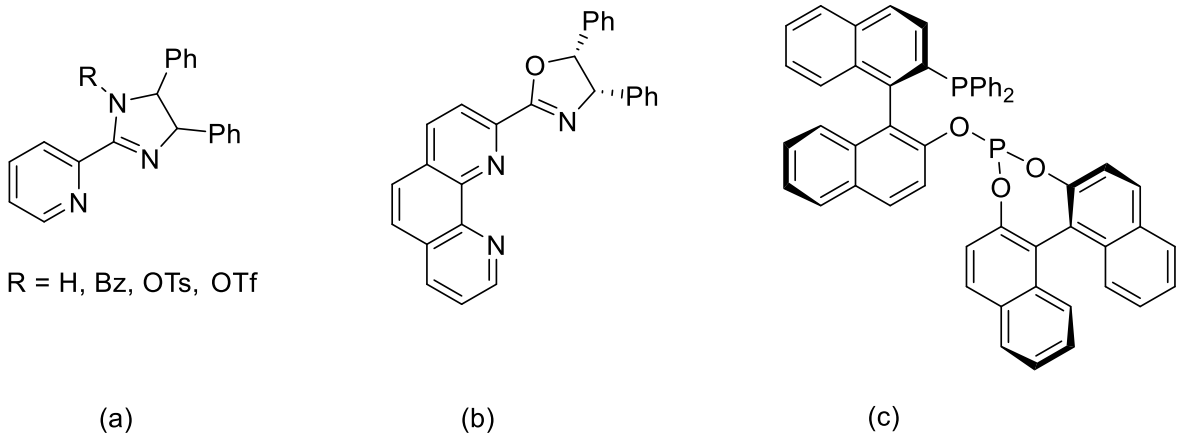

Figure 5.8. Examples of ligands with a C_1 symmetry.

Mechanistic studies allowed to understand that when low-symmetry ligands are used, the stereochemistry control depends on the site-selective coordination of the vinyl arene,[15c] meaning that the structure of the ligand selectively directs the coordination of the incoming vinyl arene on one of the two possible coordination sites. When chiral P-N* or N-N* ligands with the same stereogenic group in the oxazoline moiety are used, it is observed that in the first case, the arene selectively coordinates *trans* to the P atom and *cis* to the stereogenic group, thus making the stereochemistry controlled by the *catalytic site*, and yielding an isotactic copolymer; whereas for N-

N* ligands, the coordination of the arene occurs *trans* to the oxazoline ring, and therefore the stereochemistry is under *chain-end* control, yielding a syndiotactic copolymer.[15c]

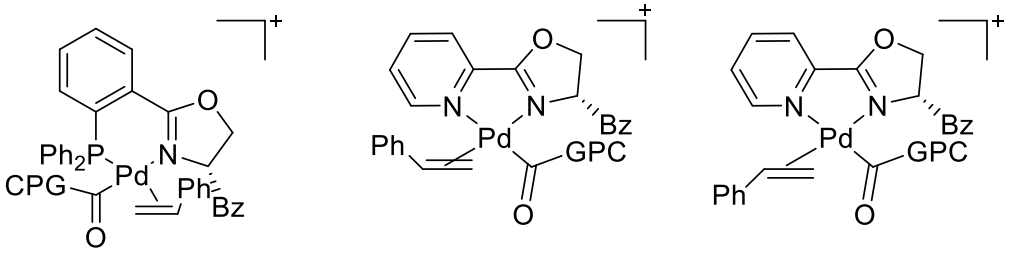

Figure 5.9. Coordination of styrene with Pd(II) complexes having a C_1 chiral ligand.

5.1.1. Pyridylimines in the CO/vinyl arene copolymerization.

As presented in Chapter 2, pyridylimines (N-N') have been widely studied and applied as ancillary ligands with transition metals, and the relevant complexes applied to several catalytic reactions, including the copolymerization of carbon monoxide with alkenes, in particular vinyl arenes. Palladium complexes with pyridylimines were tested for the first time by Sen and coworkers in 1994, yielding prevailingly syndiotactic copolymers, with a content of the *uu* triad that depends on the bulkiness of the substituents on the iminic nitrogen atom.[32]

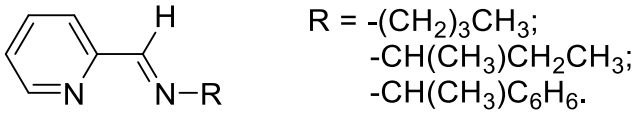

Figure 5.10. Pyridylimines reported by Sen for the CO/styrene and CO/4–methyl styrene copolymerization.

Palladium complexes with pyridylimines bearing an aryl group on the iminic nitrogen have been applied in the carbonylation of styrene in methanol, yielding the product that is the result of a double carbonylation of styrene;[33] supported pyridylimines have been used to build dendritic catalysts for the copolymerization of CO and 4-*tert*-butyl styrene, yielding a prevailingly syndiotactic copolymer (% *uu* = 60 ÷ 71).[34]

As reported in Chapter 2, in the group of Prof. Milani pyridylimines derived from the condensation of pyridine-2-aldehyde and 2-acetyl pyridine with either the simple aniline or 2,6-dimethyl aniline were studied (Figure 5.11), and the relevant palladium complexes of the general formula

[Pd(CH_3)(CH_3CN)(N–N')][PF_6] (N–N' = **L55** – **L58**; **L55b** – **L58b**) tested in the copolymerization of CO with styrene (S) or 4-methyl styrene (MS) (Table 5.1).[11e]

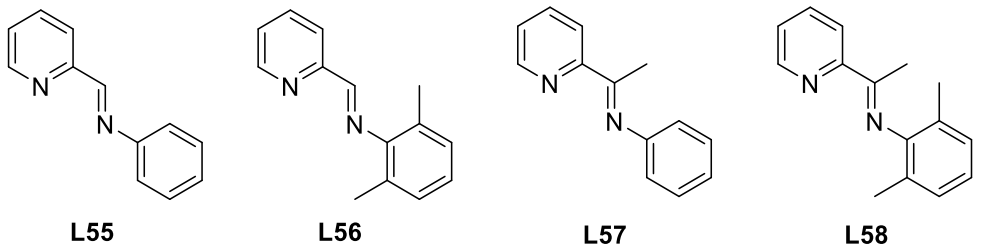

Figure 5.11. Pyridylimine ligands reported by Milani *et al*.[11e]

Table 5.1. Copolymerization of CO/vinyl arene: effect of the ligand and of the comonomer. [a] Precatalyst: [Pd(CH_3)($NCCH_3$)(**N–N'**)][PF_6], **L55b**–**L58b**.

run	**N–N'**	Vinyl arene	Yield (g)	Productivity (kg CP/g Pd)	Mw (g/mol)	Mw/Mn
1	**L55**	S	1.54	1.14	8,000	2.6
2	**L56**	S	4.82	3.57	84,000	1.7
3	**L57**	S	5.86	4.34	138,000	2.4
4	**L58**	S	3.56	2.64	278,000	1.4
5	**L55**	MS	0.80	0.59	11,000	1.6
6	**L56**	MS	3.61	2.67	46,000	1.7
7	**L57**	MS	5.23	3.87	85,000	2.8
8	**L58**	MS	4.24	3.14	244,000	2.0

[a] Reaction conditions: n_{Pd} = 1.27 x 10^{-5} mol; V_{TFE} = 20 mL; $V_{vinyl\ arene}$ = 10 mL; [BQ]/[Pd] = 5; [S]/[Pd] = 6800; [MS]/[Pd] = 6000; T = 303 K; P_{CO} = 1 bar; t = 24 h.

The productivity depends on the ancillary ligand: the less productive precatalyst, both for styrene and 4-methyl styrene is the one with **L55**, whereas **L57** generates the most productive one. Moreover, in the CO/MS copolymerization the ketimine ligands give better results in terms of productivity with respect to the relevant aldimines (**L57** *vs* **L55**, **L58** *vs* **L56**), likely thanks to the higher stability of the active species in the first case, where no inactive palladium metal is observed. The trend is valid also in the CO/S copolymerization for ligands **L55**, **L57**, whereas is opposite for **L56** and **L58**. For both of them there is decomposition to inactive palladium black, so the higher productivity of the aldimine might be due to its higher intrinsic activity with respect to the catalyst with ligand **L58**.[11e] The effect of the ancillary ligand is also reflected by the Mw, that is higher for the ketimine-derived catalysts than the aldimine ones, and it's the highest for **L58**, since in this case the termination step is hampered by the presence of methyl substituents on the *ortho* positions of the N-aryl ring. The tacticity of the products was evaluated with ^{13}C NMR spectroscopy, by

recording the spectra in a mixture of $CDCl_3$ and 1,1,1,3,3,3–hexafluoro isopropanol (HFIP) (Table 5.2).

Table 5.2. Triad distribution in CO/vinyl arene polyketones.[a]
Precatalyst: [Pd(CH_3)($NCCH_3$)(**N–N'**)][PF_6].

run	N–N'	Vinyl arene	*ll (%)*	*lu (%)*	*ul (%)*	*uu (%)*
1	**L55**	S	1	12	11	**76**
2	**L56**	S	3	17	16	**64**
3	**L57**	S	–	7	8	**85**
4	**L58**	S	5	16	17	**62**
5	**L55**	MS	7	17	14	**62**
6	**L56**	MS	3	15	16	**66**
7	**L57**	MS	–	12	9	**79**
8	**L58**	MS	5	17	17	**61**

[a] On the basis of integration of the *ipso* carbon atom signals in the ^{13}C NMR spectra recorded in HFIP/$CDCl_3$.

With all precatalysts a prevailingly syndiotactic polyketone is synthesized, with a content of *uu* triad that goes from 61 to 85 %. In the ^{13}C NMR spectra of the polyketones obtained with catalyst with **L57**, no signal for the *ll* triad is present, thus indicating a *chain-end* control.

Up to now, the stereochemistry of the synthesized copolymers synthesized was observed to vary upon variation of the ancillary ligand on the metal center, and it was never observed that for systems with the same ancillary ligand the stereochemistry varies going from styrene to 4-substituted styrene derivatives.

Complexes with pyrene-tagged pyridylimines, both aldimine and ketimine derivatives, have also been applied in the copolymerization of CO with styrene, 4-methyl styrene and 4-*tert*-butylstyrene (TBS) (Figure 5.12, Table 5.3).[11f]

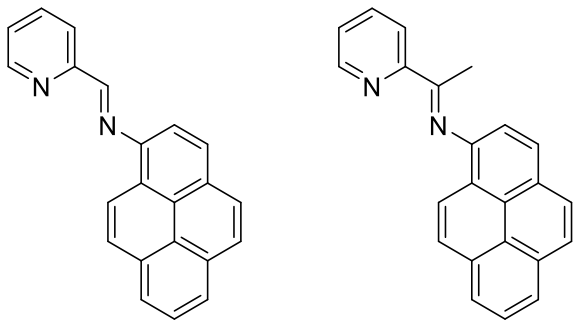

L59 **L60**

Figure 5.12. Pyrene-tagged pyridylimines.

Table 5.3. Copolymerization of CO/vinyl arene: effect of the ligand and of the comonomer. [a] Precatalyst: [Pd(CH_3)($NCCH_3$)(**N–N'**)][PF_6], **L59b**–**L60b**.

run	N–N'	Vinyl arene	Yield (g)	Productivity (kg CP/g Pd)	Mw (g/mol)	Mw/Mn
1	**L59**	S	0.86	0.64	31,000	2.0
2	**L59**	MS	0.57	0.42	8,000	1.5
3	**L59**	TBS	0.39	0.29	8,000	1.7
4	**L60**	S	5.10	3.78	256,000	2.2
5	**L60**	MS	7.27	5.38	302,000	2.6
6	**L60**	TBS	6.26	4.64	471,000	2.1

[a] see Table 5.1.

Also in this case, going from the aldimine to the ketimine derivative an increase of one order of magnitude in the productivity was achieved, and it is related to the stability of the catalyst, that is higher for the ketimine. The molecular weight of the copolymers produced with **L60** (250000-500000 g/mol) are among the highest ever reported for this class of catalysts.[11c] The productivity is influenced by the comonomer: for **L59**, it decreases going from S to MS to TBS, whereas for **L60** the lowest productivity is that in the CO/styrene copolymerization.[11f]

Table 5.4. Triad distribution in CO/vinyl arene polyketones.[a] Precatalyst: [Pd(CH_3)($NCCH_3$)(**N–N'**)][PF_6].

run	N–N'	Vinyl arene	*ll (%)*	*lu (%)*	*ul (%)*	*uu (%)*
1	**L59**	S	16	16	16	**52**
2	**L59**	MS	**47**	17	18	18
3	**L59**	TBS	30	37		33
4	**L60**	S	–	13	16	**71**
5	**L60**	MS	–	21	19	**60**
6	**L60**	TBS	–	15	10	**75**

[a] see Table 5.2.

Precatalyst with ligand **L60** yields copolymers with prevailingly syndiotactic microstructure with all comonomers, with a content of *uu* triad of 70 %, as reported for the system with ligands **L55-L58**, and again no signal due to the *ll* triad is observed in the NMR spectrum, meaning the stereochemistry is under *chain end* control. With the aldimine ligand **L59**, in the ^{13}C NMR spectrum of all products all the four triads are present, and the stereochemistry changes upon changing the comonomer: with S the copolymer is prevailingly syndiotactic, with MS isotactic and with TBS atactic. These data represent the first time that a dependence of the tacticity of the macromolecule on the nature of the comonomer was reported.

The aim of this Chapter is to further study this phenomenon by investigating a new series of pyridylimines (Figure 5.13, **14**-**22**). The relevant neutral [Pd(CH_3)Cl(**N**-**N**')] and monocationic [Pd(CH_3)(CH_3CN)(**N**-**N**')][PF_6] complexes have been synthesized, characterized and applied as precatalysts in the reaction of interest. These N-N' ligands have different substituents on the iminic carbon atom, such as hydrogen, methyl or phenyl, and on the iminic nitrogen atom, substituents with an increased number of fused aromatic rings (naphthyl, anthracenyl) are placed, in order to evaluate their effect on the copolymerization. This work is part of a collaboration with Prof. Jérôme Durand of the CNRS in Toulouse.

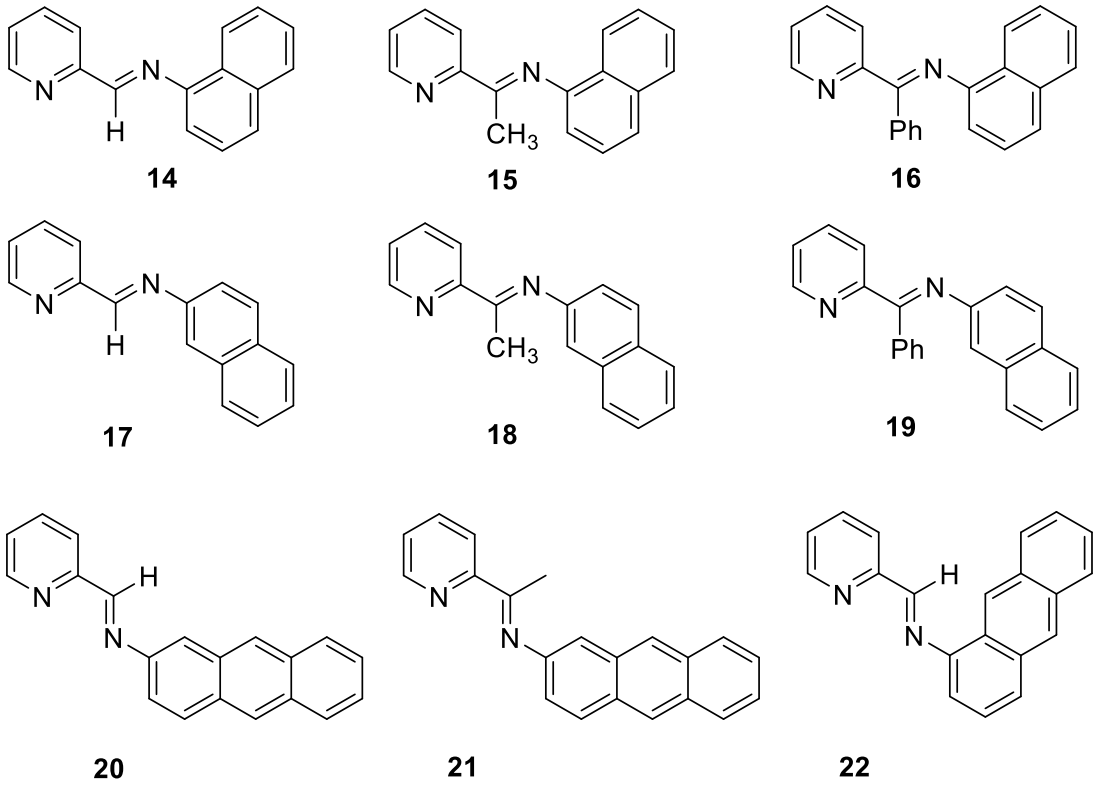

Figure 5.13. The pyridylimine ligands under investigation.

5.2. Results and discussion.

*5.2.1. Synthesis and characterization of ligands **16**-**22**.*

The pyridylimines under study have been synthesized by following different procedures. Ligand **14** and **15**, already known in literature,[35] were synthesized in the laboratories of Prof. Durand in Toulouse and used as received. Ligands **17**, **20** and **22** were obtained with a similar procedure, based on the condensation reaction between pyridine-2-aldehyde and the desired aniline in a Dean-Stark apparatus, in toluene, under reflux, for 6 h (Scheme 5.3). The difference lies in the acid catalyst employed: for ligand **20** it consists in a heterogeneous catalyst (silica-alumina),[36] whereas

for **17** and **22** acetic acid was used. The ligands were isolated as yellow solids all in acceptable to good yields (43-58 %)

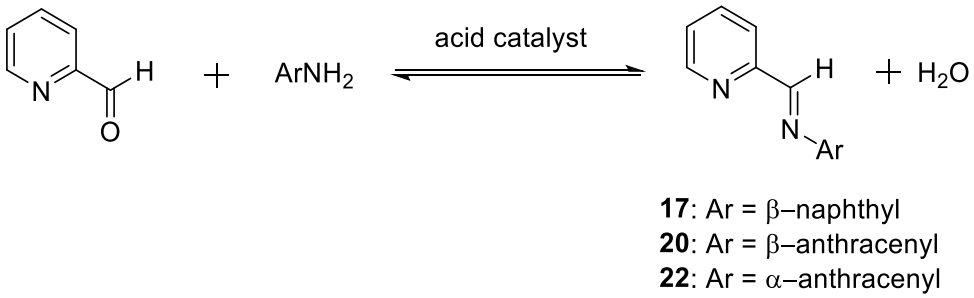

Scheme 5.3. General synthesis for pyridylimines **17**, **20**, **22**.

Ligands **16**, **19**, **21** were synthesized according to a previously reported procedure,[37] involving the use of $ZnCl_2$ as templating agent (Scheme 5.4). In this case, **16** and **19** were isolated as brown oils, in good yields (61 and 65%), whereas **21** was obtained as an ochre solid, in 41% yield.

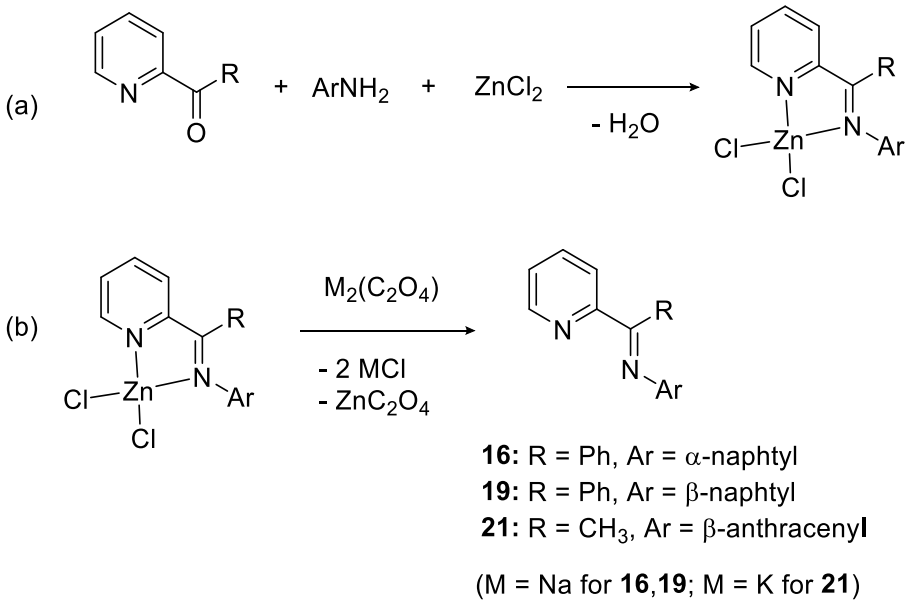

Scheme 5.4. General procedure for the template synthesis for pyridylimines **16**, **19** and **21**.

None of the procedures mentioned above was effective for the synthesis of ligand **18**, that was not obtained in the free form, but the relevant palladium(II) neutral complex was directly synthesized with a template synthesis using [Pd(cod)(CH_3)Cl]. All of the ligands were characterized by NMR spectroscopy. As an example, we report the ^{1}H NMR spectra of the aldimine and the ketimine derivatives of with 2-aminoanthracene, ligands **20** and **21** respectively, are reported (Figures 5.14 and 5.15).

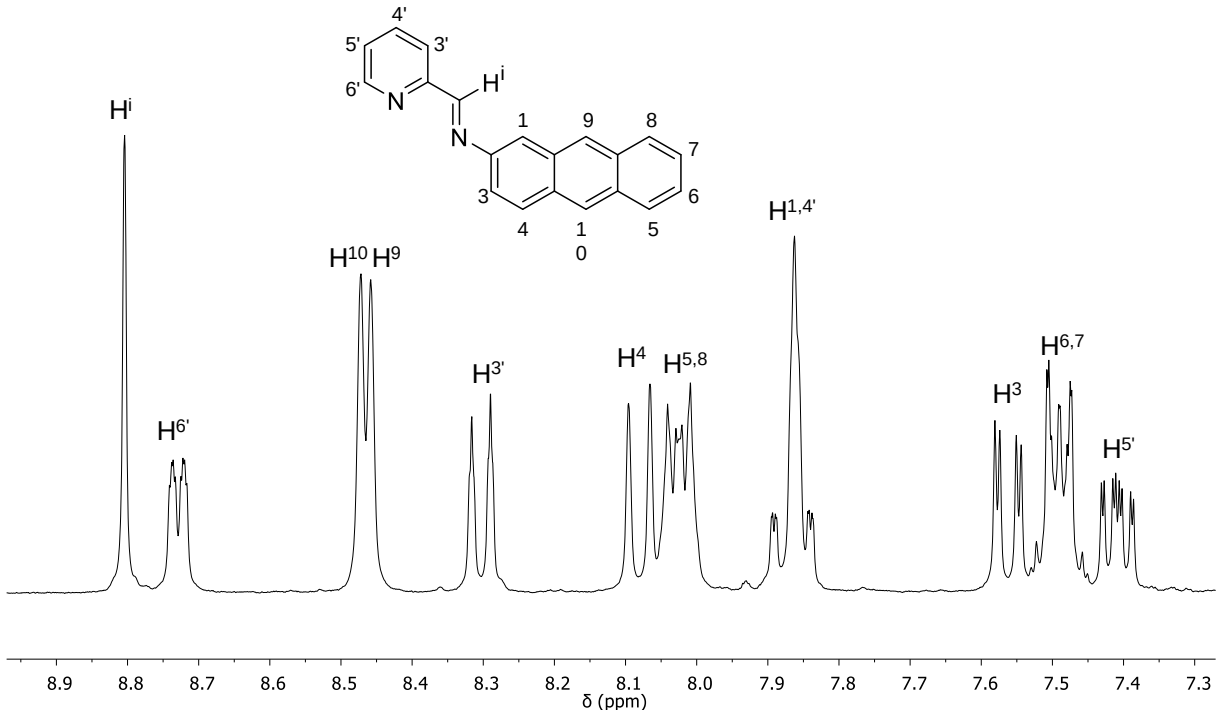

Figure 5.14. ^{1}H NMR spectrum (CD_2Cl_2, 298 K) of ligand **20**.

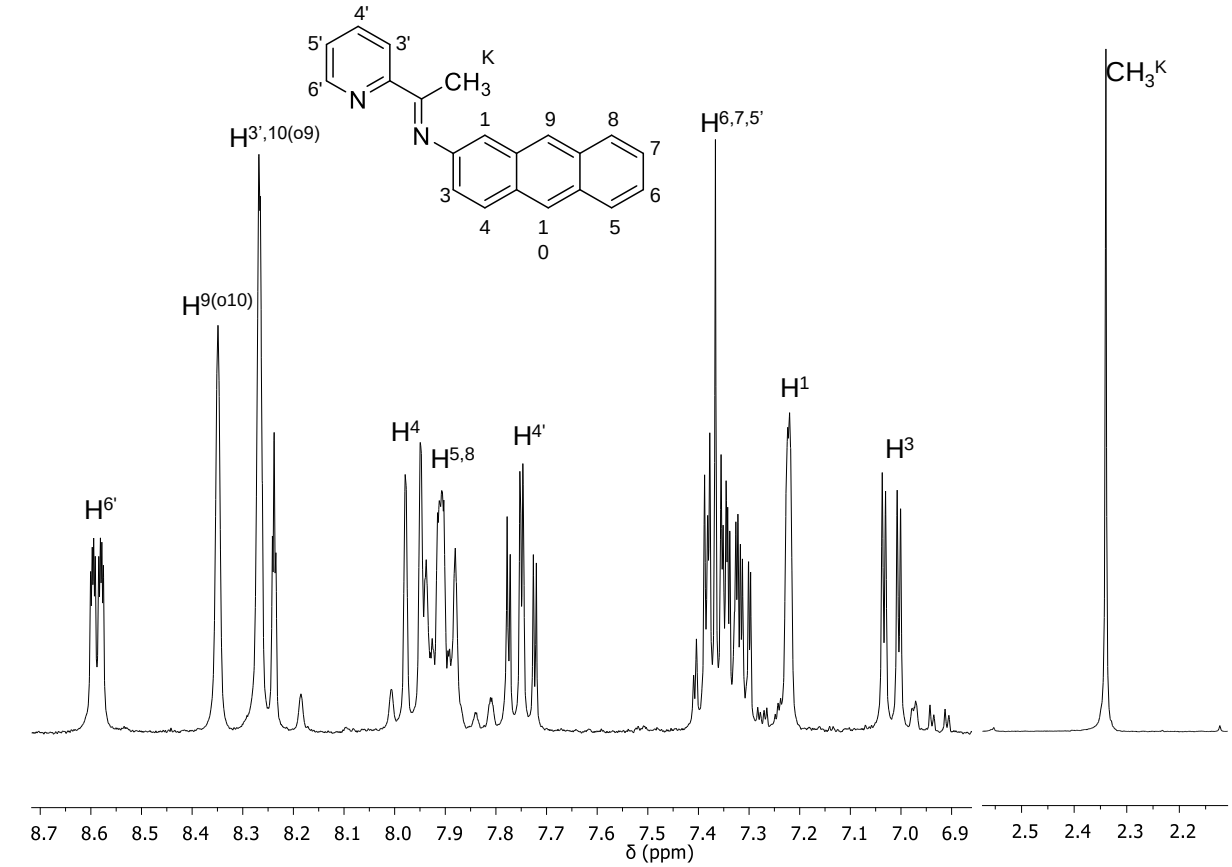

Figure 5.15. ^{1}H NMR spectrum (CD_2Cl_2, 298 K) of ligand **21**; aliphatic and aromatic region not in scale.

*5.2.2. Synthesis and characterization of neutral Pd-complexes **14a-22a**.*

The neutral palladium complexes **14a**-**22a**, with the exception of **18a**, have all been synthesized according to the usual procedure involving the reaction of the desired ligand with the palladium precursor, [Pd(cod)(CH_3)Cl] (Scheme 5.5). The products were all isolated as yellow or orange solids, in good yields (49 – 92 %).

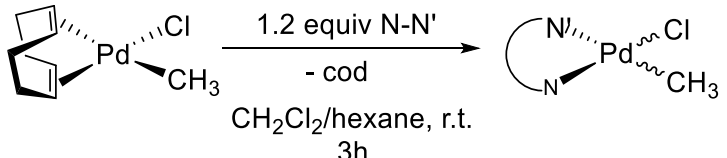

	N-N'	yield (%)
14a	**14**	92
15a	**15**	74
16a	**16**	57
17a	**17**	69
19a	**19**	90
20a	**20**	94
21a	**21**	88
22a	**22**	81

Scheme 5.5. Synthesis of the neutral Pd(II) complexes.

The neutral complex **18a** was obtained with a template synthesis that consists in reacting the 2-acetyl pyridine and β-naphthylamine (in a 1 : 1.2 ratio), with few drops of formic acid, in methanol, for 2 h at room temperature, and then adding [Pd(cod)(CH_3)Cl] as a templating agent. The reaction is further run for 1.5 h, during which the product precipitates as a yellow solid (yield 49 %).

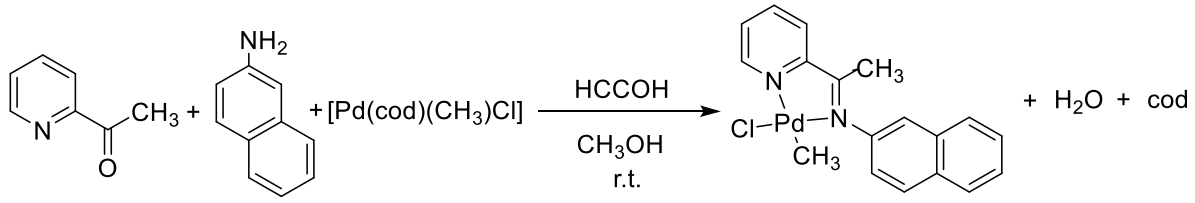

Scheme 5.6. Template synthesis of complex **18a**.

The complexes of the general formula [Pd(N-N')(CH_3)Cl] were all characterized in solution by mono- and bidimensional NMR spectroscopy and, when possible, also in the solid state with X-ray diffraction. The ^{1}H NMR spectra of **20a** and **21a** are hereby reported as an example (Figure 5.16, 5.17).

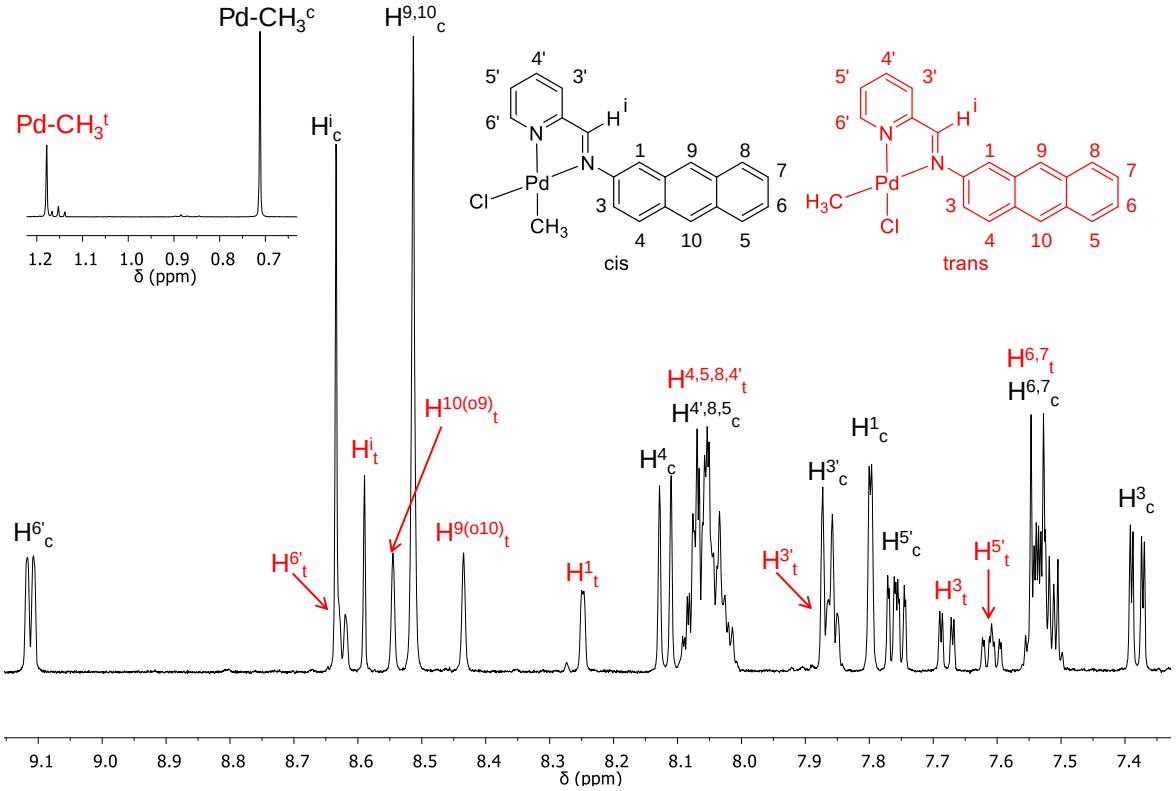

Figure 5.16. ^{1}H NMR spectrum (CD_2Cl_2, 298 K) of complex **20a**.

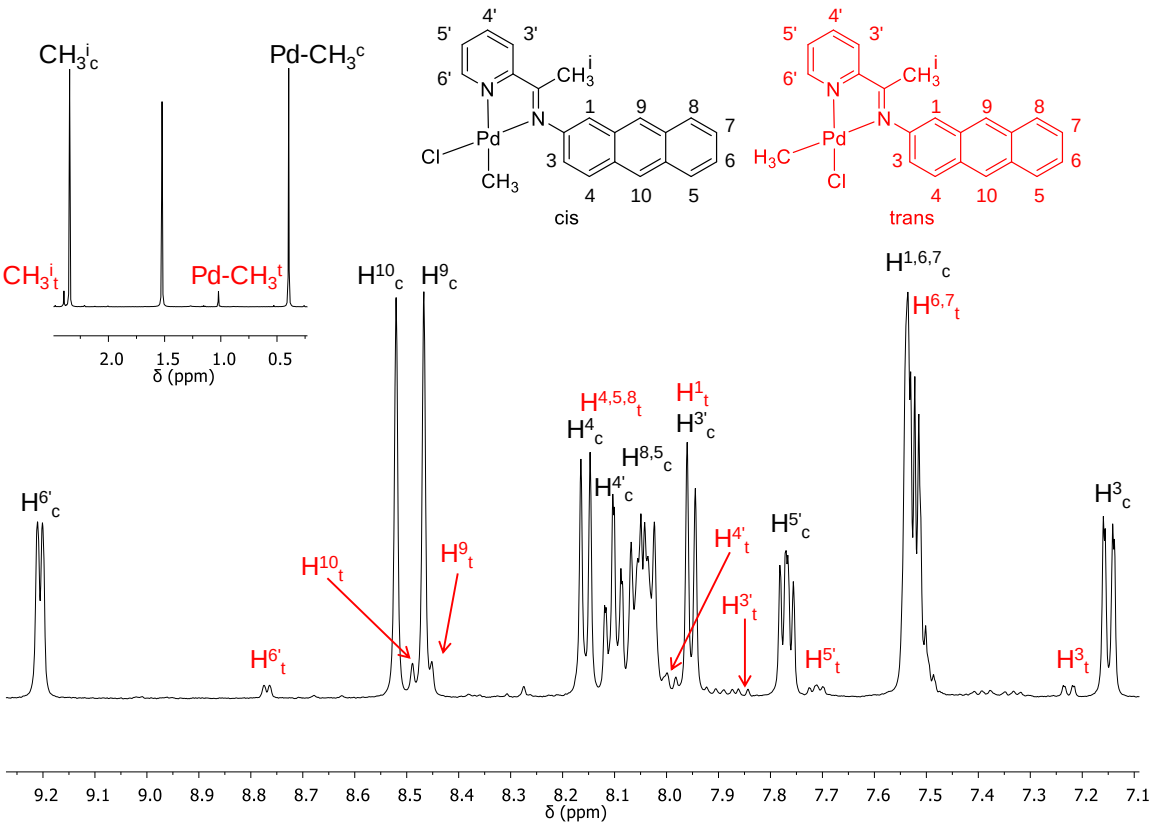

Figure 5.17. ^{1}H NMR spectrum (CD_2Cl_2, 298 K) of complex **21a**.

As seen in Chapter 2 for neutral and cationic complexes with pyridylimines, also in this case it is possible to recognize in solution two different isomers, according to the position of the Pd-C bond with respect to the iminic nitrogen atom: *cis*, when the Pd-C bond is on the same side of the iminic nitrogen, and *trans* when it is on the other side. The distribution of the isomers for the reported complexes will be discussed in the next paragraph along with that of monocationic derivatives. The main isomer can be easily recognized with a NOESY experiment, that is also useful to see exchange between the two species in solution (Figures S5.36, S5.54, S5.58, S5.64-65).

Single crystals suitable for X-ray diffraction of **14a**, **15a**, **17a**, **21a** and **22a** were obtained upon layering either diethyl ether or n-hexane over the dichloromethane solution of the complex. The structures and the most significant bond distances and angles will be reported (Figures 5.18, 5.19).

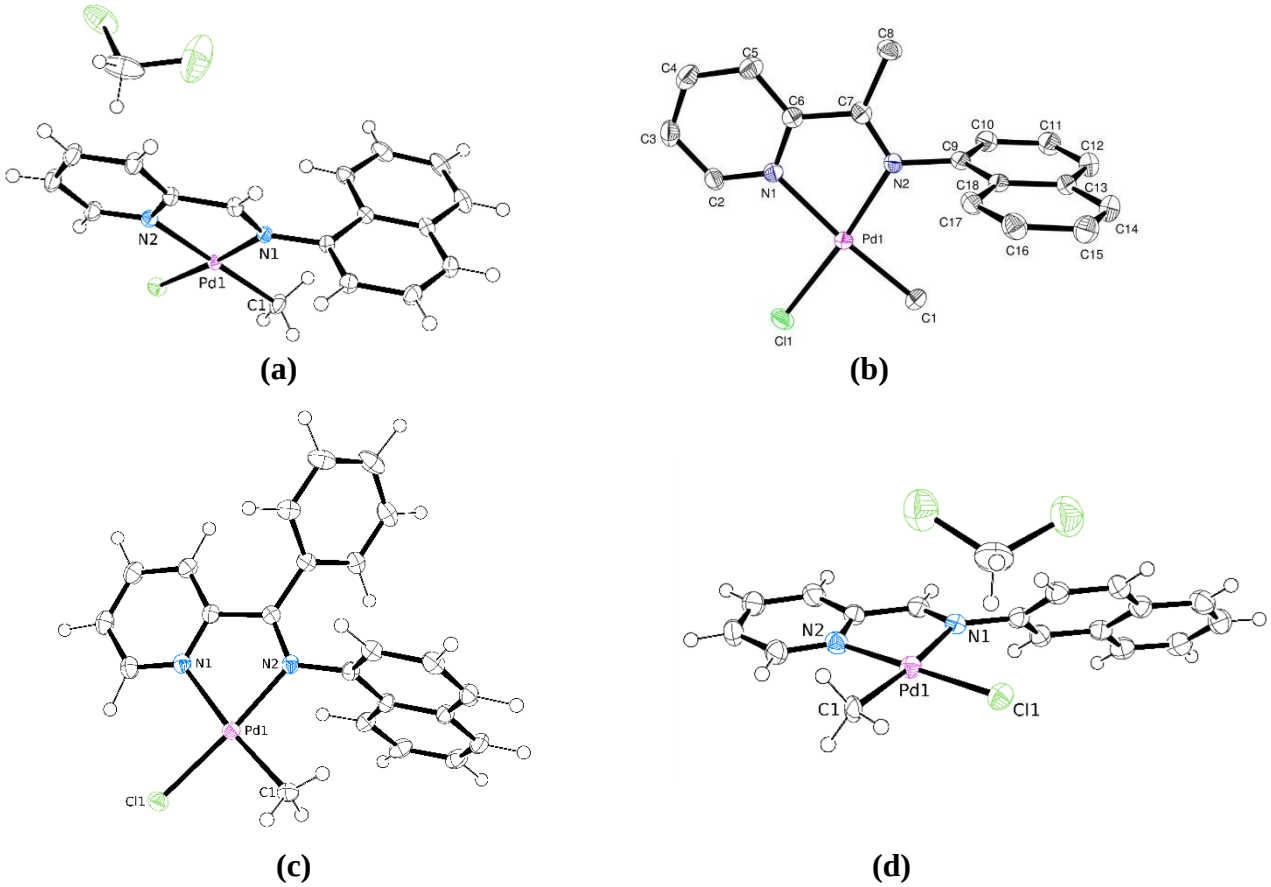

Figure 5.18. ORTEP representations of a) **14a**, b) **15a**, c) **16a**, d) **17a**; relevant bond distances and angles reported in Table 5.5.

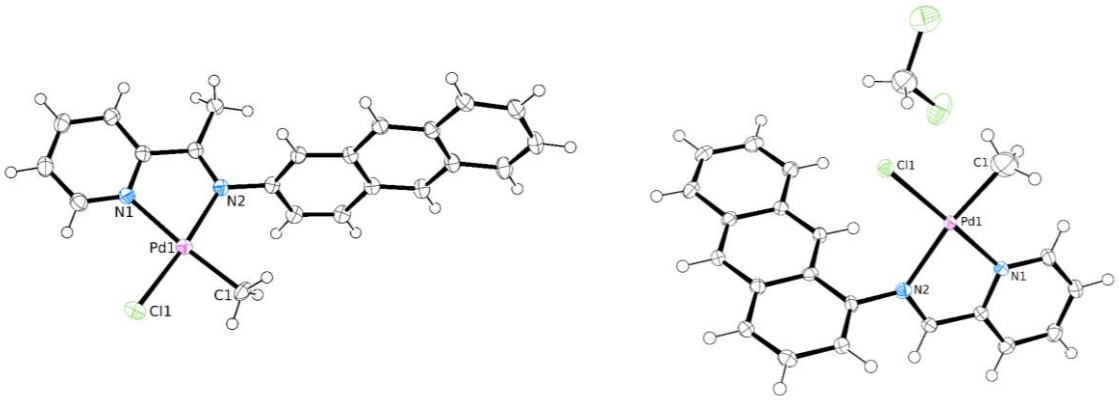

(a) **(b)**

Figure 5.19. ORTEP representations of a) **21a**, b) **22a**; relevant bond distances and angles reported in Table 5.5.

All of the complexes have the expected square planar geometry, and the coordination is completed by the bidentate ligand, a methyl and a chlorido group (Figures 5.18, 5.19). The bite angle values for the pyridylimines are similar (around 78-79°) and are in agreement with typical values reported for cyclometalled 5-membered rings (Table 5.5).[11d,e]

For all of the complexes the two Pd-N bond distances are significantly different, due to the *trans*-influence of the ligands, that is higher for methyl rather than chlorido; in fact, for **14a**, **15a**, **16a** and **21a**, for which the *cis* isomer is the only species present in the unit cell, the Pd-$N_{pyridine}$ *trans* to the methyl is the longest one, whereas for **17a** and **22**a, for which the trans isomer is present in the unit cell, the Pd-N_{imino} is the longest (Table 5.5). The values of the bond distances are very similar for the complexes that have the same configuration, and are quite similar to those already reported by Milani *et al*,[11e,f] but shorter than those reported for complex **3a** in Chapter 2, with the exception of **16a**, that has a phenyl substituent on the iminic carbon atoms, and has similar values of bond distances and angles.

The dihedral angle between the coordination plane of palladium and the plane that contains the naphtyl or anthracenyl moiety varies according to the different ligand: going from the aldimine *cis*-**14a** to the ketimine *cis*-**15a** there is an increase in this value, from 69° to 96° respectively. For *trans*-**17a**, this value is of nearly 50°, indicating that the β-naphtyl group is less orthogonal to the square planar plane with respect to the α-naphtyl group. For *cis*-**21a** and *trans*-**22a**, instead, the dihedral angles are similar, and respectively of 71° and 68°, whereas for *cis*-**16a** the value is intermediate between the highest and the lowest (79°).

Table 5.5. Most significant distances and angles for complexes **14a**, **15a**,**16a**, **17a**, **21a**, **22a**.

	***cis*-14a**	***cis*-15a**	***cis*-16a**	***trans*-17a**	***cis*-21a**	***trans*-22a**
	Distance (Å)					
Pd-CH_3	2.027(2)	2.030(2)	2.047(1)	2.098(4)	2.032(2)	2.05(1)
Pd-Cl	2.2998(6)	2.3127(6)	2.3129(8)	2.298(1)	2.3064(6)	2.313(3)
Pd-N_{pyr}	2.132(1)	2.125(2)	2.129(1)	2.059(4)	2.131(2)	2.058(4)
Pd-N_{imm}	2.056(2)	2.057(2)	2.049(1)	2.151(4)	2.060(2)	2.152(5)
	Angle (°)					
CH_3-Pd-Cl	89.64(5)	88.65(7)	89.23(4)	87.8(1)	87.98(7)	87.4(3)
CH_3-Pd-N_{imm}	94.98(6)	96.45(9)	95.93(5)	173.4(2)	97.11(8)	171.3(3)
Cl-Pd-N_{imm}	175.36(4)	174.83(6)	174.76(3)	98.8(1)	174.77(4)	98.8(2)
CH_3-Pd-N_{pyr}	173.21(7)	174.22(9)	174.19(4)	94.2(2)	175.33(7)	95.0(3)
Cl-Pd-N_{pyr}	96.21(4)	96.91(6)	96.58(3)	177.5(1)	96.68(5)	174.3(2)
N_{imm}-Pd-N_{pyr}	79.21(5)	78.01(8)	78.26(4)	79.2(2)	78.25(6)	79.3(2)
Dihedral angle	69.24(4)	95.70	78.62(4)	49.7(1)	70.64(4)	67.94(6)

The data obtained from the solid state analysis are in agreement with what was observed in solution for complexes having the α-naphthyl group: the chemical shift values of the Pd-CH_3 decreases going from **14a** to **15a** (0.35 ppm *vs* 0.11 ppm), that is expected since there is the introduction of a methyl on the iminic carbon and also from the position of the naphthyl moiety, that is more perpendicular to the coordination plane in **15a** with respect to **14a**, thus contributing more to the shielding cone of the Pd-CH_3 fragment.

*5.2.3. Synthesis and characterization of cationic Pd-complexes **14b-22b.***

The monocationic complexes were synthesized according to the dehalogenation reaction procedure involving a silver salt, $AgPF_6$ (Scheme 5.7). They were all isolated upon concentration and precipitation with diethyl ether as either yellow or orange solids, with yields ranging from 55 % to 95 %.

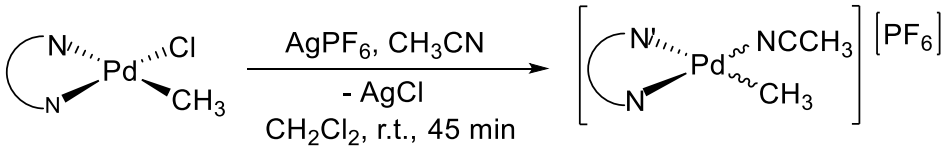

	N-N'	yield (%)		N-N'	yield (%)
14b	**14**	70	**19b**	**19**	65
15b	**15**	83	**20b**	**20**	55
16b	**16**	70	**21b**	**21**	78
17b	**17**	80	**22b**	**22**	95
18b	**18**	84			

Scheme 5.7. Synthesis of the monocationic complexes **14b-22b**.

The monocationic complexes were all characterized in solution by NMR spectroscopy; due to the very low solubility in CD_2Cl_2 and in other common organic solvents, complexes **20b** and **21b** were characterized in CD_3CNO_2, and the spectra are here reported as an example.

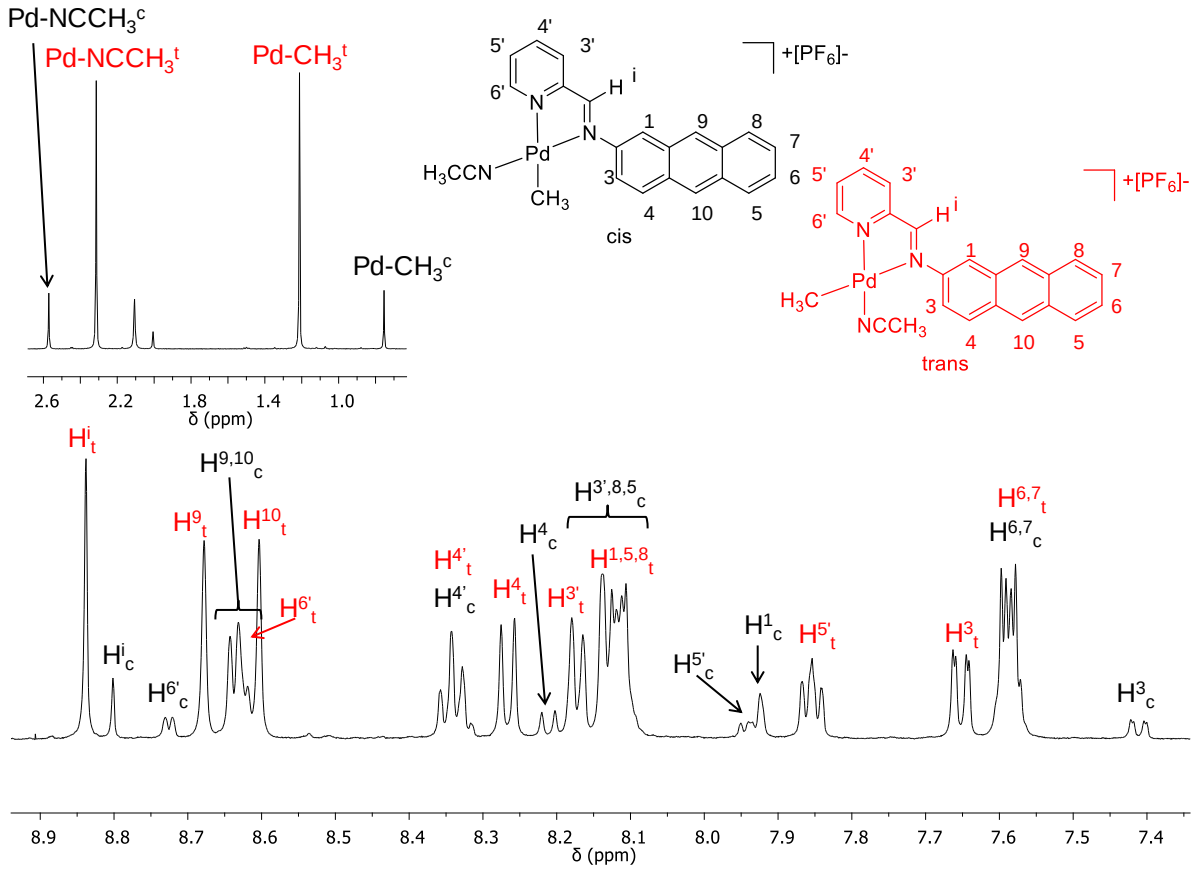

Figure 5.20. ^{1}H NMR spectrum (CD_3NO_2, 298 K) of complex **20b**.

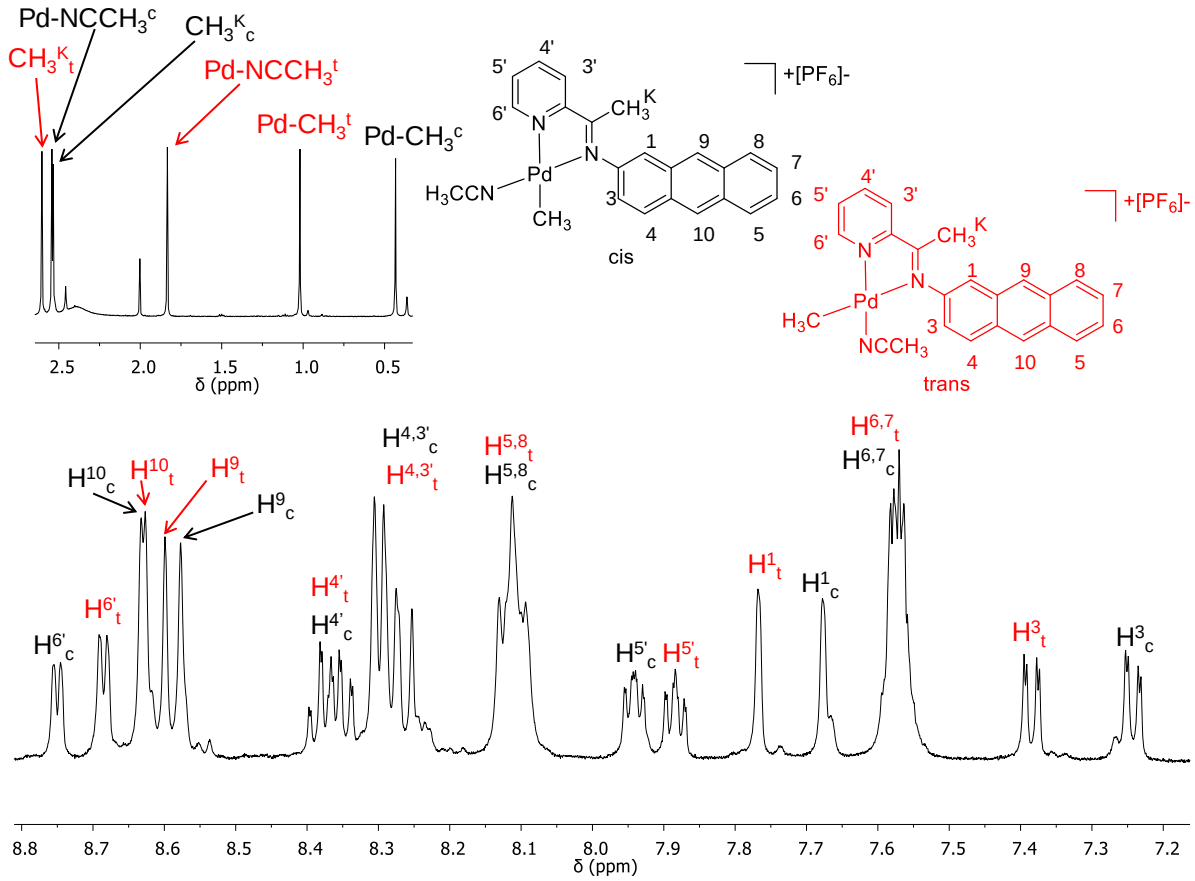

Figure 5.21. ^{1}H NMR spectrum (CD_3NO_2, 298 K) of complex **21b**.

As already observed for the corresponding neutral complexes and for other Pd-complexes with pyridylimines (see Chapter 2), also for the cationic derivatives under investigation *cis* and *trans* isomers are present in solution.

From the NMR data analysis, some conclusions regarding the isomeric distribution in solution of Pd(II) complexes with pyridylimines are discussed (Table 5.6).

Table 5.6. Isomeric distribution at the equilibrium of the investigated neutral and cationic complexes (from NMR spectra, CD_2Cl_2, 298 K).

	[Pd(CH_3)(Cl)(**N-N'**)]		[Pd(CH_3)($NCCH_3$)(**N-N'**)][PF_6]	
N-N'	*cis* (%)	*trans* (%)	*cis* (%)	*trans* (%)
14	93	7	31	69
15	96	4	65	35
16	96	4	44	56
17	78	22	25	75
18	95	5	50	50
19	92	8	42	58
20	72	28	21*	79*
21	94	6	48*	52*
22	95	5	35	65

* These data are obtained from CD_3NO_2 solution, 298 K.

As reported in Chapter 2 and for other complexes with pyridylimines,[11e,f] also in this case for neutral complexes there is a clear preference for the *cis* isomer is found regardless of the nature of the ligand used. The *trans* species is present in more relevant amounts for **17b** and **20b**, and this effect could be due to the lower Lewis basicity of such ligands, that makes the Pd-N bonds more labile and more prone to cleave, thus starting the isomerization process (see Chapter 2, Scheme 2.6). When the coordination sphere of palladium changes upon dehalogenation, generally speaking there is a loss in stereoselectivity of the coordination. For complex **15b** there is still a prevalence of the *cis* isomer, for the aldimine derivatives **14b**, **17b**, **20b** and **22b** there is a preference for the *trans* isomer, and for **16b**, **18b**, **19b** and **21b**, instead, the ratio between the two isomers is almost 1 : 1. As previously discussed in Chapter 2, the preference for the *cis* isomer in the neutral species could be indicative of electronic reasons behind it, whereas for the cationic complexes also steric effects can play a role in driving which is the favourite species. Differently from the pyridylimines complexes reported in Chapter 2, here the aldimine cationic derivatives have the highest content of *trans* isomer, regardless of the substituent on the N-aryl ring, while the methyl-ketimine and the phenyl-substituted ketimine have an almost 1 : 1 isomeric distribution or a prevalence of the *cis* isomer. The preference for the *trans* isomer for the aldimine complexes might be a result of both electronic and steric effects acting in the same direction: the iminic nitrogen atom might have a lower Lewis basicity than the $N_{pyridine}$ one due to the presence of the fused aromatic ring substituent, that also creates a higher steric hindrance than on the side of the pyridine moiety favouring the

coordination of the linear acetonitrile ligand *cis* to it. In the case of the ketimine complexes the electronic effect of the methyl group on the iminic nitrogen might counterbalance the steric hindrance of the fused aromatic ring substituents leading to an almost equal distribution of the two isomers. Anyhow, in the corresponding NOESY spectra exchange peaks between the two isomers are observed at room temperature, thus indicating that the energy difference between the two species is not so high. (E' vero che ci sono I picchi di scambio??)

Table 5.7. Selected chemical shifts (in ppm) for complexes **14a**-**19a**, **14b**-**19b** (^{1}H NMR spectra, CD_2Cl_2, 298 K).

	Pd-CH_3 *cis* (ppm)	Pd-CH_3 *trans* (ppm)		Pd-CH_3 *cis* (ppm)	Pd-CH_3 *trans* (ppm)
14a	0.35	1.12	**17a**	0.60	1.17
14b	0.50	1.23	**17b**	0.81	1.27
15a	0.11	0.98	**18a**	0.34	1.00
15b	0.26	1.05	**18b**	0.49	1.08
16a	0.20	1.11	**19a**	0.43	1.12
16b	0.35	1.19	**19b**	0.57	1.21

For all of the complexes with ligands **14**-**19**, being either neutral or cationic, and both for the *cis* and *trans* isomers, if the substituent on the N-aryl ring is the same, the Pd-CH_3 singlet moves to lower frequencies going from aldimine ligands (**14, 17**) to the phenyl-derived ones (**16**, **19**) to the ketimine ones (**15**, **18**) (Table 5.7). This trend suggests that the 2-acetyl pyridine derived ligands are better σ-donors than those derived from pyridine-2-aldehyde and that those derived from benzoyl pyridine have an intermediate donor ability. When the ligand backbone is the same, it is possible to notice that for *cis* isomers the resonance of the Pd-CH_3 for 1-naphthylamine derived complexes is lower than that of 2-naphthylamine derived species, in agreement with the different orientation of the aromatic fragment with respect to the coordination plane, being the one of 1-naphthylamine more perpendicular, thus its shielding cone affects more the methyl group bound to palladium *cis* to it.

Table 5.8. Selected chemical shifts (in ppm) for complexes **20a**-**22a**, **20b**-**22b** (^{1}H NMR spectra, CD_2Cl_2, 298 K).

	Pd-CH_3 *cis* (ppm)	Pd-CH_3 *trans* (ppm)
20a	0.71	1.18
20b*	0.75	1.21
21a	0.40	1.02
21b*	0.43	1.02
22a	0.35	1.14
22b	0.48	1.25

* These data are obtained from CD3NO2 solution, 298 K.

Also for the 2-amminoanthracene derivatives a shift to lower frequencies of the Pd-CH_3 singlet going from the aldimine to the ketimine complex is observed (Table 5.8, **20a** *vs* **21a** and **20b** *vs* **21b**), thus confirming that the latter has a more donating ancillary ligand. Considering the aldimine with the 1- and the 2-amminoanthracene substituent (Table 5.8, **20a** *vs* **22a** and **20b** *vs* **22b**), the same trend reported for the naphthyl derivatives is found: the singlet of the Pd-CH_3 bond is at lower frequencies for the 1-amminoanthracene complexes.

*5.2.4. CO/vinyl arene copolymerization with Pd-complexes **14b-22b**.*

The monocationic complexes **14b**-**22b** were tested as precatalysts in the copolymerization of carbon monoxide and vinyl arenes such as styrene (S), 4-methyl styrene (MS) and 4-*tert*-butyl styrene (TBS), in the presence of 1,4-benzoquinone (BQ) as cocatalyst, in the ratio [BQ]/[Pd] = 5. The reactions were run for 24 h in 2,2,2-trifluoroethanol (TFE) as solvent, with a pressure of CO of 1 bar and at 303 K. These reaction conditions are the same reported in literature for similar pyridylimine complexes,[11e,f] allowing a direct comparison of the catalytic data.

The complexes generated active catalysts for the reaction under study, yielding the desired copolymers, that precipitate in the reactor as white or grey solids, and are separated by filtration. In the copolymerization of CO/TBS catalyzed by **20b** and **22b** a slightly different procedure was followed: the content of the reactor was poured into a beaker with 50 mL of methanol, left to stir for 2 h and then filtered off. However, the solid obtained could not be taken from the filter itself, so it was directly dissolved in chloroform, later removed under reduced pressure, yielding a dark green, glass-like solid.

The obtained catalytic data points out that the productivity depends both on the nature of the ancillary ligand and the vinyl arene used (Table 5.9). The most productive catalyst for styrene and 4-*tert*-butyl styrene is the one generated from complex **18b** (Table 5.9, run 13 and 15), whereas for 4-methyl styrene it is the one that derives from **21b** (Table 5.9, run 23). The least productive catalysts are those bearing an aldimine ligand, such as **14b**, **17b**, **20b** and **22b** (Table 5.9, runs 1-3, 10-12, 19-21, 26-27); the precatalysts having the phenyl ring on the iminic carbon atom have productivities that are close to those of the ketimine derivatives (Table 5.9, runs 7-9, 16-18).

Table 5.9. CO/vinyl arene copolymerization: effect of the ancillary ligand and the vinyl arene.[a] Precatalyst: $[Pd(CH_3)(NCCH_3)(\mathbf{N–N'})][PF_6]$, **14b-22b**.

run	N-N'	Precat.	Vinyl arene	Yield (g)	Productiviy (kg CP/g Pd)	Mw (Mw/Mn)
1	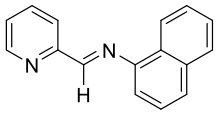	**14b**	S	0.51	0.37	16 000 (1.8)
2			MS	0.42	0.31	9 000 (1.6)
3			TBS	0.11	0.08	n.d. [b]
4	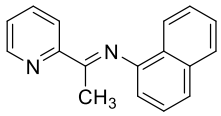	**15b**	S	5.63	4.17	141 000 (1.9)
5			MS	6.05	4.48	174 000 (2.7)
6			TBS	5.74	4.25	151 000 (2.4)
7	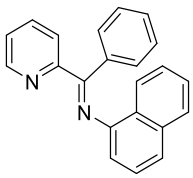	**16b**	S	5.01	3.71	134 000 (2.0)
8			MS	5.21	3.86	191 000 (2.4)
9			TBS	6.26	4.63	245000 (2.8)
10	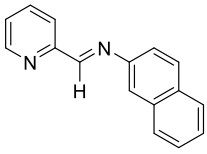	**17b**	S	0.97	0.72	19 000 (2.1)
11			MS	0.56	0.41	13 000 (1.8)
12			TBS	0.34	0.25	21 000 (2.0)
13	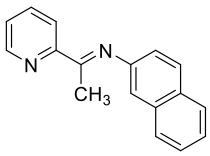	**18b**	S	7.56	5.60	209 000 (2.5)
14			MS	6.02	4.46	138 000 (2.5)
15			TBS	7.77	5.75	236 000 (2.4)

run	N-N'	Precat.	Vinyl arene	Yield (g)	Productiviy (kg CP/g Pd)	Mw (Mw/Mn)
16	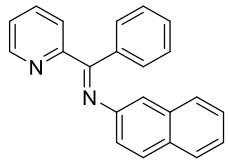	**19b**	S	5.62	4.16	117 000 (2.0)
17			MS	5.83	4.31	147 000 (2.9)
18			TBS	7.00	5.18	162 000 (3.0)
19	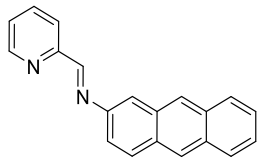	**20b**	S	0.60	0.44	19 000 (2.0)
20			MS	0.43	0.32	11 000 (1.5)
21			TBS	0.35	0.26	15 000 (1.7)
22	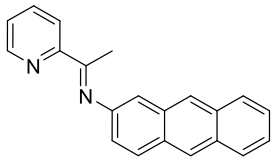	**21b**	S	5.77	4.27	104 000 (2.7)
23			MS	6.20	4.58	209 000 (2.7)
24			TBS	6.93	5.13	284 000 (3.0)
26	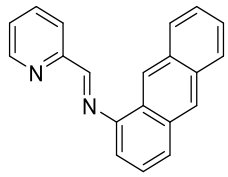	**22b**	S	0.63	0.47	26 000 (2.9)
27			MS	0.40	0.30	17 000 (2.8)
28			TBS	0.23	0.17	31 000 (2.8)

[a] Reaction conditions: n_{Pd} = 1.27 x 10^{-5} mol; V_{TFE} = 20 mL; $V_{vinyl\ arene}$ = 10 mL; [BQ]/[Pd] = 5; [S]/[Pd] = 6800; [MS]/[Pd] = 6000; [TBS]/[Pd] = 4300; T = 303 K; P_{CO} = 1 bar; t = 24 h; [b] n.d = not determined.

Comparing these results with those reported in Table 5.1 and 5.3 it is possible to state that, in all cases, the productivity of the catalyst depends on the nature of the ligand, and in particular, that ketimine-derived catalysts have productivities that are one order of magnitude higher than those of the relevant aldimine counterparts (Table 5.1, run 5 *vs* run 6; Table 5.3 runs 1-3 *vs* run 4-6; Table 5.9, runs 1-3 *vs* run 4-6, runs 10-12 *vs* runs 13-15, runs 19-21 *vs* runs 22-24). This effect is connected to the stability of the active species: in the copolymerization reactions run with precatalysts having an aldimine ancillary ligand, palladium black is present in the reaction mixture, in particular after 1 h for **14b** and **17b**, after 1.5 h for **20b** and after 4 h for **22b**; in all other cases, no palladium black is visible in the reactor, even after 24 h.

The higher stability of ketimine catalysts with respect to aldimine ones might be attributed to the higher electron donor capability of the ketimine ligand, that increases the strength of the Pd-(N-N') bond, thus disfavouring ligand dissociation from the palladium-hydride intermediate formed after the reaction of termination of the growing polymeric chain. This termination consists in a β–

hydrogen elimination on the Pd-alkyl intermediate, leading to the Pd-hydride species that can follow two different pathways: the migratory insertion of a new vinyl arene molecule, starting a new polymer chain, or the hydrogen dissociation as a proton, with the contemporary reduction of Pd(II) to Pd(0) and dissociation of the pyridylimine ligand leading to inactive palladium metal (Scheme 5.8). The higher Lewis basicity of the ligand stabilises the hydride species.

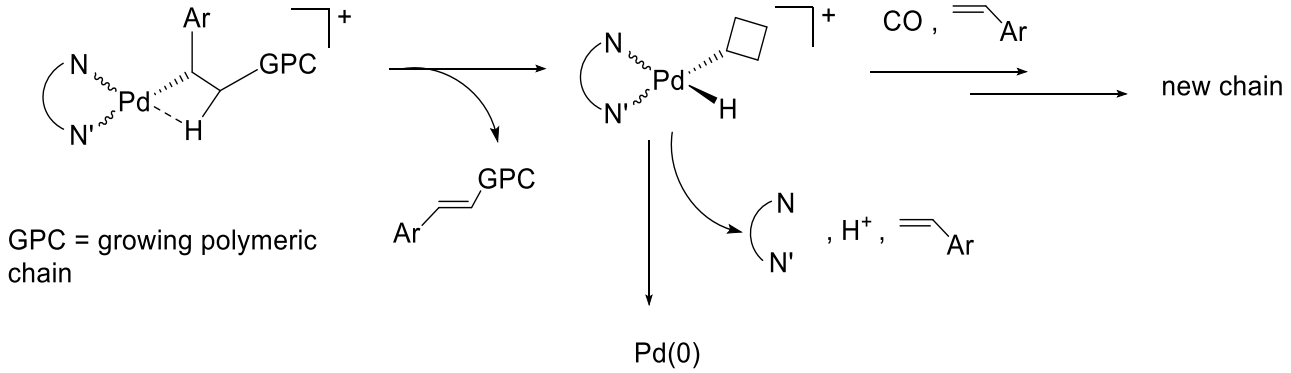

Scheme 5.8. Termination step of the catalytic cycle.

An increase in productivity was found going from α– to β–naphthylamine for all of the three comonomers (Table 5.9), and this effect might be related to the different orientation of the aromatic fused ring with respect to the coordination plane that creates a different steric hindrance both in the coordination plane and towards the axial positions.

As far as it concerns the effect of the vinyl arene on productivity, it is observed that for catalysts having aldimine ligands, such as **14b**, **17b**, **20b** and **22b** the productivity decreases going from styrene to 4-methyl styrene to 4-*tert*-butyl styrene (Table 5.9). This is analogous to what has been previously observed for other pyridylimines-based catalysts (Tables 5.1, 5.3).[11e,f]

Detailed kinetic studies on catalysts with α–diimine ligands allowed the evaluation of kinetic constant for the propagation of the growth of the polymeric chain (k_1) and for the decomposition of the catalyst (k_2) (Scheme 5.9), showing that the higher activity in the CO/S copolymerization is associated to a higher rate of propagation and a higher deactivation of the catalyst with respect to CO/MS.[38] Supposing that these conclusions are valid also for pyridylimine complexes, and considering that the aldimine catalysts always undergo decomposition regardless of the vinyl arene in use, it is acceptable to state that the lower productivity going from S to MS to TBS is due to a decrease in the propagation rate.

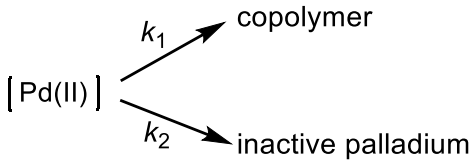

Scheme 5.9. Propagation reaction rate *vs* decomposition rate of the catalyst.

For ketimine catalysts, similar productivities are obtained for all of the three vinyl arenes starting from **15b** and **18b** (Table 5.9, run 4-6 and run 13-15), whereas for **16b**, **19b** and **21b** the productivity increases going from styrene to 4-methyl styrene to 4-*tert*-butyl styrene. However, the different mass of the vinyl arene, that is reflected in a different mass of the repetitive unit, has to be considered, and the productivity is better expressed as mol of repetitive units per gram of palladium (Table 5.10). Doing so, the productivity of the catalysts decreases on going from S to MS to TBS, in agreement with the hypothesis of a decrease in the propagation rate.

Table 5.10. Productivity in kg CP/g Pd and mol RU/g Pd.

run	**Precat.**	**Vinyl arene**	**Productivity (kg CP/g Pd)**	**Productivity (mol RU[b]/g Pd)**
1	**16b**	S	3.71	28.07
2		MS	3.86	26.39
3		TBS	4.63	24.60
4	**19b**	S	4.16	31.45
5		MS	4.31	29.51
6		TBS	5.18	24.60
7	**21b**	S	4.27	32.33
8		MS	4.58	31.36
9		TBS	5.13	27.25

[a] Reaction conditions: n_{Pd} = 1.27 x 10^{-5} mol; V_{TFE} = 20 mL; $V_{vinyl\ arene}$ = 10 mL; [BQ]/[Pd] = 5; [S]/[Pd] = 6800; [MS]/[Pd] = 6000; [TBS]/[Pd] = 4300; T = 303 K; P_{CO} = 1 bar; t = 24 h; the masses of terminal groups have been neglected; [b] RU = repetitive unit.

The molecular weight values of the synthesized macromolecules, measured at the University of Urbino in the group of Prof. Carla Carfagna, show that the aldimine derivatives yield copolymers with lower molecular weights than those obtained with their ketimine counterparts. The lowest Mw is that of CO/MS copolymer obtained with **14b** (9000 g/mol), and the highest is that of the CO/TBS copolymer obtained with **21b**. The polydispersity index in some cases (Table 5.9, runs 5, 9, 17, 18,

22-28) is higher than 2.0, suggesting that the presence of *cis* and *trans* isomers for the precatalysts in solution might lead to different active species.

The stereochemistry of the synthesized polyketones has been studied by ^{13}C NMR spectroscopy, recording the spectra in a 2 : 1 mixture of deuterated chloroform and 1,1,1,3,3,3–hexafluoropropanol (HFIP). As already mentioned in Section 5.1, the most diagnostic signal for the stereochemistry of the produced macromolecules is that of the *ipso* carbon atom.

Table 5.11. CO/vinyl arene copolymer triad distribution, in red and bold the prevailing triad.[a] Precatalyst: [Pd(CH_3)($NCCH_3$)(**N–N'**)][PF_6].

run	N–N'	Precat.	Vinyl arene	Triads			
				***ll* (%)**	***lu* (%)**	***ul* (%)**	***uu* (%)**
1	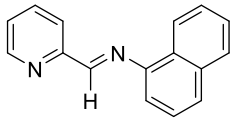	**14b**	S	28	15	16	**41**
2			MS	**50**	17	15	18
3			TBS	31	26		**43**
4	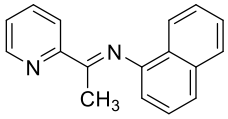	**15b**	S	3	16	15	**66**
5			MS	4	16	15	**65**
6			TBS	5	26		**69**
7	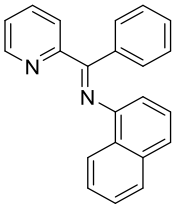	**16b**	S	2	14	13	**71**
8			MS	< 1	13	13	**74**
9			TBS	2	23		**75**
10	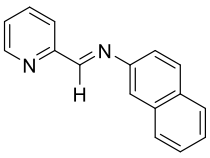	**17b**	S	7	10	12	**71**
11			MS	24	15	13	**48**
12			TBS	18	22		**60**
13	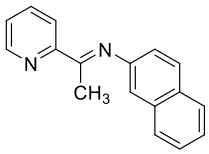	**18b**	S	-	11	10	**79**
14			MS	-	12	11	**77**
15			TBS	-	18		**82**

run	N–N'	Precat.	Vinyl arene	Triads			
				***ll* (%)**	***lu* (%)**	***ul* (%)**	***uu* (%)**
16	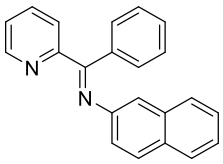	**19b**	S	–	8	7	**85**
17			MS	–	9	7	**84**
18			TBS	–	15		**85**
19	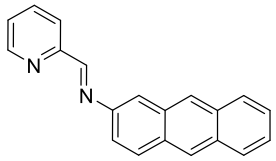	**20b**	S	17	15	16	**52**
20			MS	30	19	16	35
21			TBS	24	35		**41**
22	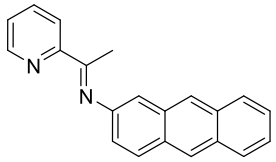	**21b**	S	–	10	9	**81**
23			MS	–	12	10	**78**
24			TBS	–	19		**81**
25	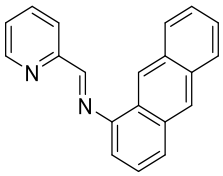	**22b**	S	**38**	16	13	33
26			MS	**56**	8	9	27
27			TBS	33	27		**40**

[a] on the basis of integration on the *ipso* carbon atom in the ^{13}C NMR spectrum.

As expected, the polymer tacticity is affected by the ancillary ligand: all the copolymer synthesized with catalysts having the ketimine ligand have a prevailingly sindiotactic microstructure, regardless of the vinyl arene comonomer (Table 5.11, runs 4-9, 13-18, 22-24). In particular, in the ^{13}C NMR spectra of those obtained with catalysts having ligands **18**, **19** and **21** (Figures 5.22, S5.112) no signal of the *ll* triad is present, thus indicating that the enantioface selection is under *chain end* control. In addition, for the ketimine catalysts, the phenyl substituent on the iminic carbon also influences the tacticity of the copolymer: for complexes bearing pyridylimines with the same aromatic system on the iminic nitrogen, the content of *uu* triad increases moving from methyl to the phenyl substituted ketimine (Table 5.11, runs 4-6 *vs* 7-9 and 13-15 *vs* 16-18), thus indicating that the phenyl group on the iminic carbon atom leads to a more efficient enantioface discrimination than the methyl substituent.

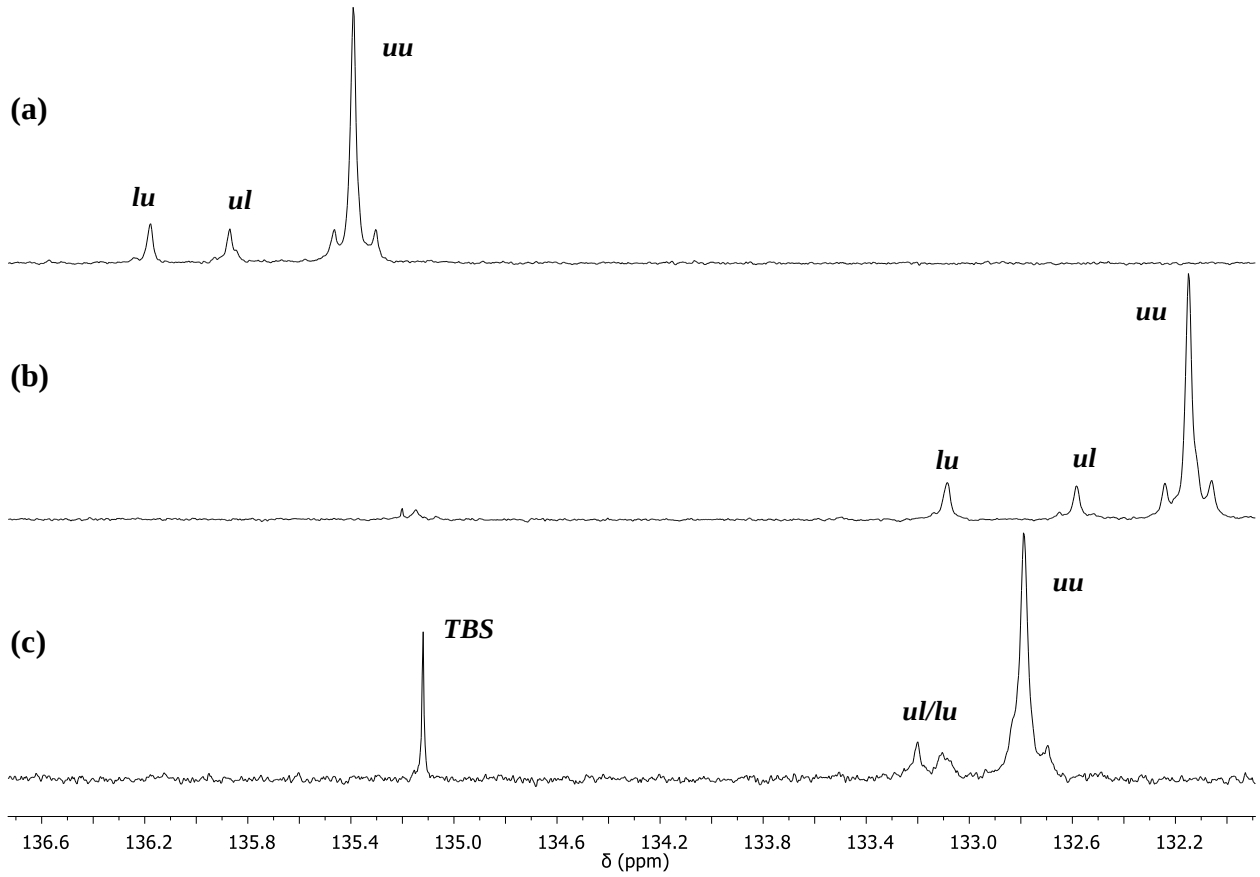

Figure 5.22. ^{13}C NMR spectra (HFIP/$CDCl_3$ = 1:2, T = 298 K) of: (a) CO/S; (b) CO/MS and (c) CO/TBS copolymers, obtained with **21b**; *ipso* carbon atom region.

A completely different situation is found when catalysts with aldimine ligands are used. In the ^{13}C NMR spectra of the synthesized macromolecules the signals of all the four triads are present with a different intensity depending on the vinyl arene comonomer (Table 5.11, runs 1-3, 10-12, 19-21, 25-27). As a general trend, by using the same catalyst an increase in the content of the *ll* triad with a concomitant decrease of the *uu* triad is observed going from the CO/S to the CO/MS copolymers, thus confirming our discovery found for pyrene-tagged pyridylimine complexes, [11f] that for catalysts with these peculiar ligands the stereochemistry of the macromolecules is affected by the substituent in *para* position of the vinyl arene comonomer. For all these macromolecules, but those obtained with catalyst with ligand **22**, the content of each heterotactic triad is around 15 %. The found triad distribution might be due either to a mixture of prevailingly isotactic and syndiotactic macromolecules with stereoerrors or to one kind of macromolecules with isotactic and syndiotactic stereoblocks. The monomodal distribution of the GPC curves for the molecular weight measurements indicates that the synthesized copolymers are formed by only one kind of macromolecules, that consists of isotactic and syndiotactic stereoblocks with the hetereotactic triads

representing the junction points among the different stereoblocks. A closer look to the triad distribution points out that: *i.* going from styrene to 4-methyl styrene the length of the isotactic blocks increases and that this increase is more marked for the copolymers synthesized with catalysts having the α-naphthyl or α-anthracenyl fragments than for those produced with the corresponding beta fused aromatic rings; *ii.* in CO/MS copolymer produced with catalyst with ligand **22** the content of the heterotactic triads is the lowest found indicating that a lower number of stereoblocks is present (Figure 5.23).

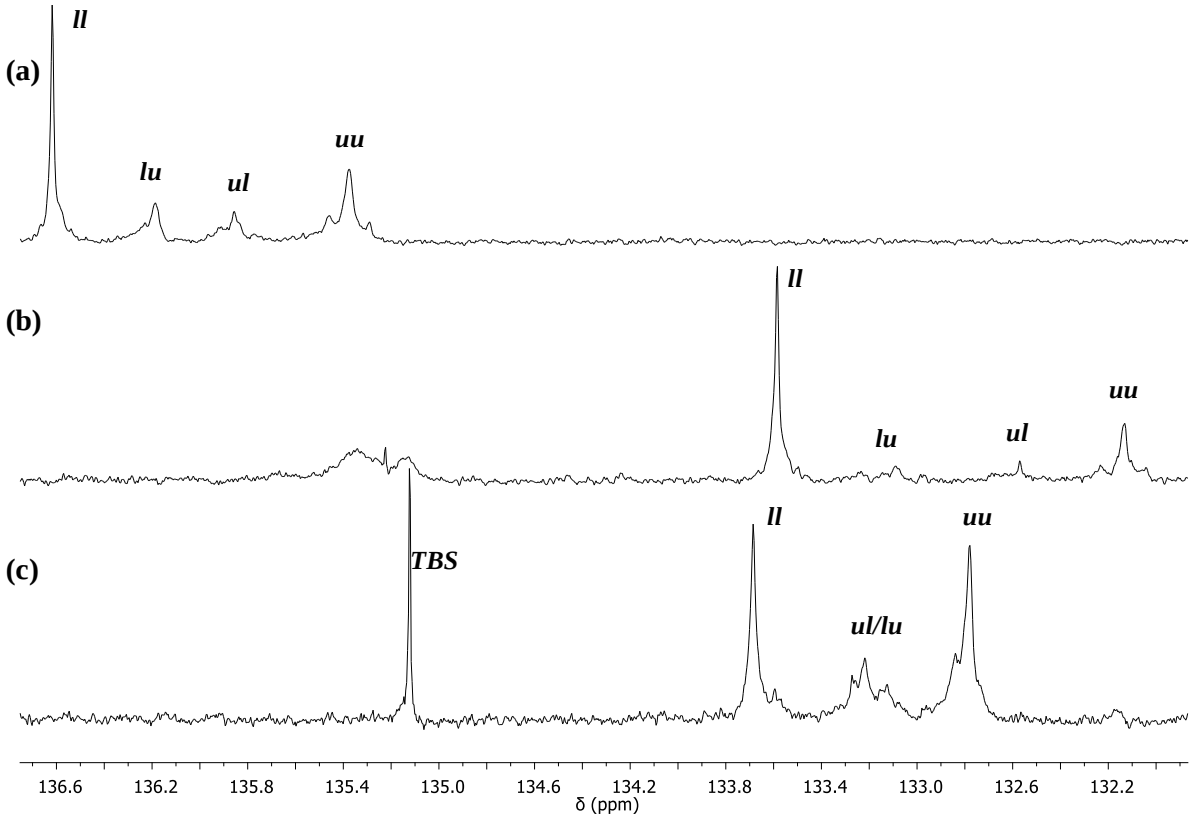

Figure 5.23. ^{13}C NMR spectra (HFIP/$CDCl_3$ = 1:2, T = 298 K) of: (a) CO/S (b) CO/MS and (c) CO/TBS copolymers, obtained with **22b**; *ipso* carbon atom region.

To tentatively explain the remarkable effect of catalysts under investigation on the stereochemistry of the synthesized polyketones the possible intermediates responsible for the enantioface selection are considered. In agreement with literature,[17] the enantioface discrimination takes places on the 6-membered metallacycle intermediate, for which two isomers are possible due to the nonsymmetric nature of pyridylimine ligands. These isomers differ for the position of the Pd-acyl bond of the growing polymer chain with respect to two non-equivalent halves of the ligand. Therefore, when the vinyl arene coordinates, four diastereoisomers can be obtained (Figure 5.24), depending on the

prochiral face (*Re* or *Si*) coordinated to the metal center. Since with N-donor ancillary ligands the insertion of the vinyl arene regiospecifically occurs with a secondary regiochemistry, the diastereoisomers that would lead to the insertion with a primary regiochemistry are not be considered.

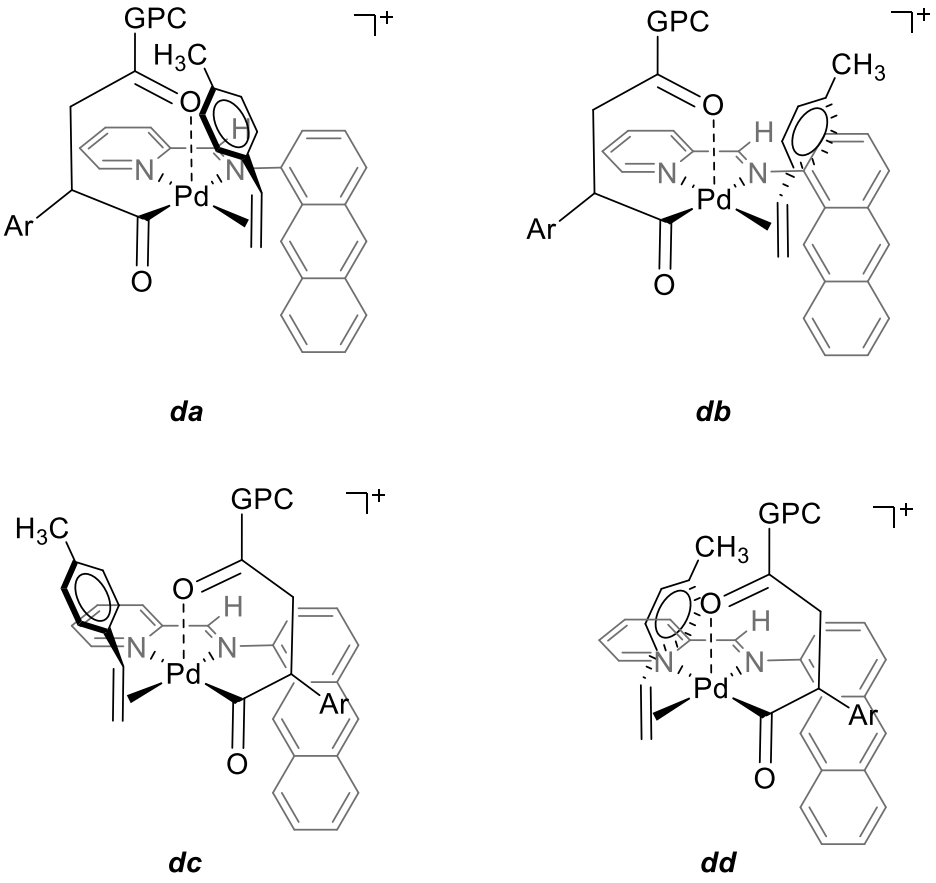

Figure 5.24. The four possible diasteroisomers of the metallacycle intermediate in the case of copolymerization with **22b**.

The NMR analysis of the precatalysts indicates a different distribution of the *cis* and *trans* isomers depending on the N-N' ligand. If we assume that a similar distribution is valid also for the 6-membered diastereoisomers it is possible to correlate the stereochemistry of the produced macromolecules to the isomer distributions.

The syndiotactic macromolecules are obtained with catalysts originated by precatalysts **16b**, **18b**, **19b** and **21b**, for which no preference for the *cis* or the *trans* isomer is observed (Table 5.6). This implies that during the copolymerization both sites can host either the growing polymeric chain or the incoming comonomer, with no site-selective coordination. Therefore, all of the four mentioned

diastereoisomers are possible, and the stereogenic centre of the last repetitive unit inserted determines the enantioface discriminations of the incoming vinyl arene, thus leading to a syndiotactic copolymer, due to the *chain-end* control.

For precatalyst **15b** a prevalence of the *cis* isomer is observed (Table 5.6), suggesting a preferential site-selective coordination of the growing polymeric chain *cis* to the naphthyl group during the copolymerization, and as a consequence the vinyl arene coordinates *cis* to the pyridine. The ***dc*** and ***dd*** diastereoisomers are the preferential ones, and again the enantioface discrimination is under *chain end* control.

For the other precatalysts, namely **14b**, **17b**, **20b** and **22b**, the prevailing isomer is *trans*, so the coordination of the growing polymer chain happens preferentially on the position *cis* to the pyridine, thus directing the coordination of the vinyl arene *cis* to the aromatic group on the N_{imino}. The aromatic group can discriminate between the enantiotopic faces, and of the four possible diastereoisomers just one is favoured, either ***da*** or ***db***. In this case the stereochemistry can depend on the nature of the comonomer, and this is linked to the efficiency of the interaction between the vinyl arene and the extend aromatic system. Going from styrene to 4-methyl styrene, the interactions between the vinyl arene and the polycyclic fragment (either π–stacking or between the group in *para* position and the ring current) are stronger, thus increasing the *ll* triad content: the content of *ll* triad is the highest for **22b**, suggesting more favourable interactions in this case than for other precatalysts.

DFT calculations on these intermediates might support or not this hypothesis.

5.3. Conclusions

A series of pyridylimine ligands (**14-22**) and the relevant Pd(II) organometallic complexes, both neutral and cationic, of general formula [Pd(N-N')(CH_3)Cl] **1a-4a** and [Pd(N-N')(CH_3)(CH_3CN)][PF_6] **1b-4b** were investigated. The ligands derive from the condensation of either pyridine-2-aldehyde or 2-acetylpyridine or benzoylpyridine and the relevant aniline, in particular α- or β-naphthylamine or α- or β-amino anthracene. Part of this work is the result of a collaboration with the group of Prof. Durand at the École Polytechnique of Toulouse.

All of the synthesized products were characterized in solution by NMR spectroscopy, both mono- and bidimensional, highlighting in particular the *cis*/*trans* isomeric distribution for the neutral and the cationic Pd(II) complexes. As discussed in Chapter 2 and as previously reported in literature, going from the neutral complexes, for which the *cis* isomer is always the prevailing one in solution, to the cationic, a loss in the stereoselectivity of the coordination of the ligand is found.

Neutral palladium complexes bearing ligands **14**-**17**, **21** and **22** were also characterized in the solid state. For complexes **14a**-**16a** and **21a** the *cis* isomer is the prevailing species in solution and that one present in the unit cell, whereas for **17a** and **22a** the minor species in solution, the *trans* isomer, is present in the unit cell in the solid state. The crystallographic data show that for all complexes the palladium presents the expected square planar geometry, and the coordination is completed by the bidentate nitrogen-donor ligand, a chlorido ligand and the methyl group. Moreover, the analysis allows to observe that the value of the dihedral angle between the naphthyl fragment and the coordination plane of the palladium depends on the nature of the ligand, and increases going from the β- to the α-naphthylamine derived ligand, and also from the aldimine to the phenyl-substituted and to the methyl-substituted ketimine; the anthracenyl fragments, instead, have a very similar orientation with respect to the metallacycle plane.

The monocationic complexes were tested in the copolymerization of carbon monoxide with vinyl arenes, in particular with styrene, 4-methyl styrene and 4-*tert*-butyl styrene. The catalytic data highlight the following points:

- Catalysts having ketimine ligands have productivities one order of magnitude higher than those of aldimine derivatives, that undergo decomposition under the applied reaction conditions;
- Moving from the α-naphthyl to the β-naphthyl fragment or from the β-anthracenyl to the α-anthracenyl an increase in the productivity is achieved, regardless of the vinyl arene used;
- The presence of *para* substituents on the vinyl arene influences the productivity of the catalysts, and this is more evident for aldimine derivatives, for which the productivity decreases in the order S > MS > TBS;

The analysis of ^{13}C NMR spectra of the synthesized copolymers allows to observe that the nature of the ancillary ligand influences the stereochemistry of the obtained polyketones. In particular, when catalysts with the ketimine ligands are used, polyketones with a prevailingly syndiotactic microstructure are obtained. The highest content of *uu* triad is found in the copolymers produced with complexes **19b** and **21b**, and for the macromolecules obtained with **18b**, **19b** and **21b** the lack of the signal of the *ll* triad in the ^{13}C NMR spectrum indicates that the stereochemistry is exclusively under *chain end* control.

When catalysts with the aldimine ligands are used, copolymers with isotactic and syndiotactic stereoblocks are obtained. In addition, by using the same catalyst the content of the *ll* triad increases on going from styrene to 4-methyl styrene, indicating that the stereoblock length is affected by the vinyl arene comonomer. To the best of our knowledge, this effect is reported here for the first time.

The combination of statistical study and DFT calculation could be helpful in supporting or not our hypothesis on the nature of effect of the vinyl arene on the stereochemistry of the polyketones, and if this is somehow connected to the isomeric distribution of the precatalysts, that is reflected on the isomeric distribution of the active species, thus imposing a shift from the *chain end* to the *enantiomorphic site* control of the stereochemistry of the macromolecule.

5.4. Experimental

All complex manipulations were performed using standard Schlenk techniques under argon. Deuterated solvents (Cambridge Isotope Laboratories, Inc. (CIL)) were stored as recommended by CIL. 2-acetylpyridine, 2-acetyl-6-methylpyridine, 2-benzoylpyridine, 1- and 2-naphthylamine, 1- and 2-aminoanthracene, TFE and the vinyl arenes were purchased from Sigma-Aldrich and used without further purification for synthetic, spectroscopic and catalytic purposes. Carbon monoxide (purity ≥ 99.9%) was purchased from SIAD and used as it is. Palladium(II) neutral complexes were synthesized using [Pd(cod)(CH_3)Cl], synthesized from [Pd($OCOCH_3$)$_2$] (Engelhard Italia), Benzonitrile (Sigma-Aldrich), HCl 37% (Fluka) and *cis*–*cis*–1,5–cyclooctadiene (Fluka) without further purification. The cationic complexes were synthesized from the appropriate $AgPF_6$ salt and anhydrous acetonitrile (Sigma-Aldrich). Dichloromethane (Sigma-Aldrich) used in the synthesis of Pd complexes was distilled over CaH_2 under argon atmosphere. Mono- and bidimensional NMR spectra were recorder on a Varian 500 spectrometer (500 MHz for ^{1}H, 125.68 MHz for ^{13}C), or on a Varian400 (400 MHz for ^{1}H, 100.55 MHz for ^{13}C, 376.3 MHz for ^{19}F and 161.9 MHz for ^{31}P), using the residual solvent peak as reference (CD_2Cl_2: 5.32 ppm for^{1}H–NMR, 54.00 ppm for ^{13}C–NMR; $CDCl_3$: 7.26 ppm for ^{1}H–NMR, 77.16 ppm for ^{13}C–NMR).

*5.4.1. Synthesis of ligands **14-22**.*

Ligand **14** and **15**, already reported in literature, were synthesized in the group of Prof. Durand of the École Polytechnique of Toulouse and used as received.

For ligands **17**, **20**, **22** the following procedure was used:

In a flask equipped with a Dean-Stark apparatus the desired aniline (1 equiv) and pyridine-2-aldehyde (1.5 equiv) are dissolved in toluene, in the presence of an acid catalyst (acetic acid for 17, 22 and silica-alumina for 20). The mixture is left under reflux for 6 h, then left to cool and concentrated under reduced pressure until precipitate starts to appear. The precipitation is favoured with the addition of a pentane : diethyl ether mixture (1 : 1). The flask is kept at 248 K overnight, then the obtained solid is filtered off and washed with additional pentane/diethyl ether mixture.

For ligands **16**, **19**, **21** the following procedure was used:

In a flask, 2-acetylpyridine or benzoylpyridine (1 equiv) and 1.1 equiv of $ZnCl_2$ are dissolved in acetic acid. 1 equiv of the desired aniline is then added. The mixture is left under reflux for 3.5 h, then cooled down, and the obtained solid filtered off and washed with petroleum ether. The solid is then dissolved in dichloromethane, to which a 1.00 M solution of sodium (**16**, **19**) or potassium (**21**) oxalate is added. The organic phase is separated and washed with distilled water, then dried over Na_2SO_4. The solution is then separated and the solvent removed under reduced pressure.

16. (brown oil, 61%) ^{1}H NMR (500 MHz, CD_2Cl_2, 298 K) δ = 8.63 (d, 1H, H^6), 8.56 (d, 1H, H^{15}), 8.44 (d, 1H, H^3), 7.91 (t, 1H, H^4), 7.44-7.39 (m, 2H, $H^{5,10}$), 7.19-7.13 (m, 6H, $H^{p,11,14,13,o}$), 7.07 (d, 1H, H^{12}), 6.90 (d, 1H, H^9), 6.48 (t, 2H, H^m); ^{13}C NMR (500MHz, CD_2Cl_2, 298 K) δ = 149 (C^{15}), 148 (C^6), 135 (C^{10}), 136 (C^4), 129 (C^{12}), 128 (C^p), 127 (C^o), 125 ($C^{13,14}$), 124 (C^5), 123 ($C^{3,9,11}$), 114 (C^m).

17. (yellow solid, 43%) (500 MHz, CD_2Cl_2, 298 K) δ = 8.73 (s, 1H, H^i), 8.72 (d, 1H, H^6), 8.27 (d, 1H, H^3), 7.94-7.82 (m, 4H, $H^{4,10}$, $H^{11,14(o12,13)}$), 7.70 (s, 1H, H^{15}), 7.55-7.45 (m, 3H, H^9, $H^{12,13(o11,14)}$), 7.40 (d, 1H, H^5); ^{13}C NMR (500 MHz, CD_2Cl_2, 298 K) δ = 161.55 (C^i), 150.14 (C^6), 136.94-128.14 ($C^{4,10}$, $C^{11,14(o12,13)}$), 125.58 (C^5), 126.20-121.07 ($C^{12,13(o11,14)}$), 121.85 (C^3), 119.04 (C^{15}).

19. (brown oil, 65%) ^{1}H NMR (500 MHz, CD_2Cl_2, 298 K) δ = 8.61 (m, 2H, $H^{6,14}$), 8.31 (d, 1H, H^3), 7.87 (t, 1H, H^4), 7.76 (d, 1H, H^{11}), 7.66-7.62 (m, 3H, $H^{o,p}$) 7.51-7.36 (m, 3H, $H^{10,12,5}$), 7.18-7.15 (m, 4H, H^{13}), 7.10 (s, 1H, H^{15}), 7.05 (d, 1H, H^9), 6.98-6.95 (m, 2H, H^m); ^{13}C NMR (500MHz, CD_2Cl_2, 298 K) δ = 149 ($C^{6,14}$), 137 (C^4), 130 (C^{11}), 129 ($C^{12,o,p}$), 128 (C^{10}), 12 (C^5), 125 (C^9), 124 (C^{13}), 123 (C^3), 122 (C^m) 117 (C^{15}).

20. (pale yellow solid, 57%) ^{1}H NMR (300 MHz, CD_2Cl_2, 298 K) δ (ppm) = 8.80 (s, 1H, H^i), 8.73 (ddd, 1H, $H^{6'}$), 8.47 (s, 1H, H^{10}), 8.46 (s, 1H, H^9), 8.30 (d, 1H, $H^{3'}$), 8.08 (d, 1H, H^4), 8.05–7.99 (m, 2H, $H^{5,8}$), 7.90–7.82 (m, 2H, $H^{1,4'}$), 7.56 (dd, 1H, H^3), 7.53–7.46 (m, 2H, $H^{6,7}$), 7.41 (ddd, 1H, $H^{5'}$); ^{13}C NMR (75.41 MHz, CD_2Cl_2, 298 K) δ (ppm) = 155.16 (C^i), 150.19 ($C^{6'}$), 137.10 ($C^{4'}$), 129.85 (C^4), 128.57,128.49 ($C^{5,8}$), 126.86–126.64 ($C^{9,10}$), 126.14,126.00 ($C^{6,7}$), 125.65 ($C^{5'}$), 122.01 ($C^{3'}$), 121.52 (C^3), 119.01 (C^1).

21. (ocher solid, 41 %) ^{1}H NMR (300 MHz, CD_2Cl_2, 298 K) δ (ppm) = 8.68 (ddd, 1H, $H^{6'}$), 8.44 (s, 1H, H^9), 8.39–8.33 (m, 2H, $H^{10,3'}$), 8.10–7.96 (m, 3H, $H^{8,5,4}$), 7.84 (ddd, 1H, $H^{4'}$), 7.51–7.43 (m, 2H, $H^{6,7}$), 7.40 (ddd, 1H, $H^{5'}$), 7.32 (s, 1H, H^1), 7.12 (dd, 1H, H^3), 2.44 (s, 3H, $CH_3{}^i$); ^{13}C NMR (75.41 MHz, CD_2Cl_2, 298 K) δ (ppm) = 148.93 ($C^{6'}$), 136.72 ($C^{4'}$), 129.86 (C^4), 128.64–128.16 ($C^{5,8}$), 126.45 (C^9), 125.46–125.26 ($C^{6,7,5'}$), 125.44 (C^{10}), 122.09 (C^3), 121.70 ($C^{3'}$), 114.01 (C^1), 16.73 ($CH_3{}^i$).

22. (brown solid, 58 %) ^{1}H–NMR (500 MHz, CD_2Cl_2, 298 K) δ (ppm) = 8.92 (s, 1H, H^{9}), 8.77 (s, 1H, H^{i}), 8.75 (ddd, 1H, $H^{6'}$), 8.50 (dd, 1H, $H^{3'}$), 8.47 (s, 1H, H^{10}), 8.08–8.03 (m, 2H, $H^{5,8}$), 7.97–7.91 (m, 2H, $H^{4',4}$), 7.53–7.47 (m, 3H, $H^{3,6,7}$), 7.46 (ddd, 1H, $H^{5'}$), 7.13 (d, 1H, H^{2}); ^{13}C–NMR (125.68 MHz, CD_2Cl_2, 298 K) δ (ppm) = 161.38 (C^{i}), 149.97 ($C^{6'}$), 136.84 ($C^{4'}$), 128.79–128.14 ($C^{5,8}$), 126.91 (C^{4}), 126.37–125.58 ($C^{3,6,7}$), 126.21 (C^{10}), 125.48 ($C^{5'}$), 122.88 (C^{9}), 122.05 ($C^{3'}$), 111.65 (C^{2}).

5.4.2. Synthesis and characterization of [Pd(CH$_3$)Cl(N–N')] ***14a–22a.***

General procedure: To 1 equiv. of [Pd(cod)(CH_3)Cl] dissolved in 10 mL of distilled dichloromethane, 1.2 equiv. of ligand were added. The solution was left to stir at room temperature for 3 h. The solution was then concentrated under reduced pressure and diethyl ether was added to favour the precipitation of the product. The yellow precipitates were then filtered and washed with additional cold diethyl ether, then dried under vacuum.

Template synthesis for **18a**: 1 equiv of 2-acetylpyridine and 2 drops of formic acid are added to a solution of 1.2 equiv of β-naphthylamine in methanol. The colourless mixture is left to stir at room temperature in the dark, observing the progressive colour change to yellow. After 2.5 h, a suspension of 1 equiv of [Pd(cod)(CH_3)Cl] in methanol is added to the mixture, and the yellow colour intensifies. The mixture is left to stir for an additional 1.5 h, after which the resulting solid is filtered off and washed with cold diethyl ether.

14a. (yellow solid, 92 %) ^{1}H NMR (400 MHz, CD_2Cl_2, 298 K) *cis* = 93%, *trans* = 7%. *Cis*: δ = 9.14 (d, 1H, H^{6}), 8.59 (s, 1H, H^{i}), 8.20 (m, 1H, H^{15}), 8.10 (t, 1H, H^{4}), 7.98-7.83 (m, 3H, $H^{11,12,3}$), 7.81 (d, 1H, H^{5}), 7.63-7.51 (m, 3H, $H^{10,13,14}$), 7.23 (d, 1H, H^{9}), 0.35 (s, 3H, Pd-CH_3). *Trans*: δ = 8.75 (d, 1H, H^{6}), 8.49 (d, 1H, H^{i}), 8.32-8.30 (m, 1H, H^{15}), 8.16 (m, 1H, H^{4}), 8.00-7.77 (m, 3H, $H^{11,12,3}$) 7.74 (m, 1H, H^{5}), 7.63-7.51 (m, 3H, $H^{10,13,14}$), 7.19 (d, 1H, H^{9}), 1.12 (s, 3H, Pd-CH_3); ^{13}C NMR (400 MHz, CD_2Cl_2, 298 K) *Cis:* δ = 168.96 (C^{i}), 150.07 (C^{6}), 139.37 (C^{4}), 128.56-127.43 ($C^{11,12,3}$), 127.31-125.54 ($C^{10,13,14}$), 123.35 (C^{15}), 121.41 (C^{5}), 118.50 (C^{9}), -1.07 (Pd-CH_3).

15a. (yellow solid, 74 %)^{1}H NMR (500 MHz, CD_2Cl_2, 298 K) *cis* = 96%, *trans* = 4%. *Cis*: δ = 9.23 (d, 1H, H^{6}), 8.12 (t, 1H, H^{4}), 8.01-7.93 (m, 2H, $H^{12,13}$), 7.90-7.82 (m, 2H, $H^{11,15}$), 7.79 (t, 1H, H^{5}), 7.62-7.50 (m, 3H, $H^{10,13,14}$), 7.09 (d, 1H, H^{9}), 2.17 (s, 3H, $CH_3{}^{i}$), 0.11 (s, 3H, Pd-CH_3); ^{13}C NMR (500 MHz, CD_2Cl_2, 298 K) *Cis:* δ = 149.68 (C^{6}), 139.30 (C^{4}), 129.22 (C^{5}),

128.93,125.63 ($C^{12,13}$), 127.4,122.72 ($C^{11,15}$), 127.45-125.64 ($C^{10,13,14}$), 118.56 (C^{9}), 18.86 (CH_3^{i}), -1.06 (Pd-CH_3).

16a. (orange solid, 57 %) ^{1}H NMR (500 MHz, CD_2Cl_2, 298 K) *cis* = 96% , *trans* = 4%. *Cis:* δ = 9.25 (d, 1H, H^6), 8.12 (d, 1H, H^{15}), 7.95 (t, 1H, H^4), 7.81 (t, 1H, H^5), 7.795 (d, 1H, H^{12}), 7.63-7.57 (m, 2H, $H^{11,14}$), 7.53 (t, 1H, H^{13}), 7.36-7.26 (m, 5H, $H^{o',m',3,10,p}$), 7.00 (t, 1H, H^m), 6.94 (d, 1H, H^9), 6.81 (d, 1H, H^o), 0.13 (s, 3H, Pd-CH_3); ^{13}C NMR (500MHz, CD_2Cl_2, 298 K) *Cis*: δ = 149 (C^6), 139 (C^4), 130 (C^p), 129 ($C^{12,m,m'}$), 128 ($C^{5,3}$), 127 ($C^{13,14,11}$), 126 ($C^{o,o'}$), 125 (C^{10}), 123 (C^{15}), 119 (C^9), -0.58 (Pd-CH_3).

17a. (yellow solid, 69 %) ^{1}H NMR (500 MHz, CD_2Cl_2, 298 K) *cis* = 78%, *trans* = 22%. *Cis*: δ = 9.11 (d, 1H, H^6), 8.57 (s, 1H, H^i), 8.07 (t, 1H, H^4), 7.98-7.82 (m, 4H, $H^{3,10}$, $H^{11,14(o12,13)}$), 7.76 (t, 1H, H^5), 7.64 (s, 1H, H^{15}), 7.62-7.50 (m, 2H, $H^{12,13(o11,14)}$), 7.37 (d, 1H, H^9), 0.66 (s, 3H, Pd-CH_3). *Trans:* δ = 8.68 (d, 1H, H^6), 8.55 (s, 1H, H^i), 8.11 (t, 1H, H^4), 8.00 (s, 1H, H^{15}), 7.98-7.82 (m, 4H, $H^{3,10}$, $H^{11,14(o12,13)}$), 7.70-7.66 (m, 2H, $H^{5,9}$), 7.62-7.50 (m, 2H, $H^{12,13(o11,14)}$), 1.17 (s, 3H, Pd-CH_3); ^{13}C NMR (500 MHz, CD_2Cl_2, 298 K) *Cis:* δ = 167.84 (C^i), 149.94 (C^6), 139.25 (C^4), 129.34-127.31 ($C^{3,10}$, $C^{11,14(o12,13)}$), 129.18 (C^5), 127.44-127.26 ($C^{12,13(o11,14)}$), 122.01 (C^9), 120.21 (C^{15}), -0.03 (Pd-CH_3). *Trans:* δ = 161.51 (C^i), 149.13 (C^6), 139.25 (C^4), 129.34-127.31 ($C^{3,10}$, $C^{11,14(o12,13)}$), 128.61 (C^5), 127.44-127.26 ($C^{12,13(o11,14)}$), 122.43 (C^9), 121.91 (C^{15}), 0.71 (Pd-CH_3).

18a. (yellow solid, 49 %) *cis* = 95%, *trans* = 5%. *Cis*: δ = 9.19 (d, 1H, H^6), 8.09 (t, 1H, H^4), 7.98 (d, 1H, H^{10}) 7.96-7.85 (m, 3H, H^3, $H^{11,14(o12,13)}$), 7.76 (t, 1H, H^5), 7.61-7.48 (m, 2H, $H^{12,13(o11,14)}$), 7.40 (s, 1H, H^{15}), 7.14 (d, 1H, H^9), 2.29 (s, 3H, CH_3^{i}), 0.34 (s, 3H, Pd-CH_3). ^{13}C NMR (500 MHz, CD_2Cl_2, 298 K) *Cis:* δ = 149.61 (C^6), 139.24 (C^4), 129.83 (C^{10}), 129.07 (C^5), 128.34-125.53 (C^3, $C^{11,14(o12,13)}$), 127.54,126.78 ($C^{12,13(o11,14)}$), 121.49 (C^9), 119.52 (C^{15}), 19.06 (CH_3^{i}), -0.07 (Pd-CH_3).

19a. (orange solid, 90 %) ^{1}H NMR (500 MHz, CD_2Cl_2, 298 K) *cis* = 92% , *trans* = 8%. *Cis:* δ = 9.25 (d, 1H, H^6), 7.93 (t, 1H, H^4), 7.77-7.72 (m, 4H, $H^{5,10,12,15}$), 7.47-7.41 (m, 2H, $H^{13,14}$), 7.35 (d, 1H, H^3), 7.30-7.22 (m, 6H, $H^{o,m,p,11}$), 7.08 (d, 1H, H^9), 0.43 (s, 3H, Pd-CH_3); ^{13}C NMR (500MHz, CD_2Cl_2, 298 K) *Cis*: δ = 149 (C^6), 139 (C^4), 130 (C^p), 129 ($C^{12,11,m}$), 128 ($C^{3,5,10,15}$), 127 ($C^{13,14}$), 122 (C^9), 121 (C^o), 1.36 (Pd-CH_3).

20a. (yellow solid, 94 %)^{1}H NMR (500 MHz, CD_2Cl_2, 298 K) *cis* = 72%, *trans* = 28%. *Cis*: δ (ppm) = 9.12 (bd, 1H, $H^{6'}$), 8.63 (s, 1H, H^i), 8.51 (s, 2H, $H^{9,10}$), 8.12 (d, 1H, H^4), 8.10–8.00 (m, 3H, $H^{4',5,8}$), 7.86 (d, 1H, $H^{3'}$), 7.80 (d, 1H, H^1), 7.76 (ddd, 1H, $H^{5'}$), 7.56–7.50 (m, 2H, $H^{6,7}$), 7.38 (dd, 1H, $H^{3'}$), 0.71 (s, 3H, Pd–CH_3). *Trans*: δ (ppm) = 8.63 (d, 1H, $H^{6'}$), 8.59 (s, 1H, H^i), 8.55 (s, 1H, $H^{10(o9)}$), 8.43 (s,1H, $H^{9(o10)}$), 8.25 (s, 1H, H^1), 8.10–8.00 (m, 4H, $H^{4',4,5,8}$), 7.86 (d, 1H, $H^{3'}$), 7.67 (dd, 1H, H^3), 7.61 (ddd, 1H, $H^{5'}$), 7.56–7.50 (m, 2H, $H^{6,7}$), 1.18 (s, 3H, Pd–CH_3); ^{13}C NMR (125.68

MHz, CD_2Cl_2, 298 K). *Cis*: δ (ppm) = 167.05 (C^{i}), 149.42 ($C^{6'}$), 138.77 ($C^{4'}$), 129.38 (C^{4}), 128.78 ($C^{5'}$), 128.51 ($C^{5,8}$), 126.92 ($C^{3'}$), 126.84 ($C^{9,10}$), 126.07 ($C^{6,7}$), 121.89 (C^{3}), 119.54 (C^{1}), –0.88 (Pd–CH_3).

21a. (yellow solid, 88 %) ^{1}H–NMR (500 MHz, CD_2Cl_2, 298 K) *cis* = 94%, *trans* = 6%. *Cis*: δ (ppm) = 9.20 (d, 1H, $H^{6'}$), 8.52 (s, 1H, H^{10}), 8.47 (s, 1H, H^{9}), 8.16 (d, 1H, H^{4}), 8.13–8.00 (m, 3H, $H^{4',5,8}$), 7.95 (d, 1H, $H^{3'}$), 7.79–7.75 (m, 1H, $H^{5'}$), 7.55–7.48 (m, 3H, $H^{1,6,7}$), 7.15 (dd, 1H, H^{3}), 2.34 (s, 3H, $CH_3{}^{K}$), 0.40 (s, 3H, Pd–CH_3). *Trans*: δ (ppm) = 8.77 (d, 1H, $H^{6'}$), 8.49 (s, 1H, H^{10}), 8.45 (s, 1H, H^{9}), 8.16–8.14 (m, 1H, $H^{4'}$), 8.12–8.01 (m, 3H, $H^{4,5,8}$), 8.00 (d, 1H, $H^{3'}$), 7.71 (dd, 1H, $H^{5'}$), 7.55–7.48 (m, 2H, $H^{6,7}$), 7.22 (dd, 1H, H^{3}), 2.40 (s, 3H, $CH_3{}^{i}$), 1.02 (s, 3H, Pd–CH_3); ^{13}C–NMR (125.68 MHz, CD_2Cl_2, 298 K). *Cis*: δ (ppm) = 149.46 ($C^{6'}$), 139.09 ($C^{4'}$), 130.22 (H^{4}), 128.93 ($C^{5'}$), 128.47–128.20 ($C^{5,8}$), 126.87 (C^{10}), 126.64 (C^{9}), 126.20 ($C^{6,7}$), 125.36 ($C^{3'}$), 121.69 (C^{3}), 118.85 (C^{1}), 18.95 ($CH_3{}^{K}$), –0.19 (Pd–CH_3).

22a. (yellow solid, 81 %) ^{1}H–NMR (500 MHz, CD_2Cl_2, 298 K) *cis* = 95%, *trans* = 5%. *Cis*: δ (ppm) = 9.18 (d, 1H, $H^{6'}$), 8.72 (s, 1H, H^{9}), 8.67 (s, 1H, H^{i}), 8.55 (s, 1H, H^{10}), 8.12 (dt, 1H, $H^{4'}$), 8.09–8.04 (m, 3H, $H^{4,5,8}$), 7.88 (d, 1H, $H^{3'}$), 7.83 (ddd, 1H, $H^{5'}$), 7.56–7.50 (m, 3H, $H^{3,6,7}$), 7.22 (d, 1H, H^{2}), 0.35 (s, 3H, Pd–CH_3). *Trans*: δ (ppm) =8.82 (s, 1H, H^{9}), 8.77 (d, 1H, $H^{6'}$), 8.57 (s, 1H, H^{i}), 8.49 (s, 1H, H^{10}), 8.16 (t, 1H, $H^{4'}$), 8.13–8.04 (m, 2H, $H^{5,8}$), 8.01 (d, 1H, H^{4}), 7.89 (d, 1H, $H^{3'}$), 7.76 (t, 1H, $H^{5'}$), 7.56–7.47 (m, 3H, $H^{3,6,7}$), 7.17 (d, 1H, H^{2}), 1.14 (s, 3H, Pd–CH_3); ^{13}C–NMR (125.68 MHz, CD_2Cl_2, 298 K). *Cis*: δ (ppm) = 168.77 (C^{i}), 149.72 ($C^{6'}$), 139.06 ($C^{4'}$), 129.31 ($C^{5'}$), 128.68–128.37 ($C^{4,5,8}$), 127.21 ($C^{3'}$), 127.06 (C^{10}), 126.48 ($C^{3(o6,7)}$), 124.28 ($C^{6,7(o3)}$), 121.98 (C^{9}), 117.42 (C^{2}), –0.95 (Pd–CH_3).

5.4.3. Synthesis and characterization of [Pd(CH_3)($NCCH_3$)(N–N')][X] ***14b–22b.***

General procedure: To 1 equiv. of the neutral precursor dissolved in 6 mL of distilled dichloromethane, 1.2 equiv. of $AgPF_6$ salt dissolved in 1.5 mL of dry acetonitrile were added. The reaction mixture was left to stir in the dark for 2.5 h. The suspension of AgCl was filtered over Celite® and washed with dichloromethane. The solution was then concentrated under reduced pressure and diethyl ether was added to favour the precipitation of the product. The bright yellow solids were then filtered under reduced pressure, washed with cold diethyl ether and dried under vacuum.

14b. (yellow solid, 70 %) ^{1}H NMR (500 MHz, CD_2Cl_2, 298 K) *cis* = 31%, *trans* = 69%. *Cis:* δ = 8.84 (d, 1H, H^{6}), 8.58 (s, 1H, H^{i}), 8.24 (t, 1H, H^{4}), 8.06 (d, 1H, H^{15}), 8.02-7.91 (m, 4H, $H^{3,5,11,12}$), 7.72-7.55 (m, 3H, $H^{10,13,14}$), 7.25 (d, 1H, H^{9}), 2.50 (s, 3H, Pd-$NCCH_3$), 0.50 (s, 3H,

Pd-CH_3). *Trans:* δ = 8.69 (s, 1H, H^i), 8.64 (d, 1H, H^6), 8.38 (d, 1H, H^{15}), 8.31 (t, 1H, H^4), 8.14 (d, 1H, H^3), 8.02-7.91 (m, 2H, $H^{11,12}$), 7.84 (t, 1H, H^5), 7.72-7.55 (m, 3H, $H^{10,13,14}$), 7.31 (d, 1H, H^9), 1.42 (s, 3H, Pd-$NCCH_3$), 1.23 (s, 3H, Pd-CH_3); ^{13}C NMR (500 MHz, CD_2Cl_2, 298 K) *Cis:* δ = 172.68 (C^i), 150.07 (C^6), 140.87 (C^4), 131.33-128.88 ($C^{3,5,11,12}$), 127.94-125.75 ($C^{10,13,14}$), 122.75 (C^{15}), 118.85 (C^9), 3.92 (Pd-CH_3), 3.64 (Pd-$NCCH_3$). *Trans*: δ = 164.41 (C^i), 150.07 (C^6), 141.61 (C^4), 131.33-128.88 ($C^{11,12}$), 130.34 (C^3), 129.67 (C^5), 127.94-125.75 ($C^{10,13,14}$), 124.24 (C^{15}), 118.08 (C^9), 3.48 (Pd-CH_3), 2.14 (Pd-$NCCH_3$).

15b. (yellow solid, 83 %)^{1}H NMR (500 MHz, CD_2Cl_2, 298 K) *cis* = 65%, *trans* = 35%. *Cis:* δ = 8.82 (d, 1H, H^6), 8.26 (t, 1H, H^4), 8.09 (d, 1H, H^3), 8.04-7.87 (m, 3H, $H^{5,11,12}$), 7.76 (d, 1H, H^{15}), 7.69-7.54 (m, 3H, $H^{10,13,14}$), 7.09 (d, 1H, H^9), 2.47 (s, 3H, Pd-$NCCH_3$), 2.28 (s, 3H, $CH_3{}^i$), 0.26 (s, 3H, Pd-CH_3). *Trans:* δ = 8.66 (d, 1H, H^6), 8.35 (t, 1H, H^4), 8.17 (d, 1H, H^3), 8.04-7.87 (m, 3H, $H^{11,12,15}$), 7.85 (t, 1H, H^5), 7.69-7.54 (m, 3H, $H^{10,13,14}$), 7.12 (d, 1H, H^9), 2.41 (s, 3H, $CH_3{}^i$), 1.40 (s, 3H, Pd-$NCCH_3$), 1.05 (s, 3H, Pd-CH_3); ^{13}C NMR (500 MHz, CD_2Cl_2, 298 K) *Cis:* δ = 150.30 (C^6), 140.78 (C^4), 131.05-128.09 ($C^{5,11,12}$), 127.69-125.62 ($C^{10,13,14}$), 127.03 (C^3), 122.00 (C^{15}), 118.85 (C^9), 19.32 ($CH_3{}^i$), 3.80 (Pd-CH_3), 3.64 (Pd-$NCCH_3$). *Trans:* δ = 150.06 (C^6), 141.58 (C^4), 131.05-128.02 ($C^{11,12}$), 129.56 (C^5), 127.69-125.62 ($C^{10,13,14}$), 123.07 (C^{15}), 117.61 (C^9), 18.15 ($CH_3{}^i$), 3.21 (Pd-CH_3), 1.87 (Pd-$NCCH_3$).

16b. (yellow solid, 70 %) ^{1}H NMR (500 MHz, CD_2Cl_2, 298 K) *cis* = 44% , *trans* = 56%. *cis:* δ = 8.87 (d, 1H, H^6), 8.09 (t, 1H, H^4), 8.00-7.97 (m, 2H, $H^{15,5}$), 7.85 (t, 1H, H^{12}), 7.63-7.53 (m, 3H, $H^{11,14,13}$), 7.49 (m, 1H, H^3), 7.36 (d, 1H, $H^{m'}$), 7.35-7.28 (m, 3H, $H^{o',p,10}$), 7.01 (t, 1H, H^m), 6.915 (d, 1H, H^9), 6.79 (d, 1H, H^o), 2.50 (s, 3H, Pd-$NCCH_3$), 0.24 (s, 3H, Pd-CH_3). *trans:* δ = 8.70 (d, 1H, H^6), 8.22 (d, 1H, H^{15}), 8.17 (t, 1H, H^4), 7.90 (d, 1H, H^{12}), 7.85 (t, 1H, H^5), 7.71-7.63 (m, 4H, $H^{3,11,13,14}$), 7.53-7.49 (m, 2H, $H^{o',m'}$), 7.45-7.40 (m, 1H, H^p), 7.35-7.28 (m, 1H, H^{10}), 7.10 (t, 1H, H^m), 6.84 (d, 1H, H^o), 6.76 (d, 1H, H^9), 1.28 (s, 3H, Pd-$NCCH_3$), 1.11 (s, 3H, Pd-CH_3); ^{13}C NMR (500MHz, CD_2Cl_2, 298 K) *cis*: δ = 150 (C^6), 140 (C^4), 131 ($C^{p,5}$), 130.03 (C^3), 129 ($C^{12,m',m}$), 128 (C^{10}), 127 ($C^{11,14,13}$), 126 ($C^{o,o'}$), 120 (C^9), 4.40 (Pd-CH_3), 3.84 (Pd-$NCCH_3$). *trans:* δ = 150 (C^6), 141 (C^4), 131 ($C^{p,3}$), 130 (C^m), 129 ($C^{m',o'}$), 128 ($C^{5,12}$), 127 ($C^{o,11,14}$), 12 (C^{15}), 118 (C^9), 3.70 (Pd-CH_3), 1.82 (Pd-$NCCH_3$)

17b. (yellow solid, 80%) ^{1}H NMR (500 MHz, CD_2Cl_2, 298 K) *cis* = 25%, *trans* = 75%. *Cis:* δ = 8.77 (d, 1H, H^6), 8.57 (s, 1H, H^i), 8.22 (t, 1H, H^4), 8.07-7.90 (m, 5H, $H^{3,5,10}$, $H^{11,14(o12,13)}$), 7.67-7.57 (m, 3H, $H^{12,13(o11,14)}$, H^{15}), 7.30 (d, 1H, H^9), 2.52 (s, 3H, Pd-$NCCH_3$), 0.81 (s, 3H, Pd-CH_3). *Trans:* δ = 8.68 (s, 1H, H^i), 8.60 (d, 1H, H^6), 8.27 (t, 1H, H^4), 8.12 (d, 1H, H^3), 8.07-7.90 (m, 3H, H^{10}, $H^{11,14(o12,13)}$), 7.86 (s, 1H, H^{15}), 7.80 (t, 1H, H^5), 7.67-7.57 (m, 2H, $H^{12,13(o11,14)}$), 7.52 (d, 1H, H^9), 2.17 (s, 3H, Pd-$NCCH_3$), 1.27 (s, 3H, Pd-CH_3) ; ^{13}C NMR (500

MHz, CD_2Cl_2, 298 K) *Trans:* δ = 163.21 (C^{i}), 149.84 (C^{6}), 141.58 (C^{4}), 130.27 (C^{3}), 130.12 (C^{10}), 129.42 (C^{5}), 128.84-128.43 ($C^{11,14(o12,13)}$), 128.08 ($C^{12,13(o11,14)}$), 120.77 (C^{15}), 120.71 (C^{9}), 4.40 (Pd-CH_3), 3.56 (Pd-NCCH_3).

18b. (yellow solid, 84 %)^{1}H NMR (500 MHz, CD_2Cl_2, 298 K) *cis* = 50%, *trans* = 50%. *Cis:* δ = 8.76 (d, 1H, H^{6}), 8.24 (t, 1H, H^{4}), 8.07 (m, 1H, H^{3}), 8.02 (m, 1H, H^{10}), 7.99-7.85 (m, 3H, $H^{5,11,14}$), 7.65-7.54 (m, 2H, $H^{12,13}$), 7.38 (s, 1H, H^{15}), 7.09 (d, 1H, H^{9}), 2.49 (s, 3H, Pd-NCCH_3), 2.39 (s, 3H, CH_3^{i}), 0.49 (s, 3H, Pd-CH_3). *Trans*: δ = 8.63 (d, 1H, H^{6}), 8.30 (t, 1H, H^{4}), 8.13 (d, 1H, H^{3}), 8.02 (m, 1H, H^{10}), 7.99-7.85 (m, 2H, $H^{11,14}$), 7.81 (t, 1H, H^{5}), 7.65-7.54 (m, 2H, $H^{12,13}$), 7.48 (s, 1H, H^{15}), 7.22 (d, 1H, H^{9}), 2.48 (s, 3H, CH_3^{i}), 1.70 (s, 3H, Pd-NCCH_3), 1.08 (s, 3H, Pd-CH_3) ; ^{13}C NMR (500 MHz, CD_2Cl_2, 298 K) *Cis:* δ = 150.20 (C^{6}), 140.77 (C^{4}), 130.87 (C^{5}), 130.22 (C^{10}), 128.43-128.37 ($C^{11,14}$), 128.13-127.73 ($C^{12,13}$), 126.92 (C^{3}), 120.88 (C^{9}), 119.76 (C^{16}), 19.58 (CH_3^{i}), 4.81 (Pd-CH_3), 3.70 (Pd-NCCH_3). *Trans:* δ = 150.03 (C^{6}), 141.55 (C^{4}), 130.22 (C^{10}), 129.46 (C^{5}), 128.27 (C^{3}), 128.43-128.37 ($C^{11,14}$), 128.13-127.73 ($C^{12,13}$), 120.73 (C^{9}), 119.14 (C^{15}), 18.12 (CH_3^{i}), 3.26 (Pd-CH_3), 2.75 (Pd-NCCH_3).

19b. (yellow solid, 65 %) ^{1}H NMR (500 MHz, CD_2Cl_2, 298 K) *cis* = 42%, *trans* = 58%. *Cis:* δ = 8.87 (d, 1H, H^{6}), 8.07 (t, 1H, H^{4}), 7.96 (t, 1H, H^{5}), 7.80-7.74 (m, 3H, $H^{10,11,14}$), 7.50-7.43 (m, 6H, $H^{3,12,13,m,p}$), 7.47-7.30 (m, 3H, $H^{o,15}$), 7.02 (d, 1H, H^{9}), 2.53 (s, 3H, Pd-NCCH_3), 0.57 (s, 3H, Pd-CH_3). *Trans:* δ = 8.715 (d, 1H, H^{6}), 8.14 (t, 1H, H^{4}), 7.80-7.74 (m, 4H, $H^{5,10,11,14}$), 7.61 (d, 1H, H^{3}), 7.50-7.43 (m, 6H, $H^{12,13,m,p}$), 7.47-7.30 (m, 3H, $H^{o,15}$), 7.07 (d, 1H, H^{9}), 1.72 (s, 3H, Pd-NCCH_3), 1.21 (s, 3H, Pd-CH_3); ^{13}C NMR (500MHz, CD_2Cl_2, 298 K) *cis*: δ = 15 (C^{6}), 140 (C^{4}), 131 (C^{3}), 130 (C^{5}), 129 ($C^{m,p,10.o}$) 12 ($C^{11,14}$), 127 ($C^{12,13}$), 122 (C^{9}), 4.84 (Pd-CH_3), 3.54 (Pd-NCCH_3). *trans:* δ = 150 (C^{6}), 141 (C^{4}), 131 (C^{3}) 130 ($C^{m,p}$) 129 ($C^{5,10,o}$), 128 ($C^{11,14}$), 127 ($C^{12,13}$), 121 (C^{9}), 3.36 (Pd-CH_3), 2.36 (Pd-NCCH_3).

20b. (orange solid, 55 %) ^{1}H NMR (500 MHz, CD_3NO_2, 273 K) *cis* = 17%, *trans* = 83%. *Cis*: δ (ppm) = 8.80 (s, 1H, H^{i}), 8.72 (d, 1H, $H^{6'}$), 8.65–8.57 (m, 2H, $H^{9,10}$), 8.36–8.32 (m, 1H, $H^{4'}$), 8.22–8.10 (m, 4H, $H^{4,3',5,8}$), 7.96–7.92 (m, 2H, $H^{5',1}$), 7.62–7.55 (m, 2H, $H^{6,7}$), 7.42 (dd, 1H, H^{3}), 2.57 (s, 3H, Pd–NCCH_3), 0.75 (s, 3H, Pd–CH_3). *Trans*: δ (ppm) = 8.84 (s, 1H, H^{i}), 8.68 (d, 1H, H^{9}), 8.65–8.57 (m, 2H, $H^{6',10}$), 8.36–8.32 (m, 1H, $H^{4'}$), 8.27 (d, 1H, H^{4}), 8.22–8.10 (m, 4H, $H^{3',1,5,8}$), 7.86 (td, 1H, $H^{5'}$), 7.66 (dd, 1H, H^{3}), 7.62–7.55 (m, 2H, $H^{6,7}$), 2.31 (s, 3H, Pd–NCCH_3), 1.21 (s, 3H, Pd–CH_3); ^{13}C NMR (125.68 MHz, CD_3NO_2, 273 K). *Cis*: δ (ppm) = 173.57 (C^{i}), 150.52 ($C^{6'}$), 141.56 ($C^{4'}$), 131.11 ($C^{5'}$), 129.75 ($C^{3'}$), 130.44 (C^{4}), 129.25 ($C^{5,8}$), 128.44–127.44 ($C^{9,10}$), 127.52 ($C^{6,7}$), 122.88 (C^{3}), 120.92 (C^{1}), 3.25 (Pd–CH_3), 3.24 (Pd–NCCH_3). *Trans*: δ (ppm) = 164.61 (C^{i}), 150.73

($C^{6'}$), 142.17 ($C^{4'}$), 131.11 (C^{4}), 130.68 ($C^{3'}$), 130.01 ($C^{5'}$), 129.25 ($C^{5,8}$), 128.45 (C^{9}), 127.83 (C^{10}), 127.52 ($C^{6,7}$), 121.85 (C^{3}), 121.75 (C^{1}), 3.29 (Pd–CH_3), 3.08 (Pd–$NCCH_3$).

21b. (yellow solid, 78 %)^{1}H–NMR (500 MHz, CD_3NO_2, 273 K) *cis* = 48%, *trans* = 52%. *Cis*: δ (ppm) = 8.75 (dd, 1H, $H^{6'}$), 8.63 (s, 1H, H^{10}), 8.58 (s, 1H, H^{9}), 8.35 (dt, 1H, $H^{4'}$), 8.32–8.24 (m, 2H, $H^{4,3'}$), 8.14–8.08 (m, 2H, $H^{5,8}$), 7.94 (ddd, 1H, $H^{5'}$), 7.68 (s, 1H, H^{1}), 7.59–7.55 (m, 2H, $H^{6,7}$), 7.24 (dd, 1H, H^{3}), 2.54 (s, 3H, Pd–$NCCH_3$), 2.53 (s, 3H, CH_3^K), 0.43 (s, 3H, Pd–CH_3). *Trans*: δ (ppm) = 8.68 (dd, 1H, $H^{6'}$), 8.63 (s, 1H, H^{10}), 8.60 (s, 1H, H^{9}), 8.38 (dt, 1H, $H^{4'}$), 8.32–8.24 (m, 2H, $H^{4,3'}$), 8.14–8.08 (m, 2H, $H^{5,8}$), 7.88 (ddd, 1H, $H^{5'}$), 7.77 (s, 1H, H^{1}), 7.59–7.55 (m, 2H, $H^{6,7}$), 7.38 (dd, 1H, H^{3}), 2.60 (s, 3H, CH_3^K), 1.83 (s, 3H, Pd–$NCCH_3$), 1.02 (s, 3H, Pd–CH_3); ^{13}C–NMR (125.68 MHz, CD_3NO_2, 273 K). *Cis*: δ (ppm) = 149.89 ($C^{6'}$), 141.82 ($C^{4'}$), 131.02 (C^{4}), 130.70 ($C^{5'}$), 129.77–128.33 ($C^{5,8}$), 128.07 (C^{4}), 127.68 (C^{10}), 127.51 (C^{9}), 127.25–126.20 ($C^{6,7}$), 122.44 (C^{3}), 120.28 (C^{1}), 19.70 (CH_3^K), 3.51 (Pd–CH_3), 3.39 (Pd–$NCCH_3$). *Trans*: δ (ppm) = 150.58 ($C^{6'}$), 141.96 ($C^{4'}$), 130.77 (C^{4}), 129.84 ($C^{5'}$), 129.77–128.33 ($C^{5,8}$), 128.97 (C^{4}), 127.64 (C^{10}), 127.42 (C^{9}), 127.25–126.20 ($C^{6,7}$), 122.50 (C^{3}), 119.58 (C^{1}), 18.19 (CH_3^K), 2.46 (Pd–$NCCH_3$), 2.11 (Pd–CH_3).

22b. (orange/red brick solid, 95 %)^{1}H–NMR (500 MHz, CD_2Cl_2, 298 K) *cis* = 35%, *trans* = 65%. *Cis*: δ (ppm) = 8.88 (d, 1H, $H^{6'}$), 8.66 (s, 1H, H^{i}), 8.60 (s, 1H, H^{9}), 8.59 (s, 1H, H^{10}), 8.31 (dt, 1H, $H^{4'}$), 8.21–8.17 (m, 2H, $H^{5,8}$), 8.14–8.07 (m, 1H, H^{4}), 8.04 (d, 1H, $H^{3'}$), 8.01 (dd, 1H, $H^{5'}$), 7.63–7.56 (m, 2H, $H^{6,7}$), 7.55 (t, 1H, H^{3}), 7.25 (d, 1H, H^{2}), 2.49 (s, 3H, Pd–$NCCH_3$), 0.48 (s, 3H, Pd–CH_3). *Trans*: δ (ppm) = 8.91 (s, 1H, H^{9}), 8.78 (s, 1H, H^{i}), 8.67 (d, 1H, $H^{6'}$), 8.58 (s, 1H, H^{10}), 8.33 (dt, 1H, $H^{4'}$), 8.17 (d, 1H, $H^{3'}$), 8.14–8.07 (m, 3H, $H^{4,5,8}$), 7.86 (dt, 1H, $H^{5'}$), 7.63–7.56 (m, 3H, $H^{6,7,3}$), 7.31 (d, 1H, H^{2}), 1.25 (s, 3H, Pd–CH_3), 1.05 (s, 3H, Pd–$NCCH_3$); ^{13}C–NMR (125.68 MHz, CD_2Cl_2, 298 K). *Cis*: δ (ppm) = 172.43 (C^{i}), 150.74 ($C^{6'}$), 140.67 ($C^{4'}$), 130.96 ($C^{5'}$), 129.69 (C^{4}), 128.69 ($C^{3'}$), 128.47 ($C^{5,8}$), 127.56 (C^{10}), 126.98–126.84 ($C^{6,7}$), 124.34 (C^{3}), 121.19 (C^{9}), 117.98 (C^{2}), 3.98 (Pd–CH_3). *Trans*: 163.88 (C^{i}), 149.82 ($C^{6'}$), 141.43 ($C^{4'}$), 130.21 ($C^{3'}$), 129.96 (C^{4}),129.49 ($C^{5'}$), 128.35 ($C^{5,8}$), 127.23 (C^{10}), 126.98–126.84 ($C^{6,7}$), 125.04 (C^{3}), 123.17 (C^{9}), 117.21 (C^{2}), 4.28 (Pd–CH_3), 1.69 (Pd–$NCCH_3$).

5.4.4. CO/vinyl arene copolymerization reactions.

All the catalytic experiments were carried out at atmospheric carbon monoxide pressure in a three-necked, thermostated 75 mL glass reactor equipped with a magnetic stirrer. After establishment of the reaction temperature (303 K), the precatalyst (n_{Pd} = 12.7 x 10^{-6} mol), 1,4-benzoquinone ([BQ]/[Pd] = 5), vinyl arene (10 mL, [S]/[Pd] = 6800; [MS]/[Pd] = 6000; [TBS]/[Pd] = 4300) and TFE (20 mL) were added. CO was bubbled through the solution for 10 min; afterwards two 4 L

balloons previously filled with CO were connected to the reactor. After the desired time (24 h), the reaction mixture was poured into 100 mL of methanol and stirred for 1.5 h at room temperature. The solid was filtered off and washed thoroughly with methanol, then dried under vacuum to constant weight.

5.4.5. Preparation of copolymer samples for NMR spectroscopy.

70 mg of copolymer are weighted and dissolved in 0.70 mL of HFIP, to which 1.40 mL of CDCl3 are then added. 0.70 mL of the resulting solution are taken and used for the NMR analysis.

5.4.6. Recrystalization of CO/vinyl arene polyketones.

The polyketones were recrystalized to eliminate any possible trace of palladium metal due to decomposition of the catalyst. 250 mg of copolymer are dissolved in 20 mL of chloroform (or more, depending on the copolymer solubility). The solution is left to stir until complete dissolution of the copolymer, then filtered over Celite® and washed with additional chloroform. The solvent is partially removed until few millilitres of solution are obtained. The solution is slowly dropped into 40 mL of ethanol, observing precipitation of a white solid that is then filtered off, washed with additional ethanol and left to dry under reduced pressure.

When the polyketones are unsoluble in chloroform another procedure is applied:[cit 46 tesi MF] 200 mg of copolymer are suspended in 20 mL of ethyl acetate ad left under stirring at room temperature for 4 h. The polymer is then filtered off, washed with the same solvent and dried, and then re-suspended in diethyl ether and left to stir at room temperature for an additional 2 h. The solid is then filtered off, washed with diethyl ether and dried under vacuum.

5.5. Bibliography

1. a) Sen, A.; Lai, T.W., *J. Am. Chem. Soc.*, **1982**, 104, 3520; b) Drent, E.; Budzelaar, P.H.M., *Chem. Rev.*, **1996**, *96*, 663; c) Nozaki, K.; Hiyama, T., *J. Organomet. Chem.*, **1999**, *576*, 248; d) Bianchini, C.; Meli, A., *Coord. Chem. Rev.*, **2002**, *225*, 35; e) Mul W.P.; van der Made A.W.; Smaardijk A.A.; Drent, E., in *Catalytic Synthesis of Alkene-Carbon Monoxide Copolymers and Cooligomers*, Ed.: A. Sen, Kluwer Academic Publisher, **2003**, Capitolo 4, p. 87; f) Belov, G.P.; Novikova, E.V., *Russian Chem. Rev.*, **2004**, *73* (3), 267.

2. Milani, B.; Crotti, C.; Farnetti, E., *Dalton Trans.*, **2008**, 4659.

3. Reppe, W.; Magin, A., *US Pat. 2577208*, **1950**; *Chem. Abstr.*, **1952**, *46*, 6143c.

4. Gough, A., *British Pat. 1081304*, **1967**; *Chem. Abstr.*, **1967**, *67*, 100569.

5. Sen, A.; Lai, T.W., *Organometallics*, **1984**, *3*, 866.

6. a) Drent, E., *Eur. Pat. Appl. 121965 A2*, **1984**; *Chem. Abstr.*, **1985**, *102*, 46423; b) Drent, E.; Van Broekhoven, J.A.M.; Doyle, M.J., *J. Organomet. Chem.*, **1991**, *417*, 235.

7. a) Garbassi, F., *CHEMTEC*, **1999**, *29*, 48; b) Alperwicz, N., *Chem. Week.*, **1995**, *22*.

8. http://www.poly-ketone.com/utl/web/mediadownload.do?subpath=/download/catalogEn/poketone_catalogue2017_en.pdf

9. Pisano, C.; Mezzetti, A.; Consiglio, G., *Organometallics*, **1992**, *11*, 20.

10. a) Milani, B.; Scarel, A.; Mestroni, G.; Gladiali, S.; Taras, R.; Carfagna, C.; Mosca, L., *Organometallics*, **2002**, *21*, 1323; b) Milani, B.; Anzilutti, A.; Vicentini, L.; Sessanta o Santi, A.; Zangrando, E.; Geremia, S.; Mestroni, G., *Organometallics*, **1997**, *16*, 5064.

11. a) Brookhart, M.; Wagner, M.I.; Balavoine, G.G.A.; Haddou, H.A., *J. Am. Chem. Soc.*, **1994**, *116*, 3641; b) Carfagna, C.; Gatti, G.; Martini, D.; Pettinari, C., *Organometallics*, **2001**, *20*, 2175; c) Durand, J.; Zangrando, E.; Stener, M.; Fronzoni, G.; Carfagna, C.; Binotti, B.; Kamer, P.C.J.; Muller, C.; Caporali, M.; van Leeuwen, P.W.N.M.; Vogt, D.; Milani, B., *Chem. Eur. J.*, **2006**, *12*, 7639; d) Rosar, V.; Meduri, A.; Montini, T.; Fini, F.; Carfagna, C.; Fornasiero, P.; Balducci, G.; Zangrando, E.; Milani, B., *ChemCatChem*, **2014**, *6*, 2403; e) Rosar, V.; Dedeic, D.; Nobile, T.; Fini, F.; Balducci, G.; Alessio, E.; Carfagna, C.; Milani, B., *Dalton Trans.*, **2016**, *45*, 14609; f) Canil, G.; Rosar, V.; Dalla Marta, S.; Bronco, S.; Fini, F.; Carfagna, C.; Durand, J.; Milani, B., *ChemCatChem*, **2015**, *7*, 2255.

12. Barsacchi, M.; Consiglio, G.; Medici, L.; Petrucci, G.; Suter, U.W., *Angew. Chem. Int. Ed. Engl.*, **1991**, *8*, 989.

13. Milani, B.; Alessio, E.; Mestroni, G.; Zangrando, E.; Randaccio, L.; Consiglio, G., *J. Chem. Soc., Dalton Trans.*, **1996**, 1021.

14. a) Aeby, A.; Consiglio, G., *Inorg. Chim. Acta*, **1999**, *296*, 45; b) Sirbu, D.; Consiglio, G.; Gischig, S., *J. Organomet. Chem.*, **2006**, *691*, 1143.
15. a) Sperrle, M.; Aeby, A.; Consiglio, G.; Pfaltz, A., *Helv. Chim. Acta*, **1996**, *79*, 1387; b) Aeby, A.; Bangerter, F.; Consiglio, G., *Helv. Chim. Acta*, **1998**, *81*, 764; c) Aeby A.; Gsponer, A.; Consiglio, G., *J. Am. Chem. Soc.*, **1998**, *120*, 11000; d) Gsponer, A.; Consiglio, G., *Helv. Chim. Acta*, **2003**, *86*, 2170; e) Nozaki, K.; Sato, N.; Takaya, H., *J. Am. Chem. Soc.*, **1995**, *117*, 9911; f) Iggo, J.A.; Kawashima, Y.; Liu, J.; Hiyama, T.; Nozaki, K., *Organometallics*, **2003**, *22*, 5418.
16. Corradini, P.; De Rosa, C.; Panuzi, A.; Petrucci, G.; Pino, P., *Chimia*, **1990**, *44*, 52.
17. Barsacchi, M.; Batistini, A.; Consiglio, G.; Suter, U.W., *Macromolecules*, **1992**, *25*, 3604.
18. a) Consiglio, G.; Milani, B., in *Catalytic synthesis of alkene-carbon monoxide copolymers and cooligomers* Ed. Ayusman Sen, Kluwer Academic Press, **2003**, Capitolo 6, p. 189; b) Durand, J.; Milani, B., *Coord. Chem. Rev.*, **2006**, *250*, 542; c) Milani, B.; Masdeu-Bultò, A. M., in *Organometallic Chirality* Ed. G. Pályi, C. Zucchi e L. Caglioti Mucchi Editore, **2008**, Chapter 8, 161.
19. a) Carfagna, C.; Gatti, G.; Paoli, P.; Binotti, B.; Fini, F.; Passeri, A.; Rossi, P.; Gabriele, B., *Organometallics*, **2014**, *33*, 129; b) Carfagna, C.; Gatti, G.; Paoli, P.; Rossi, P., *Organometallics*, **2009**, *28*, 3212.
20. Brookhart, M.; Rix, F.C.; DeSimone, J.M.; Barborak, J.C., *J. Am. Chem. Soc.*, **1992**, *114*, 5894.
21. Carfagna, C.; Gatti, G.; Martini, D.; Pettinari, C., *Organometallics*, **2001**, *20*, 2175.
22. Milani, B.; Corso, G.; Mestroni, G.; Carfagna, C.; Formica, M.; Seraglia, R., *Organometallics*, **2000**, *19*, 3435.
23. Brookhart, M.; Wagner, M.I.; Balavoine, G.G.A.; Haddou, H.A., *J. Am. Chem. Soc.*, **1994**, *116*, 3641
24. Bartolini, S.; Carfagna, C.; Musco, A., *Macromol. Rapid Commun.*, **1995**, *16*, 9.
25. Reetz, M-T.; Haderlein; G.; Angermund, K., *J. Am. Chem. Soc.*, **2000**, *122*, 996.
26. Schatz, A.; Scarel, A.; Zangrando, E.; Mosca, L.; Carfagna, C.; Gissibl, A.; Milani, B.; Reiser, O., *Organometallics*, **2006**, *25*, 4065.
27. Sen, A.; Jiang, Z., *Macromolecules*, **1993**, *26*, 911
28. Bastero, A.; Ruiz, A.; Reina, J.A.; Claver, C.; Guerrero, A.M.; Jalon, F.A.; Manzano, B.R., *J. Organomet. Chem.*, **2001**, *619*, 287.
29. Aeby, A.; Consiglio, G., *Inorg. Chim. Acta*, **1999**, *296*, 45.
30. Meduri, A.; Cozzula, D.; D'Amora, A.; Zangrando, E.; Gladiali, S.; Milani, B., *Dalton Trans.*, **2012**, *41*, 7474.

31. Nozaki, K.; Komaki, H.; Kawashima, Y.; Hiyama, T.; Matsubara, T., *J. Am. Chem. Soc.*, **2001**, *123*, 534.

32. Jiang, Z.; Adams, S.E.; Sen, A., *Marcomolecules*, **1994**, *27*, 2694.

33. Bianchini, C.; Lee, H.M.; Mantovani, G.; Meli, A., *New J. Chem.*, **2002**, *26*, 387.

34. Benito, J. M.; de Jesus, E.; de la Mata, F.J.; Flores, J.C.; Gomez, R., *Organometallics*, **2006**, *25*, 3045.

35. a) Dinda, J.; Sinha, C., *Transition Metal Chemistry*, **2003**, *28*, 864; b) Koppl, A.; Alt, H.G., *J. Mol. Cat. A: Chem.*, **2000**, *154*, 45.

36. Qian, C., Gao, F., Chen, Y., Gao, L. Synlett. 2003, 10, 1419.

37. a) Chen Z.; Allen E. K.; White S. P.; Daugulis O.; Brookhart M., *Organometallics*, **2016**, *35*, 1756; b) Zhang, L., Yue, E., Liu, B., Serp, P., Redshaw, C., Sun, W-H., Durand, J. *Catalysis Communication* **2014**, *43*, 227.

38. Amoroso, F.; Zangrando, E.; Carfagna, C.; Muller, C.; Vogt, D.; Hagar, M.; Ragaini, F.; Milani, B., *Dalton Trans*., **2013**, *42*, 14583.

OTHER PROJECTS

N-S and P-P donor ligands in Pd(II) catalyzed copolymerization reactions.

With the aim of investigate further the concept of ligand desymmetrisation presented in *Chapter 2*, thiophenylimines (Figure 1a) have been considered as potential ancillary ligands for Pd(II). A series of Pd(II) complexes with thiophenylimines has been synthesized and characterized both in solution and in solid state and will be tested later on in the copolymerization reactions of interest. The work on P-P donor ligands has been done partly in collaboration with the group of Prof. Paolo Tecilla (UniTs) and partly in collaboration with the group of Prof. Matthias Beller and Dr. Ralf Jackstell (LIKAT, Rostock).

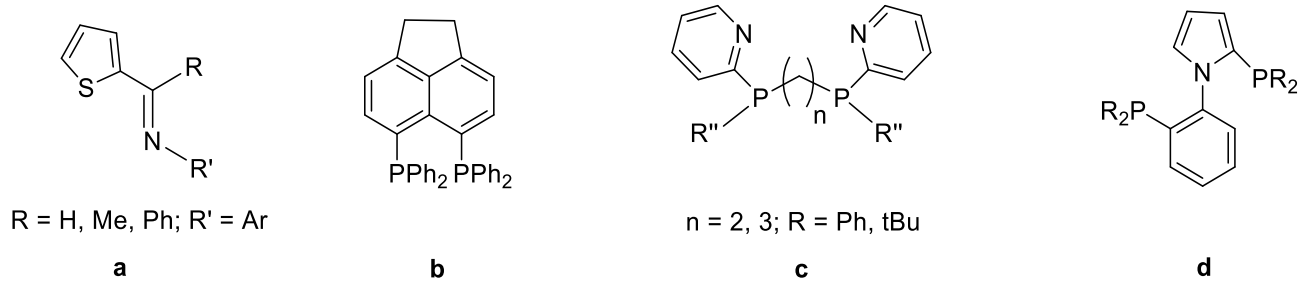

Figure 1. N-S and P-P donor ligands tested.

In the first case, an acenaphthene-derived P-P ligand (DppAc, Figure 1b) was the focus of our investigation, and its coordination chemistry to Pd(II) was evaluated by synthesizing the neutral complex [Pd(DppAc)(CH_3)Cl] and the cationic complexes [Pd(DppAc)(CH_3)(L)][SbF_6] (where L = CH_3CN, 3,5-lutidine) and [Pd(DppAc)(μ-OH)]$_2$[SbF_6]$_2$, all characterized by NMR spectroscopy and, when possible, by X-ray diffraction. A preliminary study of the reactivity of complex [Pd(DppAc)(CH_3)(CH_3CN)][SbF_6] shows that it reacts fast with the olefin, and it represents an efficient and selective catalyst for the dimerization of ethylene to *cis*-2-butene; moreover, several organometallic intermediates are found, and in particular the species having the Pd-CH_2CH_3 fragment represents the catalyst resting state. The complex will be tested in the homopolymerization of ethylene and in the copolymerization of ethylene and methyl acrylate.

I've spent 3 months (Sept 2018- Dec 2018) at the Leibniz-Institut für Katalyse, Rostock, in the group of Prof. Matthias Beller, supported by a DAAD scholarship. The main objective of this research program deals with the investigation of homogeneous catalysts for the copolymerization of carbon monoxide with ethylene. The focus was the study of in situ catalytic systems based on Pd(II) salts ($Pd(OAc)_2$ and $Pd(TFA)_2$, where OAc= acetate, TFA= trifluoroacetate) and P-P donor ligands (Figure 1c, 1d). A catalytic study varying the reaction conditions was performed, and also higher olefins, such as 1- and 2-octene and butenes, were tested. As a side project, I've also studied the hydrogenation of carbonates catalysed by non-noble metals, that resulted in a publication.

Publications

1. Baron, M.; Dall'Anese, A.; Tubaro, C.; Orian, L.; Di Marco, V.; Bogialli, S.; Graiff, C.; Basato, M. "A square planar gold(III) bis-(1,1′-dimethyl-3,3′-methylene-diimidazol-2,2′-diylidene) trication as an efficient and selective receptor towards halogen anions: the cooperative effect of Au···X and X···HC interactions" *Dalton Trans*., **2018**, *47*, 935. I.F. = 4.052, N.C. = 4

2. Milocco, F.; de Vries, F.; Dall'Anese, A.; Rosar, V.; Zangrando, E.; Otten, E.; Milani, B. "Palladium alkyl complexes with a formazanate ligand: synthesis, structure and reactivity" *Dalton Trans*., **2018**, *47*, 14445. I.F. = 4.052, N.C. = 3

3. Ferretti, F.; Scharnagl, F. K.; Dall'Anese, A.; Jackstell, R.; Dagstir, S.; Beller, M. "Additive-free cobalt-catalysed hydrogenation of carbonates to methanol and alcohols" *Catal. Sci. Technol.* **2019**, *9*, 3548. I.F. = 5.726, N.C. = 1

4. Dall'Anese, A.; Rosar, V.; Cusin, L.; Montini, T.; Balducci, G.; D'Auria, I.; Pellecchia, C.; Fornasiero, P.; Felluga, F.; Milani, B. "Palladium-Catalyzed Ethylene/Methyl Acrylate Copolymerization: Moving from the Acenaphthene to the Phenanthrene Skeleton of α-Diimine Ligands" *Organometallics*, **2019**, *38*, 3498. I.F. = 4.1, N.C. = 0

Conference partecipation

1. A. Dall'Anese, F. Felluga, G. Balducci, B. Milani
"Effect of the α-diimine skeleton in Pd(II)-catalyzed copolymerization reactions"
Poster 15, presented by Dall'Anese A., accepted for flash presentation
Assignee of grant to attend the **11th International School of Organometallic Chemistry**, Camerino (Italy) September 2nd-September 6th 2017

2. A. Dall'Anese, T. Montini, G. Balducci, P. Fornasiero, F. Felluga, B. Milani
"From acenaphthene to phenanthrene: effect of the skeleton in Pd(II)-α-diimine catalysts for the copolymerization of ethylene with methyl acrylate"
Oral Communication, presented by A. Dall'Anese
XV PhD Day – TRIESTE organized by CIRCC (Consorzio Interuniversitario Reattività Chimica e Catalisi), April 6th, 2018

3. A. Dall'Anese, T. Montini, P. Fornasiero, F. Felluga, G. Balducci, B. Milani
"Pd(II)-α-diimines catlysts for functionalized polyolefin synthesis: from the acenaphthene to the phenanthrene skeleton"
Poster, presented by A. Dall'Anese
28th International Conference on Organometallic Chemistry (ICOMC), Florence, July 15th-20th, 2018. - Book of Abstract: P048

4. A. Dall'Anese, T. Montini, P. Fornasiero, F. Felluga, G. Balducci, B. Milani
"Pd(II)-catalysed copolymerization reactions: effect of symmetrical and nonsymmetrical α-diimines with a phenanthrene skeleton"
Oral communication, presented by A. Dall'Anese

XLVI Congresso Nazionale di Chimica Inorganica, Bologna, September 10th-13th, 2018 – Book of abstract: OC51

5. A. Dall'Anese, G. Balducci, F. Felluga, T. Montini, C. Pellecchia, P. Fornasiero, B. Milani
"Electron-rich metal cations in the copolymerization of ethylene and methyl acrylate"
Flash communication and poster, presented by A. Dall'Anese
XII International School on Organometallic Chemistry "Marcial Moreno Mañas", Castellon de la Plana, June 12th-14th, 2019 – Book of abstract: FP-7

6. A. Dall'Anese, M. Degrassi, G. Balducci, T. Montini, P. Fornasiero, B. Milani
"Ligand desymmetrization: application of Pd(II)-pyridilimine complexes in copolymerization reactions"
Oral communication, presented by A. Dall'Anese
XXIII European Conference on Organometallic Chemistry, Helsinki, June 16th-20th, 2019 – Book of abstract: O38

ACKNOWLEDGEMENTS

The research project of this PhD thesis involves some collaborations related to specific aspects. In particular, I want to thank:

Dr. Gabriele Balducci of University of Trieste for the X-ray structure analysis (Chapter 2-5);

Prof. Tiziano Montini and Prof. Paolo Fornasiero of University of Trieste for the GC-MS analysis of some catalytic products (Chapter 2 and 3);

Prof. Carla Carfagna of University of Bologna for the measurement of the molecular weight of the synthesized CO/vinyl arene copolymers (Chapter 5);

Dr. Jerome Durand of the ENSIACET of Toulouse for the synthesis of ligands 14, 15, 20, 21 (Chapter 5);

Prof. Cyril Godard of University Rovira i Virgili of Tarragona for the synthesis of ligands 10-13 (Chapter 4);

Prof. Claudio Pellecchia of University of Salerno for the measurement of the molecular weight of the synthesized ethylene/methyl acrylate copolymers (Chapter 3 and 4).